Characterization of the subcellular localization of the TGF-β receptors in the wing imaginal disc

Inauguraldissertation

zur

Erlangung der Würde eines Doktors der Philosophie

vorgelegt der

Philosophisch-Naturwissenschaftlichen Fakultät

Der Universität Basel

von

Ilaria Alborelli

aus Mailand, Italien

Basel, 2016

Genehmigt von der Philosophisch-Naturwissenschaftlichen Fakultät

auf Antrag von

Prof. Dr. Markus Affolter

Dr. Giorgos Pyrowolakis

Basel, den 19 April 2016

Prof. Dr. Jörg Schibler

Dekan

TABLE OF CONTENTS

ABSTRACT

The TGF-β pathway has been extensively studied *in vivo* in the wing imaginal disc of *D. melanogaster*. In particular, many investigations focus on the TGF-β ligand Dpp (BMP2/4 orthologue) that acts as a morphogen, regulating patterning and growth of wing disc cells.

It was reported that Dpp forms an extracellular gradient consisting of an apical and a basolateral fraction (Entchev, Schwabedissen, & González-Gaitán, 2000; Gibson, Lehman, & Schubiger, 2002; Teleman & Cohen, 2000). However the function of these distinct fractions and the subcellular localization of the molecules responsible for ligand perception have not yet been characterized in this developmental context.

Therefore, in this thesis I investigated the localization of BMP receptors and co-receptors expressed in the wing disc. I found that the *D. melanogaster* TGF-β superfamily type-I receptors have different subcellular localizations: while the BMP receptors Tkv and Sax distribute along the apical and the basolateral side of the wing disc epithelium, the TGF-β/Activin receptor Babo is only basolaterally localized. This subcellular bias in localization is also found in the TGF-β type-II receptors, Punt and Wit. Punt localizes only to the basolateral compartment, whereas Wit is also present at the apical compartment and shows a clear enrichment in this domain. The glypicans Dally and Dlp localize to both apical and basolateral compartments, as previously reported (Ayers, Gallet, Staccini-Lavenant, & Thérond, 2010; Gallet, Staccini-Lavenant, & Thérond, 2008).

In order to understand the functional importance of the polarized subcellular localization of TGF-β receptors, I tried to mislocalize the TGF-β receptors using different approaches. In a first approach I have been using membrane-bound nanobodies. Despite the fact that these nanobody-tools were

designed to trap secreted GFP-tagged proteins, I will show that they are also potential tools to mislocalize polarized membrane proteins. In another approach, I tried to mislocalize the TGF-β receptors through the mutation of "targeting domains". Finally, to address whether signalling polarization has important consequences on physiological development, I attempted to modify the subcellular localization of the endogenous type-I receptor Tkv. To this end, I used a landing site in the *tkv* locus, generated by replacing the last two exons of *tkv* with an *attP* landing site and resulting in a *tkv* null allele. This tool allows manipulation of the receptor at the endogenous locus, important to understand the developmental impact of its proper subcellular localization. I achieved to generate different tagged versions of Tkv, with either an extracellular or a C-terminal mCherry tag. Moreover, I deleted a conserved targeting domain in the Tkv protein and obtained apical enrichment of Tkv localization.

In the following, I will discuss these different methods and their implications for studying TGF-β signalling polarization in the wing disc.

1 INTRODUCTION

The concept of polarity is present in a multitude of scientific fields, ranging from the polarization of waves in physical sciences, to chemical polarity and racial polarization in social sciences.

In any of these disciplines, the term "polarity" is used to describe the property of having two different poles or aspects, characterized by contradictory features. Notably, this asymmetry is often the reason why many processes happening in polarized systems acquire a specific orientation.

Concerning biology, the idea of polarization pervades both macroscopic and microscopic scales. A common example of "macroscopic" polarization is the division of a living organism – as wells as its tissues and organs – into different axes of symmetry. This phenomenon is particularly evident during initial phases of *Drosophila melanogaster* development, where its molecular bases have been associated with the discovery of a set of genes, called the "egg/segment-polarity genes". These genes are expressed in a polarized fashion and responsible for specifying the anterior-posterior axis of the embryo and, later on, of the embryonic segments (Nüsslein-Volhard & Wieschaus, 1980).

At the microscopic scale many cell types are polarized, as they accommodate asymmetrically localized domains and structures, which enables them to carry out specialized functions at distinct cell poles (Figure 1.1).

For example, neurons are polarized cells. They contain specialized structures at opposite ends, e.g. dendrites receiving the signal at one end and axon terminals propagating the signal at the other end. As a consequence of this polarization the propagation of the nerve impulse is unidirectional, always travelling from the dendrites to the axon terminals (Figure 1.1D, reviewed in Horton & Ehlers, 2003).

Another example of polarization is found in migrating cells. The leading edge (front) of migrating cells is often characterized by actin-based structures such as lamellipodia or filopodia. At the trailing edge (rear) there are stress fibers, caused by the contractile forces needed for the edge retraction (Figure 1.1C). In general, migrating cells are described as polarized because migration itself is an oriented behaviour (Vicente-Manzanares, Webb, & Horwitz, 2005).

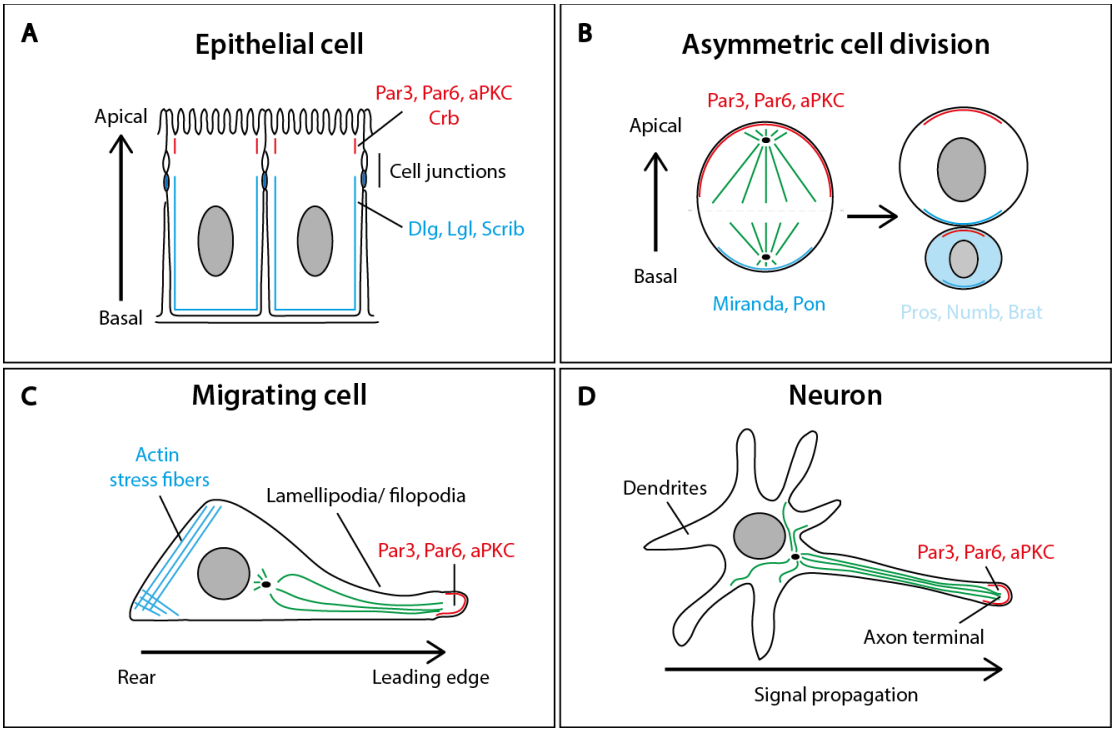

Figure 1.1 Examples of polarization in different cell types. A. Epithelial cells are subdivided by tight junctions (dark blue) in an apical and a basolateral domain. The apical domain (red) faces the lumen (or the outside of the body for e.g. skin cells), and is determined by the presence of specific members of the Par complex. The basolateral domain (light blue) is characterized by the presence of SCRIB complex components. **B.** During asymmetric cell division the mitotic spindle is oriented parallel to the apical-basal axis. This results in the asymmetric distribution of cell fate determinants into the daughter cells (here depicted a *D. melanogaster* neuroblast). **C.** Migrating cells are characterized by an asymmetric distribution of functional structures, such as filopodia or lamellipodia at the leading edge and stress fibers due to the contracting rear. **D.** Neurons are clearly polarized cells, as molecules and structures needed for signal propagation are arranged in a unidirectional fashion. Note that, in all the examples mentioned, Par3, Par6 and aPKC localize to an exclusive pole. Figure adapted from (Suzuki, 2006) and http://www.eb.tuebingen.mpg.de/

Stem cells can divide asymmetrically, giving rise to daughter cells with different fates, balancing self-renewal and differentiation. This mechanism relies on the polarized distribution of fate determinants (Figure 1.1B, reviewed in Knoblich, 2010).

Above all, polarity has been studied in epithelial cells (Figure 1.1A). The next pages are dedicated to epithelial cell polarity and to the pathways that are responsible for controlling and shaping these asymmetries along the apical-basal axis.

1.1 Epithelial cell polarity

Epithelial cells are polarized structures, subdivided by sealing junctions (septate junctions in *D. melanogaster*, tight junctions in vertebrates) in apical and basolateral compartments. These domains are characterized by differential distribution of molecules at the cell cortex, the plasma membrane and in the extracellular space.

Epithelial polarity is essential to generate and maintain specific cellular functions and, if disrupted, can lead to loss of tissue homeostasis and cancer. A handful of molecules act as key regulators of epithelial cell polarity, since they are responsible for establishing and maintaining apical or basolateral compartment identity.

These molecules belong to three main complexes: the Par, the Crumbs and the Scribble complexes (Figure 1.2A,C).

Par proteins (Partition defective) were first discovered in a screen in *C. elegans* and found to be required for the correct segregation of cytoplasmic material among anterior and posterior cells of the early worm embryo (Kemphues, Priess, Morton, & Cheng, 1988). Homologues of the *par* gene family are found throughout the animal kingdom. Par proteins are ubiquitously expressed (Figure 1.1) and they regulate not only polarity, but

also processes such as proliferation and differentiation. The Par group consists of proteins with diverse functions, such as kinases (PAR1, PAR4 and aPKC), scaffold (PAR3) and adaptor proteins (PAR6), the phospho-protein interactor PAR5 and the GTPase CDC42.

To coordinate the epithelial polarity module, Par proteins need to interact with two main protein complexes, the Crumbs and the Scribble complex. Most of these proteins were discovered through genetic screens in *D. melanogaster* and they are conserved amongst metazoans. In contrast to Par proteins, the expression of Crumbs and Scribble group members is restricted to epithelial cells.

The Crumbs complex consists of Crumbs (Crb), Stardust (Std in *D. melanogaster,* PALS1 in mammalian) and PALS1-associated tight-junction (PATJ) (Tepass, 2012). The complex localizes to the apical compartment of epithelial cells and it is required for the specification of this domain.

In contrast, the Scribbled group is restricted to the basolateral side and contains Discs-large (Dlg), Lethal giant larvae (Lgl) and Scribble (Bilder, Li, & Perrimon, 2000). Additional regulators of basolateral domain identity were discovered in *D. melanogaster*, as the Coracle complex, that includes Yurt, Coracle, Neurexin IV and Na^+K^+-ATPase (Laprise et al., 2009).

In addition to the asymmetric distribution of the proteins discussed above, the plasma membrane of apical and basolateral compartments differs in its lipid composition. A specific class of lipids, the phosphoinositides, is distributed in a polarized fashion in mammalian epithelia. The tri-phosphorylated form of phosphatidylinositol (PtdIns-3,4,5-trisphosphate) is found in the basolateral plasma membrane, whereas the bi-phosphorylated form (PtdIns-4,5-bisphosphate) determines apical membrane identity (Gassama-Diagne et al., 2006; Martin-Belmonte et al., 2007). No correspondent role of phosphatidylinositol has been observed in *D.*

melanogaster. However PTEN, the phosphatase required to switch from tri- to bi-phosphorylated phosphatidylinositol, localizes apically in the fly embryonic epithelial cells and neuroblasts (Stein, Ramrath, Grimm, Müller-Borg, & Wodarz, 2005).

Many other molecules are involved in the control of epithelial cell polarity and further players and interactions will be elucidated due to large-scale protein interaction mapping (Koorman et al., 2016).

1.1.1 The epithelial polarity cascade

Coordinated molecular networks are required to establish and maintain epithelial cell polarity. These mechanisms depend on feedback loops and interactions between proteins belonging to the different apical/basolateral domains (Figure 1.2A). Indeed, an important feature of the polarity regulators is their subcellular localization bias (except for Par5, which is uniformly distributed throughout the cytoplasm). Two kinases of the Par complex have a crucial role in segregating polarized proteins into specific subcellular domain, aPKC and Par1.

Only few polarity determinants are transmembrane proteins (Crb, Neurexin IV and Na^+K^+-ATPase). Among them, Crb serves as a docking station for PALS1 (Stardust). Binding of PALS1 to Crb is crucial for the exclusion of basolateral proteins from the apical domain: PALS1 binds to PAR6, which is required for the apical positioning of aPKC (atypical Protein Kinase C) (David, Tishkina, & Harris, 2010). The GTPase CDC42 interacts with Par6 and is required for the apical localization of aPKC. CDC42 localizes apically through a PTEN and PtdIns-4,5-bisphosphate-dependent mechanism in mammalians.

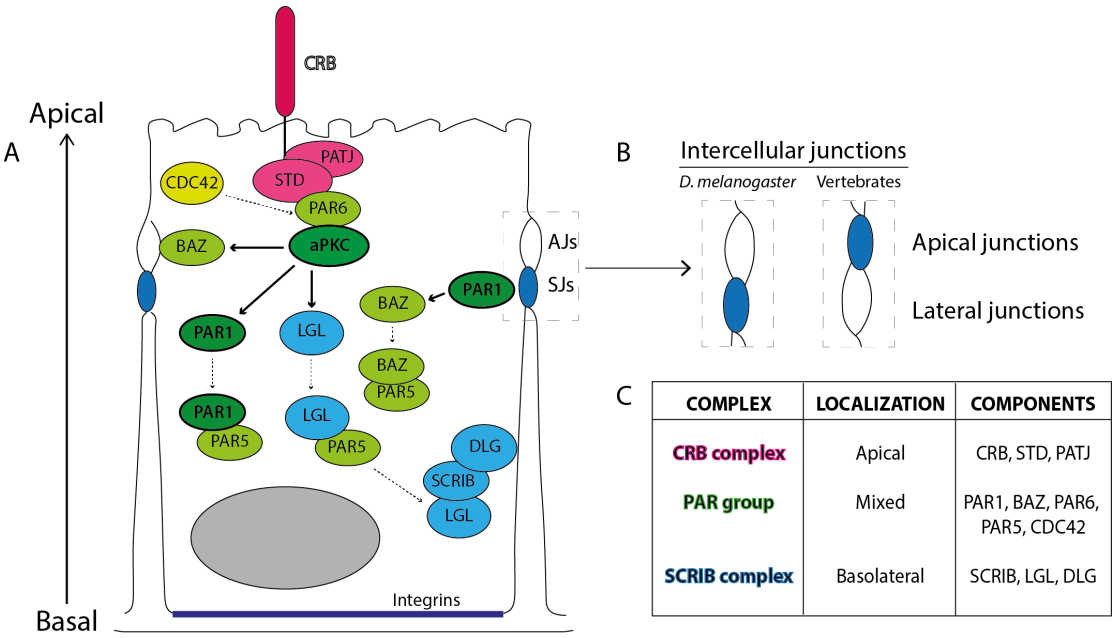

COMPLEX	LOCALIZATION	COMPONENTS
CRB complex	Apical	CRB, STD, PATJ
PAR group	Mixed	PAR1, BAZ, PAR6, PAR5, CDC42
SCRIB complex	Basolateral	SCRIB, LGL, DLG

Figure 1.2 The epithelial polarity pathway. A. The subcellular localization of polarity determinants is regulated by a series of feedback loops. Crb binds Std (PALS1), which binds PATJ. Std recruits Par6 and Par6 recruits aPKC to the apical side. CDC42 localizes apically and is required for Par6 and aPKC function. aPKC and PAR1 actively maintain the borders of apical and basolateral domain, respectively. aPKC phosphorylates Baz (Par3), Par1, LGL to prevent their apical localization. Par1 phosphorylates Baz, to prevents its basolateral localization. Indeed Baz ends up localizing to the adherens junctions (AJs). Solid arrows represent phosphorylation events. Dashed arrows represent formation of protein complexes. **B.** Intercellular junctions have different subcellular distribution in D. *melanogaster* compared to vertebrate cells. In *D. melanogaster* the sealing junctions, called septate junctions (SJs) are basal to the AJs. In vertebrates the sealing junctions, called tight junctions, are apical to the AJs. **C.** Subcellular distribution of the epithelial polarity complexes represented in A.

aPKC is actively maintaining epithelial polarity by phosphorylation of basolateral proteins, causing their exclusion from the apical domain (Rodriguez-Boulan & Macara, 2014; St Johnston & Sanson, 2011). The most important target of aPKC is PAR1, which is phosphorylated and banished from the apical side (Figure 1.2A).

PAR1 is the basolateral counterpart of aPKC, since it has the crucial role of excluding apical proteins from the basolateral side.

A special member of the Par complex is the adaptor protein Bazooka (Baz, PAR3). Baz has a crucial role as a polarity determinant, since it is required for the assembly of junctional components and for the apical localization of

aPKC (St Johnston & Sanson, 2011). Remarkably, Baz is phosphorylated by both aPKC and PAR1 (Benton & St Johnston, 2003; Horikoshi et al., 2009; Morais-de-Sá, Mirouse, & St Johnston, 2010) (Figure 1.2A). This forces Baz to localize at the apical side of the intercellular junctions (tight junctions in mammalians and adherens junctions in *D. melanogaster*).

In summary, aPKC and PAR1 are responsible for the generation of complementary apical/basolateral cortical domains. However, they both rely on PAR5 (also named 14-3-3) to mediate proper "re-shuttling" of the phosphorylated proteins. PAR5 localizes uniformly across the apical/lateral domains and binds to the proteins targeted by aPKC and PAR1. Binding of PAR5 to phospho-proteins triggers their release from the cell cortex (Goldstein & Macara, 2007). Importantly, PAR5 can also bind to both PAR1 and Baz and is necessary for their proper localization (Benton & St Johnston, 2003; Rodriguez-Boulan & Macara, 2014).

The molecules and the mechanisms involved in the control of epithelial polarity are well conserved in the animal kingdom. Nevertheless, important variations have been recorded in different developmental contexts, tissues and species.

One example of diversity is the position of the junctions in *D. melanogaster* compared to mammalian epithelial cells. Two main types of junctions are present at the border between apical and lateral domain: sealing junctions (septate junctions (SJs) in *D. melanogaster* and tight junctions in mammalians) and adherens junctions (AJs) (Figure 1.2B). The sealing junctions form a barrier that segregate the internal medium from the outside environment or lumen, therefore physically separating apical and basolateral compartments.

In vertebrates tight junctions localize apically, above AJs, whereas in *D. melanogaster* SJs are described as components of the basolateral domain,

and harbour important members of the lateral determinants (reviewed in Giepmans & van Ijzendoorn, 2009). AJs are part of the subapical region in *D. melanogaster* and they are labelled by the apical determinant Baz and DE-cadherin (St Johnston & Sanson, 2011).

Outside the cell, external cues play an important role in determining epithelial polarity, mainly by directing the orientation of the apical-basal axis. During mesenchymal-to-epithelial transition (MET) cells rely on the contacts with the other cells and with the basal membrane (mediated by integrins), in order to develop polarized epithelial features (O'Brien et al., 2001; W. Yu, 2004). Accordingly, external cues are translated inside the cell, resulting in restructuring of the polarity network. This applies similarly to epithelial-to-mesenchymal transition (EMT), where the TGF-β receptor type-II affects cell polarity by phosphorylating PAR6, which leads to loss of tight junctions (Ozdamar et al., 2005).

In the results part of this thesis, I will show the attempts of mislocalizing the apical determinant Crb to the basolateral side of the wing imaginal disc epithelium. Therefore, I will summarize the characterization of Crb as an apical determinant and growth regulator in *D. melanogaster* in the following section.

1.1.2 The transmembrane protein Crumbs regulates polarity and growth during *D. melanogaster* development

Crb was the first protein to be described as an apical determinant (Tepass & Knust, 1990; Tepass, Theres, & Knust, 1990). This definition is based on the observation that in embryonic epithelium Crb is necessary and sufficient to specify the apical membrane, since *crb* mutants loose apical membrane identity (Wodarz, Grawe, & Knust, 1993) and Crb overexpression causes

expansion of the apical plasma membrane domain (Wodarz, Hinz, Engelbert, & Knust, 1995).

Crb is a type-I transmembrane protein, with a large extracellular domain of more than 2000 amino acids (aa), characterized by several EGF-like repeats and four laminin AG-like repeats. The considerably smaller (37 aa) cytoplasmic domain is required to interact with Std, PATJ and Lin7 (Bulgakova & Knust, 2009). The function of the extracellular domain of Crb is controversial. *D. melanogaster* embryos mutant for *crb* show severe epithelial polarity defects (Tepass & Knust, 1990), which can be fully rescued by a version of Crb lacking the extracellular domain (Crb^{intra}) (Klebes & Knust, 2000; Wodarz et al., 1995). In support of this observation, the Crb homologous proteins in human, CRB1, CRB2 and CRB3, have a shorter extracellular domain, with CRB3 completely lacking the extracellular domain (P. Li, Mao, Ren, & Liu, 2015). Nevertheless, Crb^{intra} is mislocalized in the *D. melanogaster* photoreceptor cells, whereas a membrane-bound Crb extracellular domain is correctly targeted to the apical compartment (stalk) (Pellikka et al., 2002). Moreover, in the zebrafish retina interactions between the extracellular domains of CRB2a and CRB2b are required for cell adhesion and epithelial integrity (Zou, Wang, & Wei, 2012). Consistently, mutations falling in the extracellular domain of CRB1 are associated with retinal dystrophies in humans (Bujakowska et al., 2012).

Crb is expressed in most epithelial cells of *D. melanogaster* and at different developmental stages, starting from embryonic blastoderm cells, to larval imaginal discs and ovarian follicle cells (Tepass & Knust, 1990). In all these cells Crb has the same restricted subcellular distribution, localizing specifically to the apical portion of the plasma membrane situated above the AJs, named the subapical or marginal region (Tepass, 1996; 2012). This specific localization suggests that Crb might have the same function in all

these different epithelia. However, this is not the case. Crb is not required to maintain cell polarity during late embryonic development (Tanentzapf & Tepass, 2003), in larval eye imaginal discs (Pellikka et al., 2002) and Malphighian tubes epithelium (K. Campbell, Knust, & Skaer, 2009). In particular, *crb* mutants show no perturbation of AJs and β_{Heavy}-spectrin localization (an apical cytoskeletal protein required for membrane integrity) in the eye imaginal disc. Nevertheless, in the same study overexpression of Crb caused loss of epithelial integrity and mislocalization of apical proteins (Pellikka et al., 2002). In the wing imaginal disc, Crb is required for the localization of other apical components, but the basolateral proteins seem unaffected (Hamaratoglu et al., 2009). The lack of polarity defects in some *crb* mutant epithelia, suggests that Crb functions redundantly with other polarity determinants, such as Baz (Pellikka et al., 2002; Tanentzapf & Tepass, 2003).

Crb has been implicated in the regulation of cell growth. Both Crb overexpression and Crb loss give rise to overgrowth (C.-L. Chen et al., 2010; Grzeschik, Parsons, Allott, Harvey, & Richardson, 2010; Ling et al., 2010; Lu & Bilder, 2005; Robinson, Huang, Hong, & Moberg, 2010).

Crb was shown to regulate growth acting through one of the major growth regulatory pathways, the Hippo pathway. The main players of the Hippo pathway are the kinases Hippo and Warts and their adaptor proteins Salvador and Mats. Active Hippo phosphorylates Warts that ultimately phosphorylates and inactivates Yorkie. Yorkie is a transcriptional co-activator that promotes cell growth and survival. Therefore, by inhibiting Yorkie function, the Hippo pathway acts as a tumour suppressor. The Hippo-Salvador complex is recruited to cell membrane via the adaptor protein Expanded, a cytoplasm protein associated to the apical membrane.

Expanded requires Crb for proper apical localization (C.-L. Chen et al., 2010; Ling et al., 2010). Expanded binds to Crb through its FERM domain (Ling et al., 2010) and is lost from the subapical region in both Crb loss and overexpression conditions (C.-L. Chen et al., 2010; Ling et al., 2010). Consequently, Crb acts as a tumour suppressor, by supporting Hippo pathway activity. Moreover Crb has been linked to Notch signalling, another important pathway implicated in cell-cell communication and differentiation. The heads of *crb* mutant flies show an increased size compared to wild-type flies, as a consequence of ectopic Notch signalling (E. C. N. Richardson & Pichaud, 2010). In this system Crb acts as a negative regulator of Notch by restricting apical endocytosis of Notch and its ligand Delta. Crb regulation of Notch signalling has been observed also in zebrafish neuroepithelial cells, where the Crb extracellular domain directly binds to the receptor Notch1a (Ohata et al., 2011).

In conclusion, Crb function as a polarity determinant is context-dependent and varies in different tissues and developmental stages. Tissues expressing *crb* might not rely on it for apical domain specification. For example, in the wing and eye imaginal disc, Crb is important for proper targeting of many apical proteins (for example Expanded and PatJ) and for apical domain size control; however, it is not essential to maintain epithelial cell polarity (Genevet et al., 2009; Hamaratoglu et al., 2009; Pellikka et al., 2002).

1.2 The wing imaginal disc as a model system

1.2.1 The life cycle of *D. melanogaster*

D. melanogaster is a fruit fly belonging to the *Drosophilidae* family and is a powerful model organism for studying developmental and cell biology.

The life cycle of *D. melanogaster* lasts around 10 days and is subdivided in four major stages: embryonic, larval, pupal and adult stage.

The embryonic stage lasts until 22-24 hours after egg laying (AEL), and it is followed by the first larval instar. Three instar stages take place during the larval development, in which the larva eats and grows. The transition from one instar to the next is marked by a molting event. First and second larval instars development requires around 24 hours each, while the third instar stage lasts 30-40 hours, which in total accounts for the four days of larval development. Subsequently, metamorphosis begins during the pupal stage. The pupal stage lasts five days and results in the hatching of the adult fly (imago) from the pupal case. Most larval tissues are degraded during the pupal stage, with the notable exceptions of histoblasts and the fifteen imaginal discs. Histoblasts will give rise to the abdominal epidermis and internal organs of the adult fly. The imaginal discs will give rise to many epidermal structures, such as adult wings, legs, eyes, mouthparts, antenna, genital ducts and parts of the head and thorax. Developmental biologists have used *D. melanogaster* imaginal discs as a paradigm to study tissue and organ development. In particular, the wing imaginal disc emerged a model system to study the regulation of growth and patterning (Held & Held, 2005) and is the model tissue chosen for this study .

1.2.2 The wing imaginal disc structure

Larval imaginal discs are sac-like structures composed of two joined epithelial sheets separated by a lumen. The two epithelia composing the imaginal discs are named disc proper (DP) and peripodial membrane (PM) (Figure 1.3B, B'). Throughout first and second larval instar, the cells of these two epithelial layers have a cuboidal shape. At late-second larval instar the cells undergo drastic shape changes, which lead to transformation of the DP into a

pseudostratified columnar monolayer and the PM into a squamous monolayer (McClure & Schubiger, 2005). In mid to late-third instar, the molting hormone 20-hydroxyecdysone drives further changes in the imaginal discs, leading to a process called eversion. In this event, the imaginal discs PMs simultaneously contract and push the DP towards the outside of the body (Gibson & Schubiger, 2001).

After metamorphosis, the DP and PE develop into different adult tissues. In particular, in the wing imaginal disc, the DP gives rise to the adult wing, hinge and notum (Figure 1.4), whereas the PM contributes to the formation of a minor portion of the adult body, specifically the ventral and lateral pleura (body wall) and ventral wing hinge (Gibson & Schubiger, 2001). For this reason, most studies focus on the DP cells, in particular on the pouch of the wing imaginal disc, which gives rise to the adult wing blade. However, as pointed out by the studies below, the PM of the wing disc might have additional roles than just acting as mechanical support during eversion.

In particular, cell-cell communication between DP and PM of the wing imaginal disc has been observed in several instances. Expression of the gene Ubithorax (Ubx) or Vestigial (Vg) in the DP cells, causes reduction or increase in the number of PM cells (Pallavi & Shashidhara, 2003). Repression of EGFR/RAS pathway in the PM induces notum/hinge-to-wing transformations in the DP (Pallavi & Shashidhara, 2003). Furthermore, inhibition of the Decapentaplegic (Dpp) signalling in PM cells caused reduction in adult wing size and patterning defects (Gibson et al., 2002). Cellular protrusions crossing the wing disc lumen have been visualized and they appear to directly interconnect DP and PM cells (Demontis & Dahmann, 2007).

Additional manipulations provided evidence for cell-cell interaction between DP and PM cells. Overexpression of Delta, a Notch ligand, in the PM induces expression of Notch target gene Wingless (Wg) expression in the DP (Pallavi

& Shashidhara, 2005). Similarly, expression of wild-type and membrane tethered versions of Hedgehog (Hh) in PM cells caused activation of the Hh target gene Dpp in DP cells. These results suggest the existence of physical cell-cell interaction between PM and DP cells. Notably, both the Notch and the Hh pathways require apical membranes interactions in order to activate signalling into neighbouring cells. This observation is consistent with the orientation of DP and PM cells, since the apical compartments of these two epithelial sheets face each others (Pallavi & Shashidhara, 2005).

1.2.3 The wing imaginal disc cell polarity

The sac-like structure of the wing imaginal disc is characterized by an internal cavity, or lumen, that separates the DP from the PM epithelium (Figure 1.3B, B'). This should per se define the orientations of the apical surface of both epithelia, since the apical membrane is defined as the side of the epithelial cell facing the lumen. Indeed the orientation of DP and PM epithelial cells was confirmed, by using markers with different and specific subcellular localization. Armadillo is a junctional protein that marks the subapical region. Indeed, it was found that Armadillo localizes to the cell surface facing the lumen in DP and PM cells. Cortical actin (labelled with Phalloidin, that binds to filamentous-actin (F-actin) in Figure 1.3A', B'') is enriched at the apical side of epithelial cells and indeed localized above Armadillo. In agreements, the basolateral markers Fasciclin III and Dlg label the opposing cell surface of DP and PM cells facing away from the lumen (Pallavi & Shashidhara, 2005). Dlg is not only basolateral, but also enriched at the SJs, whereas the apical side of the junctions (AJs) is marked by the *Drosophila* Epithelial-cadherin (DE-cadherin) (Figure 1.3B'''). The subapical region (SAR) is characterized by the presence of important apical determinants, as Crb and aPKC (Figure 1.3B'''). The polarity of the wing disc epithelium has an important impact on major cellular events, like cell division and cell death.

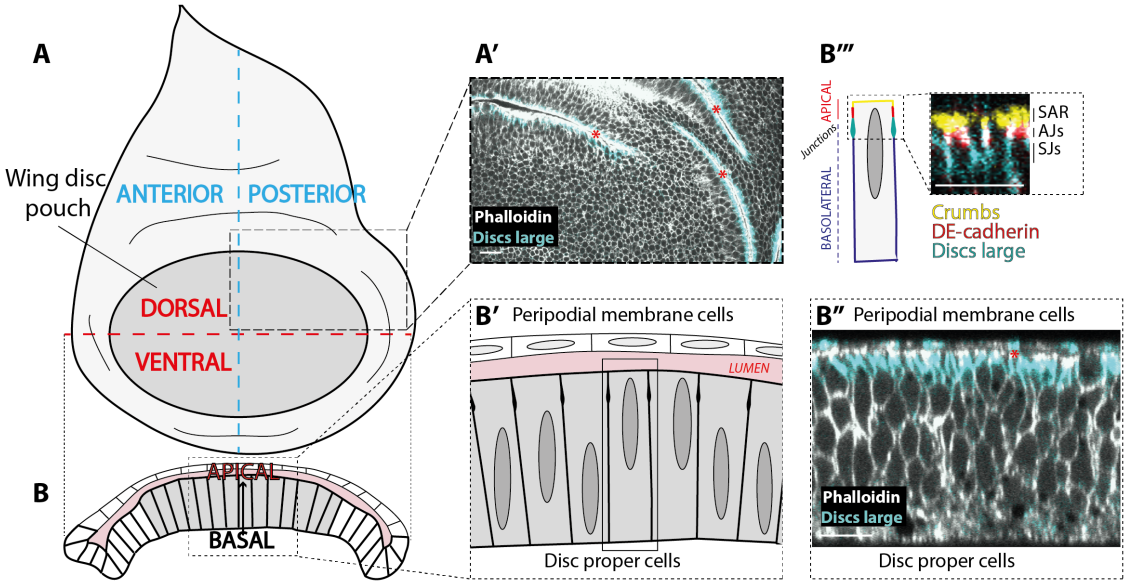

Figure 1.3 Wing imaginal disc structure and cell polarity. A. Schematic representation of the top view of a wing disc, the pouch area is shaded in grey. **A'.** Top view of a wing imaginal disc labeled with Phalloidin (marks F-actin, grey) and Discs large (cyan). The apical surface of DP cells contacts in the folds (red asterisks). The apical surface is visualized through cortical F-actin enrichment (Phalloidin in grey). Discs large (cyan) marks the septate junctions, visualized basal to the Phalloidin enrichment. **B.** Schematic representation of a cross section of the wing imaginal disc, pouch cells are coloured in grey. The apical surface of wing disc cells faces the lumen. **B'.** Peripodial membrane cells (B', top) are separated from disc proper cells (B', bottom) by the lumen. **B''**. Cross section of the imaginal disc shown in (A'). Phalloidin (grey) labels cortical F-actin, enriched at the apical side of the cells. Disc large (cyan) labels the septate junctions, just below the apical compartment. PM cells are squamous cells, thus the junctions are less dense. The red asterisk marks the lumen. **B'''.** Magnification showing the apical region of a wing disc cross-section. Discs large (cyan) labels the SJs, DE-cadherin (red) labels the adherens junctions (AJs) and Crumbs localizes to the subapical region (SAR).

Nuclear division happens at the apical side of the wing imaginal disc and involves a process called interkinetic nuclear migration (Meyer, Ikmi, & Gibson, 2011). Cells destined to die undergo a process of cell extrusion, also referred as delamination. This process leads to the removal of a group of cells from the epithelium, without interfering with the epithelial barrier function. For example, wing pouch clones with inappropriate Dpp or Wg signalling are extruded in a polarized fashion, characterized by apical surface retraction and extrusion to the basal side (Gibson, 2005; Widmann & Dahmann, 2009a).

Another process affected by the apical-basal polarization of the wing disc cells is signalling, which will be discussed in chapter 1.4.2.

1.2.4 The wing imaginal disc cell shape

Epithelial sheets often need to change their shape during development, for example during morphogenetic movements or cell division. Epithelial cell shape falls into three main categories: squamous, cuboidal or columnar. Importantly, the relative size of the apical, lateral or the basal surface is different in these three types of epithelia: apical and basal surfaces are predominant in squamous cells, at the expenses of the lateral domain; vice versa the elongation of the lateral compartment and the narrowing of the apical and basal surfaces are responsible for the cuboidal-to-columnar transition (St Johnston & Sanson, 2011).

The DP and PM cells derive from a common set of precursors cells in the embryo. The two cell populations diverge during the early larval stages. During first and early-second larval instar these two epithelia have a similar shape: at this stage both PM and DP cells are cuboidal (McClure & Schubiger, 2005). At late-second instar, PM cells flatten and undergo a cuboidal-to-squamous transition. On the other side of the disc, DP cells are rapidly dividing. In order to accommodate the drastic cell number increase, DP cells transform into a pseudostratified monolayer and undergo cuboidal-to-columnar transition (McClure & Schubiger, 2005). At late third instar, the DP contains around 50,000 columnar cells (Bryant & Levinson, 1985; Martin, Herrera, & Morata, 2009), and the PM 400-450 squamous cells (Pallavi & Shashidhara, 2005) . However, since PM squamous cells are much larger that the DP cells, these epithelia overlay and occupy virtually the same space (Figure 1.3B', B'', B''').

The DP cells will go back to cuboidal shape during pupal stage, contributing to the surface area extension required for the final formation of the adult wing blade (D. Fristrom & Fristrom, 1993).

Dpp and Wg signalling is cell-autonomously required to promote and maintain the columnar cell shape of DP cells (Widmann & Dahmann, 2009b; 2009a). In particular, Dpp acts by regulating Rho1, a GTPase responsible for activating the myosin-II regulatory chain Spaghetti squash (Sqh). Active Rho1 causes contraction of actin-myosin filaments and increase in cortical tension, acting through Sqh. Dpp regulates the subcellular localization of Rho1 activity and keeps it higher at the apical side of columnar cells. Locally activated Rho1 can generate the anisotropic cortical tension that drives cell elongation, by increasing apical constriction and decreasing lateral cortical tension (Widmann & Dahmann, 2009a).

Wg instead acts, at least partially, by maintaining the target gene Vestigial (Vg) expression: the transcription factor Vg is required to induce the actin capping protein alpha (*cpa*). Cpa restricts actin polymerization and therefore affects actin cytoskeleton and cell shape (Widmann & Dahmann, 2009b).

1.2.5 Compartmentalization of the wing imaginal disc

The wing imaginal disc consists of different cell populations, subdivided in discrete regions. As introduced above, the two cell layers form the wing disc, the DP and the PM.

Fate map data (Bryant, 1979), recently decorated by transcriptional profiling data (Butler et al., 2003), subdivide DP cells into presumptive territories along the proximal-distal axis: the notum forming the adult body wall (proximal), the wing hinge (central) and the wing blade (distal) (Figure 1.4).

The Iroquois-complex (Iro-C) genes are induced by Epidermal Growth Factor Receptor (EGFR) and they are required to specify notum identity. Vein, the ligand that activates EGFR in the notum, is specifically repressed in presumptive pouch cells by Wg. Dpp and the hinge factor Muscle segment homeodomain (Msh) further confine the notum by repressing Iro-C genes in the wing pouch and hinge respectively (Cavodeassi, Rodriguez, & Modolell, 2002; S. H. Wang, Simcox, & Campbell, 2000; Zecca & Struhl, 2002b; 2002a). Moreover, the cells expressing Iro-C genes do not intermingle with the ones that do not express Iro-C (Zecca & Struhl, 2002b).

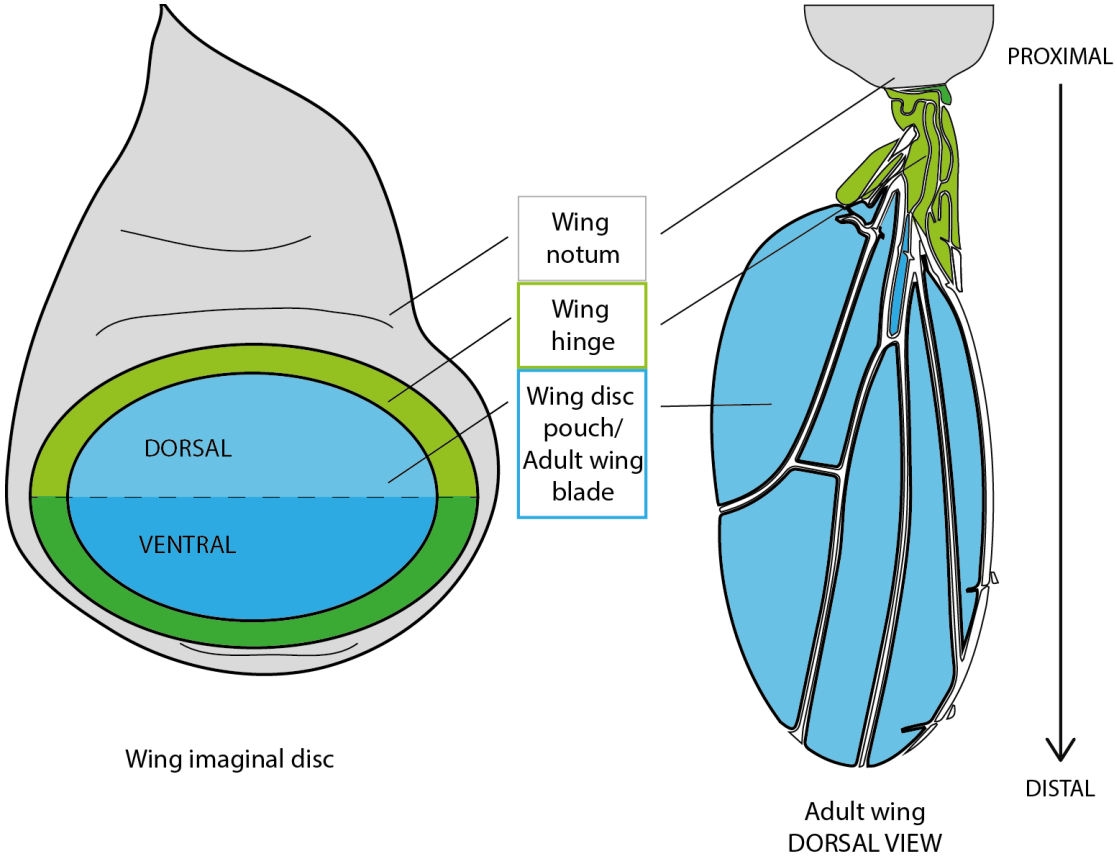

Figure 1.4 The division of the wing on the proximal/distal axis. Left: The wing imaginal disc is divided into concentric sections along its promal/distal axis: notum, hinge and pouch. After metamorphosis, the dorsal and ventral surfaces of the wing disc hinge and pouch, will fold on top of each other. **Left:** The adult fly's body and wings are subdivided along the proximal/distal axis into different structures, arising from the wing disc precursor.

The wing hinge is specified by the transcription factors Teashirt (Tsh), Nubbin (Nub), Rotund (Rn) and the homeodomain factor Homothorax (Hth). Mutation of any of these genes leads to loss of the hinge region in adult flies (Azpiazu & Morata, 2000; Casares & Mann, 2000; Rodríguez Dd, Terriente, Galindo, Couso, & Diaz-Benjumea, 2002).

Tsh and Hth are expressed in all the wing disc cells, but during second instar they are repressed in the wing pouch (Azpiazu & Morata, 2000; Wu & Cohen, 2002). Nub and Rd are instead expressed in both the wing pouch and the distal hinge, and Nub is also required for wing blade patterning and growth (Rodríguez Dd et al., 2002; St Pierre, Galindo, Couso, & Thor, 2002). Wg is required for hinge cells proliferation and is expressed in two concentric rings in the hinge (Whitworth & Russell, 2003; Zecca & Struhl, 2010). The activation of the JAK/STAT pathway is important for hinge fate specification and growth, since adult flies mutants for the JAK/STAT-ligand Unpaired lack the hinge region (Ayala-Camargo et al., 2013; Johnstone, Wells, Strutt, & Zeidler, 2013). Furthermore, ectopic STAT activity in the wing pouch perturbs wing blade development (Ayala-Camargo et al., 2013).

The wing pouch will give rise to the adult wing blade, structured by five longitudinal veins and two cross veins. Amongst others, Wg and Dpp are essential for wing development, as they are required for the formation of the adult wing (Neumann & Cohen, 1997; Spencer, Hoffmann, & Gelbart, 1982; Zecca, Basler, & Struhl, 1996).

The wing disc is also a model to study tissue compartments, defined as non-intermingling population of cells. The wing disc is divided into four different compartments, marked by two compartment boundaries: the anterior-posterior (A/P) and the dorsal-ventral (D/V) compartment boundary.

The generation of different compartments is important for the control of tissue growth and patterning, since it ultimately leads to the generation of an

organizing centre associated with the compartment boundary. The organizing centre produces a secreted molecule with a very special organizing power, a so-called morphogen. Morphogens are diffusible signalling molecules that form concentration gradients and organise tissue pattern in a concentration-dependent manner. During wing disc development, three signalling molecules have been described as morphogens, Hh, Dpp and Wg. In particular, Dpp forms a concentration gradient across the anterior and posterior compartments, with highest morphogen concentration at its source located next to the A/P boundary. Wg diffused from its source along the D/V boundary into the dorsal and ventral compartments.

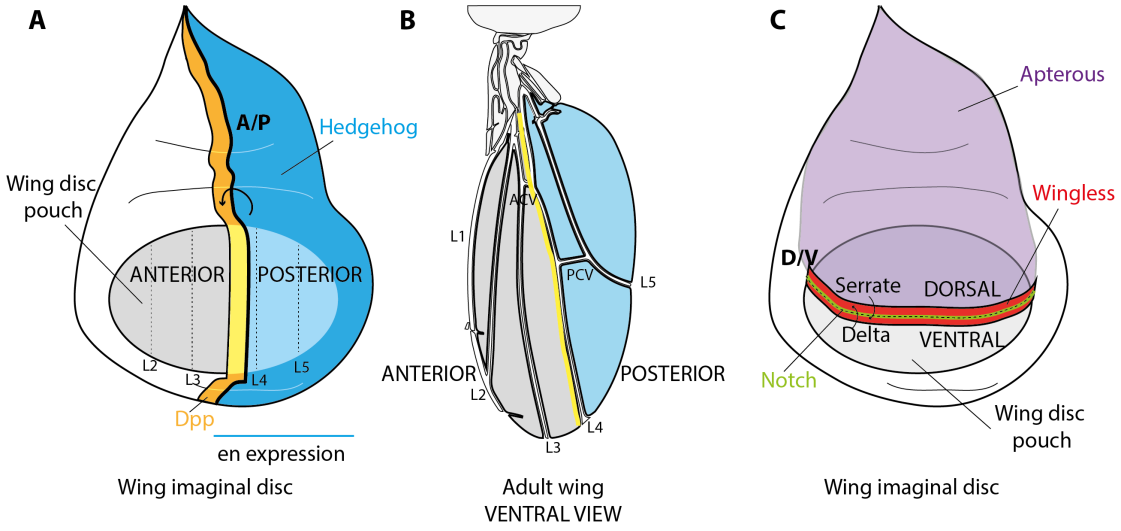

Figure 1.5 Compartmentalization of the wing imaginal disc. A. The wing disc is subdivided in anterior and posterior compartments. The selector gene *engrailed* is expressed in the posterior compartment. Engrailed induces Hedgehog, which in turn induces the Dpp organizer in an anterior stripe of cells adjacent to the border (thick line). **B.** The adult wing is subdivided in anterior and posterior compartments. The longitudinal veins L1, L2, L3 are located in the anterior compartment, whereas L4 and L5 are located in the posterior compartment. ACV: anterior cross vein. PCV: posterior cross vein. **C.** The wing disc is subdivided in dorsal and ventral compartments. The selector gene *apterous* induces a bi-directional Notch signalling cascade, which activates Wg expression in a stripe of cells at the D/V border.

The subdivision into anterior and posterior compartments is established during embryogenesis. The embryonic parasegments are patterned by the segment-polarity genes; one of the latter, *engrailed* (*en*), is expressed at the posterior side of each segments. Importantly, *en* is a transcription factor responsible for inducing posterior fate (Garcia-Bellido, 1975; Morata & Lawrence, 1975).

The wing imaginal disc segregates from a small group of cells, located in the second thoracic segment of the *D. melanogaster* embryo (Bate & Arias, 1991). This group of cells resides at the region of the *en* expression boundary, so that it consists of cells with posterior identity (En+) and cells with anterior identity (En-). Therefore the wing disc is "pre-patterned" during the embryonic stage. Through wing disc development, En induces the expression of a secreted signalling molecule, the morphogen Hh in the posterior cells of the wing disc (Tabata, Eaton, & Kornberg, 1992; Zecca, Basler, & Struhl, 1995) (Figure 1.5A).

While inducing Hh, En renders posterior cells insensitive to Hh signalling, by repressing the Cubitus Interruptus (Ci) transcription factor, which is required for Hh signalling transduction (S. Eaton & Kornberg, 1990). From posterior source cells, Hh disperses into the anterior compartment, where Ci is not repressed and cells can respond to Hh signalling. In a stripe of anterior cells Hh activates *dpp* (Zecca et al., 1995), one of its target genes (Figure 1.5A). This creates a stripe of *dpp* expression just anterior to the A/P boundary. This stripe acts as an organizer region that starts to secret Dpp, which acts as a morphogen forming a concentration gradient that controls growth and patterning along the A/P axis (reviewed in Affolter & Basler, 2007; Zecca et al., 1995). Another target gene of Hh is Patched (Ptc) that acts as the primary receptor for Hh and, as *dpp*, is activated in a stripe of anterior cells along the A/P border of the wing disc (Torroja, Gorfinkiel, & Guerrero, 2005).

The segregation of dorsal and ventral compartments happens during second larval instar. Here the selector gene is *apterous* (*ap*), a transcription factor expressed in the dorsal compartment (Diaz-Benjumea & Cohen, 1993) (Figure 1.5C). On the one hand, Ap restricts Notch signalling at the D/V border by activating the transcription of the Notch transmembrane ligand Serrate and of the signalling modulator Fringe in the dorsal compartment (Klein & Arias, 1998). On the other hand, the receptor Notch and the ligand Delta are not restricted to the dorsal compartment, but expressed broadly in the wing disc. Fringe is required to inhibit Notch-Serrate signalling and to enhance Notch-Delta signalling (Fleming, Gu, & Hukriede, 1997; Panin, Papayannopoulos, Wilson, & Irvine, 1997). This leads to the activation of Notch at both sides of the D/V boundary, depending on Serrate in ventral cells (Fringe free) and on the transmembrane ligand Delta in dorsal cells (Diaz-Benjumea & Cohen, 1995; Doherty, Feger, YoungerShepherd, Jan, & Jan, 1996) (Figure 1.5C). Notch signalling induces Wg at the D/V boundary, which acts as a morphogen to organize the tissue along D/V axis (Neumann & Cohen, 1997; Zecca et al., 1996). However the long-range morphogen function of Wg is currently disputed, since a membrane-tethered form of Wg can support relatively normal development and patterning, without considerably affecting growth (Alexandre, Baena-Lopez, & Vincent, 2014).

1.3 The TGF- β superfamily

1.3.1 TGF-β signalling overview

Transforming Growth Factor-β (TGF-β) signalling mediates a variety of cellular processes in a context dependent fashion.

The TGF-β pathway can block or stimulate cell proliferation, it can act as a tumour suppressor or support tumorigenesis by promoting EMT, stimulate differentiation (e.g. in myoblasts and neuroblasts) but also maintain

pluripotency of embryonic stem cells (Akhurst & Padgett, 2015; Massagué, 2012).

The conventional TGF-β pathway cascade involves interaction of the ligand with one of the transmembrane type-I and type-II serine/threonine kinase receptors, which are or will associate into a heteromeric receptor complex (Figure 1.6). In the complex, the type-II receptor activates the type-I receptor, by phosphorylating a GS (Glycine-Serine) rich region of the type-I receptor.

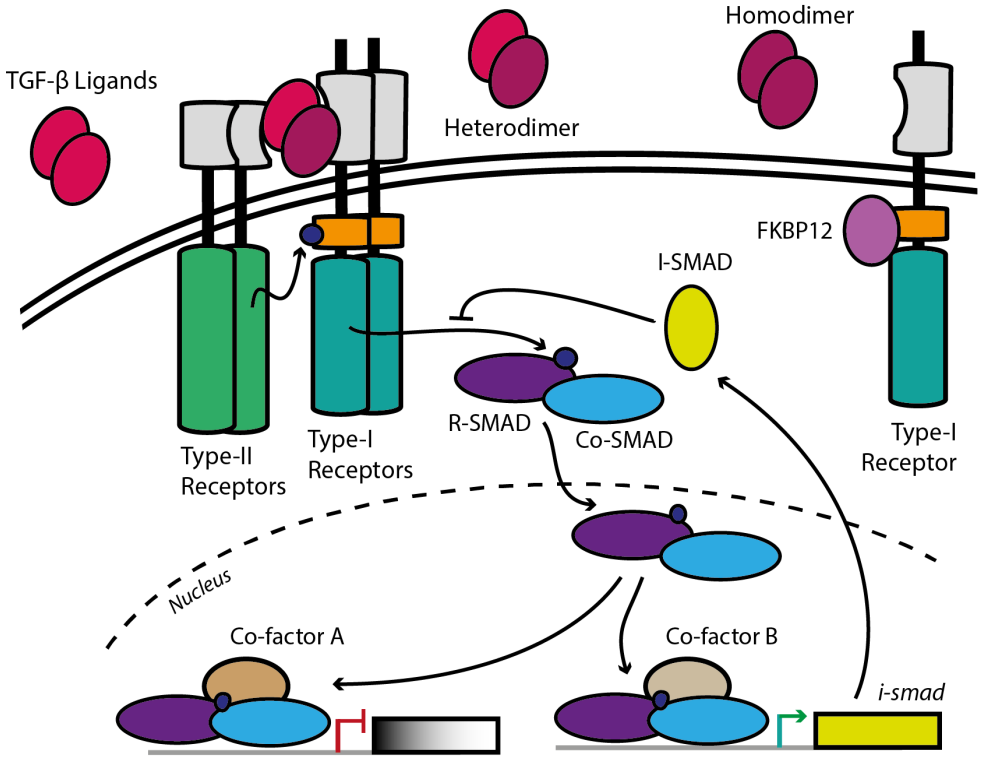

Figure 1.6 The TGF-β signal transduction. TGF-β ligands (pink) act as homodimers or heterodimers. They activate signalling by binding to type-I and type-II receptors. The receptor complex is heterotetrameric, made of two type-I and two type-II receptors. The receptor type-II initiates the signalling by phosphorylating (blue spot=phosphorylation) the GS region (orange box) of the type-I receptor. This triggers a conformational change and actives the type-I receptor. The type-I receptor phosphorylates (blue spot) a specific R-SMAD (purple). Phosphorylated R-SMADs associate with the Co-SMAD (blue) and move to the nucleus where they regulate transcription, together with other co-factors (brown). Among the target genes induced by TGF-β signalling, we find the I-SMADs (yellow). I-SMADs act as feedback regulators, interacting with type-I receptors and inhibiting the activation of R-SMADs. In an inactive state (right side), the GS domain of the type-I receptor is bound by FKBP12 (light purple). The kinase domains of type-II and type-I receptors are depicted as green boxes.

The GS region is well conserved and is located N-terminal to the kinase domain. The phosphorylation of the GS region triggers a conformational switch: from a site that binds 12 kDa FK506-binding protein (FKBP12), which inhibits the kinase domain, into a surface that binds and phosphorylates substrate SMAD proteins (Huse et al., 2001). FKBP12 directly binds the GS region, whereas SMAD proteins bind the L45 loop of the type-I receptor.

Upon phosphorylation by the type-I receptor, the so called receptor-SMAD (R-SMAD) associates with the common-mediator SMAD (co-SMAD, Smad4) and this complex moves to the nucleus, where it acts as a transcriptional regulator (Massagué, 2012).

Based on ligand sequence similarity the TGF-β superfamily can be divided in two major subfamilies: the TGF-β/Activin/Nodal subfamily and the BMP subfamily (Massagué, 2012; Shi & Massagué, 2003). The eleven members of the class of Growth and Differentiation Factors (GDFs) are represented in both subfamilies (Moustakas & Heldin, 2009; Schmierer & Hill, 2007; Shi & Massagué, 2003) (Figure 1.7).

All TGF-β superfamily ligands are synthetized as pre-pro-peptides that undergo subsequent steps of proteolytic cleavage during maturation. The pre-domain is a signal peptide, usually removed at the endoplasmic reticulum. The pro-domain is required for proper folding and trafficking, but needs to be removed to allow signalling, with some exceptions (Peterson & O'Connor, 2012). The pro-domain is also required for ligand dimerization, which occurs intracellularly. TGF-β superfamily ligands act prevalently as homodimers, but they can function also in combination with other ligands as in the case of Nodal-BMP4, Nodal-BMP7, Activin-βA-Activin-βB, Dpp-Screw (Scw), Dpp-Glass bottom boat (Gbb) (Massagué, 2012; Schmierer & Hill, 2007; Shi & Massagué, 2003).

A conserved structural feature of all TGF-β ligands is the cysteine knot motif, made of three intramolecular disulphide bonds between six conserved cysteine residues.

The ligands of the two subfamilies are selective for receptor complexes, consisting of specific combination of type-I and type-II receptors, that end up activating specific R-SMADs (Feng & Derynck, 2005; Schmierer & Hill, 2007). The basis of this specificity is not yet clear, however diffusible inhibitors and co-receptor are important regulators of ligand-receptor interactions (Schmierer & Hill, 2007). Moreover, TGF-β ligand can bind to a specific type-I or type-II receptor, or require a preformed heterotetrameric receptor complex for high affinity (Feng & Derynck, 2005).

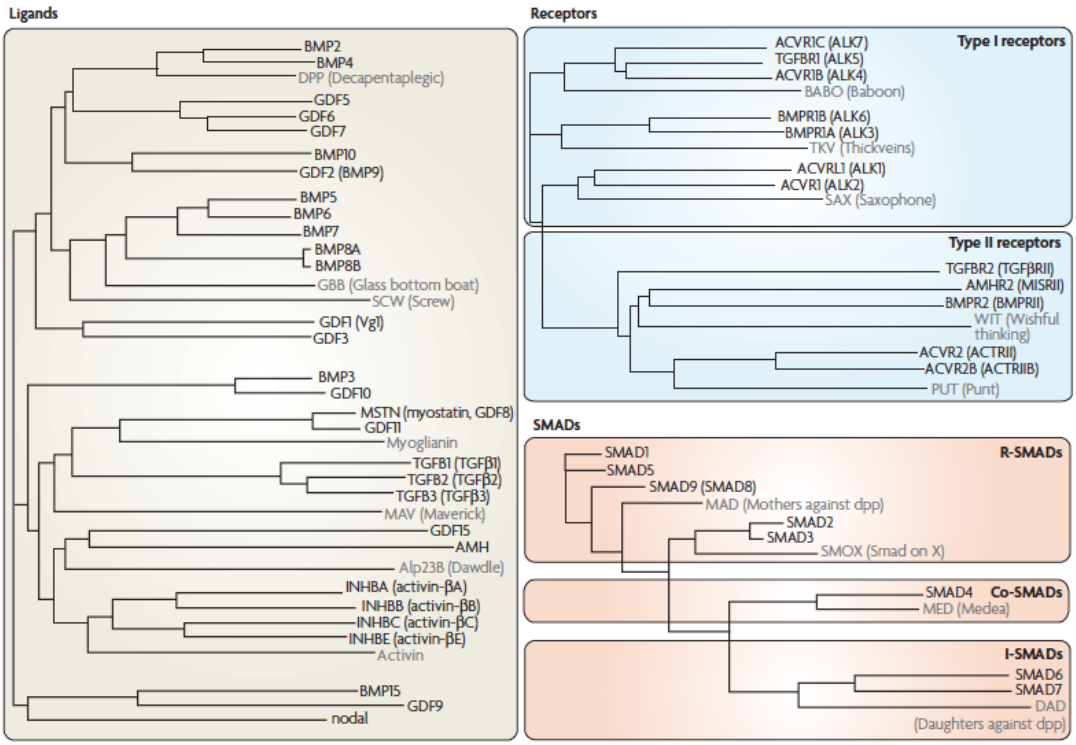

Figure 1.7 TGF-β superfamily ligands, receptors and SMAD proteins. Phylogenetic trees obtained from protein alignments of the TGF-β family components found in human (black) and in D. melanoster (grey). The phylogenetic trees were prepared using ClustalW web tool **(Chenna et al., 2003)**. Figure obtained from **(Schmierer & Hill, 2007)**.

Multiple type-I and type-II receptor combinations are possible. The seven human type-I receptors bind to one specific type-II receptor, with the exception of BMPR-1A/B and ALK2 that can bind to at least two different type-II receptors (Feng & Derynck, 2005). The type-II receptors are more promiscuous and can be shared by both TGF-β subfamilies; the extreme case is the ACTR-IIB receptor, which can bind to six different type-I receptors in response to different ligands (Schmierer & Hill, 2007).

The interaction between type-I receptors and R-SMADs is much more restricted. Each type-I receptor activates a specific set of R-SMADs, with Smad1/5/8 responsible for the BMP branch and Smad2/3 for the TGF-β/Activin/Nodal ligands (Massagué, 2000; Moustakas & Heldin, 2009) (Figure 1.8).

In addition to R-SMADs and Co-SMAD, there is a third class of SMAD proteins, the inhibitory SMADs (I-SMADs, Smad6 and Smad7 in humans, Dad in *D. melanogaster*). I-SMADs act as feedback regulators, since they are transcriptionally induced by TGF-β signalling and responsible for signal attenuation. They act either by competing for receptor binding or by enhancing receptor degradation and dephosphorylation (reviewed in Miyazono, 2007). Importantly, SMAD proteins share a similar structure, with a conserved N-terminal MH1-domain, responsible for DNA binding, and a C-terminal MH2-domain, responsible for type-I receptor binding, separated by a divergent linker region (Figure 1.8). Only the MH2 domain is conserved in the I-SMADs (Massagué, 2000).

Non-canonical TGF-β signal transduction has been reported, where TGF-β receptors can phosphorylate and active non-SMAD proteins (Moustakas, 2005). A notable example is the phosphorylation of the polarity regulator Par6 by TGF-β type-I and TGF-β type-II receptors, linked to disassembly of tight junctions and induction of EMT (Ozdamar et al., 2005).

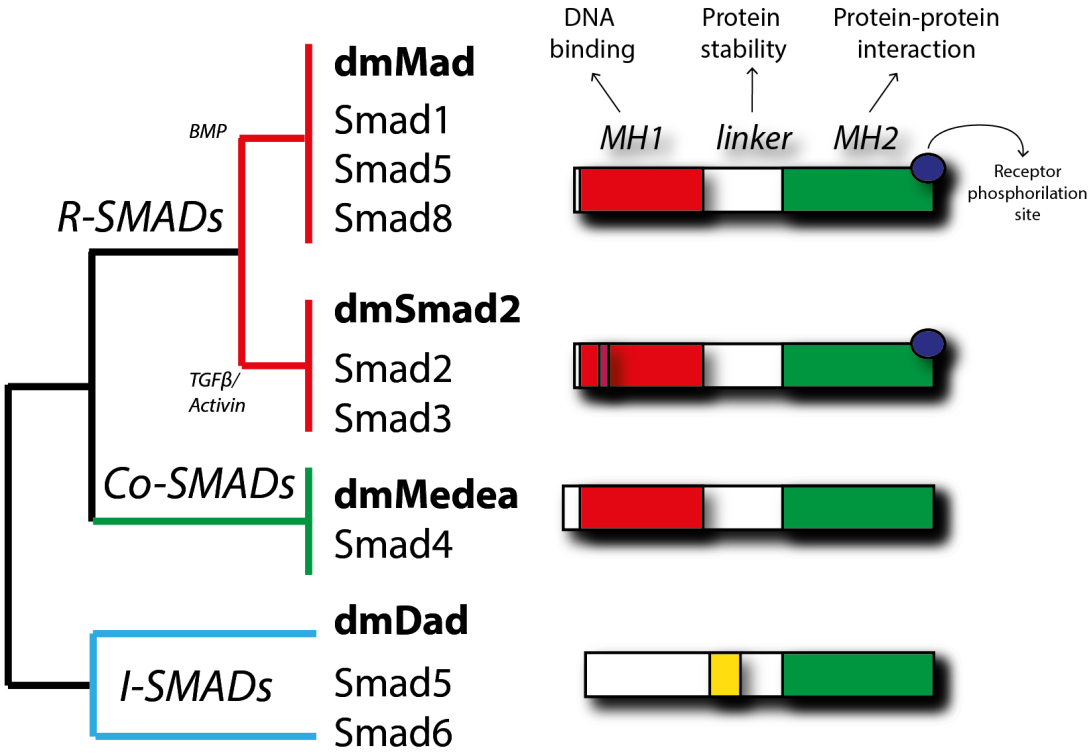

Figure 1.8 The SMAD protein family. Simplified dendrogram based on sequence similarity between the three SMAD subfamilies. R-SMADs and Co-SMADs contain conserved N-terminal (MH1) and C-terminal (MH2) domains separated by a divergent linker region. Only the MH2 domain is conserved in the inhibitory Smads (I-Smads). The blue spots represent the receptor phosphorylation sites. The darker purple stripe represents the alternatively spliced insert in Smad2. The yellow box represents the PY domain, required for I-SMADs protein turnover. Figure modified from **(Massagué, 2000)**.

Additionally, BMP2 can induce the activation of the p38/MAPK cascade, alternatively to SMAD activation. The choice between these two possible signalling outputs was suggested to depend on the state of the receptor complexes: BMPR-1a/BMPR-2 preassembled complexes mediate SMAD1 phosphorylation, whereas when BMP2 induces the formation of the receptor complex the output is p38 phosphorylation (Guzman et al., 2012; Hassel et al., 2003). Finally, BMPR-2 and the *D. melanogaster* type-II receptor Wishful thinking (Wit) were shown to activate the LIM1 kinase during dendrogenesis and synapse development (Foletta et al., 2003; Lee-Hoeflich et al., 2004).

The TGF-β signalling is an ancient invention of the animal kingdom, already found in sponges and trichoplax (Huminiecki et al., 2009). The number of

TGF-β ligands drastically increased during evolution: five potential ligands are found in *C. elegans*, seven in *D. melanogaster* and thirty in humans. The ligands number expansion does not correlate with an increase in receptors number: two type-I and one type-II receptors are found in *C. elegans*, three type-I and two type-II receptors in *D. melanogaster*, and seven type-I and five type-II receptors in humans (Mueller & Nickel, 2012; Sebald, Nickel, Zhang, & Mueller, 2004). This observation implies the existence of promiscuity in ligand-receptor recognition. Alternatively, splicing variants of the same receptor could code for proteins with different extracellular domains, recognizing different ligands (Jensen, Zheng, Lee, & O'Connor, 2009).

1.3.2 TGF-β signalling in *D. melanogaster*

The TGF-β superfamily in *D. melanogaster* is represented by seven ligands, of which four belong to the TGF-β/Activin family and three to the BMP family. *Drosophila* Activin (dAct, also called Actβ), Dawdle (Daw), Myoglianin (Myo) and Maverick (Mav) belong to the TGF-β/Activin branch, whereas Dpp, Gbb and Scw belong to the BMP branch (Figure 1.7, Figure 1.9). This classification was initially based on the number of conserved cysteine in the C-terminal portion of the ligand: seven for BMPs and nine for TGF-β/Activin. However Mav is the most divergent of the TGF-β/Activin homologues and it cannot be easily classified based on sequence conservation (Figure 1.7) (Schmierer & Hill, 2007).

1.3.2.1 The SMAD family in D. melanogaster

Two R-SMADs have been found in *D. melanogaster*: Mothers against Dpp (Mad) is required for pathway transduction of the BMP branch and Smad2 (also known as SmoX, Smad on the X) for the TGF-β/Activin branch (Figure 1.8).

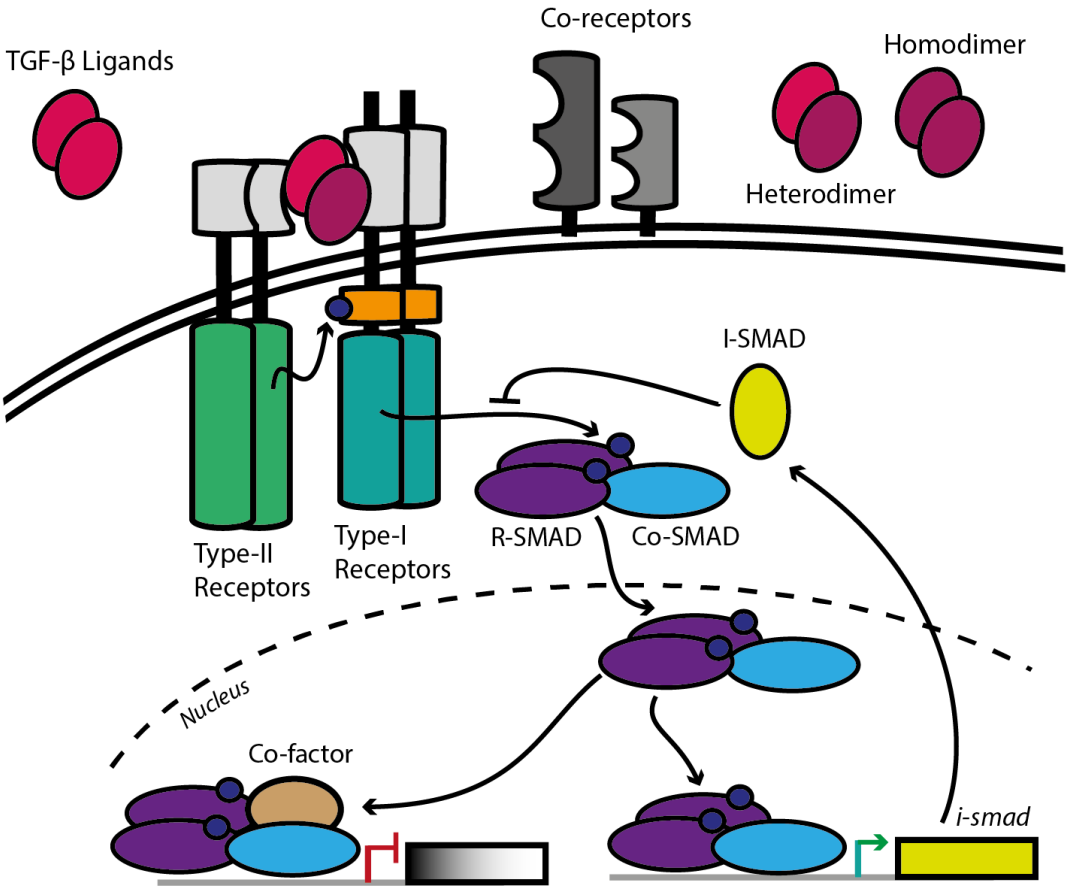

	BMP branch	TGF-β branch
Ligands	Dpp, Gbb, Scw	dAct, Daw, Myo, Mav
Receptors Type-I	Tkv, Sax	Babo
Receptors Type-II	Punt, Wit	Punt, Wit
Co-receptors	Dally, Dlp	?
R-SMADs	Mad	Smad2
Co-SMAD	Medea	Medea
I-SMAD	Dad	?

Figure 1.9 The TGF-β superfamily components in *D. melanogaster*. (Top) Schematic representation of the core components of the pathway and their signalling implications. The components and the mechanism are well conserved from *C.elegans* to humans. (**Bottom**) The relevant members of the TGF-β superfamily of *D. melanogaster* are classified based on their function and association with the BMP or TGF-β/Activin branch.

Mad was shown to be phosphorylated by the type-I receptors and to associate with the only Co-SMAD Medea (Med). Upon phosphorylation, a Mad-Med trimeric complex translocates into the nucleus and regulates Dpp target genes (J J Sekelsky, 1995; Raftery, Twombly, Wharton, & Gelbart,

1995). Dpp signalling activity is conventionally visualized using an antibody that specifically recognizes the phosphorylated form of Mad (α-P-Mad) (Figure 1.10, right panel).

Mad is also associated with signal transduction of two other BMP ligands, Scw and Gbb, mostly when these ligands act together with Dpp in heterodimers (Ferguson & Anderson, 1992; Wharton, Ray, & Gelbart, 1993) (Bangi & Wharton, 2006a; 2006b).

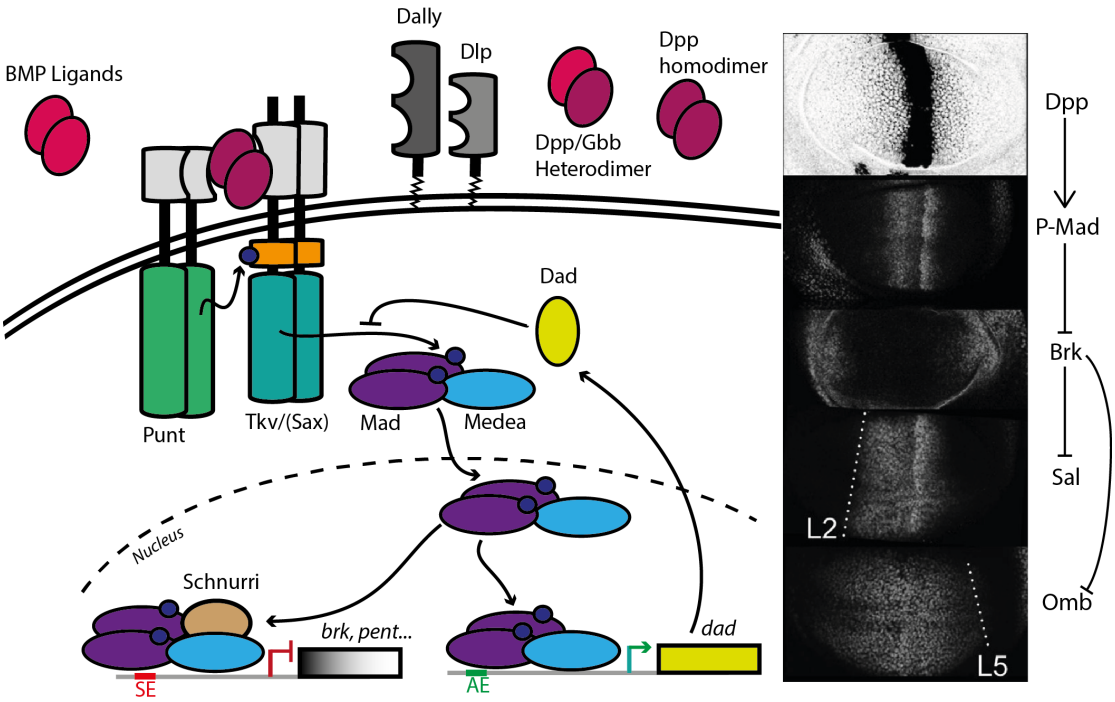

Figure 1.10 The Dpp/BMP pathway in the wing imaginal disc. (Left) Schematic representation of the Dpp signalling pathway in the wing disc. Dpp functions in homodimers (dark pink), using the type-I receptor Tkv (green), or in heterodimers together with Gbb (pink-dark pink), which also require the type-I receptor Sax. However, the specific function of each dimer combination is unclear. Punt (green) is the receptor type-II associated with the Dpp pathway. A trimolecular complex consisting of two Mad molecules and one Medea, acts in the nucleus to regulate the transcription of Dpp target genes. This complex acts together with Schnurri (brown) to repress the gene *brk* by binding to the Silencer Element (SE, red). The Mad/Medea complex also activates the expression of *dad* (yellow) by binding the Activating Element (AE, green). Dad is the I-SMAD required for signal modulation. **(Right)** The Dpp signalling cascade. Patterning of the wing disc depends on the proper spatial regulation of Dpp target genes. The anterior expression border of *sal* will specify position of longitudinal vein 2 (L2) in the adult wing. The posterior expression border of *omb* will define the position of L5 in the adult wing. The right panel was modified from **(Matsuda, Harmansa, & Affolter, 2015)**.

Also the TGF-β/Activin branch can activate Mad, through its type-I receptor Baboon (Babo) as shown in *in vitro* cell culture studies (Gesualdi & Haerry, 2007; Peterson et al., 2012). *In vivo* Babo can phosphorylate Mad only in absence of its specific substrate, the R-SMAD Smad2 (Hevia & De Celis, 2013; Peterson et al., 2012).

In the wing disc, P-Mad levels are highest near the Dpp source and graded towards the lateral pouch region. Interestingly, the levels of P-Mad are low in the Dpp source cells (see chapter 1.3.3.1, Figure 1.10, right panel).

The effects of the P-Mad signalling gradient on transcriptional regulation have been characterized in detail in the context of wing development.

Activated Mad, together with Medea, moves to the nucleus where it regulates transcription. The most important action of activated Mad is the downregulation of *brinker* (*brk*) (Marty, Müller, Basler, & Affolter, 2000; Torres-Vazquez, Warrior, & Arora, 2000). Brk acts as a general transcriptional repressor of Dpp target genes and as a suppressor of growth (G. Campbell & Tomlinson, 1999; Jaźwińska, Kirov, Wieschaus, Roth, & Rushlow, 1999; Minami, Kinoshita, Kamoshida, Tanimoto, & Tabata, 1999). The downregulation of *brk* is mediated by a molecular complex, consisting of Mad, Medea and the nuclear co-repressor Schnurri (Arora, Dai, Kazuko, Jamal, & O'Connor, 1995; Grieder, Nellen, Burke, Basler, & Affolter, 1995; Marty et al., 2000; Staehling-Hampton, Laughon, & Hoffmann, 1995; Torres-Vazquez et al., 2000). This complex acts on specific silencer-elements (SEs), located in the *brk cis*-regulatory region: two molecules of P-Mad and one Medea bind to specific DNA motifs in the SE and recruit Schnurri, in order to mediate repression (Gao, Steffen, & Laughon, 2005; Müller, Hartmann, Pyrowolakis, Affolter, & Basler, 2003; Pyrowolakis, Hartmann, Müller, Basler, & Affolter, 2004). SEs have been found in other genes regulated by Dpp signal, of which an eminent example is *pentagone (pent)*, a factor involved in

modulating Dpp signalling and the Dpp spreading range in the wing disc (Hamaratoglu, de Lachapelle, Pyrowolakis, Bergmann, & Affolter, 2011; Vuilleumier et al., 2010). Mad and Medea, without Schnurri, can also activate target genes by binding to a so-called activating-element (AE), as it is the case for the *daughters against dpp* (*dad)* cis-regulatory region (Weiss et al., 2010) (Figure 1.10).

The integration of P-Mad input and the inverse Brk input gives a functional read-out of the Dpp morphogen gradient and defines the activation threshold of the Dpp target genes. This is visualized by the nested expression of Dpp target genes, such as spalt (*sal*) (Barrio & De Celis, 2004), optomotor blind (*omb*) and *dad* (Sivasankaran, Vigano, Müller, Affolter, & Basler, 2000) (reviewed in Affolter & Basler, 2007).

The Dpp target genes are directly implicated in wing patterning events, by positioning the wing longitudinal vein 2 (L2) and 5 (L5): L2 is induced in the anterior compartment of the wing disc at the border of *sal* expression, L5 is induced in the posterior compartment at border between *omb* and *brk* expression (reviewed in (Affolter & Basler, 2007; Blair, 2007; De Celis & Diaz-Benjumea, 2003; Matsuda et al., 2015) (Figure 1.10, right panel).

As mentioned above, Smad2 is the main R-SMAD for the TGF-β/Activin branch (Brummel et al., 1998). Smad2 phosphorylation was visualized *in vitro* thanks to an anti-Phospho-Smad2 (P-Smad2) antibody (Brummel et al., 1998; Gesualdi & Haerry, 2007). When the same antibody was used *in vivo*, P-Smad2 was detected uniformly in all wing disc cells (Hevia & De Celis, 2013). More recently, a Smad2-GFP-FLAG genomic rescue was used to visualize signalling activation, by measuring Smad2-GFP-FLAG nuclear translocation (Ayyaz, Li, & Jasper, 2015).

The type-I receptor Babo is the only type-I shown to phosphorylate Smad2 *in vitro* and to induce the formation of Smad2-Medea complexes (Brummel et

al., 1998; Gesualdi & Haerry, 2007). However, the phenotypes of *babo* or *smad2* mutant wing discs are different. While *babo* mutant wing discs shows a moderate size reduction, *smad2* mutants show overgrowth of the lateral areas of the disc (Brummel et al., 1994; Hevia & De Celis, 2013; Peterson & O'Connor, 2013; Sander, Eivers, Choi, & De Robertis, 2010). Moreover patterning defects are associated with loss of Smad2, but not with *babo* mutants. These results might be explained by ectopic BMP signalling activation in *smad2* mutants (see chapter 1.3.3.3).

Also the type-I receptor Saxophone (Sax), commonly associated with the BMP branch, can mediate Smad2 phosphorylation in testis and intestinal stem cells (Ayyaz et al., 2015; C.-Y. Li, Guo, & Wang, 2007).

Only one I-SMAD, Dad, was found in *D. melanogaster* (Tsuneizumi et al., 1997). As mentioned above, *dad* is induced by Dpp signalling and negatively regulates Dpp activity, acting as feedback inhibitor. Buffering of receptor levels and ectopic signalling activity depend on Dad: in the absence of Dad, increase of Tkv levels cause increase of P-Mad levels (Ogiso, Tsuneizumi, Masuda, Sato, & Tabata, 2011). Interestingly, Dad has been shown to interact with and inhibit Tkv and Sax, but not Babo (Kamiya, Miyazono, & Miyazawa, 2008). This suggests that Dad regulates BMP signalling, but not TGF-β/Activin signalling.

1.3.2.2 The role of TGF-β/Activin ligands in fly development

The TGF-β/Activin branch of *D. melanogaster* has been mainly characterized for its implications during neural development.

In particular, dAct and Daw have redundant roles in regulating larval brain proliferation (Zhu et al., 2008), whereas they act independently in the regulation of motor neuron axon guidance (Parker, Ellis, Nguyen, & Arora, 2006; Serpe & O'Connor, 2006). dAct regulates neuromuscular junction

(NMJ) synapse development (M.-J. Kim & O'Connor, 2014). Recently, Daw was found to act as a systemic signal that regulates sugar homeostasis (Ghosh & O'Connor, 2014). Daw transcription was found to be regulated by insulin/IGF1 signalling, being a target of the forkhead transcription factor dFOXO (Bai, Kang, Hernandez, & Tatar, 2013).

The role of the ligands Mav and Myo is less well characterized. Myo was identified as homologue of the vertebrate muscle differentiating factor Myostatin (Lo & Frasch, 1999). Myo is expressed in muscle and glia cells and its interaction with Babo and the type-II receptor Wit activates the TGF-β/Activin signalling pathway (Lee-Hoeflich, Zhao, Mehra, & Attisano, 2005).

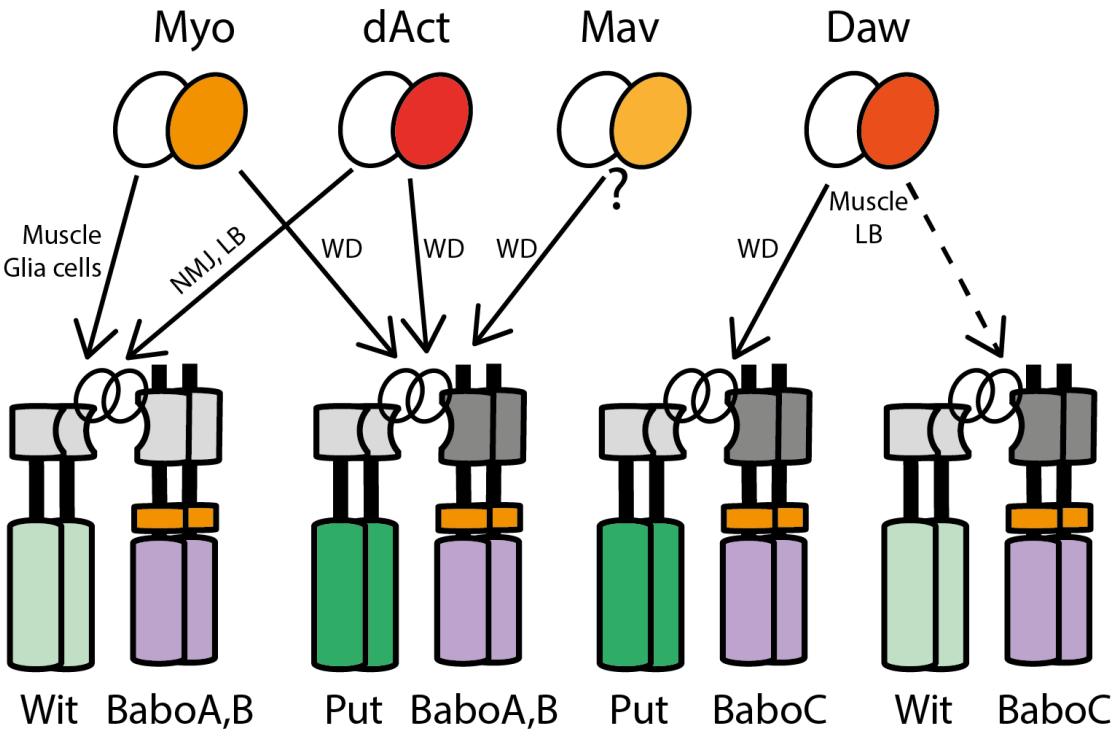

Figure 1.11 TGF-β ligands interaction with receptor complexes in different target tissues. TGF-β ligands share the type-I receptor Babo and the two type-II receptors Punt and Wit. However Babo is expressed in three splicing isoforms (BaboA, B, C), of which BaboC is specific for Daw. BaboC was shown to require the type-II receptor Punt in order to mediate Smad2 phosphorylation in cell culture. However BaboC could function together with either type-II receptor *in vivo*, in larval brain and muscle tissue. The type-II receptors are represented as homodimers, but they could potentially act as heterodimers in tissues where they are coexpressed. NMJ: neuromuscular junction. LB: larval brain. WD: wing disc.

Glial-secreted Myo makes neurons responsive to ecdysone-driven remodelling by up-regulating the ecdysone nuclear receptor in larval neurons (Awasaki, Huang, O'Connor, & Lee, 2011).

Very little is known about Mav. Mav was identified as third among members of the TGF-β/Activin subfamily (M. Nguyen, Parker, & Arora, 2000) and is expressed dynamically in the developing embryo and at late stage during egg chamber development (M. Nguyen et al., 2000).

Recently, the function of all four TGF-β/Activin ligands in regulating wing growth and patterning has been investigated.

Loss of function of the only TGF-β/Activin type-I receptor, Babo and its R-SMAD Smad2, results in reduced wing size without clear patterning defects (Brummel et al., 1998; Hevia & De Celis, 2013). However patterning defects linked to Smad2 loss of function have been reported in another publication (Sander et al., 2010). It was reported that only dAct, among the ligands, could recapitulate the wing over-growth phenotype observed by expressing constitutively active Babo (Gesualdi & Haerry, 2007). However dAct expression was not detected in the wing disc, suggesting paracrine or systemic delivery (Gesualdi & Haerry, 2007).

Later, it was reported that the four Act ligands are all expressed in the wing imaginal disc, in a uniform pattern (Hevia & De Celis, 2013). The pattern of expression is more specific or restricted in other imaginal discs and in larval brain. Knockdown of each ligand resulted in minor wing size reduction without causing patterning defects. The authors conclude that all four TGF-β/Activin contribute to Smad2 activation and Babo function in the wing disc (Hevia & De Celis, 2013).

1.3.2.1 *The role of BMP ligands in fly development*

The BMP branch was thoroughly characterized in different contexts of *D. melanogaster* development. Dpp is the homologue of vertebrate BMP2/4, Gbb and Scw are both homologue of BMP5/6/7/8, however Scw is more distantly related.

The ligand Scw is required for embryonic development, where it acts synergistically with Dpp to pattern the dorsal-ventral axis (Arora, Levine, & O'Connor, 1994). Embryos mutant for *dpp* or *scw* are ventralized, lacking most of the dorsal structures.

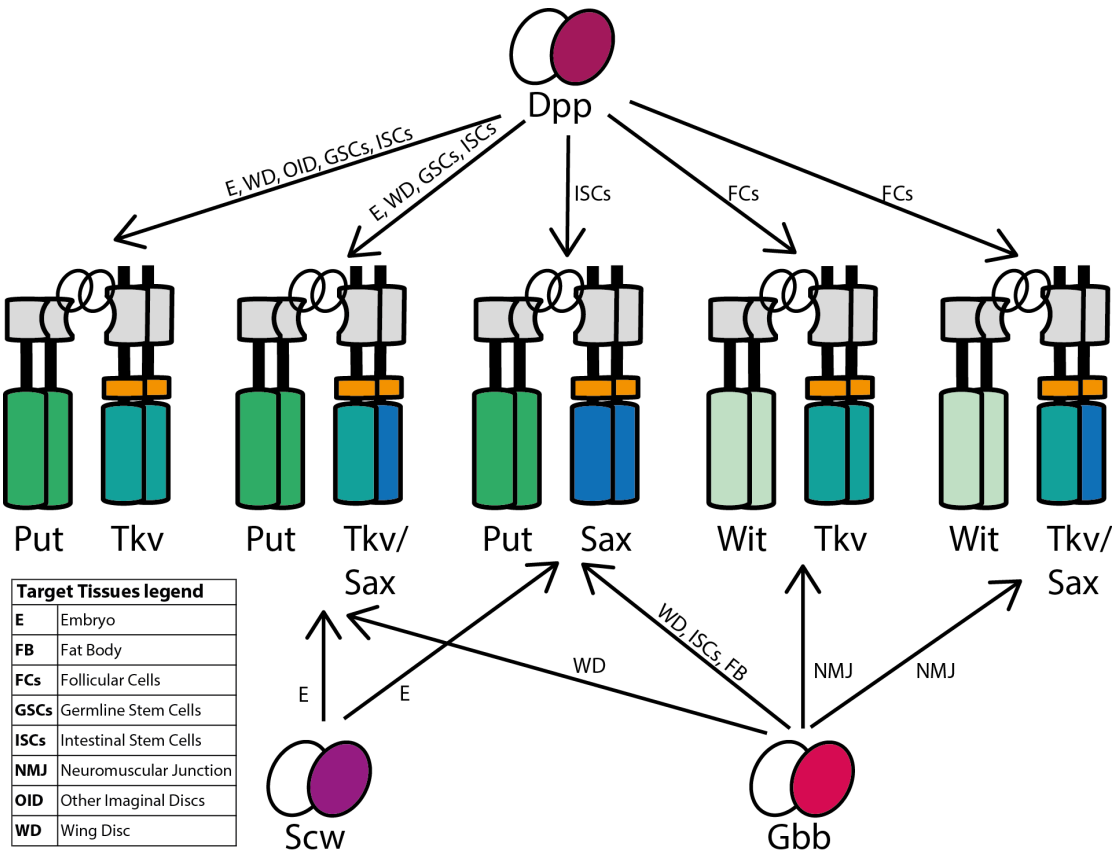

Figure 1.12 BMP ligands interaction with receptor complexes in different target tissues. BMP ligands share a common set of receptors, which are preferentially activated in different tissues. The main type-I receptor for Dpp is Tkv, whereas Gbb and Scw signal through Sax. The type-II receptors are represented as homodimers, but they could potentially act as heterodimers in tissues where they are coexpressed (e.g. FCs).

The phenotype is most dramatic in *dpp* mutants, where all dorsal cells become neurogenic ventral ectoderm (Sutherland, 2003). TGF-β ligands can act as homodimers or heterodimers, and it was shown that Dpp/Scw heterodimers show the highest signalling activity (Shimmi, Umulis, Othmer, & O'Connor, 2005b). Dpp/Scw heterodimers act through the type-I receptors Tkv and Sax and the type-II receptor Punt (Put) (Shimmi et al., 2005b).

In the embryo, high BMP signalling activity specifies the dorsal-most tissue, the amnioserosa, whereas lower signalling levels specify the dorsal-lateral ectoderm. In particular, low levels of P-Mad are detected throughout the dorsal compartment at embryonic blastoderm stage; during cellularization, the P-Mad gradient sharpens with highest levels in the dorsal midline region (Ferguson & Anderson, 1992; Wharton et al., 1993).

Other extracellular molecules than the Dpp and Scw ligands are involved in the formation of the Dpp signalling gradient. In particular, Short gastrulation (Sog) (Francois, Solloway, O'Neill, Emery, & Bier, 1994) and Twisted gastrulation (Tsg) (Chang et al., 2001; Ross et al., 2001) are BMP inhibitors that hinder Dpp-receptor interaction and regulate Dpp spreading, actively enhancing its long-range action (Ashe, Ashe, Levine, & Levine, 1999; Levine & Ashe, 1999; Marqués, Musacchio, & Shimell, 1997; Shimmi et al., 2005b). Another extracellular factor, the metalloprotease Tolloid (Tld), is involved in the regulation of signalling gradient formation: Tld cleaves and inactivates Sog at the dorsal ectoderm, in a process promoted by Dpp (Marqués et al., 1997; Shimell, Ferguson, Childs, & O'Connor, 1991; Shimmi, 2003). A similar mechanism has been observed in the pupal wing, where Dpp is actively transported from the LVs toward the posterior cross vein (PCV) by Sog and the paralog of Tsg, Crossveinless (Matsuda & Shimmi, 2012; Shimmi, Ralston, Blair, & O'Connor, 2005a).

Among the TGF-β superfamily, Dpp is the most discussed and characterized. Mutations of the *dpp* gene have drastic consequences for development, affecting the morphogenesis of all fifteen larval imaginal discs (Spencer et al., 1982). Dpp was the first secreted molecule to embody the morphogen concept. Dpp spreads from a localized source, forming a concentration gradient that provides positional information to receiving cells in the target tissue, thereby controlling patterning events (Ferguson & Anderson, 1992; Lecuit et al., 1996; Nellen, Burke, Struhl, & Basler, 1996). The morphogen function of Dpp has been studied in the context of dorsal–ventral patterning in the early embryo and anterior–posterior patterning and growth of the wing imaginal disc.

In the wing imaginal disc, *dpp* is expressed in a stripe of anterior cells at the A/P compartment boundary, from where it spreads and establishes a gradient in the target tissue. As a result, the Dpp gradient has the highest intensity levels in the central source region and decays in a shallow fashion at both sides of the A/P compartment boundary (Entchev et al., 2000; Teleman & Cohen, 2000). The Dpp gradient was visualized thanks to two GFP-Dpp fusion proteins, expressed in the central stripe region (Entchev et al., 2000; Teleman & Cohen, 2000). GFP-Dpp fusions can at least partially rescue *dpp* mutant growth and patterning defects (Entchev et al., 2000; Harmansa, Hamaratoglu, Affolter, & Caussinus, 2015).

Four different mechanisms have been proposed for Dpp spreading: free extracellular diffusion (Lander, Nie, & Wan, 2002; S. S. Zhou et al., 2012), restricted extracellular diffusion (Akiyama et al., 2008; Belenkaya et al., 2004; Lecuit & Cohen, 1998; Muller, Rogers, Yu, Brand, & Schier, 2013; Schwank, Dalessi, et al., 2011a), receptor-mediated transcytosis (Entchev et al., 2000; González-Gaitán, 2003; González-Gaitán & Jäckle, 1999; Kruse, Pantazis, Bollenbach, Jülicher, & González-Gaitán, 2004) and cytoneme-based active

transport (Hsiung, Ramirez-Weber, Iwaki, & Kornberg, 2005; Ramirez-Weber & Kornberg, 1999; Roy, Hsiung, & Kornberg, 2011; Roy, Huang, Liu, & Kornberg, 2014). These mechanisms will be discussed in chapter 1.3.3.1, concerning their involvement of TGF-β receptors and co-receptors, and were recently reviewed in (Matsuda et al., 2015).

In the wing imaginal disc, the patterning function of the Dpp gradient is well established (see chapter 1.3.2.1), however its role in growth control and cell proliferation is still unclear and under debate. On the one hand, removal of Dpp from the wing imaginal disc, using mutations specific for the *dpp* wing disc enhancer, leads to severe reduction of adult wing size (Spencer et al., 1982; Zecca et al., 1995). On the other hand, Dpp overexpression and ectopic Dpp signalling lead to wing disc duplications and over-growth (Burke & Basler, 1996; Capdevila & Guerrero, 1994; Martín-Castellanos & Edgar, 2002). Further research set forth two main models explaining how the Dpp gradient acts to regulate growth: the growth-equalization model (GEM) and the temporal rule model (TRM). In the GEM, the Dpp gradient has only a permissive/indirect role on growth control, that is the removal of the growth-suppressor Brk from medial cells of the wing disc; lateral cells have a proliferation advantage and grow independently from Dpp (Restrepo, Zartman, & Basler, 2014; Schwank, Restrepo, & Basler, 2008; Schwank, Tauriello, et al., 2011b). According to the TRM, Dpp act as an instructive growth signal, as cells divide upon sensing 40% increase in Dpp signalling (Wartlick et al., 2011). These two models were examined in a recent publication (Harmansa et al., 2015). Using a novel nanobody-derived tool, Dpp morphogen spreading was blocked by tethering Dpp to the membrane of Dpp source cells. As a result, wing disc patterning was disrupted, whereas growth was affected only in the medial region of the disc, in support of the GEM (Harmansa et al., 2015). In another work, Dpp removal was induced in

different spatial and temporal patterns, using a Flippase-dependent conditional *dpp* null allele (Akiyama & Gibson, 2015). Removal of Dpp from wing disc source cells lead to disturbance of tissue patterning, but not to major growth defects.

In conclusion, these observations demonstrate that the Dpp gradient is essential for wing patterning, whereas its role on growth regulations is still poorly understood.

A second molecule contributes to the BMP signalling in the wing imaginal disc, the ligand Gbb. Interestingly, the Gbb expression pattern in the wing disc is complementary to the Dpp expression pattern. In contrast to Dpp distribution, the Gbb protein is more broadly distributed with higher expression levels in the lateral regions (Khalsa, Yoon, Torres-Schumann, & Wharton, 1998).

Gbb functions are partially redundant to Dpp, since *dpp* duplications can rescue some of patterning defects in the *gbb* mutants (Ray & Wharton, 2001). A loss of Gbb function strongly impacts the posterior compartment, resulting in a severe shrinking of the P-Mad gradient in this compartment (Bangi & Wharton, 2006a). This correlates with the loss of L5 specification in the wing disc for the strongest *gbb* mutant alleles (Bangi & Wharton, 2006a). This effect is also visible in adult wings, where Gbb reduction causes L4 and L5 truncations, loss of the PCV and decrease in the size of the L4–L5 intervein territory (Khalsa et al., 1998). Gbb is required for BMP signalling and Dpp transport into the PCV region of the pupal wing, presumably functioning as Dpp–Gbb heterodimer (Matsuda & Shimmi, 2012). Importantly, *gbb* mutant clones located in the anterior compartment can affect patterning (L5 specification) and growth on the posterior compartment, suggesting a long-range function of Gbb (Bangi & Wharton, 2006a; Ray & Wharton, 2001). In *gbb* null mutants the BMP signalling gradient severely shrinks and disc size is

reduced (Bangi & Wharton, 2006a). Taken together, these observations suggest that Dpp-Gbb heterodimers are required to specify L5 and that Gbb is required for some aspects of the long-range function of Dpp (Bangi & Wharton, 2006a).

In the nervous system, Gbb signalling has a great impact on synapse development. Gbb is produced both by post-synaptic muscle and pre-synaptic motor neuron participating to the NMJ and is required for retrograde signalling that regulates neurotransmitter release and synaptic growth (Allan, Pierre, Miguel-Aliaga, & Thor, 2003; Goold & Davis, 2007; Marqués, 2003; McCabe et al., 2003). It is interesting to observe that in the NMJ system, the two branches of TGF-β superfamily function on opposite sides, where dAct (TGF-β/Activin branch) controls post-synaptic membrane physiology and Gbb (BMP branch) controls pre-synaptic development (M.-J. Kim & O'Connor, 2014). During larval development, Gbb is also required to positively regulate nutrient storage and control of energy homeostasis (Ballard, Jarolimova, & Wharton, 2010).

1.3.3 TGF-β receptors and co-receptors in *D. melanogaster*

Five TGF-β family receptors are present in *D. melanogaster*: the type-I receptors Tkv, Sax and Babo and the type-II receptors Put and Wit.

Type-I receptors have a crucial role in both signalling and internalization of the ligand, while type-II receptor are constitutively active serine/threonine kinases able to phosphorylate the type-I receptors to initiate signalling.

The type-I receptors are specific for either TGF-β/Activin or BMP ligands, while type-II receptors are able to function for both ligand families (F. Huang & Chen, 2012; Schmierer & Hill, 2007).

In *D. melanogaster* the members of a specific family of heparan sulfate proteoglycans, the glypicans Dally and Dally-like protein (Dlp), are proposed

to act as co-receptors. The glypicans are thought to stimulate signalling by supporting ligand-receptor interactions or increase ligand concentration at the cell surface (Akiyama et al., 2008; Belenkaya et al., 2004; Fujise et al., 2003; Yan & Lin, 2009).

In the following section I provide a description of the different TGF-β receptors and co-receptors, particularly focusing on their implications on wing development.

1.3.3.1 The type-I receptor Thickveins

The type-I receptor Tkv (Nellen, Affolter, & Basler, 1994; Penton et al., 1994) is involved in the signalling transduction of all three BMP ligands Dpp, Gbb and Scw (Khalsa et al., 1998; Nellen et al., 1996; Neul & Ferguson, 1998; Singer, Penton, Twombly, Hoffmann, & Gelbart, 1997; Tanimoto, Itoh, Dijke, & Tabata, 2000). Tkv binds Dpp with high affinity, comparable to BMP2, and Gbb with lower affinity (Penton et al., 1994; Schwank, Dalessi, et al., 2011a).

Tkv influences the extracellular distribution of Dpp by promoting ligand removal from the pool of extracellular Dpp (Lecuit & Cohen, 1998; Tanimoto et al., 2000). High Tkv level sensitize cells to Dpp signalling and at the same time limit Dpp spreading (Crickmore & Mann, 2006; Lecuit & Cohen, 1998) (Figure 1.13). Tkv is necessary for BMP signalling in the wing imaginal disc, since eliminating Tkv leads to a lack of P-Mad, and is required for wing patterning and growth (Singer et al., 1997; Tanimoto et al., 2000) (Figure 1.13). Tkv is also required for the survival of medial wing disc cells, since medial clones mutant for *tkv* are smaller and they are extruded from the disc (Burke & Basler, 1996; Gibson, 2005; Nellen et al., 1996).

Many reports indicate that Tkv mediates Dpp internalization via endocytosis (Entchev et al., 2000; Teleman & Cohen, 2000) (Figure 1.13). Endocytosis could be required for Dpp signalling, since Dpp activity is cell-autonomously reduced in clones in which endocytosis is blocked using a mutant of the small

GTPase Dynamin (Belenkaya et al., 2004). Alternatively, endocytosis could be required for signal modulation, as was reported for the NMJ, where the protein Nervous wreck interacts with Tkv and components of the endocytosis machinery to negatively regulate Gbb signalling and synaptic growth (O'Connor-Giles, Ho, & Ganetzky, 2008). Receptor-mediated endocytosis is also reported to be essential for signalling modulation and termination of the vertebrate TGF-β and BMP ligands (reviewed in Ehrlich, 2015).

Repeated cycles of receptor-mediated Dpp-endocytosis followed by re-secretion towards the neighbour cell has been proposed as a possible transport mechanism for Dpp, termed receptor-mediated transcytosis (Entchev et al., 2000; González-Gaitán, 2003; Kicheva et al., 2007; Kruse et al., 2004). This mechanism was supported by the observation that GFP-Dpp cannot cross but accumulates at the surface of clones in which endocytosis was blocked (dynamin-mutant clones) (Entchev et al., 2000). This mechanism has been challenged by the evidence that Dpp can disperse over receptor mutant clones (Schwank, Dalessi, et al., 2011a). Moreover, Dpp accumulation at the surface of dynamin-mutant clones has been explained by the fact that these cells have enriched Tkv levels, and therefore exhibit enhanced ligand trapping (Belenkaya et al., 2004; Lander et al., 2002).

Another mechanism proposed for Dpp gradient formation is restricted extracellular diffusion, for which the ligand dispersal is hindered by is receptors and extracellular matrix molecules at cell surface (Akiyama et al., 2008; Belenkaya et al., 2004; Lecuit & Cohen, 1998). For this mechanism regulation of receptor levels is required to control the range of Dpp spreading (Crickmore & Mann, 2006; Lecuit et al., 1996; Lecuit & Cohen, 1998; Ogiso et al., 2011). Indeed, this has been proposed to explain the size regulation of haltere versus the wing disc tissue: in the haltere, the hox gene *ultrabithorax* (*ubx*) restricts Dpp diffusion, and thus organ size, by increasing

tkv expression (Crickmore & Mann, 2006). A similar mechanism has been described for ovarian stromal cells, where *tkv* is up-regulated by Wnt ligands produced by the stem cell niche (Luo, Wang, Fan, Liu, & Cai, 2015).

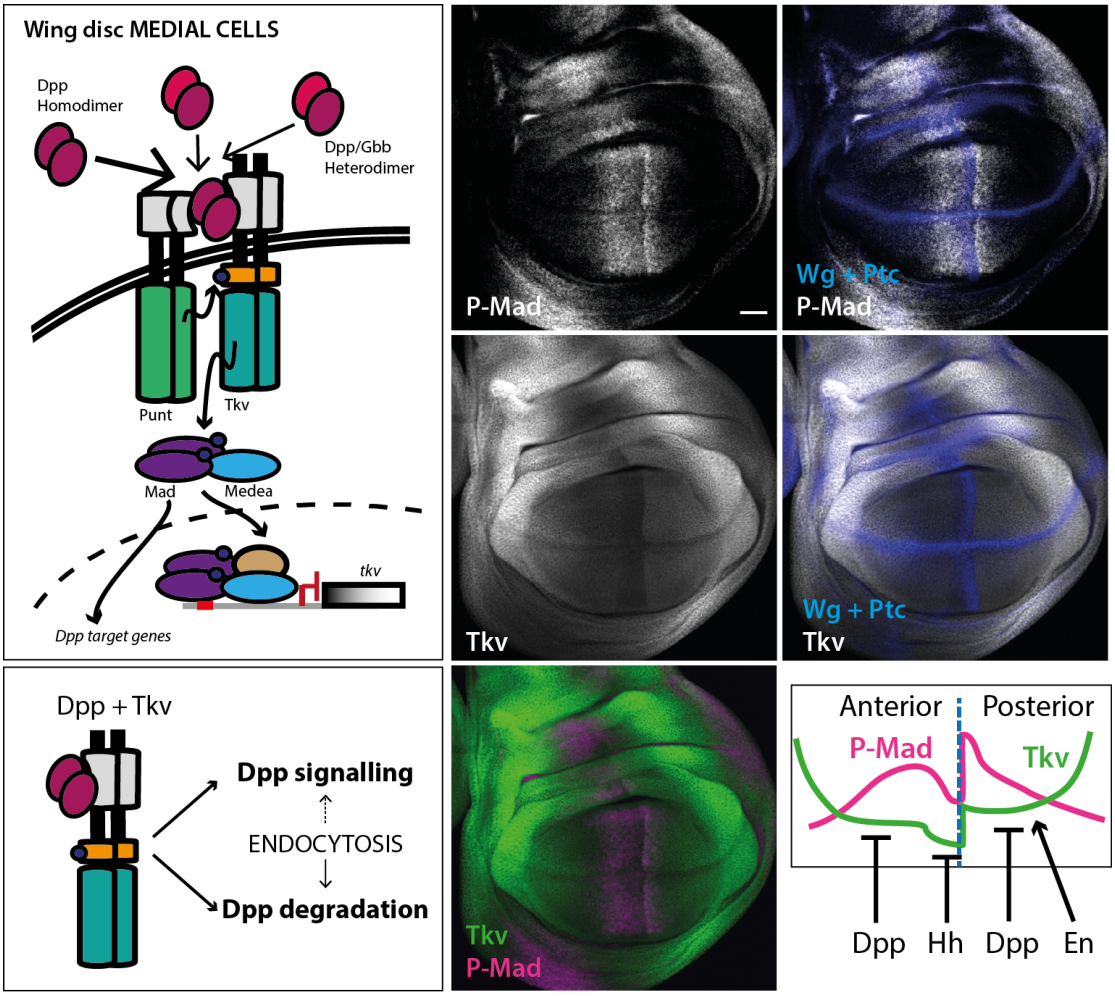

Figure 1.13 Tkv transcriptional regulation and impact on Dpp signalling. (Top left) In the medial cells of the wing imaginal disc Tkv is repressed by Dpp signalling. **(Bottom left)** The formation of Dpp-Tkv complexes has a double effect on Dpp. On one hand, Tkv mediates and sensitizes cells to Dpp signalling. On the other hand, Tkv captures and sequester extracellular Dpp, targeting it for subsequent degradation. **(Right panel)** Dpp signalling in the wing disc is visualized by P-Mad antibody staining. The signalling gradient of P-Mad strongly correlates with and depends on the *tkv* expression pattern. Tkv expression is regulated by Dpp, Hh and En. Dpp and Hh repress *tkv* in medial cells. Hh is responsible for the hyper-repression in the Dpp stripe. The basal levels of Tkv are higher in the posterior compartment due to the action of En. Wingless (Wg) and Patched (Ptc) antibody stainings are used to label the pouch (Wg) and the compartment boundaries (Wg – D/V, Ptc – A/P).

The expression of *tkv* in the wing disc is regulated by Hh, En and Dpp signalling (Funakoshi, Minami, & Tabata, 2001; Lecuit & Cohen, 1998; Tanimoto et al., 2000) (Figure 1.13). Dpp represses *tkv* transcription, since clones ectopically expressing Dpp in the lateral region of the wing disc show drastic reduction of *tkv* expression (Lecuit & Cohen, 1998). In Dpp source cells, Hh induces *dpp* expression, but diminishes Dpp signalling by repressing *tkv* transcription through the nuclear protein Master of Thickveins (Mtv) (Funakoshi et al., 2001; Tanimoto et al., 2000).

En contributes to the regulation of *tkv* transcription, by repressing *mtv* in the posterior compartment: this leads to asymmetric *tkv* expression, such that basal Tkv levels are higher in posterior medial cells compared to anterior medial cells (Funakoshi et al., 2001). As a result, high levels of *tkv* are present in the lateral regions of the disc and low basal levels in medial cells; the basal levels are higher in the posterior compartment (Figure 1.13). The expression pattern of *tkv* directly impacts the P-Mad signalling pattern. P-Mad levels are low in Dpp source cells, but high in cells immediately adjacent to it, creating one anterior and one posterior signalling peak that fade gradually towards the lateral region.

The posterior P-Mad gradient has a higher peak intensity compared to the anterior one, but short length scale, due to higher *tkv* expression in the posterior compartment (Figure 1.13).

The subcellular distribution of Tkv has not been characterized, however Tkv has been visualized in some apical protrusions of cell bodies in the wing imaginal disc and in testis (Demontis & Dahmann, 2007; Hsiung et al., 2005; Inaba, Buszczak, & Yamashita, 2015). These protrusions, named cytonemes (actin-based) or nanotubes (microtubule-based), are though to mediate cell-cell communication and in particular Dpp signalling. Cytonemes orient from cells in the target tissue toward Dpp source cells and carry moving *puncta* of

Tkv-GFP (Hsiung et al., 2005) and their shape and distribution depends on *dpp* expression (Roy et al., 2011). Basal cytonemes protruding from the air sac primordium contact Dpp producing cells in the wing disc, and they carry Dpp ligand together with activated Tkv receptor back to the recipient cells bodies (Roy et al., 2014).

BMP signalling activity has been traced with subcellular resolution in testis cells, where activated Tkv is found at AJ between hub and germline stem cells (Michel, Raabe, Kupinski, Pérez-Palencia, & Bökel, 2011).

This allows local activation and restriction of BMP signalling at the niche. The activation of Tkv was monitored using a fluorescent-based reporter that emits a fluorescent signal relative to the displacement of FKBP12, therefore sensing Tkv activation (Michel et al., 2011).

Finally, Tkv has been reported to accumulate in *puncta* in different contexts (Demontis & Dahmann, 2007; Hsiung et al., 2005; Inaba et al., 2015; O'Connor-Giles et al., 2008; Roy et al., 2014; Teleman & Cohen, 2000).

Different reasons have been proposed to explain this local accumulation, as for example big complexes of endocytosed receptor and ligand (O'Connor-Giles et al., 2008; Teleman & Cohen, 2000), moving receptor-ligand complexes (Hsiung et al., 2005; Inaba et al., 2015; Roy et al., 2014) or transversal section of cytoplasmic protrusions (Demontis & Dahmann, 2007).

1.3.3.2 The type-I receptor Saxophone

Sax is a type-I receptor associated with the BMP pathway (Brummel et al., 1994). Loss of function of *sax* causes embryonic lethality, however ubiquitous expression of a *tkv* transgene can rescue *sax* mutants (Brummel et al., 1994). This suggests that Tkv and Sax have partially overlapping roles during development.

In contrast to the restricted expression pattern of *tkv*, *sax* is reported to be expressed ubiquitously in all tissues and in all developmental stages (Brummel et al., 1994). Sax has different affinities for the three BMP ligands. Sax cannot bind Dpp and is proposed to have high affinity for Scw and Gbb ligands (Haerry, 2010). During embryonic development, Sax can function in homodimers or heterodimers with Tkv, recognizing Scw homodimers or Dpp-Scw heterodimers, respectively (Neul & Ferguson, 1998; M. Nguyen, Park, Marqués, & Arora, 1998; Shimmi et al., 2005b).

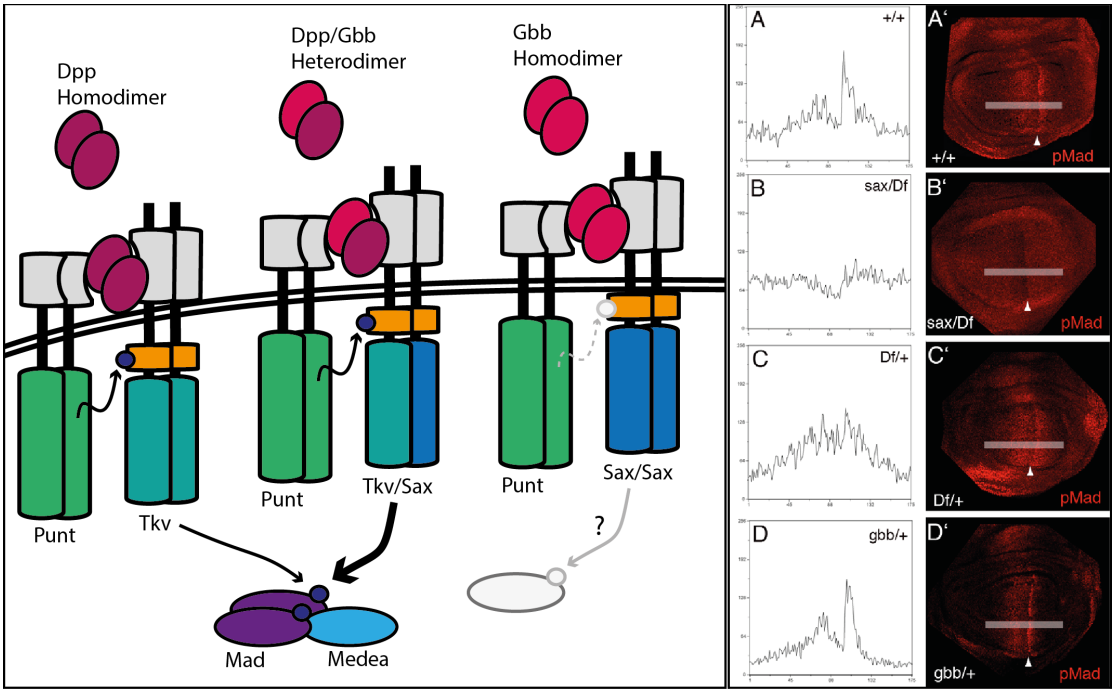

Figure 1.14 The role of Sax in BMP signalling transduction in the wing disc. (Left) Tkv has a higher affinity for Dpp (dark pink), than for Gbb (light pink). Sax (dark blue) cannot bind Dpp, but can bind Gbb. Sax has a dual function in mediating BMP signalling in the wing disc. When coupled in heteromeric receptor complexes with Tkv (petrol blue), it mediates phosphorylation of Mad. Mad is also phosphorylate by Tkv homodimers, however Tkv-Sax contributes stronger to the signalling (thicker arrow). Sax homodimers fail to phosphorylate Mad, potentially acting on another molecule or being signalling ineffective. **(Right)** P-Mad profiles in wt (A, A'), *sax*^{4}/Df(2R)H23 (B, B'), Df(2R)H23/+ (C,C'), *gbb*^{1}/+ (D,D') wing discs. Complete loss of Sax caused expansion of P-Mad gradient (B, B'), seen to a lesser extent also in discs with only one functional copy of *sax* (C, C'). Conversely, *gbb* heterozygous mutants show shrinking of P-Mad gradient. Right panel from **(Bangi & Wharton, 2006b)**.

Similarly, in the wing imaginal disc Sax is thought to recognise Gbb homodimers or Dpp-Gbb heterodimers when acting in homodimers or heterodimers with Tkv, respectively (Bangi & Wharton, 2006b; Haerry, 2010; Haerry, Khalsa, O'Connor, & Wharton, 1998). However, effective signalling output (P-Mad phosphorylation) comes only from Sax-Tkv heterodimers and not from Sax-Sax homodimers (Haerry, 2010). This observation has very important consequences on the function of Sax as a mediator of BMP signalling. Specifically, in the wing disc Sax can both promote and antagonise BMP signalling.

On one hand, Sax mediates Gbb signalling, since a dominant-negative version of Sax suppresses the overexpression phenotype of Gbb (Haerry et al., 1998; Singer et al., 1997). Moreover, complete loss of Sax enhances the wing phenotype of a weak *gbb* mutant allele (Bangi & Wharton, 2006b). In the wing disc, *sax* mutant clones show a cell-autonomous reduction of P-Mad. Strangely, the cells adjacent to the *sax* mutant clones show increased P-Mad levels.

On the other hand, Sax can negatively regulate Gbb signalling. For example, *sax* overexpression suppresses the wing phenotype caused by overexpression of *gbb*. In contrast, *tkv* overexpression enhanced the wing phenotype caused by increase of both Gbb and Dpp (Bangi & Wharton, 2006b). Moreover, loss of *sax* in the wing disc does not recapitulate the loss of *gbb* phenotype. Wing discs completely lacking Sax show a dramatic reduction of P-Mad intensity accompanied by broadening of the gradient. However, loss of *gbb* causes the opposite phenotype, by narrowing the P-Mad gradient (Figure 1.14, right panel).

This suggests that Sax both supports and antagonizes BMP signalling, when acting in heterodimers with Tkv or alone in homodimers, respectively (Figure 1.14).

1.3.3.3 *The type-I receptor Baboon*

Babo is the type-I receptor specific for the TGF-β/Activin pathway. Babo is not necessary for embryogenesis, however *babo* mutants die during late larval or early pupal stages, suggesting an essential role of Babo during this developmental phase (Brummel et al., 1998). Loss of *babo* causes a general reduction in size of the imaginal discs, and a severe size reduction of the larval brain lobes (Brummel et al., 1998). The only tissue that is enlarged in *babo* mutants are the larval anal pads, from which the gene name is derived (Brummel et al., 1998). Importantly, no effect on patterning is observed in *babo* mutant wings and *babo* does not perturb the expression of BMP target genes (Brummel et al., 1998).

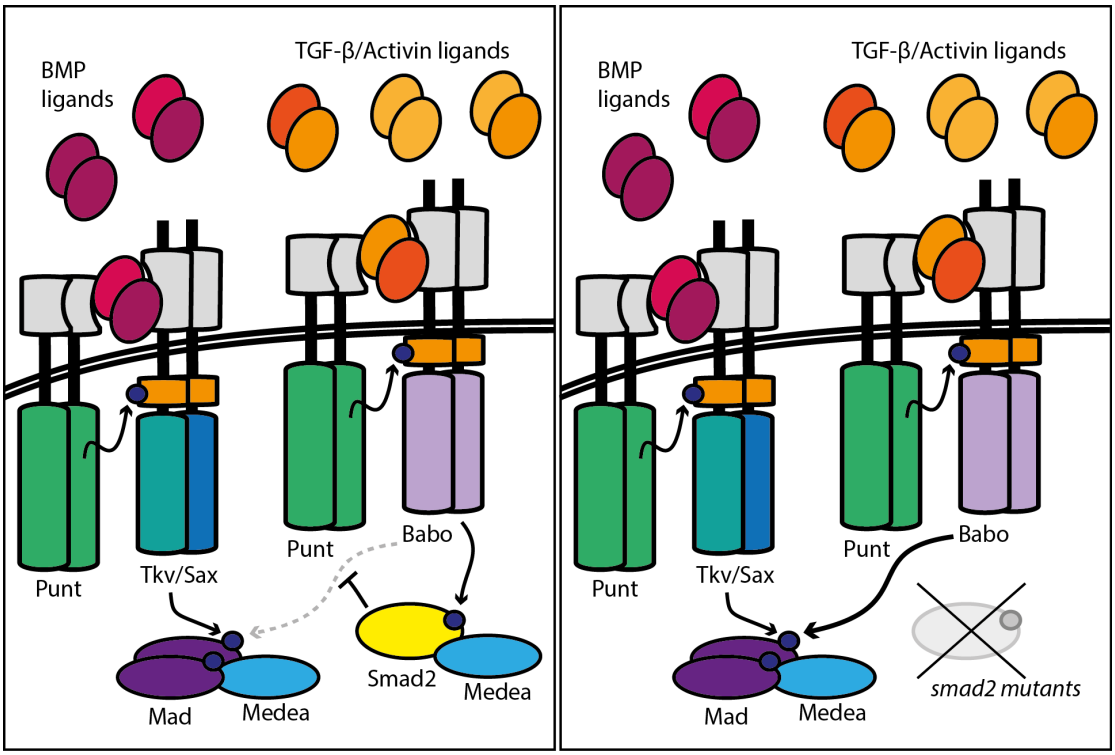

Figure 1.15 Signal transduction of the type-I receptor Babo. (Left panel) In wild-type wing disc cells, Babo (purple) transduces TGF-β/Activin signalling by phosphorylating the R-SMAD Smad2 (yellow). Smad2 prevents Babo from ectopically activating Mad. **(Right panel)** In *smad2* mutants, Babo ectopically activates Mad. This possibly leads to repression of the Dpp target gene *brk* in the lateral areas of the wing disc.

In the brain lobes a severe reduction in proliferation, but not cell death, appear to be the main reason for size reduction (Brummel et al., 1998; Zhu et al., 2008). However, the cause for size reduction in *babo* mutant imaginal discs seems to be more complex. The *babo* loss of function causes cell size increase, but cell number decrease in wing imaginal discs and adult wings (Hevia & De Celis, 2013).

Babo acts through the R-SMAD Smad2 and is able to induce Smad2 phosphorylation in cell culture in a process that requires Punt and Medea (Brummel et al., 1998; Gesualdi & Haerry, 2007; Zheng et al., 2006; Zhu et al., 2008) (Figure 1.15). However, in the wing imaginal disc, the phenotypes caused by *babo* or *smad2* loss are different: *babo* mutant wing discs shows a moderate size reduction, whereas *smad2* mutants show overgrowth of the lateral areas of the disc (Brummel et al., 1994; Hevia & De Celis, 2013; Peterson & O'Connor, 2013; Sander et al., 2010). These results were interpreted in the light of antagonistic connection between the TGF-β/Activin and the BMP pathway (Figure 1.15). The three TGF-β type-I receptors compete for the available type-II receptors and for the co-SMAD Medea. An additional level of competition occurs at the level of the substrate R-SMAD.

R-SMADs should be specific for the type-I receptor, with Tkv and Sax phosphorylating only Mad and Babo only Smad2. Loss of *babo* does not alter P-Mad (Hevia & De Celis, 2013), however constitutively active Babo can activate Mad in cell culture (Gesualdi & Haerry, 2007; Peterson et al., 2012) and *in vivo* in absence of Smad2 (Hevia & De Celis, 2013; Peterson et al., 2012). The activation of Mad observed in *smad2* mutants is key to the difference between *smad2* and *babo* mutant phenotypes. Indeed patterning defects observed by perturbing Smad2 function depend on Mad (Peterson & O'Connor, 2013; Sander et al., 2010). The overgrowth of the lateral wing disc

region observed in *smad2* mutant discs, was associated to repression of the Dpp target gene *brk* caused by Mad ectopic activation.

Therefore, Smad2 under normal conditions is responsible to limit P-Mad signalling, by preventing ectopic Babo-Mad interaction (Hevia & De Celis, 2013; Peterson et al., 2012) (Figure 1.15). Importantly, buffering of receptor levels and ectopic activity depends on the inhibitory SMAD Dad: in the absence of Dad, increase in Tkv levels cause increase in P-Mad levels (Ogiso et al., 2011). Interestingly, Dad has been shown to interact and inhibit Tkv and Sax, but not Babo (Kamiya et al., 2008). Therefore Smad2 could have an important effect on the regulation of TGF-β/Activin signalling, hindering cross-interactions with the BMP branch.

Babo is the only type-I receptor found for the four proposed TGF-β/Activin ligands. However, *babo* encodes for three different splicing isoforms (*baboA*, *baboB*, *baboC*), characterized by differential extracellular domain. Indeed, this three different isoforms bind TGF-β/Activin ligands with different affinities: only *baboC* can mediate Daw signalling, whereas *baboA* and *baboB* are responsive to dAct (Jensen et al., 2009). The splicing isoform *baboA* has been associated with Myoglianin signalling in mushroom body neurons (Awasaki et al., 2011). Since these splicing isoforms are expressed in different tissues during larval development (Jensen et al., 2009), they could be the key for cell type-specificity of TGF-β/Activin signals.

1.3.3.4 The type-II receptors Punt and Wit

The type-I receptors share two type-II receptors Punt (put) (Letsou et al., 1995) and Wishful Thinking (Wit) (Aberle et al., 2002; Marqués et al., 2002).

The type-II receptor Punt was shown to be required for the function of all three type-I receptors (Burke & Basler, 1996; Das et al., 1999; Letsou et al., 1995; Nellen et al., 1996; Ruberte, Marty, Nellen, Affolter, & Basler, 1995).

Punt has been implicated mainly in Dpp signalling, based on the finding that the *punt* and *dpp* mutant phenotypes are extremely similar (Simin, Bates, Horner, & Letsou, 1998).

In contrast to its vertebrate orthologues (ACTRII and ACTRIIB), Punt does not bind to Dpp and does not influence ligand spreading (Haerry, 2010; Letsou et al., 1995; Penton et al., 1994; Schwank, Dalessi, et al., 2011a). Punt is required during early embryogenesis and in many different larval tissues, including the wing imaginal disc (Affolter & Basler, 2007; Ruberte et al., 1995). As a type-II receptor, Punt functions as a constitutively active kinase that just needs to be in close proximity of a type-I receptor to activate downstream signalling. Indeed, clones overexpressing *punt* cell-autonomously activate P-Mad in the wing discs (Nellen et al., 1996; Schwank, Dalessi, et al., 2011a).

Wit, a second type-II receptor has been found in *D. melanogaster* (Marquès et al. 2002, Aberle et al. 2002). Wit is important in neural development. Wit is expressed in the wing disc, in the wing pouch and also in a broad area along the anterior-posterior boundary of the presumptive notum. However, Wit function in the wing imaginal disc remains unclear. The *wit* mutants die during late pupal phase, just before emerging from their cocoon (pharate). The *wit* mutants grow wings without obvious patterning defects, as observed by dissecting *wit* mutant animals out of their pupal case and artificially inflating their wings (Marqués et al., 2002).

Punt and Wit function redundantly in some developmental contexts, as in the mushroom body neurons development (Zheng et al., 2003). In other cases, the two receptors are not interchangeable: *wit* mutant motor neurons cannot be rescued by ectopic *punt* expression (Marqués et al., 2002). Moreover, Punt but not Wit can mediate Daw signalling through *baboC* (Jensen et al., 2009). Wit is required for BMP signalling in follicle cells, where also Punt is

expressed and contributes to BMP signalling (Marmion, Jevtic, Springhorn, Pyrowolakis, & Yakoby, 2013). Dpp signals through Tkv and Wit to control eggshell patterning (Marmion et al., 2013).

Gbb requires Wit for its function in motor neurons and indeed in this system Wit functions together with the type-I receptors Tkv and Sax (Marqués, 2003; Marqués et al., 2002; McCabe et al., 2003). However, Wit was also shown to interact with Babo, mediating Myoglianin and its orthologue Myostatin signalling (Lee-Hoeflich et al., 2005).

Wit as well as its homologue BMPR-II are able to activate non-canonical signalling, by phosphorylating LIM1 kinase, required for synapse stability (B. A. Eaton & Davis, 2005; Lee-Hoeflich et al., 2004). Wit and BMP-RII are characterized by a long cytoplasmic tail that extends past the kinase domain and is not common to Punt or other type-II receptors. Mutations in this region do not interfere with canonical SMAD signalling, and they are associated with pulmonary arterial hypertension (Nishihara, Watabe, Imamura, & Miyazono, 2002).

1.3.3.5 The glypicans Dally and Dlp

The glypicans Dally and Dlp are general regulators of morphogen gradients, acting as co-receptors and influencing the spreading of Wg, Hh and BMP ligands (Bornemann, 2004; Han, 2004; Yan & Lin, 2009) (see chapter 1.4.2). Specifically, they are required for BMP ligands response and extracellular distribution. Dally and Dlp have different affinities for the two BMP ligands; while Dally can bind both Dpp and Gbb, Dlp can only bind Gbb (Dejima, Kanai, Akiyama, Levings, & Nakato, 2011). This observation, together with the differential specificities of the BMP ligands for the type-I receptors Sax and Tkv, could be the reason of the distinct function of Gbb and Dpp in the wing imaginal disc.

Dally and Dlp are required for Dpp transport in the wing disc, since Dpp cannot spread across *dally/dlp* mutant clones. Dally and Dlp are also required for BMP signalling, since *dally* or *dally/dlp* mutant clones show strong reduction in P-Mad levels, except for the first row of mutant cells adjacent to wild-type cells (Belenkaya et al., 2004; Fujise et al., 2003). This interesting observation suggests that glypicans can act *in trans*, by stabilizing Dpp and activating signalling in the neighbouring cells. Therefore, they might be required to support transport of ligands along the surface from cell to cell (Belenkaya et al., 2004). Overexpression of Dally sensitizes cells to Dpp signalling, suggesting that Dally functions as a co-receptor or is sufficient to increase the Dpp concentration at cell surface (Fujise et al., 2003). Support for the role as co-receptor comes for the vertebrate orthologues, where heparan-sulfate acts to promote ligand induced dimerization of BMP receptors (Kuo, Digman, & Lander, 2010).

Dally was proposed to promote Dpp stabilization at the cell surface, also by interfering with the degradation of the Tkv-Dpp receptor-ligand complexes (Akiyama et al., 2008). In particular Tkv and Dally appear to have antagonist functions in controlling Dpp spreading, trapping or facilitating Dpp transport, respectively. Overexpression of Dally in the posterior compartment of the wing disc broadens the P-Mad gradient, whereas the gradient is restricted to medial cells in *dally* mutants (Akiyama et al., 2008; Hufnagel, Teleman, Rouault, Cohen, & Shraiman, 2007). Together, this data suggest that Dally is required to promote BMP spreading from medial to lateral region of the disc.

The role of Dlp in BMP signalling is more controversial, since overexpression of Dlp in the posterior compartment of the wing disc results in a narrower P-Mad gradient (Hufnagel et al., 2007). One possibility is that Dlp acts indirectly on BMP signalling through modulation of Hh spreading (Yan & Lin, 2009).

The transcriptional regulation of the glypican genes requires inputs from different pathways. The expression of *dally* is regulated by the same molecular pathways that regulates *tkv*, including Dpp, Hh and En (Fujise et al., 2003). This is particularly important for the regulation of the Tkv/Dally ratio, which controls Dpp spreading (Crickmore & Mann, 2007). The expression of *dally* in the wing disc is also positively regulated by Notch and Wg (Fujise, Izumi, Selleck, & Nakato, 2001). As a result of these different transcriptional inputs, *dally* expression is high in the A/P and D/V boundaries and in the lateral regions of the wing pouch (observed with a *dally-lacZ* enhancer trap and *in situ* hybridization) (Crickmore & Mann, 2007; Fujise et al., 2001; 2003). The expression of *dlp* is up-regulated in the anterior compartment as a consequence of positive Hh input (Gallet et al., 2008) and down-regulated at the D/V boundary by Wg (Han, 2005). The expression of *dally* and *dlp* is also repressed by the Hippo pathway (Alberto Baena-Lopez, Rodriguez, & Baonza, 2008).

1.4 Polarized signalling

1.4.1 The consequences and functions of polarized signalling

Polarized signalling refers to the observation that pathway activation can happen at specific positions along the cell surface (e.g. only at one cell pole) due to the restricted subcellular localization of signalling pathway components (receptors and/or ligands).

In epithelia, the function of the asymmetric distribution of signalling components is not absolute, but strictly context-dependent. In particular, (1) restricted receptor localization is necessary to prevent spurious pathway activation: ectopic autocrine signalling can be avoided by secreting the ligand apically and localizing the receptors only basolaterally (Murphy et al., 2004; Sotillos, Díaz-Meco, Moscat, & Castelli-Gair Hombría, 2008).

Alternatively, (2) signalling molecules can be polarized because they need to interact and function together with the polarity determinants (C.-L. Chen et al., 2010; Saitoh et al., 2012). Finally, (3) the presence of specific sets of receptors at different sides of the plasma membrane can lead to differential signalling outputs in response to the same ligand (Wu, Klein, & Mlodzik, 2004).

The function of signalling polarization is well established in asymmetrically dividing cells. Here, the asymmetric localization of signalling molecules is the key process leading to the generation of daughter cells with distinct fates.

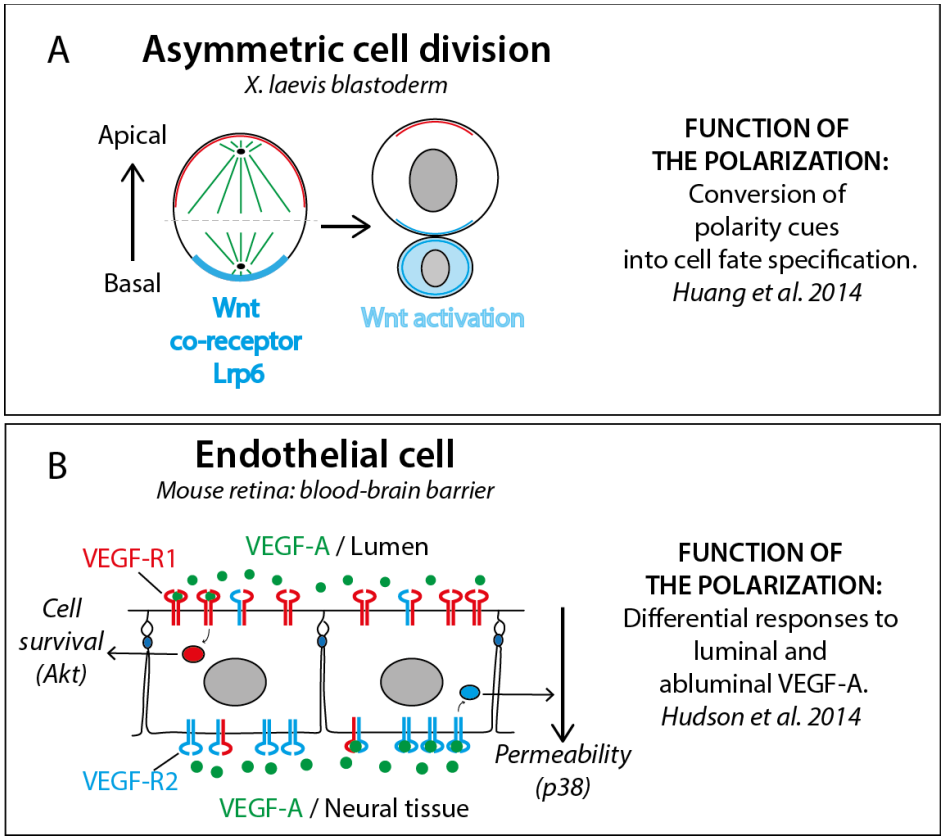

Figure 1.16 Examples of polarized signalling. A. *X. laevis* blastoderm cells divide asymmetrically to generate different daughter cells. The upregulation of Wnt signalling is crucial for the basal daughter cell fate (light blue). The asymmetrical distribution of Wnt co-receptor Lrp6 is necessary and sufficient to cause Wnt upregulation. **B.** Endothelial cells at the blood-brain barrier have different responses to luminal or abluminal VEGF-A (green). These cells achieve to activate differential responses by strictly controlling the localization of VEGF-receptors. VEGF-R1 (red) activates Akt (red), transducing signal from the luminal side, while VEGF-R2 (blue) activates p38 (blue), transducing signal from the neural tissue.

For example, the segregation of the inhibitor of Notch-Delta signalling Numb to the basal cortex is required for the generation of a basal differentiating ganglion mother cell in *D. melanogaster* neuroblasts (reviewed in (Knoblich, 2010), Figure 1.1A). Another example, highlighting the role of receptor localization, is the basolateral enrichment of the Wnt co-receptor Lrp6 observed in *X. laevis* blastoderm cells (Figure 1.16A).

These cells divide asymmetrically and Wnt signalling is known to be required for generating a ciliated daughter cell at the basal side. The enrichment of Lrp6 at the basal side of the blastoderm causes the basal daughter cell to inherit high Wnt signalling, required for its differentiation (Y.-L. Huang & Niehrs, 2014). Hence, in asymmetric cell division, the function of the polarization of signalling components is to convert polarity cues into cell fate specification.

In particular, the endothelial cells of the blood-brain barrier have developed a system to exhibit differential responses to luminal and abluminal vascular endothelial growth factor-A (VEGF-A). The localization of the receptors VEGF-R1 and VEGF-R2 is highly polarized in this system: VEGF-R1 is enriched at the luminal side, from where it mediates Akt activation and cell survival; in contrast VEGF-R2 is enriched at the abluminal side, where it stimulates permeability acting through p38. Due to these different signalling outcomes, only VEGF-A secreted from the neural tissue can increase permeability. Here, the function of the polarization is to translate spatial information into different cellular responses to the same ligand.

1.4.2 Subcellular distribution of morphogens and their receptors in the *D. melanogaster* wing imaginal disc

In polarized epithelial cells, differential distribution of signalling components can modulate the signalling output. Three morphogens are expressed in the

wing imaginal disc and they are differentially secreted and show specific activity patterns along the apical-basal axis.

Wg ligand trafficking is polarized in the wing disc. Wg is initially secreted on the apical side of DP cells, then endocytosed and re-secreted basolaterally in a process that depends on Dlp (Gallet et al., 2008; Marois, Mahmoud, & Eaton, 2006; Strigini & Cohen, 2000). Dlp is present at the apical and basolateral side of the disc and its GPI-anchor is required for Wg trafficking (Gallet et al., 2008).

The Wg receptors Frizzled1 (Fz1) and Frizzled2 (Fz2) have different subcellular localizations: Fz1 localizes to the apical junctional complexes and Fz2 to the basolateral side (Strigini & Cohen, 2000; Wu et al., 2004). This specific localization translates into different signalling outcomes, since Fz1 mediates mainly non-canonical Wg signalling via the planar cell polarity (PCP) pathway, whereas Fz2 mediates Wg signalling via the canonical β-catenin pathway (Wu et al., 2004).

In the wing disc, the Hh gradient consists of two distinct pools: an apical fraction and a basolateral fraction. The function of these different pools is controversial, since either one of them appears to be required for long-range Hh signalling and therefore activation of low threshold target genes (Callejo et al., 2011; D'Angelo, Matusek, Pizette, & Thérond, 2015). The factor Dispatched is required for Hh long range function and was shown to be implicated in apical and/or basolateral trafficking of Hh (Callejo et al., 2011; D'Angelo et al., 2015). Hh follows a similar route a Wg, being secreted apically and re-internalized in a Rab5/ Rab4/dynamin-dependent mechanism (D'Angelo et al., 2015; Gallet et al., 2008). Dally regulates apical accumulation of Hh and its spreading in the apical compartment. Possibly Dally is cleaved by the hydrolase Notum and released in complex together with Hh (Ayers et al., 2010). Dlp is required for the endocytosis of Hh and its

receptor Patched from the apical side (Gallet et al., 2008). Additionally, secretion of Hh depends on the endosomal sorting complex required for transport (ESCRT) proteins, that appear to transport Hh in specialized extracellular vesicles (Matusek et al., 2014).

Cell-derived extracellular vesicles (exosomes) were also shown to transport Hh and important signalling components – as the co-receptor Ihog – along basal cytonemes (Bischoff et al., 2013; Gradilla et al., 2014).

The Hh receptors Patched (Ptc) and Smoothened (Smo) have different subcellular localizations: Ptc localizes apical and basolateral, whereas Smo localization is limited to the basolateral domain (Denef, Neubüser, Perez, & Cohen, 2000).

The spreading of Dpp in the wing disc has been visualized using different GFP-Dpp fusion proteins (Entchev et al., 2000; Teleman & Cohen, 2000) and an anti-Dpp antibody (Gibson et al., 2002). Observing GFP-Dpp spreading, both reports conclude that GFP-Dpp forms an extracellular long-range gradient, dispersing mostly at the basolateral side of the disc (Entchev et al., 2000; Teleman & Cohen, 2000). However, experiments using an anti-Dpp antibody (Panganiban, Rashka, Neitzel, & Hoffmann, 1990) showed a strong lumenal accumulation of Dpp (Gibson et al., 2002). This observation was confirmed by expression of GFP-Dpp (Entchev et al., 2000). Thus, the subcellular localization of Dpp spreading remains debated.

The distribution of BMP receptors along the apical-basal axis has not been characterized in *D. melanogaster*. The subcellular localization of Tkv is unknown, however Tkv was visualized in apical cytonemes and protrusions, when overexpressed in wing disc and testis (Demontis & Dahmann, 2007; Hsiung et al., 2005; Inaba et al., 2015). Moreover, a Tkv-YFP protein trap was reported to localize apically during embryonic epithelial morphogenesis (stage 6-10) (supplemental table S4 Lye, Naylor, & Sanson, 2014). Sax and

Babo protein localization has never been visualized. Unpublished data report that in the wing imaginal disc Wit is apically enriched (Mundt & O'Connor, unpublished). Punt localizes only basolaterally, and a juxtamembrane intracellular domain, named Punt Targeting Domain (PTD), is required for Punt apical exclusion (Mundt & O'Connor, unpublished). Dally and Dlp are reported to localize to the apical and the basolateral side of the wing disc; importantly, their GPI-anchor works as a general motif for apical targeting (Ayers et al., 2010; Gallet et al., 2008).

1.4.3 Subcellular localization of TGF-β superfamily components in vertebrates epithelial cells

BMP receptors were shown to have a localization bias towards the basolateral side of different polarized cell types (Gleason, Akintobi, Grant, & Padgett, 2014; Saitoh et al., 2012).

In the intestinal epithelium of *C. elegans*, the BMP type-I receptor SMA-6 and the type-II receptor DAF-4 localize basolaterally (Gleason et al., 2014).

Proper subcellular localization of BMP receptors is crucial for their physiological function. BMPR-II missense mutations associated with a human lung disease, pulmonary arterial hypertension, resulted in receptor mislocalization (Jiang et al., 2011; Prewitt et al., 2015). In these mutants, the BMPR-II protein did not localize properly to specific plasma membrane domains, like caveolae and clathrin-coated pits. Caveolae are specialized lipid-rafts important for signal transduction (Prewitt et al., 2015).

In the polarized MDCK cells BMPR-II localizes exclusively to the basolateral compartment (Saitoh et al., 2012). The basolateral localization of BMPR-II is dependent on the clathrin adaptor subunit AP1-μA. As a consequence of the restricted localization of BMPR-II, the BMP4 ligand can be sensed only from the basolateral side, inducing phosphorylation of Smad1/5/8. This

observation suggests that also a BMP type-I receptor has to be localized basolaterally. Conversely, TGF-β acts on the apical side of polarized MDCK cells to activate Smad2. TGF-β is known to stimulate EMT and to repress trans-epithelial resistance (TER) by disrupting cell junctions and epithelial polarity (reviewed in J. Xu, Lamouille, & Derynck, 2009). In MDCK cells, BMP4 can counteract the reduction of TER induced by TGF-β, by up-regulating *claudin1* and *claudin4* genes, tight junctions components required for epithelial barrier function.

In contrast to these results, TGF-β2 ligand was shown to activate Smad2/3 signalling from the basolateral side of MDCK polarized cells (Murphy et al., 2004). TGF-β receptors type-I and type-II are localized to the basolateral domain of these cells. TGF-β type-I and type-II receptors require their cytoplasmic domain to prevent apical accumulation. The cytoplasmic basolateral targeting motif of TGF-β receptor type-II has been identified and characterized (Murphy, Shapira, Henis, & Leof, 2007) and will be discussed below. Moreover the cytoplasmic domain of the TGF-β type-II receptor interacts with the retromer complex, which is required to maintain proper basolateral localization (Yin, Murphy, Wilkes, Ji, & Leof, 2013).

1.5 Protein targeting and mislocalization methods

1.5.1 Apical and basolateral targeting domains

The proper subcellular localization of plasma membrane proteins depends on their interactions with the intracellular trafficking machinery.

Inside the cell, proteins are synthesized and processed at the endoplasmic reticulum. Then, they are transported to the Golgi apparatus where they become sorted at the trans-Golgi network (TGN). The TGN is the first sorting station, where apical and basolateral cargos are separated into distinct vesicles. However, additional segregation based on the specific sorting

signals happens in post-TGN or endosomal compartments. From the TGN the cargo protein can take a direct route and reach the membrane through direct vesicular trafficking. Alternatively, the cargo protein reaches its final destination indirectly (called transcytotic route): first the cargo reaches a provisional destination at the plasma membrane; then the cargo is re-internalized and transported to its final destination (reviewed in Cao, Surma, & Simons, 2012; Carmosino, Valenti, Caplan, & Svelto, 2012; Rodriguez-Boulan & Macara, 2014).

Therefore, the proper localization of plasma membrane molecules depends on the balance of biosynthetic and endocytotic routes. Targeting/sorting motifs are *cis*-regulatory motifs, found in the cargo protein. Supposedly, the trafficking machinery recognizes them, sorting the cargo to their appropriate localization. Importantly apical and basolateral targeting motifs have different localizations and features.

Apical targeting motifs can be localized at the presumptive extracellular protein side (called ectodomain), as are N- and O-linked glycans and glicosyl-phosphadylinositol(GPI)-anchors (Paladino et al., 2008; Weisz & Rodriguez-Boulan, 2009). It is proposed that glycans need to interact with Galectin 3, Galectin 4 and Galectin 9 to promote apical sorting (Rodriguez-Boulan & Macara, 2014). Additionally, a transmembrane apical sorting motif is found in hemagglutinin (HA) and mediates apical targeting through incorporation into lipid rafts (Takeda, Leser, Russell, & Lamb, 2003). A cytoplasmic domain of Rhodopsin is required for its apical translocation, since it binds the microtubule motor protein Dynein, in MDCK cells (Tai, Chuang, Bode, Wolfrum, & Sung, 1999).

Basolateral targeting motifs are usually localized in the cytoplasmic domain. Canonical motifs are dihydrophobic dileucine (LL/LI) or tyrosine-based motifs (YxxΦ, where x represents any residue, and Φ stands for a large hydrophobic

residue) (Hunziker & Fumer, 1994; Matter, Hunziker, & Mellman, 1992; Miranda et al., 2001). Basolateral motifs usually require clathrin-adaptor proteins (AP), in particular Tyr-based motifs interact with AP-1 (Carvajal-Gonzalez et al., 2012), reviewed in Rodriguez-Boulan & Macara, 2014). Additionally, specific Rab proteins and the exocyst complex have been associated with both apical and basolateral trafficking (reviewed in (Cao et al., 2012; Carmosino et al., 2012; Rodriguez-Boulan & Macara, 2014).

A unique cytoplasmic domain was found in the TGF-β type-II receptor, named LTA based on its sequence (LTAxxxVAxxR) (Murphy et al., 2007). Interestingly, LTA acts as a dominant basolateral targeting signal, since it mislocalizes the influenza HA protein to the basolateral side (causing loss of apical signal and gain of basolateral fraction).

1.5.2 Protein mislocalization tools II: nanobodies

Nanobodies are single-domain antibodies derived from the heavy-chain-only antibodies found in members of the *Camelidae* species and cartilaginous fish (Hamers-Casterman, Atarhouch, & Muyldermans, 1993). In particular, they consist of the antigen-binding variable domain of heavy-chain antibodies, called VHH (Variable domain of the Heavy-chain of the Heavy-chain antibody). The main advantage of VHHs over conventional antibodies is that they consist of a single polypeptide chain. Consequently, they are small (around 15 kDa), monomeric and they can be selected to function intracellularly (Hassanzadeh-Ghassabeh, Devoogdt, De Pauw, Vincke, & Muyldermans, 2013; Helma, Cardoso, Muyldermans, & Leonhardt, 2015; Muyldermans, 2013; Saerens et al., 2005).

The isolation of a 13 kDa anti-GFP nanobody (vhhGFP4) lead to the generation of many protein engineering applications (Rothbauer et al., 2007; 2006; Saerens et al., 2005). The greatest advantage of vhh-GFP4 is the ability

to function *in vivo* when combined with fusion proteins (Rothbauer et al., 2007).

Given the availability of large collections of GFP-tagged proteins in *D. melanogaster* (see next chapter), vhhGFP4 can be used to interact and manipulate a wide range of targets. Indeed, the anti-GFP nanobody was functionalized and used to induce protein degradation (Caussinus, Kanca, & Affolter, 2012) or extracellular trapping (Harmansa et al., 2015). To mediate protein degradation, vhhGFP4 was fused to the N-terminal domain of the Slmb protein, an adaptor protein that interacts with the E3 ubiquitin ligase complex SCF, mediating substrate recognition (Caussinus et al., 2012).

A fusion protein between vhhGFP4 and the mouse CD8 transmembrane protein was used to sequester the GFP-Dpp morphogen on producing cells and thereby prevent morphogen spreading (Harmansa et al., 2015). In both case, the expression of the functionalized nanobody tool was made inducible by the implementation of the UAS/Gal4 system (A. H. Brand & Perrimon, 1993).

In this thesis, I will investigate if nanobodies are potential tools for mislocalization of transmembrane proteins. For this I will use functionalized versions of vhhGFP4 in the context of protein mislocalization. The tools used are derived from fusing the anti-GFP nanobody to the mouse CD8 transmembrane protein or to other scaffold proteins that show different localizations along the apical-basal axis.

The anti-GFP antibody fused to red fluorescent protein (RFP) (anti-GFP chromobody) was already shown to cause subcellular mislocalization of the bacterial pathogen effector protein AvrHah1, when expressed in plant cells (Schornack et al., 2009). AvrHah1 translocates into the nucleus of plant cells in order to mediate apoptosis. Co-expression of AvrHah1-GFP with the anti-

GFP chromobody, cause AvrHah1-GFP retention in the cytoplasm and reduction of apoptosis.

Nevertheless, this same chromobody was used to visualize the GFP-tagged transmembrane protein DSCAM in *D. melanogaster* motor neurons and did not cause any mislocalization (Kamiyama et al., 2015).

1.6 Overview of the tools used for studying protein localization

The study of protein localization relies on the use of reliable tools to visualize endogenous proteins. For this work, I used different strategies, and here I briefly discuss the advantages and disadvantages of these different methods.

Immunofluorescence (IF) utilizes specific antibodies against the protein of interest (POI) and is the most widely used protein visualization technique. The classic IF techniques are "indirect", because the labeled antibody (secondary antibody, conjugated with a fluorescent dye) recognizes an unlabeled antibody (primary antibody) that is the one directly binding the target epitope. This allows for an amplification of the signal, because more than one secondary antibody will bind to the primary antibody, enabling great sensitivity to the detection.

However, a complication arising from indirect IF is the linkage error: the indirect binding leads to a label displacement of more than 10 nm (size of an antibody). Thus, the linkage error is relevant when proteins are visualized with subcellular resolution. The utilization of direct IF, in which the fluorophore is fused directly to the antigen-binding antibody, minimize the linkage error, especially when small protein binders are used (e.g. nanobody-based chromobodies Rothbauer et al., 2006). A disadvantage of IF is the need to generate new antibodies, which is a laborious, time-consuming process.

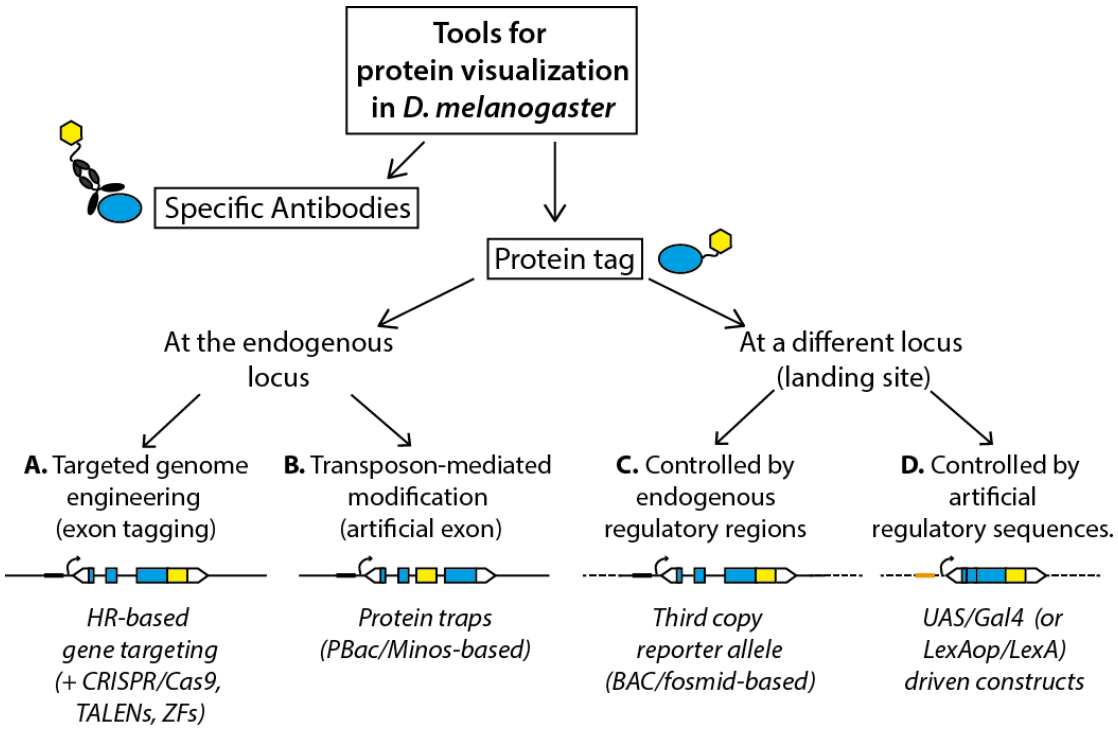

Figure 1.17 Summary of the tools used for protein visualization in *D. melanogaster*. Protein visualization commonly involves the use of fluorescent tags (yellow), which are coupled to the protein of interest (POI, blue) either by the use of specific antibodies (IF) or directly added to the POI by genetic modifications (protein tag). The tag can be inserted by modifying the endogenous locus or by introducing an additional copy of the gene of interest at a different locus. **(A)** The endogenous locus (solid line) can be tailored modified with high efficiency by coupling homologous recombination (HR)-based gene targeting with the CRISPR/Cas9 (in the past TALENs, ZFs). **(B)** The target gene can be modified by introducing an artificial exon carrying the fluorescent protein. At a different locus (dashed line), the additional gene copy can be controlled by the endogenous regulatory regions **(C)** or by artificial binary systems **(D)**. HR: homologous recombination. CRISPR: clustered regularly interspaced short palindromic repeats. TALENs: transcription activator-like effector nucleases. ZFNs: zinc finger nucleases.

Moreover some antibodies show non-specific cross-reactivity, causing off-target detection artefacts.

The generation of fluorescent protein (FP) fusions allows to visualize the target protein in native conditions, offering temporal and dynamic information. This approach is powerful, as the signal can be detected in live tissue without fixation and staining. Antibody stainings against the chosen FP can still be used for signal amplification. However, the main disadvantage of FP-tagging is the fact that it modifies the protein sequence. This could result in artefacts like protein mislocalization, as it is known that N-terminal and C-

terminal tags can influence subcellular localization of the POI (Stadler et al., 2013) and big tags can possibly interfere with protein function. Using small tags, like HA, Myc, V5 FLAG tags, reduces the chance of interfering with protein function. Another possible disadvantage is that, depending on the position of the tag, specific splicing isoforms may not be labelled.

The generation of tagged protein can be approached in different ways. The best approach is to modify genes at the endogenous locus, leaving the regulatory regions intact and the coding region almost unperturbed. In *D. melanogaster* homologous-recombination (HR) based gene targeting (Gong & Golic, 2003; J. Huang, Zhou, Dong, Watson, & Hong, 2009; Rong, 2000) was a major breakthrough, allowing direct and precise modification of target genes. Coupling this method with the CRISPR (Clustered Regularly Interspaced Short Palindromic Repeats)/Cas9 technology appears to greatly improve the HR efficiency (L. A. Baena-Lopez, Alexandre, Mitchell, Pasakarnis, & Vincent, 2013; Gratz, Cummings, Nguyen, Hamm, Donohue, Harrison, Wildonger, & O'Connor-Giles, 2013a) (see chapter 1.6.1), making genome engineering effective and convenient (Figure 1.17A).

The protein-trapping technique allows to modify the endogenous locus by introducing an artificial exon (Figure 1.17B). This method takes advantage of the power of *D. melanogaster* genetics, by relying on the mobilization of transposable elements. The transposable element contains an artificial exon encoding the tag (usually a fluorescent marker) flanked by splicing acceptor and donor sites. When the transposon integrates in an intron, with the correct orientation and reading frame, the artificial exon will be integrated in the transcript, creating a fusion protein containing the tag. This technique is very powerful, since transposable elements integrations are extremely efficient and fast. Therefore it allows large-scale protein tagging at the endogenous locus. Recent advances in protein trapping lead to select specific types of

transposable elements, that in contrast to P-elements, have a good frequency of integration in introns, like *piggyBac* (Buszczak et al., 2007) (Lowe et al., 2014) and *Minos* (Venken et al., 2011) elements. Nevertheless, careful validation of protein trap lines is needed to make sure that the artificial exon is efficiently integrated in all the transcripts and that the tagged protein is still functional (Pastor-Pareja & Xu, 2011) (Nagarkar-Jaiswal et al., 2015).

Before the CRISPR/Cas9 revolution, a great number of tagged proteins were generated by introducing artificial constructs at a specific genomic locus, different from the endogenous one (Figure 1.17C, D). The reason why this is so convenient in *D. melanogaster* is because it relies on a highly efficient site-specific insertion technology, based on ΦC31 integrase (Bischof, Maeda, & Hediger, 2007; Groth, Fish, Nusse, & Calos, 2004). Therefore, large collections of constructs were injected and integrated into a specific *landing site*, called phage attachment site (*attP).* This site is inserted in the genome and recombines with the bacterial attachment site (*attB*) in the donor plasmid, in order to mediate the integration of exogenous sequences. The specific and constant position of the landing site allows to minimize artefacts arising from genomic positional effect.

A type of collection successfully generated in *D. melanogaster* using landing sites is the so-called *third copy reporter allele* (Figure 1.17C). This approach relies on cloning large constructs (using Bacterial Artificial Chromosomes (BAC) (Venken et al., 2009) or fosmid libraries Ejsmont, Sarov, Winkler, Lipinski, & Tomancak, 2009), containing most of the region encompassing the gene of interest (GOI). By inserting a tag on the coding region, the transgene functions as an additional copy of the GOI, controlled by the endogenous regulatory regions and labelled by the tag. This type of tagging approach proved to be extremely valuable, as it recapitulates the endogenous protein localization and in most cases fully rescues genetic null

mutants (almost 70% as described in Sarov et al., 2015). The limitation of this approach is that there might still be some positional effects, deriving from the site of integration.

The size of the construct can be reduced – making it easier to clone and insert – by cloning only the cDNA of the GOI under the control of an artificial promoter (Figure 1.17D). In *D. melanogaster* the UAS/Gal4 binary system is widely used for this aim (A. H. Brand & Perrimon, 1993). More recently a LexA driven binary system has been developed and implemented in *D. melanogaster* (Yagi, Mayer, & Basler, 2010). In this case the tagged protein can be overexpressed and visualized in different tissues (Bischof et al., 2013). Nevertheless the overexpression of the tagged protein could give rise to artifacts and misrepresent the physiological condition.

1.6.1 The CRISPR/Cas9 technology

Genome editing techniques in *D. melanogaster* advanced drastically in the last decade, with the development and implementation of DNA binding factors that can be used to target specific genomic region. These factors are able to induce DNA double-strand breaks (DSBs) that are repaired by the cellular machinery through non-homologous end joining (NHEJ) or homologous recombination (HR). NHEJ leads to imprecise repair, resulting in insertion or deletion of nucleotides (Bibikova, Golic, Golic, & Carroll, 2002). HR is instead precise, since it uses the sister chromatid as a template for the repair. HR-based repair can be hitchhiked by supplying the cell with a large excess of an artificial synthetic template, modified to introduce precise changes in the targeted locus (Beumer, 2005; Beumer et al., 2008; Bibikova, 2003) (Figure 1.17D).

Initially, zinc-finger nuclease (ZFNs) and transcription activator like effector nucleases (TALENs) were used to bind DNA and induce DSBs (Beumer, 2005;

J. Liu et al., 2012). However, these factors were quickly replaced by the CRISPR/Cas9 system. The CRISPR/Cas9 was discovered as a bacterial mechanism of defence against intruding pathogens, where the crRNA (CRISPR RNA) provides binding specificity to the pathogenic template by pairing to a 20 nucleotides (nts) sequence (Barrangou et al., 2007; Ishino, Shinagawa, Makino, Amemura, & Nakata, 1987; Jansen, Embden, Gaastra, & Schouls, 2002). The crRNA forms a complex with the trans-acting crRNA (tracrRNA), in order to recruit Cas9 nuclease (Brouns et al., 2008; Gasiunas, Barrangou, Horvath, & Siksnys, 2012; Jinek et al., 2012). The CRISPR/Cas9 system has been used for genome editing in a wide variety of organism, from fungi to human cells. In the synthetic CRISPR/Cas9 system, the crRNA and tracrRNA are fused into a single guideRNA (gRNA), a 100 nts long molecule. The 20 nts of the guide sequence are located at the 5' end of the gRNA and they have to be followed by a specific protospacer adjacent motif (PAM) sequence in the genomic target site (NGG or NAG) (Mali et al., 2013).

Several groups reported successful genome editing by using the CRISPR/Cas9 system in *D. melanogaster* (Bassett, Tibbit, Ponting, & Liu, 2014; Gratz, Cummings, Nguyen, Hamm, Donohue, Harrison, Wildonger, & O'Connor-Giles, 2013b; Kondo & Ueda, 2013; X. Ren et al., 2013; Sebo, Lee, Peng, & Guo, 2014; Z. Yu et al., 2013).

Most of these groups targeted the *yellow* gene and could induce mutagenesis rates as high as 88%, which resulted from NHEJ (Bassett et al., 2014). Moreover, replacement of a concrete portion of the *yellow* gene with an *attP* landing site, was achieved by using two gRNAs and a single-strand oligodeoxynucleotide (ssODN) template (Gratz, Cummings, Nguyen, Hamm, Donohue, Harrison, Wildonger, & O'Connor-Giles, 2013b). Further advances involved the generation of transgenic flies expressing Cas9 in germline cells, under the control of the *vasa* or *nanos* promoters (Gratz et al., 2014a; Kondo

& Ueda, 2013; X. Ren et al., 2013; Sebo et al., 2014). The efficiency of gene replacement or targeted insertions is drastically increased by implementing the CRISPR/Cas9 technology, since production of a DSB at the region of exchange stimulates HR (up to 7% of targeting efficiency) (L. A. Baena-Lopez et al., 2013; Gratz et al., 2014a).

The current methods use double-stranded DNA donor plasmids, in order to mediate the integration of large synthetic sequences, usually containing a removable screening marker. This technique is HR-based and involves the exchange of the regions included between two homology arms, that often comprise part of the GOI with the desired modifications. Very often gene editing is completed in two steps: first the target gene is deleted and replaced with an attP landing site; in the second step, the landing site is used to reintroduce modified target-gene DNA into the locus (J. Huang et al., 2009).

The design of gRNAs is now supported by web-based tool for finding and evaluating CRISPR target sites, based on their off-targets and of their efficiency score (Gratz, Wildonger, Harrison, & O'Connor-Giles, 2014b; Housden et al., 2015).

2 MATERIAL AND METHODS

2.1 Fly stocks

hh-Gal4	Gal4 enhancer trap, drives expression in the posterior compartment of the wing disc (as described on FlyBase).
ci-Gal4	Gal4 enhancer trap, drives expression in the anterior compartment of the wing disc (as described on FlyBase).
tkv-3xHA	Endogenous Tkv protein tag, generated by Jennifer Gawlik and Giorgos Pyrowolakis.
vasa-ΦC31; tkvKO-attP(2)/CyO	Used for the injection of pGE re-entry vectors. Generated by Jennifer Gawlik and Giorgos Pyrowolakis.
Sax-GFP	Third-copy reporter allele, VDRC ID 318380. Generated in (Sarov et al., 2015).
Babo-GFP	Third-copy reporter allele, VDRC ID 318433. Generated in (Sarov et al., 2015).
Punt-GFP	Third-copy reporter allele. Generated and obtained by Michael O'Connor.
Wit-GFP	Third-copy reporter allele, VDRC ID 318043. Generated in (Sarov et al., 2015).
Dally-YFP	Endogenous protein trap. CPTI-001039.
Dlp-YFP	Endogenous protein trap. CPTI-000445.
Tkv-YFP	Endogenous protein trap. CPTI-002487.
Nrv1-YFP	Endogenous protein trap. CPTI-000925.

Crb-GFP-A	Endogenous Crb protein tag (extracellular GFP tag), generated and obtained from (J. Huang et al., 2009).
UAS-SBN-A_intra	Described in the PhD thesis of S. Harmansa (University of Basel, 2016), designed as VHH-GFP4-T48-Baz::mCherry (VHH-GFP4 substitutes mCherry in the intracellular version).
UAS-SBN-A_extra	Described in the PhD thesis of S. Harmansa (University of Basel, 2016), with the name of VHH-GFP4-T48-Baz::mCherry.
UAS-SBN-AB_extra	Described in (Harmansa et al., 2015).
UAS-SBN-B_extra	Described in the PhD thesis of S. Harmansa (University of Basel, 2016), with the name of VHH-GFP4-Nrv1::TagBFP.
UAS-PH-GFP	FlyBase reference FBtp0020840, generated in Zelhof & Hardy, 2004).
yv; P{TRiP.HMS02185}attP40	UAS-driven *tkvRNAi*. Bloomington 40937.
Dp(2;3)tkv3	Interchromosomal duplication containing a region including the *tkv* locus (25A2-3;25D5-E1 region of the chromosome 2), inserted in the third chromosome. Tkv is mutated in the duplicated region (*tkv3* allele). Bloomington 1164.
vasa:Cas9	Used for injection of the pGX targeting vector and pU6-chiRNA vectors (Gratz et al., 2014a).

2.2 Immunostaining

2.2.1 Immunostaining procedure for wing imaginal discs

Imaginal discs were dissected in PBS. Larvae were cut in the middle and the anterior part was inverted, keeping the imaginal discs attached to the tracheas and the larval cuticle. Fat tissue was removed to expose the wing discs. Dissected larvae were fixed in fixative solution for 20 minutes at RT, using 2 mL tubes on a rotor. Fixative was removed, by washing three times in PBT. Subsequently, the tissue was permeabilized, by washing three times in PBT for 20 minutes at RT on a rotor. After blocking in PBTN for 30 minutes. rotating at RT, the tissue was incubated with primary antibody in PBTN overnight at 4°C. The next day the primary antibody solution was removed by rinsing three times in PBT. The dissected larvae were washed in PBT, by changing the solution every 20 minutes for four times. Secondary antibody incubation was diluted in PBTN and incubated at RT for 2 hours. Afterwards, the secondary antibody solution was removed by rinsing three times in PBT and the dissected larvae were washed in PBT, by changing the solution every 20 minutes for four times. Finally, PBT was removed as much as possible and larval carcasses were covered in Vectashield fluorescent mounting medium (Vecta Laboratories, H-1000). After incubating the sample for at least 1 hours in Vectashield, wing imaginal discs were mounted.

For mounting, wing discs were positioned with apical side facing the cover slide, in order to obtain better resolution of the apical domain.

2.2.2 Extracellular immunostaining of wing imaginal discs

Larvae were dissected as described above, using ice-cold Schneider's Insect Medium (S2, Sigma-Aldrich) instead of PBS. The inverted carcasses were incubated in primary antibody diluted in S2 in 0.5 mL tubes for 1 hour on ice. The tubes were shaken every 15 minutes. The primary antibody solution was

then removed, by rinsing the dissected larvae in ice-cold PBS for three times. Larvae were transferred in 2 mL tubes and fixed using fixative solution. The procedure followed the same steps of the conventional immunostaining.

Solutions:

10x PBS: 2g KH2PO4, 1.25ml 10N NaOH, 80g NaCl, 2g KCl, 6.1g Na2HPO4 were dissolved in 1L of milliQ water.

Fixative solution: 4% Paraformaldehyde in 1xPBS

PBT: 0.3% Triton-X100 (Sigma-Aldrich) in 1xPBS

PBTN: 2% Normal Donkey Serum (Jackson Immuno Research) in PBT

2.2.3 Antibodies

Primary antibodies: rb-anti-p-Mad (1:1,500; E. Laufer); rb-anti-phospho-Smad1/5 (1:200; Cell Signaling, 9516S; used in Extended Data Fig. 4d–f); m-anti-Wg (4D4-s; 1:120; DSHB, University of Iowa); m-anti-Ptc (Apa1-s; 1:40; DSHB, University of Iowa); rb-anti-GFP (1:200 for extracellular staining; Abcam ab6556); rb-anti-mCherry (1:2000; Sigma); m-anti-Dlg (4F3-s; 1:500; DSHB, University of Iowa); m-anti-Crb (Cq4-s; 1:5; DSHB, University of Iowa); rb-anti-HA (C29F4, 1:500; Cell signalling); rat-anti-DE-cad (DCAD2-c; 1:100; DSHB, University of Iowa); rb-anti-aPKC (1:500; Santa Cruz); m-anti-PatJ (1:1500; courtesy of F. Hamaratoglu).

Secondary antibodies: AlexaFluor series, used at 1:750 dilution.

2.3 Nucleic acids extraction

2.3.1 Single fly genomic DNA extraction

Single flies (anesthetized with CO2 and transferred at -20°C for 20 minutes) are transferred into PCR tubes and squished using a pipet tip loaded with 50ml of squishing buffer. Once crushed, the squishing buffer is expelled and

mixed with the squished fly. The sample is then incubated for 30 minutes at 37°C, followed by 2 minutes at 95°C for heat-inactivation of Proteinase K. 1 µL of the sample was used as a PCR template (in a 25 µL PCR volume). Extracted DNA can be stored at 4°C for one month.

Solutions:

Squishing buffer: 10 µL 1M Tris-HCl (pH 7.5), 5 µL 500mM EDTA (pH 8.0), 5 µL 5M NaCl, 10 µL Proteinase K (20mg/ml), up to 1mL with ddH2O.

2.3.2 RNA extraction from wing imaginal discs

Approximately 50 wing discs for each genotype where used for total RNA isolation using Trizol reagent (Invitrogen). cDNA was synthesized from 2 µg of RNA with the High Capacity cDNA Reverse Transcription Kit (Applied Biosystems). An average of 50 ng of cDNA was used for semi-quantitative (semi-q) RT-PCR (33 amplification cycles). The primers used for semi-qRT-PCR are shown in Table 1. Real-time PCR (quantitativeRT-PCR or qRT-PCR) analysis was performed in a Step One Plus Real-Time PCR System machine (Applied Biosystems), using 50–200 ng of cDNA with SYBR green fast kit (Applied Biosystems) according to the manufacturer's instructions. The expression of eiF-1A (housekeeping gene, elongation factor required for protein synthesis) was used as an internal control for normalization of cDNA amounts. The primers used for semi-qRT-PCR are shown in Table 2.

Table 1 Primers used for semi-qRT-PCR:

tkvYFP_rv	GTACATCCCGGTCGTCTCATC
tkvYFP_PCRD_fw	GCGCCGAAATCCAGAAAGAAG
tkvYFP_PCRA_fw	TGCGAATGTTCAGCCAGACG

Table 2 Primers used for qRT-PCR:

eIF-1A fw	ATCAGCTCCGAGGATGACGC
eIF-1A rv	GCCGAGACAGACGTTCCAGA

FvkgReal	GCGGATGGAAAGATCTGC
RvkgReal	CGTCCAGGTGGTCCTATATCA
F1vkgRT	AGCCTGGTTTCCGTTACCTT
F2vkgRT	TCTGGGCGTCGTTTATCTGT
R1vkgRT	GCTCACCGCTTTTACCCATA
R2vkgRT	TGTCCTTTCTCGCCTTGTTC
TkvYFP_qRTPCR-PP-fw	AGGCTCATGCCCGCTCCC
TkvYFP_qRTPCR-PP-rv	CCTCCTCGTACATCCCGGTCG

2.4 Cloning

2.4.1 Cloning of the tkv homologous arm in the targeting vector

The pGX vector generated in (J. Huang et al., 2009) was used as the targeting vector to mediate the swapping of the last two exons of the *tkv* gene with a removable eye color marker and an attP landing site (Figure 4.33). The 5′ homologous arm was cloned using NotI and KpnI restriction sites, whereas the 3′ homologous arm was cloned using BglII and AscI restriction sites in the pGX vector. The primers used for the amplification of the 5′ and 3′ homologous arms are shown in Table 3. The homologous arms were amplified using yw genomic DNA as a template.

2.4.2 Cloning of the gRNAs into the pU6-chiRNA vector

The pU6-chiRNA vector (Gratz et al., 2014a) was used to clone and express the gRNAs used for *tkv* locus targeting.

The primers used are depicted in the Table 3 and were used for cloning into the pU6-chiRNA vector using a BbsI restriction site, according to the protocol described in http://flycrispr.molbio.wisc.edu/protocols/gRNA.

The gRNAs were chosen using the CRISPR Optimal Target Finder tool (http://tools.flycrispr.molbio.wisc.edu/targetFinder/) for off-targets prediction and the CRISPR evaluator tool (http://www.flyrnai.org/evaluateCrispr/) to score the efficiency of the gRNAs. All gRNAs had no predicted off-targets and variable scores (mentioned below).

The gRNAs used to generate the *tkvKO-attP(1)* allele target the following sites in the *tkv* locus:

5' gRNA site: 3'TAATATGTCCTTATGATATCCGG 5' score: 8.75.

3' gRNA site: 5'CCAAAAGCTCGATTTTCTGTTGG 3' score: 7.32.

An alternative gRNA couple was initially used and did not yield to any recombination event. This couple targets the following sites in the tkv locus:

5' gRNA site: 3'TCCATATGAAATGAAGAGTCTGG 5' score: 4.48.

3' gRNA site: 3'TTAGCTATGGATTTATTGTATGG 5' score: 7.10.

Table 3 Primers used for pGX cloning and gRNAs cloning:

NRpGX_tkv_5hom_fw	aaaaGCGGCCGCTGGAATGGAATCCGAGAGTTT
NRpGX_tkv_5hom_rv	aaaaGGTACCATCCGGTTATAATAACTAGTCGTC
NRpGX_tkv_3hom_fw	aaaaAGATCTTGTTGGTTTTATCAGCGTTCG
NRpGX_tkv_3hom_rv	aaaaGGCGCGCCATGCACACATCTCAACTCGC
NRtkv_chiRNA5'_fw	cttcgTAATATGTCCTTATGATATC
NRtkv_chiRNA5'_rv	aaacGATATCATAAGGACATATTAC
NRtkv_chiRNA3'_fw	cttcgCCAAAAGCTCGATTTTCTGT
NRtkv_chiRNA3'_rv	aaacACAGAAAATCGAGCTTTTGGc

2.4.3 Cloning of the *tkv* re-entry vectors

In order to integrate modified versions of the *tkv* genomic region, I injected different "re-entry" vectors into the *tkvKO-attP(2)* flies (Figure 4.33). As a backbone for the re-entry vectors I used the pGE plasmid, that carries an *attB* site for recombination with the *attP* in the targeted locus and a removable w^+ screening marker (Figure 4.33B) (J. Huang et al., 2009). First, I inserted the region that was deleted in the *tkvKO-attP(1)* allele (last two *tkv* exons) in the pGE vector, using NotI and SpeI sites (to generate the pGE-*tkv-rescue* plasmid). Next, I inserted a linker containing the AgeI (5') and the XbaI (3') site either in coding region corresponding to the extracellular domain of Tkv (to generate the pGE-*tkv-Extra-mCherry* plasmid) or to the C-terminal end of Tkv (to generate the pGE-*tkv-Cterm-mCherry* plasmid) (primer used for linker

insertion are shown in Table 5). I used the AgeI and XbaI restriction site to clone mCherry into the *tkv* coding region. For the amplification of the *tkv* genomic region, I used yw genomic DNA. For mCherry amplification, I used the pLOT-VHH-GFP4::CD8::mCherry plasmid (courtesy of S. Harmansa) as a template. The primers used are listed in Table 4 and Table 5.

Insertion site of mCherry into *tkv-Extra-mCherry* (exon *tkv2*, FlyBase):

5'-AGCGTACATATGGATGCATG//ATGCATGCCTCCCGAAGACA-3'

This results in the insertion of mCherry at position 118 aa in *tkv-A* and at 64 aa in *tkv-D* (61 aa from the transmembrane domain). The YFP tag of Tkv-YFP is located 114 aa from the transmembrane domain.

Table 4 Primers used for the re-entry constructs:

pGE_tkv-rescue_fw	aaaaGCGGCCGCATCATAAGGACATATTATAGGGGTC
pGE_tkv-rescue_rv	aaaaACTAGTGAAAATCGAGCTTTTGGGTTTAA
AgeI_mCherry_fw	ctggtACCGGTATGGTGAGC
XbaI_mCherry_rv	aaaatctagaCTTGTACAGCTCGTCCATGC

Table 5 Primers used to insert AgeI-XbaI linker:

Tkv_Cterm_AX	CGATGTGCCCATTAAGATTGTCggaggttccggtggaagcggaggtagcaccggtaaaatctagaTAAGCAGCTGTTTGTAGTCTCG
Tkv_Nterm_AX_se	aaaaATGCATGggaggttccggtggaagcggaggtagcaccggtaaaaaatctagaGGCGgatccggaggtagcggtggaagcggATGCATaaaa
Tkv_Ntermt_AX_as	ttttATGCATccgcttccaccgctacctccggatcCGCCtctagatttttttaccggtgctacctccgcttccaccggaacctccCATGCATtttt
LTAdel	GGCACCCGAATCCCACCGTTACGCTGGGGCGACTGGAAAC

2.4.4 Deletion of the LTA domain from pGE-tkv-Cterm-mCherry

I used the pGE-*tkv-Cterm-mCherry* plasmid to delete the LTA domain (Murphy et al., 2007) from *tkv* coding region, following PCR-based mutagenesis.

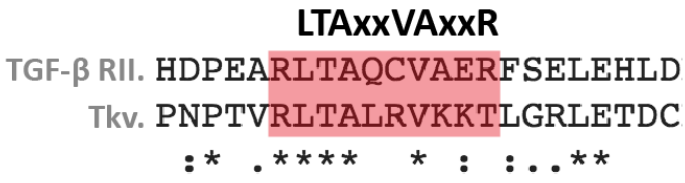

Figure 2.1 The LTA signal of the TGF-β type-II receptor and Tkv. The LTA signal of the TGF-β type-II receptor is conserved in Tkv. The LTA consensus (LTAxxVAxxR, where x is any aa) is represented above **(Murphy et al., 2007)**. The conservation was obtained by aligning the whole sequence of the TGF-β type-II receptor and Tkv, using the global alignment tool ClustalW **(Chenna et al., 2003)**.

The primer used for the PCR-based mutagenesis is shown in Table 5. The LTA signal was initially discovered in the TGF-β type-II receptor (Murphy et al., 2007). The conservation between the LTA signal of the TGF-β type-II receptor and of Tkv is shown in Figure 2.1.

2.5 Generation of transgenic flies

2.5.1 Generation of the *tkvKO-attP(1)* allele

The *tkvKO-attP(1)* allele was generated by injecting the pGX vector described in chapter 2.4.1 together with the pU6-chiRNA vectors described in chapter 2.4.2 into *vasa-Cas9* flies. The pU6-chiRNA vectors were injected at the concentration of 100 ng/µL, whereas the pGX vector at the concentration of 500 ng/µL (as recommended in (Gratz et al., 2014a). The primers used for screening of the targeting event are shown in Table 6 and Figure 4.34.

Table 6 Primer used for the screening of the *tkvKO-attP(1)* allele

3'seq_tkv_rv (P2)	AACTGCAGGCTCTGATCGAC
Tkv_intron_fw (P1)	ATACAGGTCCGAGTACGGAAG
white3_fw (P3)	TAATATCCTGCGCCAGCTCC

2.5.2 Generation of the *tkvKO-attP(1)* allele

In order to integrate modified versions of the *tkv* genomic region, I injected different re-entry vectors into the *tkvKO-attP(2)* founder line, expressing the ΦC31 integrase in the germline (under the control of the *vasa* promoter) (Figure 4.33). After injections, I recovered the following alleles: *tkv-rescue*, *tkv-Extra-mCherry*, *tkv-Cterm-mCherry*, *tkvΔLTA-Cterm-mCherry*. The primers used for screening of the *tkv-rescue* allele are shown in Table 7 and the PCR screening is shown in Figure 4.36.

Table 7 Primers used for the screening of *tkv-rescue* allele.

Tkv_lastexons_fw (P1)	GGGATAAGACCAACCCACTCG
tkv_3hom_rv (P2)	GACAAAAGGTCGGAACTGCG
3'seq_tkv_fw (P3)	GCAAAGATGTTTATAGGCCGCT
pGEseq_rv (P4)	cggggcatgacgtacgataac

The strategy for detecting the *tkv-Extra-mCherry* allele is shown in Figure 2.2 and the primer sequence is shown in Table 8.

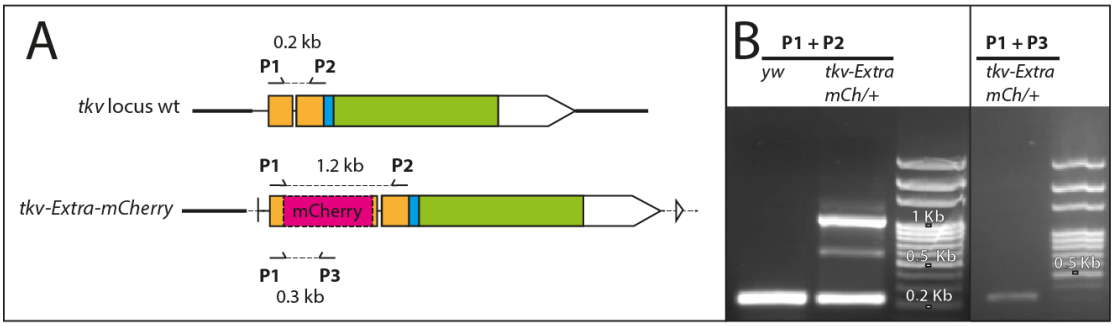

Figure 2.2 Isolation of the tkv-Extra-mCherry allele. A. Schematic representation of the PCR screening used for *tkv-Extra-mCherry* isolation. **B.** Using the primer couple P1+P2 a wild type band (0.2 bp) is visible in yw wild type flies; the wild type band shifts (1.1 kb) due to the mCherry insertion in *tkv-Extra-mCherry* heterozygous. The mCherry insertion is detected also by using the primer couple P1 + P3 (320 bp). The sequence of the primers used is presented in **Table 8**.

Table 8 Primers used for detecting the *tkv-Extra-mCherry* allele:

tkv_3hom_fw (P1)	TACGATGAGACGACCGGGAT
106_rv (P2)	GGGTACAGCGGCTACCTTGC
mCherry_rv (P3)	TTCACGTAGGCCTTGGAGCC

The strategy for detecting the *tkv-Cterm-mCherry* and *tkvΔLTA-Cterm-mCherry* alleles is depicted in Figure 2.3 and the sequence of the primers used is shown in Table 9.

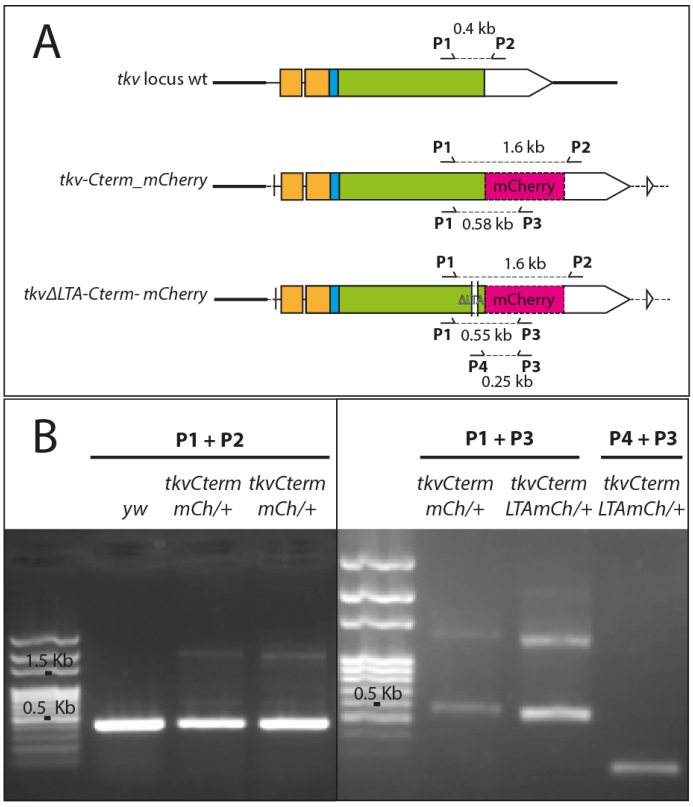

Figure 2.3 Isolation of the *tkv-Cterm-mCherry* and *tkvΔLTA-Cterm-mCherry* alleles. A. Schematic representation of the PCR screening used for *tkv-Cterm-mCherry* and *tkvΔLTA-Cterm-mCherry* isolation. **B.** Using the primer couple P1+P2 a wild type band (0.4 kb) is visible in yw wild type flies; the wild type band shifts (1.6 kb) due to the mCherry insertion in *tkv-Cterm-mCherry* and *tkvΔLTA-Cterm-mCherry* heterozygous. The mCherry insertion is detected also by using the primer couple P1 + P3 (0.58 kp for *tkv-Cterm-mCherry* and 0.55 kb for *tkvΔLTA-Cterm-mCherry*). The primer P4 is specific for the LTA deletion and amplifies a region of 0.25 kb in *tkvΔLTA-Cterm-mCherry* heterozygous. The sequence of the primers used is presented in **Table 9**.

Table 9 Primers used for the screening of *tkv-Cterm-mCherry* and *tkvΔLTA-Cterm-mCherry* alleles:

tkv_lastexonend_fw (P1)	AGATGACCCGTCGCTGCTAC
tkv_3hom_rv (P2)	GACAAAAGGTCGGAACTGCG
mCherry_rv (P3)	TTCACGTAGGCCTTGGAGCC
LTAdel_screen_rv (P4)	TCGCCCCAGCGTAACGGT

3 AIM OF THE PROJECT

The activation of different signalling pathways can happen at specific positions along the cell surface (e.g. only at one cell pole) due to the restricted subcellular localization of pathway components (receptors and/or ligands). This phenomenon is referred to as polarized signalling and has been observed in different cell types.

In epithelial cells, a number of molecules distribute differentially along the apical-basal axis. Signalling pathway components often display restricted subcellular localization or bias towards apical or basolateral domains. For example, different receptors of the TGF-β superfamily were shown to localize exclusively to the basolateral side in different epithelial systems (Gleason et al., 2014; Murphy et al., 2004; Saitoh et al., 2012). However the function of this restricted localization and the extracellular distribution of the TGF-β ligands remains unclear in these systems.

The subcellular distribution of the TGF-β superfamily ligand Dpp has been characterized in the wing disc epithelium of *D. melanogaster*. In contrast, to the aforementioned receptors, Dpp was reported to disperse at the apical (Gibson et al., 2002) and the basolateral side of the wing disc (Entchev et al., 2000; Teleman & Cohen, 2000). However, the subcellular localization of the TGF-β receptors has not yet been investigated in the wing imaginal disc.

Therefore, in this study I characterized the subcellular distribution of the three TGF-β type-I receptors and the two type-II receptors in the wing imaginal disc. I also analysed the localization of the glypicans Dally and Dlp, that have been proposed to act as co-receptors for the TGF-β signalling pathway.

In order to understand the function of the different subcellular fractions of the TGF-β receptors, I attempted to mislocalize the receptors along the apical-basal axis. To this aim, I used newly developed nanobody-based tools, here

referred to as Scaffold Bound Nanobodies (SBNs). The SBNs toolset is composed of an anti-GFP nanobody fused to transmembrane scaffold proteins that differentially localize along the apical-basal axis. I characterized the potential of these novel tools by using them to mislocalize GFP/YFP fusion proteins. Finally, I used the SBNs to mislocalize GFP/YFP tagged versions of the TGF-β receptors in the wing imaginal disc and observed the effect of receptor mislocalization on signal perception and transduction.

Additionally, I attempted to mislocalize TGF-β receptors by mutating targeting elements. In particular, I deleted a basolateral targeting sequence located in the C-terminal portion of the type-I receptor in order to achieve apical enrichment.

This work will help to gain a better understanding on how the subcellular restriction of the ligand perception machinery can control signalling and influences development of multicellular organisms.

4 RESULTS

4.1 Subcellular localization of TGF-β receptors

The subcellular distribution of the TGF-β superfamily receptors in *D. melanogaster* has not been reported. Different tools can be used to visualize proteins and could be used to address this question (see chapter 1.6). Since no good antibodies are available for the different TGF-β receptors, I made use of fly lines carrying tagged versions of the POI (Table 10). Importantly, many of these fly lines contain endogenous protein tags, generated by modifying the endogenous locus (Tkv-3xHA, Dally-YFP, Dlp-YFP). Alternatively I used third copy reporter alleles generated in BAC or fosmid-based approaches (Punt-GFP, Sax-GFP, Babo-GFP, Wit-GFP). These reporters are suitable to study protein localization at endogenous expression levels, since the tagged clones contain large sequences comprising most of the endogenous regulatory regions.

In the following, I am summarizing the results I obtained using these tools in combination with high-resolution imaging to investigate the subcellular localization of the TGF-β receptors in the wing disc.

Receptor	Protein-Tag	Tagging method	Reference
Tkv	Tkv-3xHA	Endogenous protein tag	G. Pyrowolakis
Sax	Sax-GFP	Third copy reporter allele	(Sarov et al., 2015)
Babo	Babo-GFP	Third copy reporter allele	(Sarov et al., 2015)
Punt	Punt-GFP	Third copy reporter allele	M. O'Connor
Wit	Wit-GFP	Third copy reporter allele	(Sarov et al., 2015)
Dally	Dally-YFP	Protein trap	(Lye et al., 2014)
Dlp	Dlp-YFP	Protein trap	(Lye et al., 2014)

Table 10 Summary of the tools used to visualize the TGF-β receptors and the glypicans Dally and Dlp. See chapter 1.6 for an overview of the protein tagging methods.

The use of high-resolution confocal imaging along the z-axis allowed me to compute sections through a wing disc stack and investigate the localization of pathway components along the apical-basal axis. To characterize the subcellular localization of the TGF-β receptors, I used Dlg and Crb as markers to distinguish basolateral and apical compartment, respectively.

Dlg is enriched at the SJs, therefore it labels the apical border of the basolateral compartment (Figure 1.3). Crb is an apical determinant, which localizes to the subapical region of wing disc cells, just above the AJs in the apical compartment (Figure 1.3). Therefore, molecules that localize at the same level and below Dlg are referred to as basolaterally localized. Molecules that are found above the SJs (Dlg) are localized to the apical compartment of wing disc cells. Moreover, molecules that localize at the same level as Crb localize to the subapical region of the apical compartment.

For high-resolution analysis of the subcellular localization of the TGF-β receptors, a region of the dorsal-posterior compartment of the wing disc pouch is shown as a representative area. Because of their restricted expression pattern, a dorsal-anterior area of the wing pouch is shown for Babo-GFP and Dlp-YFP.

4.1.1 The type-I receptor Tkv localizes to the apical and basolateral compartment of the wing disc

The type-I receptor Tkv was visualized using an endogenous protein tag, Tkv-3xHA (generated by J. Gawlik, G. Pyrowolakis). The *tkv-3xHA* allele was generated using a two steps HR-based method that targets and modifies the endogenous *tkv* locus (described in chapter 1.6). The 3xHA tag was introduced into the last *tkv* exon, so that it localizes at the C-terminal end of the Tkv protein (Figure 4.1B). Tkv-3xHA flies are homozygous viable and, due to the insertion site, the 3xHA-tag is common to all splicing isoforms.

Therefore, Tkv-3xHA allows the visualization of all Tkv splicing isoforms expressed in the wing disc by conventional α-HA antibody staining.

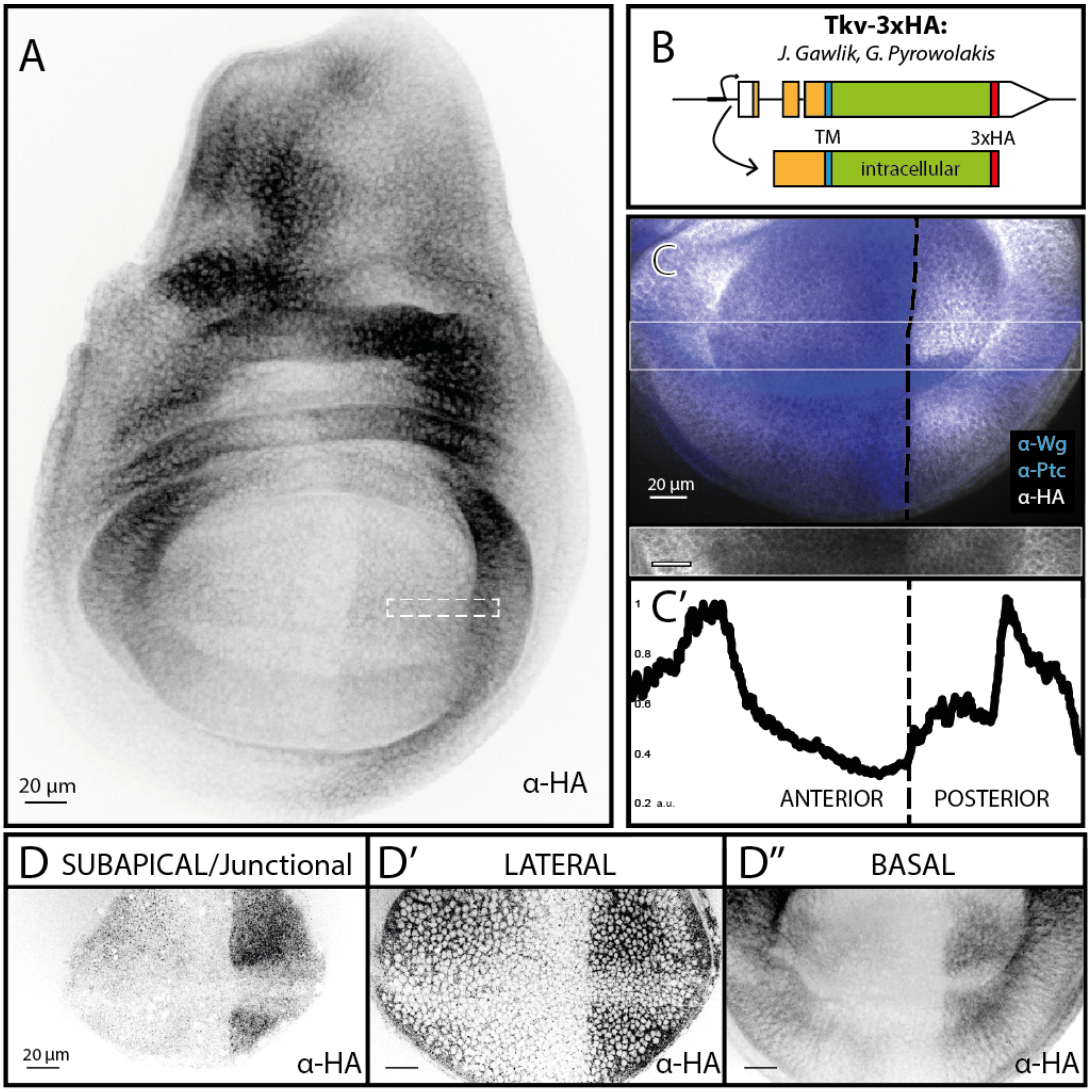

Figure 4.1 The expression pattern of Tkv-3xHA in the wing disc. A. Tkv-3xHA has a restricted expression pattern and is expressed in the notum, hinge and pouch region. The white dotted square outlines a representative dorsal posterior region, shown in **Figure 4.2**. **B.** Tkv-3xHA locus and the corresponding protein product are schematically depicted. Extracellular = orange. Intracellular = green. TM = transmembrane domain, blue. 3xHA tag = red. **C.** In the wing pouch, Tkv-3xHA precisely recapitulates the known *tkv* expression (see chapter 1.3.3.1). Wg and Ptc are used as markers for A/P (Ptc) and D/V (Wg) borders. **C′.** Profile of Tkv-3xHA fluorescence levels along the A/P axis. Tkv-3xHA shows high expression levels at the lateral regions of the pouch and lower expression levels in medial cells. The posterior medial cells experience higher levels than anterior medial cells. The area used for the intensity plot is indicated by the white box in (C). a.u.= arbitrary units. **D.** Z-projections of subapical/junctional, lateral or basal regions of Tkv-3xHA wing disc pouch. Tkv-3xHA is visualized through conventional α-HA antibody staining.

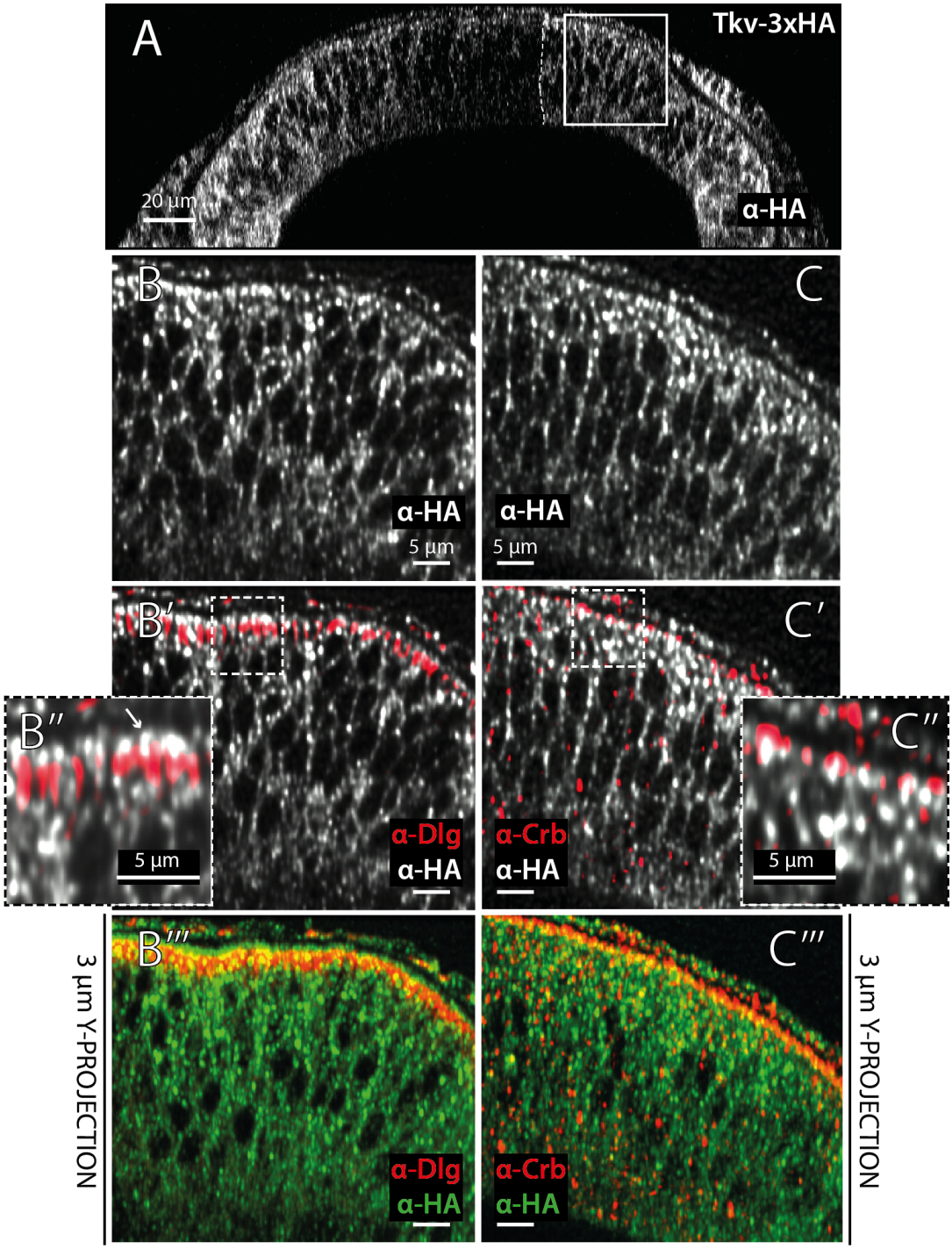

Figure 4.2 The subcellular localization of Tkv-3xHA in the wing disc pouch. A. Transversal cut of the dorsal compartment of a Tkv-3xHA wing disc Tkv-3xHA stained with α-HA antibody. The white square outlines a representative posterior region, as those shown in (B) and (C)**.** The white dotted line indicates the A/P compartment boundary. **B.** Tkv-3xHA (grey) is uniformly distributed throughout the basolateral side and localizes also apically above the junctional marker Dlg (red). **B′′** is a magnification of the inset in (B′). **B′′′** A 3 µm Y-projection shows that Tkv-3xHA (green) localizes above Dlg (red) and partially localizes at the SJs (yellow). **C.** Tkv-3xHA (grey) localizes to the level of Crb (red). **C′′** is a magnification of the inset in (C′). **C′′′** A 3 µm Y-projection shows that Tkv-3xHA (green) localizes to the level of Crb (red) and partially colocalizes (yellow).

Tkv-3xHA is expressed in the presumptive notum, the hinge and the pouch (Figure 4.1A). As expected, the Tkv-3xHA expression profile is not uniform along the A/P axis (see chapter 1.3.3.1). In the wing pouch, Tkv-3xHA levels are low in the central region and high laterally, with higher basal levels in the posterior medial region (Figure 4.1C,C'). This restricted expression pattern is consistent through the apical/junctional-basal axis of the wing disc pouch (Figure 4.1D). However, the presence of Tkv-3xHA to the apical compartment needs to be addressed using higher resolution imaging. For this reason, I looked at computed cross-sections of the wing disc pouch.

For the analysis of the subcellular localization of Tkv-3xHA, an area of the dorsal-posterior compartment of the wing disc pouch is shown (area outlined by a white square in Figure 4.1A and Figure 4.2A). However, the observed distribution was consistent for all the areas of the pouch. Tkv-3xHA signal was detected in the basolateral and apical compartments of wing disc pouch cells (Figure 4.2). In the basolateral compartment, Tkv-3xHA was distributed uniformly along the apical-basal axis (Figure 4.2B, C). Interestingly, Tkv-3xHA appeared partially excluded from the SJs (Figure 4.2B', B''). Tkv-3xHA localized also to the apical compartment of the wing disc cells, as shown by α-HA signal detected above the SJs, marked by Dlg (Figure 4.2B', B'', B''). Apical Tkv-3xHA localized to the level of the subapical marker Crb (Figure 4.2C, C', C''). However, Crb signal extends slightly above Tkv-3xHA, indicating that Tkv could be restricted to the AJs (Figure 4.2C'''). Interestingly, activation of Tkv was reported to be restricted to AJs in the GSCs niche (Michel et al., 2011).

In conclusion, Tkv-3xHA is present in both the basolateral and the apical compartment of the wing disc pouch.

4.1.2 The type-I receptor Sax localizes to the apical and basolateral compartment of the wing disc

The localization of the Sax protein has never been studied, however, this receptor was reported to be ubiquitously expressed in all tissues and all stages during development (Brummel et al., 1994).

Recently a collection of 880 transgenic fly lines, containing GFP-tagged proteins, was produced by using a fosmid-based approach (Sarov et al., 2015). Fosmid constructs allow the cloning of large genomic regions and in this study the average fosmid clone carried 36 kb (kilobase pairs). This resulted in the generation of constructs containing C-terminally GFP-tagged genes with most of the endogenous regulatory regions. All construct were inserted into a landing site on the third chromosome of the fly genome, generating transgenic fly lines carrying third copy reporter alleles (see chapter 1.6). Sax-GFP is among the lines generated (Figure 4.3B). The tagging cassette consists of a superfolder-GFP (sGFP), and other tags for affinity purification, attached to the C-terminal end of Sax. Notably, Sax-GFP fully rescues *sax* null mutants (Sarov et al., 2015).

Sax-GFP was visualized through conventional antibody staining, using α-GFP antibody. Sax-GFP is broadly expressed in the presumptive notum, hinge and pouch, with highest levels towards the anterior side of the disc (Figure 4.3A). In the wing pouch, Sax-GFP is high in the lateral region and lower in the medial region of the disc (Figure 4.3C, C'). The lateral levels are higher in the anterior compartment, whereas in the medial cells the basal levels are higher in the posterior compartment (Figure 4.3C, C'), resembling the *tkv* expression pattern. However, Sax-GFP is more broadly distributed, since the downregulation in the medial pouch cells is not as strong as what observed for Tkv-3xHA. The Sax-GFP expression pattern appears constant through the apical/junctional-basal axis of the wing disc pouch (Figure 4.3D).

To assess the subcellular localization of Sax-GFP with high resolution, I looked at computed cross-sections of the wing disc pouch and here I show a representative area of the wing disc pouch (indicated by the white square in Figure 4.3A and Figure 4.4A).

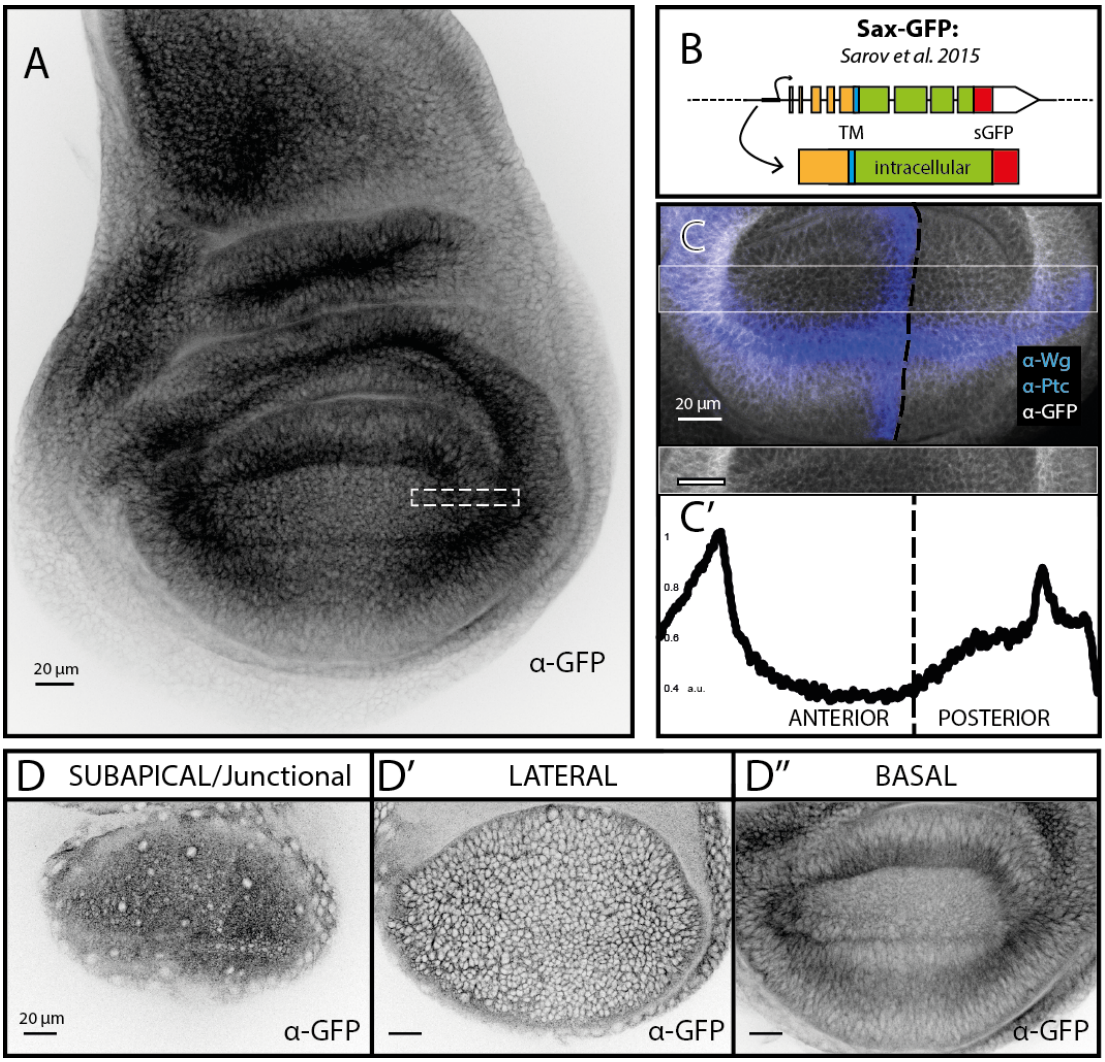

Figure 4.3 The expression pattern of Sax-GFP in the wing disc. A. Sax is expressed in the notum, hinge and pouch region. The white dotted square outlines a representative dorsal-posterior region, shown in **Figure 4.4**. **B.** Sax-GFP is a third copy reporter allele, generated in (Sarov et al., 2015). Extracellular=orange. Intracellular=green. TM= transmembrane domain, blue. sGFP tag= red. **C.** Sax-GFP levels are higher in the lateral regions of the wing pouch, in particular in the anterior compartment. Wg and Ptc are used as markers for A/P (Ptc) and D/V (Wg) boundaries. **C'.** Profile of Sax-GFP expression in the wing pouch. The area used for the intensity plot is indicated by the white box in (C). a.u.= arbitrary units. **D.** Z-projections of subapical, lateral or basal regions of a Sax-GFP wing disc pouch.

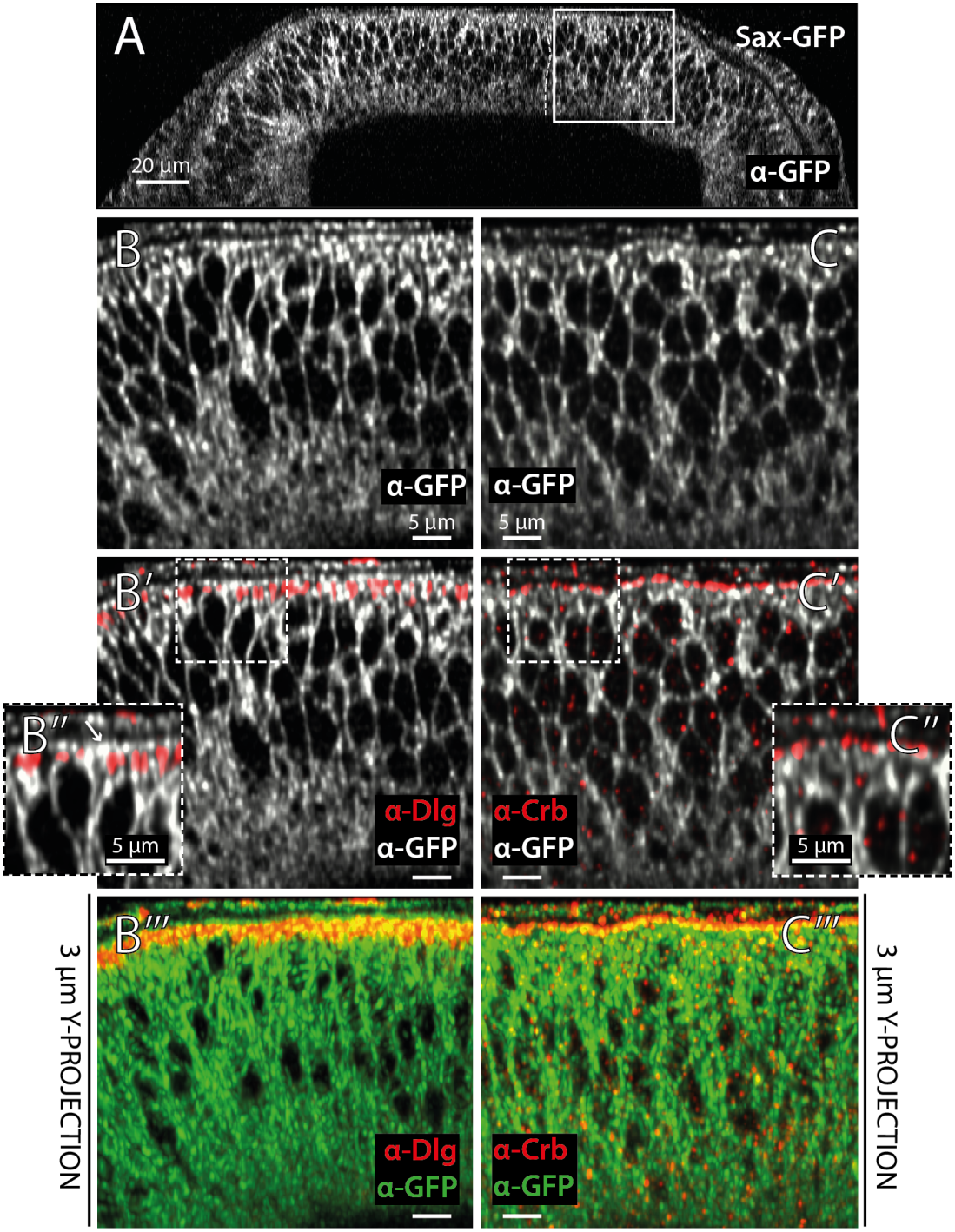

Figure 4.4 The subcellular localization of Sax-GFP in the wing disc pouch. A. Transversal cut of the dorsal compartment of Sax-GFP wing disc. The white square outlines a representative posterior region, as those shown in (B) and (C). The white dotted line indicates the A/P compartment boundary. **B.** Sax-GFP (grey) is uniformly distributed throughout the basolateral side and localizes above Dlg (red). **B''** is a magnification of the inset in (B'). **B'''** A 3 µm Y-projection shows that Sax-GFP (green) localizes apically above Dlg (red) and partially localizes at the SJs (yellow). **C.** Sax-GFP (grey) localizes at the level of Crb (red). **C''** is a magnification of the inset in (C'). **C'''** A 3 µm Y-projection shows that Sax-GFP (green) localizes to the level of Crb (red), showing partial colocalization (yellow).

Sax-GFP signal is detected in the basolateral and in the apical compartment of wing disc cells (Figure 4.4). Sax-GFP uniformly distributes along the apical-basal axis within the basolateral compartment, but is partially excluded from the SJs (Figure 4.4B, B''). Sax-GFP is also present in the apical compartment of the wing disc, as shown by α-GFP signal detected above the SJs (Figure 4.4B', B'', B'''). Similarly to what observed for Tkv-3xHA, the apical fraction of Sax-GFP could be restricted to the AJs, since it only partially overlaps with the subapical marker Crb (Figure 4.4C'', C'''). In conclusion, Sax-GFP localizes to both the basolateral and the apical compartment of the wing disc pouch.

4.1.3 The type-I receptor Babo localizes exclusively to the basolateral side of the wing disc

In *D. melanogaster* Babo is the only type-I receptor associated with the TGF-β/Activin branch of the superfamily. Loss of Babo was reported to affect wing disc size and cell proliferation (Brummel et al., 1998). Babo localization and expression have not been characterized and no antibody specific to Babo is available. A Babo-GFP third copy reporter allele was recently generated with the fosmid-based *in vivo* tagging method mentioned above and was reported to completely rescue *babo* mutant phenotype (Sarov et al., 2015) (Figure 4.5B). Babo-GFP was visualized through conventional antibody staining, using α-GFP antibody. In the wing disc, Babo-GFP was uniformly expressed at low levels in the notum, hinge and wing pouch. In addition to the uniform low levels, Babo-GFP is strongly expressed in a stripe of anterior pouch cells adjacent to the A/P boundary (Figure 4.5A, C, C'). Here, Babo-GFP is downregulated at the D/V boundary (Figure 4.5A, C). Babo-GFP is also expressed at high levels in a group of cells located at the anterior side of the notum (Figure 4.5A) and in a group of cells in the posterior compartment of the PM (data not shown). The expression pattern of Babo-GFP was

consistent throughout the apical-basal axis of the wing disc pouch (Figure 4.5D). However, when the distribution of Babo-GFP was inspected at higher resolution, Babo-GFP revealed to be excluded from the apical compartment of the wing disc pouch cells (Figure 4.6).

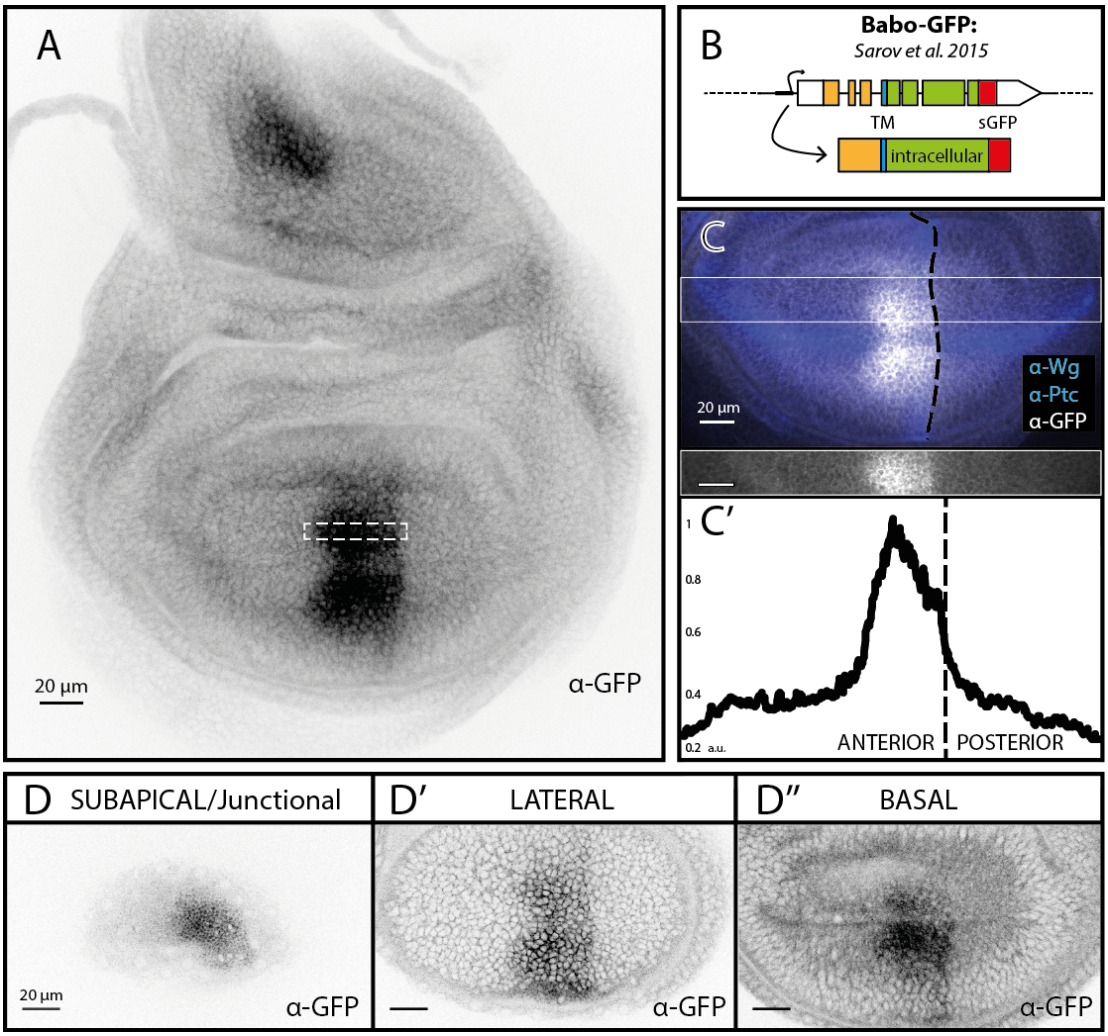

Figure 4.5 The expression pattern of Babo-GFP in the wing disc. A. Babo-GFP is expressed at high levels in a medial anterior stripe of the wing pouch and in a group of anterior notum cells. The white dotted square outlines a representative dorsal-anterior region, shown in **Figure 4.6**. **B.** Babo-GFP is a third copy reporter allele, generated in (Sarov et al., 2015). Extracellular=orange. Intracellular=green. TM= transmembrane domain, blue. sGFP tag= red. **C.** In the wing pouch, high levels of Babo-GFP are detected in a central stripe of anterior cells adjacent to the A/P boundary. Babo-GFP is downregulated at the D/V border. Wg and Ptc are used as markers for A/P (Ptc) and D/V (Wg) borders. **C′.** Expression profile of Babo-GFP. The area used for the intensity plot is indicated by the white box in (C). a.u.= arbitrary units. **D.** Z-projections of Babo-GFP located at the subapical/junctional, lateral or basal regions of the disc pouch.

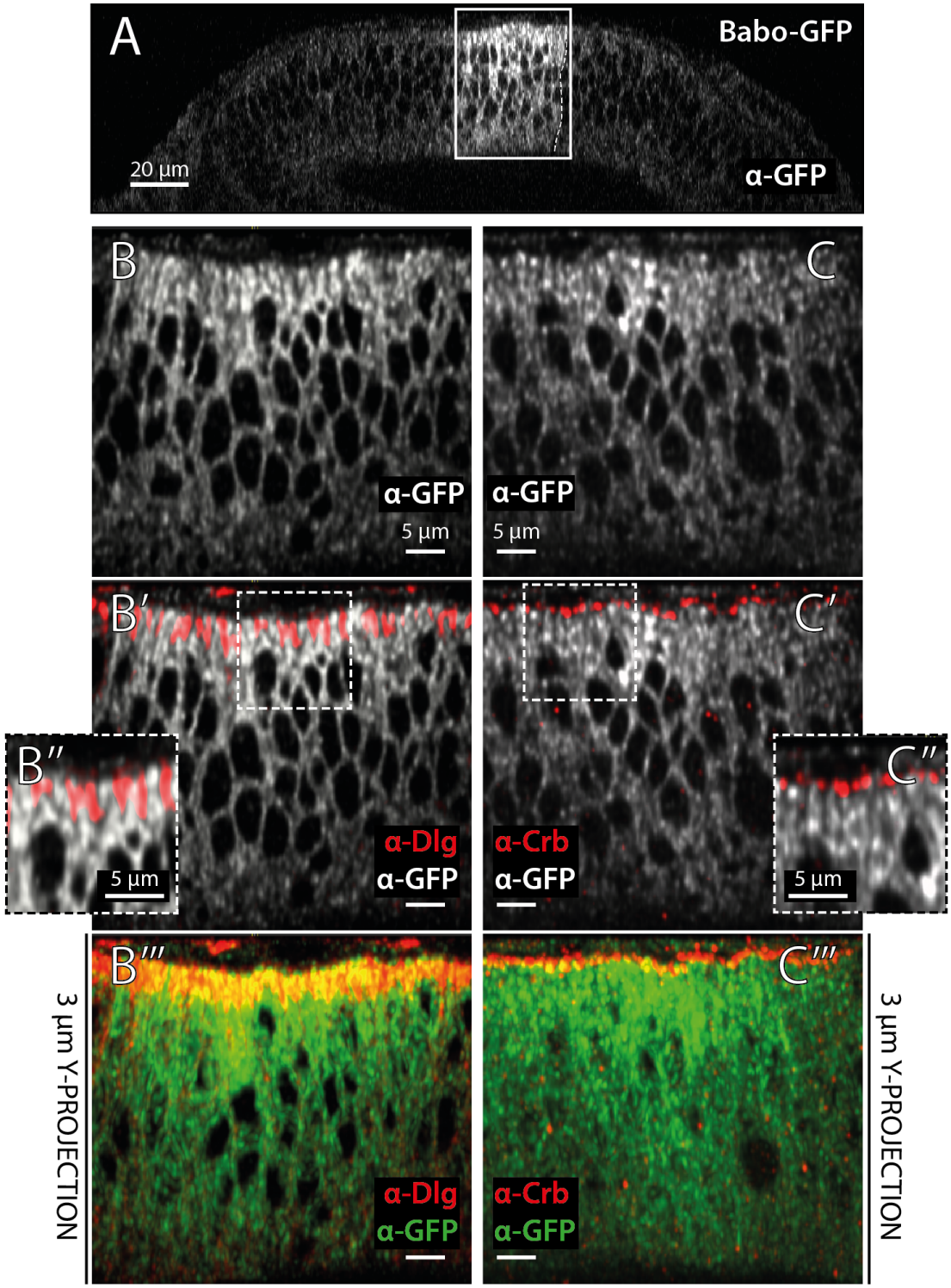

Figure 4.6 Subcellular localization of Babo-GFP. A. Transversal cut of the dorsal compartment of a Babo-GFP wing disc. The white square outlines a representative anterior region, as those shown in (B) and (C). The white dotted line indicates the A/P compartment boundary. **B.** Babo-GFP (grey) is unevenly distributed throughout the basolateral side and localizes at the same level, but not above, Dlg (red). **B''** is a magnification of the inset in B'. **B'''** A 3 µm Y-projection shows that Babo-GFP (green) localizes at the same level of Dlg (red) and colocalizes with it at the SJs (yellow). **C.** Babo-GFP (grey) localizes below Crb (red). **C''** is a magnification of the inset in C'. **C'''** A 3 µm Y-projection shows that Babo-GFP (green) localizes below Crb (red) and is excluded from the subapical region.

Babo-GFP distributes unevenly within the basolateral compartment, with increasing levels towards the junctional side (Figure 4.6B, B'). Babo-GFP localizes at the level of the SJs, but not above (Figure 4.6B, B''). Babo-GFP is not downregulated at the level of the SJs as was observed for Tkv-3xHA and Sax-GFP, and colocalizes with Dlg (Figure 4.6B''). Babo-GFP localizes below Crb and is excluded from the subapical region of the epithelial cells of the wing disc pouch (Figure 4.6C, C', C''). In conclusion, Babo-GFP localizes only to the basolateral compartment of the wing disc pouch and to the SJs, but is excluded from the apical compartment of the wing disc pouch cells.

4.1.4 The type-II receptor Punt localizes exclusively to the basolateral side of the wing disc

The type-II receptors are able to mediate signalling from both branches of the TGF-β superfamily (Zheng et al., 2003), however their positional bias could lead to a preferential association with a specific type-I receptor.

Punt is the main type-II receptor implicated in BMP signal transduction in the wing disc and it has also been associated with the TGF-β/Activin branch, acting together with the type-I receptor Babo (see chapter 1.3.3.4). Despite the fundamental role of Punt in the wing disc, the localization of Punt has not been reported. Here I characterize the localization of a GFP-tagged Punt transgenic line, generated through landing site-mediate integration of a 20.3 kb genomic region, containing the *punt* gene and most of its regulatory regions (obtained from Micheal O'Connor, unpublished) (Figure 4.7B).

Using α-GFP conventional antibody staining, Punt-GFP was detected in all cells of the wing disc. The expression levels of Punt-GFP are rather uniform throughout the disc, but higher levels were detected in the central wing pouch (Figure 4.7A, C, C'). Punt-GFP localizes uniformly through the basolateral axis of the wing disc pouch, but is absent from the

subapical/junctional region (Figure 4.7D). This observation was confirmed by high resolution imaging, as shown by cross section of a dorsal-posterior pouch area of a Punt-GFP wing disc (area indicated by the white square in Figure 4.7A and Figure 4.8A).

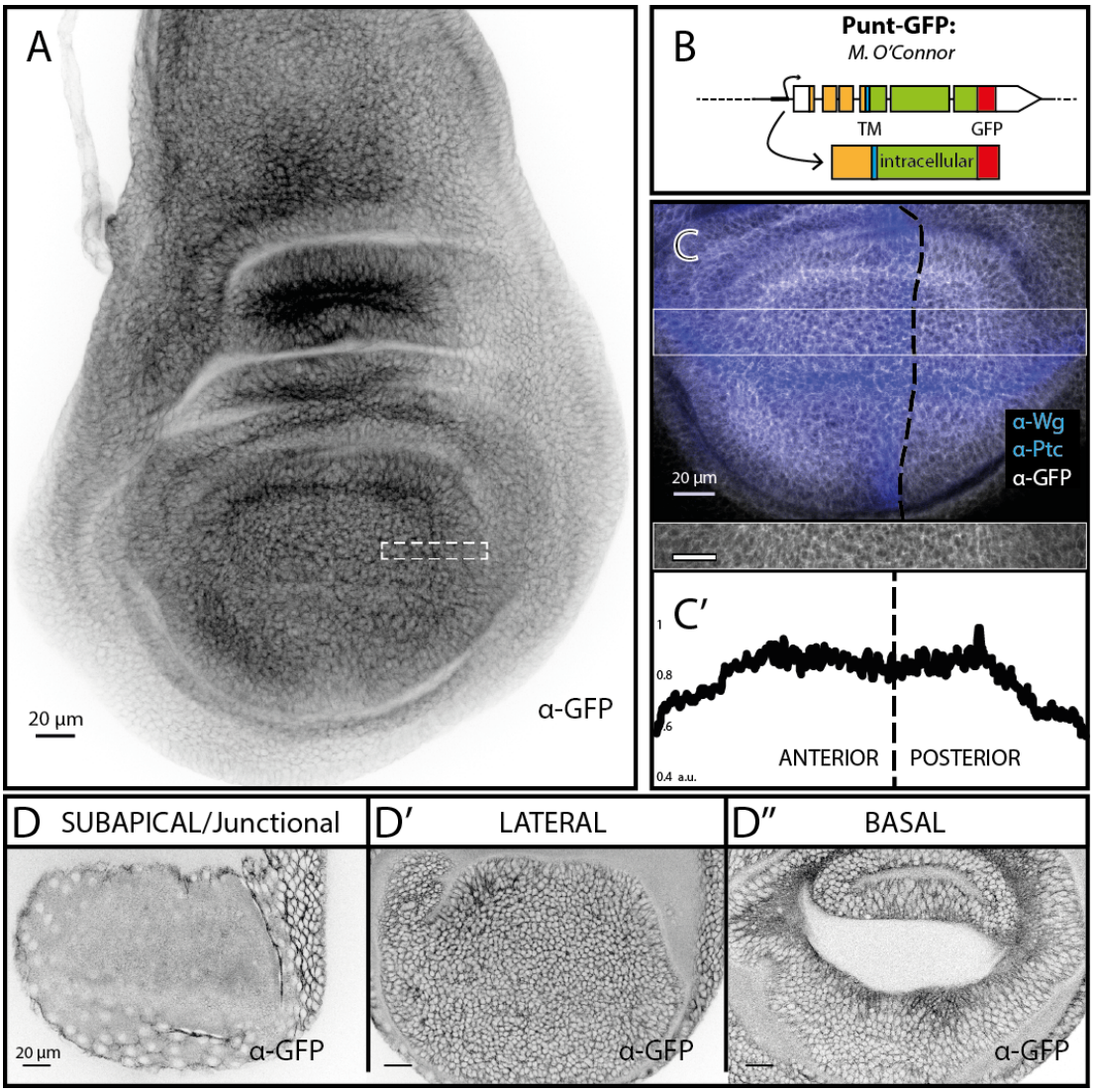

Figure 4.7 The expression pattern of Punt-GFP in the wing disc pouch. A. Punt-GFP is broadly expressed in the wing disc. The white dotted square outlines a representative dorsal posterior region, shown in **Figure 4.8**. **B.** Punt-GFP locus and corresponding protein product are depicted. Extracellular=orange. Intracellular=green. TM= transmembrane domain, blue. GFP tag= red. **C.** Punt-GFP is broadly distributed in the wing disc pouch, with higher levels in medial cells. Wg and Ptc are used as markers for A/P (Ptc) and D/V (Wg) borders. **C′.** Punt-GFP expression profile in the wing pouch. The area used for the intensity plot is indicated by the white box in (C). a.u.= arbitrary units. **D.** Z-projections of Punt-GFP located at the subapical/junctional, lateral or basal regions of the disc pouch.

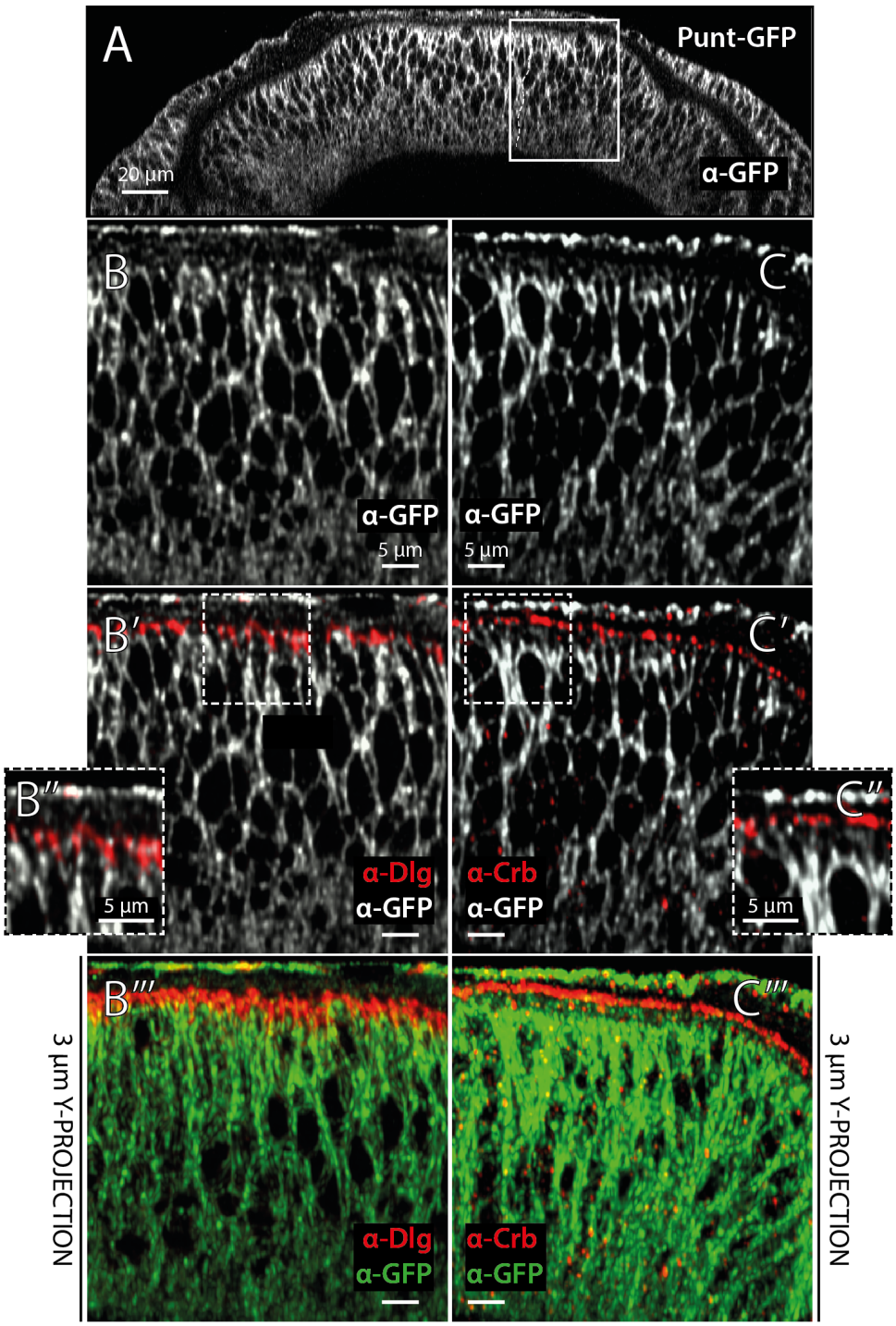

Figure 4.8 Subcellular localization of Punt-GFP. A. Transversal cut of the dorsal compartment of Punt-GFP wing disc. The white square outlines a representative posterior region, as shown in B and C. The white dotted line indicates the A/P compartment boundary. **B.** Punt-GFP (grey) is uniformly distributed throughout the basolateral side, however is partially excluded from the SJs (Dlg, red). **B''** is a magnification of the inset in (B'). **B'''** A 3 µm Y-projection shows that Punt-GFP (green) localizes at the basolateral compartment and does not colocalize with Dlg (red). **C.** Punt-GFP (grey) localizes below Crb level (red). **C''** is a magnification of the inset in (C'). **C'''** A 3 µm Y-projection shows that Punt-GFP (green) does not colocalizes with Crb (red).

Punt-GFP signal was detected exclusively in the basolateral compartment of wing disc cells (Figure 4.8). Punt-GFP distributes evenly within the basolateral compartment, with no signal detected above the SJs (Figure 4.8B, B', B''). Punt-GFP is partially excluded from the SJs, as seen by absence of colocalization with Dlg (Figure 4.8B, B''). Moreover, Punt-GFP localizes below Crb and is excluded from the subapical region of the wing pouch cells (Figure 4.8C, C', C'').

In conclusion, Punt-GFP localizes to the basolateral compartment of the wing disc pouch epithelium. These data recapitulate unpublished observations made in overexpression conditions, using a UAS-driven Punt-GFP construct (Mundt & O'Connor, unpublished).

4.1.5 The type-II receptor Wit shows apical enrichment and basolateral localization

Only two type-II receptors have been discovered in *D. melanogaster*. Type-I receptors depend on type-II receptors to activate the signalling cascade and, since Punt appears to be excluded from the apical compartment, it is important to know whether Wit could fulfil the type-II receptor functions in the apical domain of the wing disc cells.

The Wit-GFP third copy reporter allele used for this study was generated with the fosmid-based *in vivo* tagging method introduced before (Sarov et al., 2015) (Figure 4.9B). Using α-GFP conventional antibody staining, Wit-GFP was detected in the wing disc, showing a broad expression in the wing pouch, hinge and notum (Figure 4.9A). Wit-GFP recapitulates the known *wit* expression pattern visualized by *in situ* hybridization in the wing disc (Marqués et al., 2002) (see chapter 1.3.3.4). In the notum, Wit-GFP is upregulated in a large area along the A/P boundary (Figure 4.9A, C, C'). Wit-GFP is expressed at high levels in the wing pouch, with highest levels in the

centre of the pouch and decreasing levels towards the lateral regions (Figure 4.9C'). When Wit-GFP expression was analysed through the apical-basal axis of the wing disc pouch, an enrichment of the subapical/junctional fraction was clearly visible (Figure 4.9D).

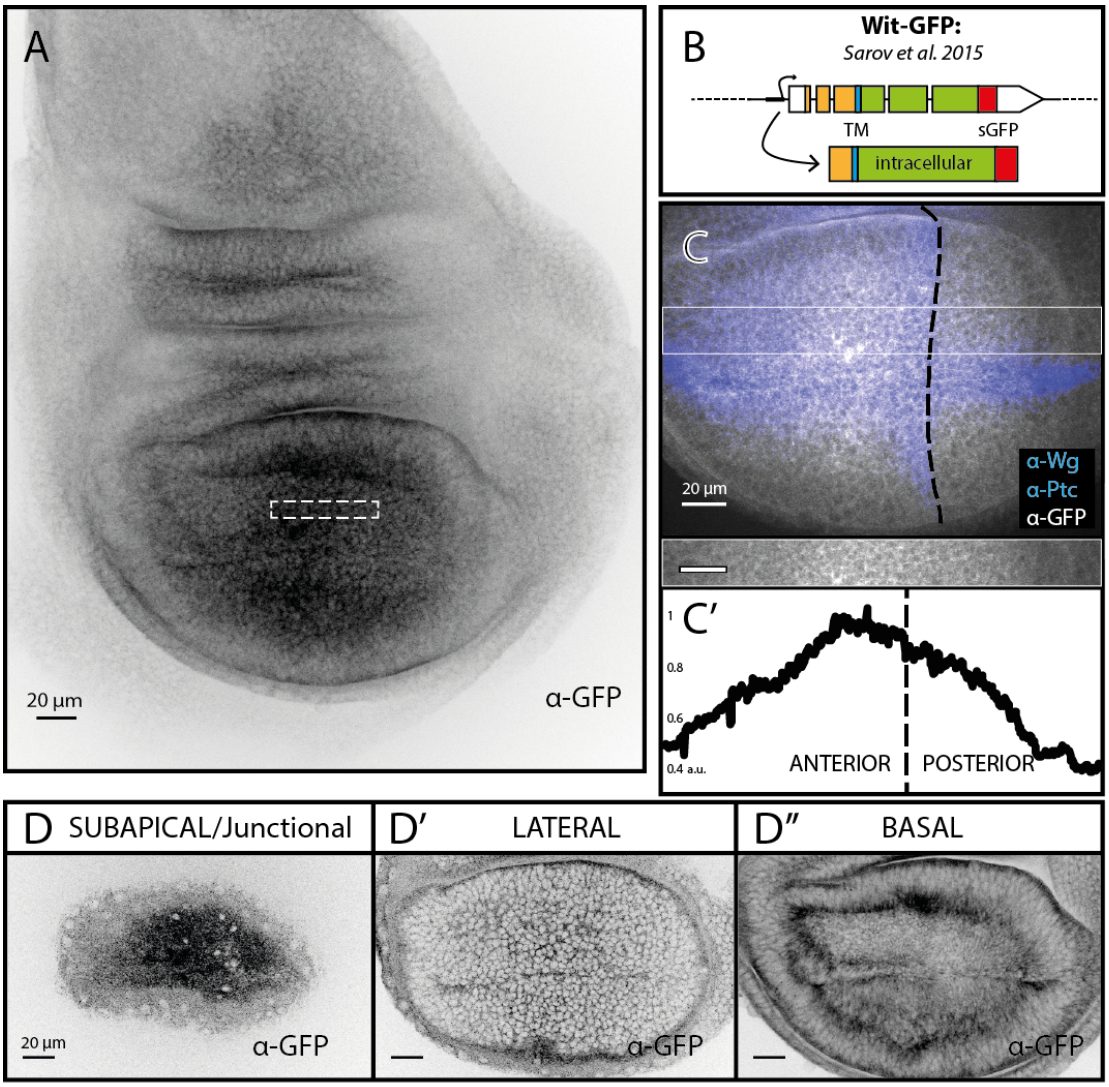

Figure 4.9 The expression pattern of Wit-GFP. A. Wit-GFP recapitulates *wit* expression pattern **(Marqués et al., 2002)**. The white dotted square outlines a representative dorsal medial region, shown in **Figure 4.10**. **B.** Wit-GFP is a third copy reporter allele, generated in (Sarov et al., 2015). Extracellular=orange. Intracellular=green. TM= transmembrane domain, blue. sGFP tag= red. **C.** In the wing pouch, Wit-GFP is higher in the central region and decreases laterally. Wg and Ptc are used as markers for A/P (Ptc) and D/V (Wg) borders. **C'.** Profile of Wit-GFP expression in the wing pouch. The peak of intensity corresponds to an area of anterior medial cells. The area used for the intensity plot is shown by the white box in (C). a.u.= arbitrary units. **D.** Z-projections of a Wit-GFP wing disc at the subapical/junctional, lateral or basal regions of the disc pouch.

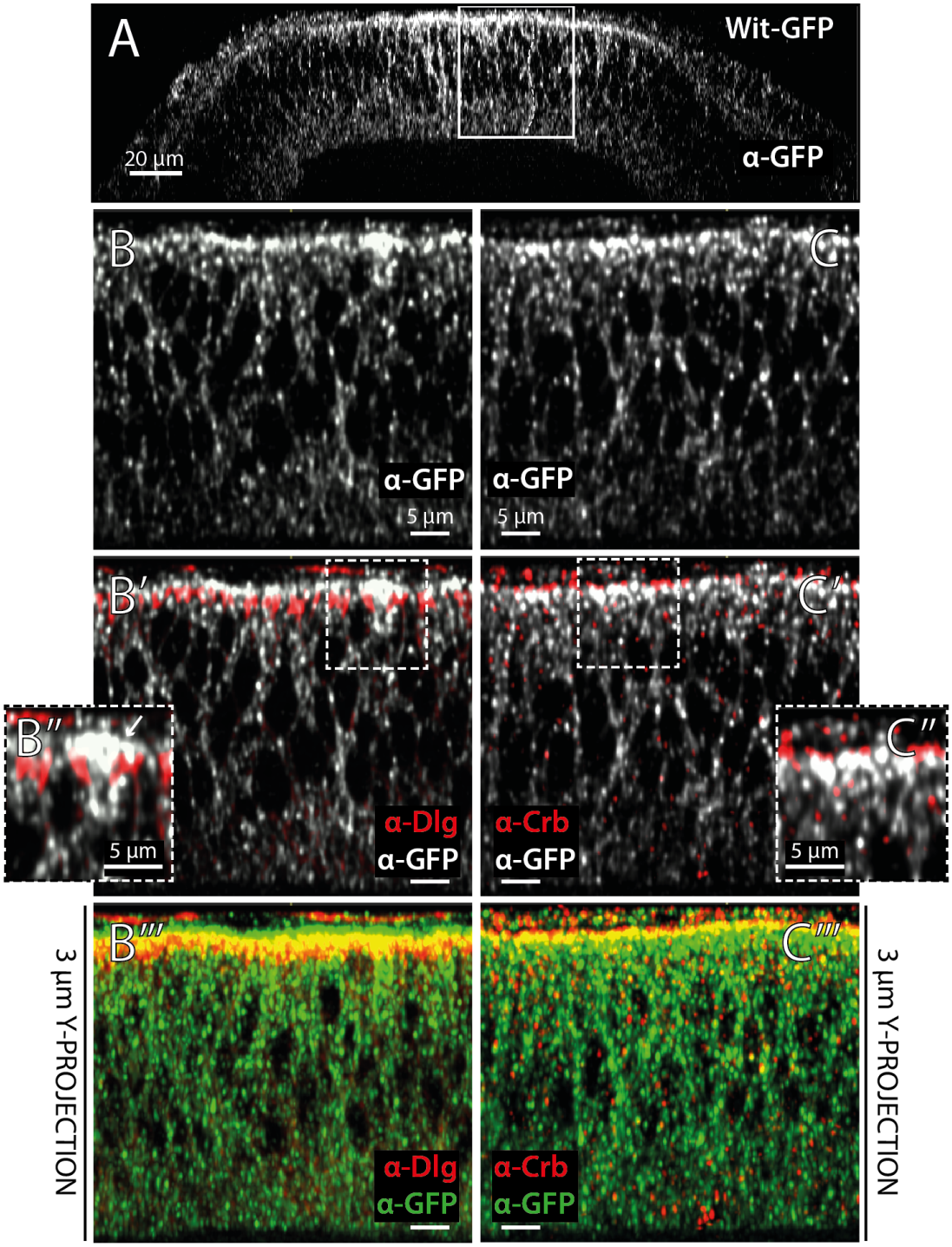

Figure 4.10 Subcellular localization of Wit-GFP. A. Transversal cut of the dorsal compartment of a Wit-GFP wing disc. The white square outlines a representative medial region, as those shown in B and C. The white dotted line indicates the A/P compartment boundary. **B,** Wit-GFP (grey) is present in the basolateral compartment and is enriched at the apical compartment, above Dlg (red). **B''** is a magnification of the inset in B'. **B'''** A 3 µm Y-projection shows that Wit-GFP (green) localizes above Dlg (red) and partially localizes at the SJs (yellow). **C, C', C''** Wit-GFP (grey) is enriched at the apical side and localizes at the same level of Crb (red). **C''** is a magnification of the inset in **C'. C'''** A 3 µm Y-projection shows that Wit-GFP (green) localizes at the same level of Crb (red) and partially colocalize (yellow).

Indeed, when analysed at subcellular resolution, Wit-GFP showed to be characterized by a prominent apical fraction (Figure 4.10). Nevertheless, Wit-GFP signal is detected also in the basolateral compartment (Figure 4.10B, B', C, C'). Wit-GFP clearly localizes above the SJs, marked by Dlg (Figure 4.10B'') and at the same level of Crb (Figure 4.10C'', C'''). Wit-GFP strongly colocalizes with Crb at the subapical region of the wing disc cells (Figure 4.10C''').

In conclusion, Wit-GFP is enriched at the apical compartment of the wing disc pouch and is the only TGF-β type-II receptor localized in this compartment. Thus, in the apical compartment the TGF-β signal transduction depends on Wit. These results recapitulate what previously observed using a UAS-driven Wit-GFP (Mundt & O'Connor, unpublished).

4.1.6 The glypicans Dally and Dlp localize to the apical and the basolateral side

Glypicans are molecules belonging to the heparan sulfate proteoglycan family and they are critically involved in the regulation of several signalling pathways. Only two glypicans have been found in *D. melanogaster*, Dally and Dlp. These molecules have been implicated in the control of the BMP signalling pathway, among others, possibly by enhancing ligand spreading or by acting as co-receptors (see chapter 1.3.3.5). Two protein trap lines (see chapter 1.6) were used to analyse the localization of the glypicans, Dally-YFP and Dlp-YFP (CPTI, Lowe et al., 2014; Lye et al., 2014) (Figure 4.11B and Figure 4.13B). Dally-YFP and Dlp-YFP were detected using α-GFP conventional antibody staining, since this antibody recognises a shared sequence between YFP and GFP. The expression of Dally-YFP partially recapitulates what was observed with a *dally-lacZ* enhancer trap line and *in situ* hybridization (Fujise et al., 2001) (see chapter 1.3.3.5). Dally-YFP is

broadly expressed in the wing disc and is upregulated in a large area of the anterior notum and the anterior hinge region (Figure 4.11A).

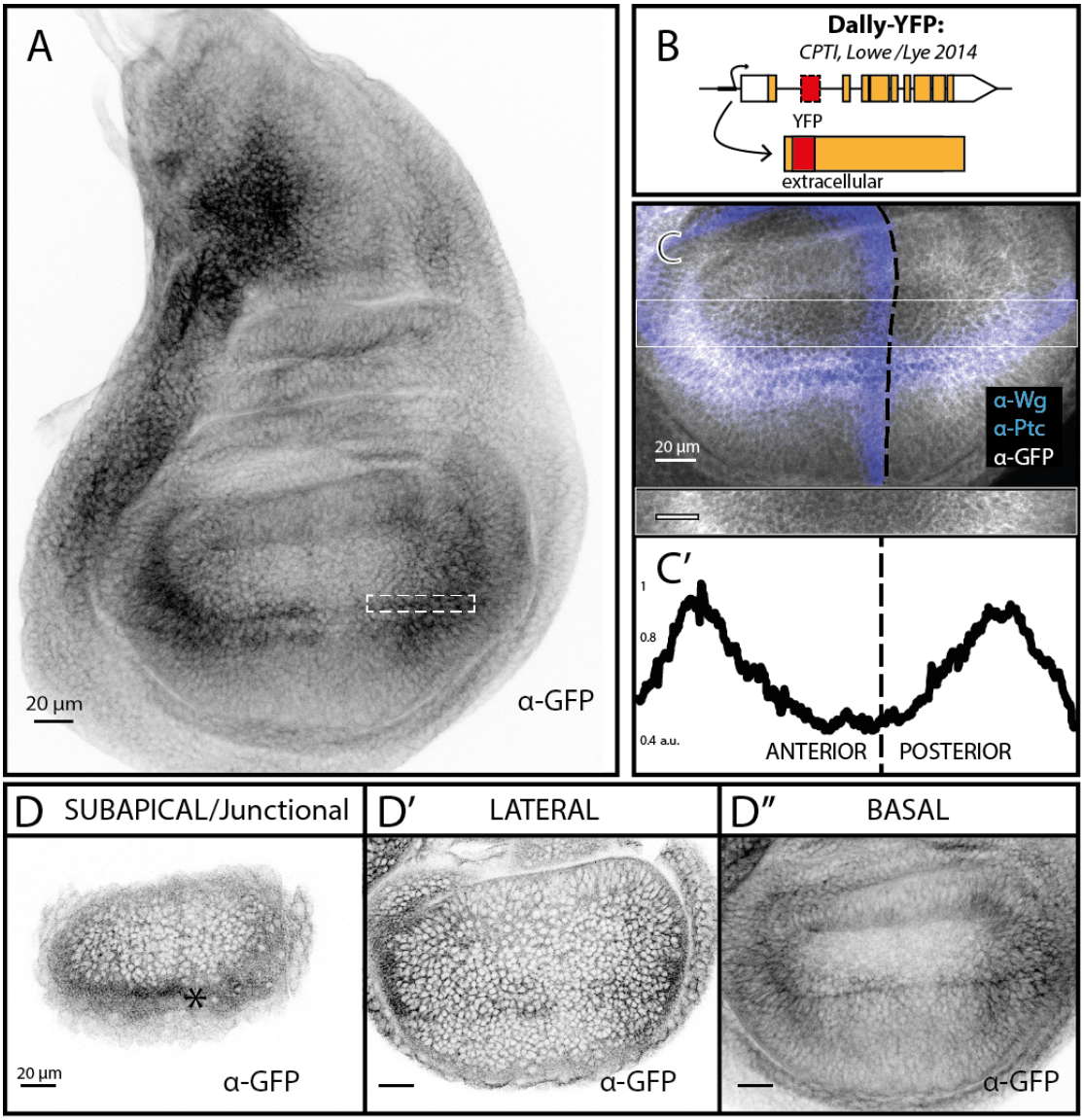

Figure 4.11 The expression pattern of Dally-YFP in the wing disc. A. Dally-YFP is upregulated in the anterior notum and hinge and along the D/V border of the wing pouch. The white dotted square outlines a representative region, shown in **Figure 4.12**. **B.** Dally-YFP is a protein trap line, generated in the Cambridge Protein Trap Insertions project (CPTI). The *dally* locus was modified by insertion of an artificial YFP exon in the first intron. Extracellular=orange. YFP tag=red. **C.** In the wing pouch, Dally-YFP is expressed at higher levels in the lateral regions and in a stripe of cells at both sides of the D/V boundary. However Dally-YFP is repressed at the D/V boundary. Wg and Ptc are used as markers for A/P and D/V borders. **C′.** Expression profile of Dally-YFP in the wing disc pouch. The area used for the intensity plot is outlined by the white box in (C). a.u.= arbitrary units. **D.** Z-projections of a Dally-YFP wing disc at the subapical/junctional, lateral or basal regions of the disc pouch.

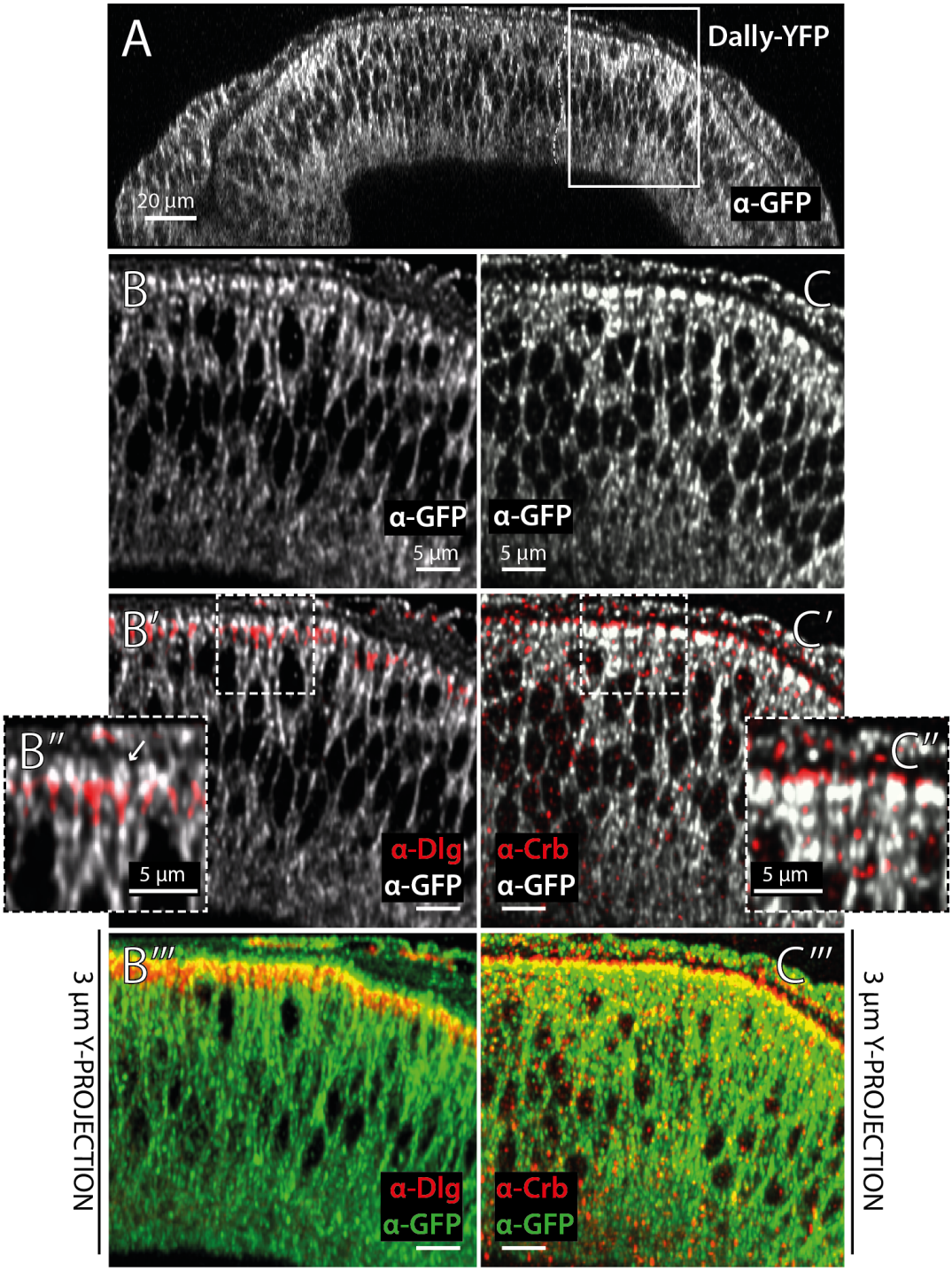

Figure 4.12 Subcellular localization of Dally-YFP. A. Transversal cut at the position of the D/V boundary of a Dally-YFP wing disc. The white square outlines a representative posterior region, as those shown in B and C. The white dotted line indicates the A/P compartment boundary. **B,** Dally-YFP (grey) is uniformly distributed within the basolateral side and localizes above Dlg (red). **B′′** is a magnification of the inset in B′. **B′′′** A 3 µm Y-projection shows that Dally-YFP (green) localizes above Dlg (red) and partially localizes to the SJs (yellow). **C.** Dally-YFP (grey) localizes at the same level of Crb (red). **C′′** is a magnification of the inset in C′. **C′′′** A 3 µm Y-projection shows that Dally-YFP (green) localizes at the same level of Crb (red) and partially colocalizes with Crb (yellow).

In the wing pouch, Dally-YFP is higher along the D/V boundary and in the lateral regions (Figure 4.11C, C'). However, in contrast to previous reports, Dally-YFP is not upregulated along the A/P boundary (Fujise et al., 2001). This discrepancy is likely due to post-transcriptional regulation. Dally-YFP expression is consistent along the apical-basal axis of the wing disc pouch, showing higher levels along the D/V boundary and at the lateral region (Figure 4.11D). When investigated at subcellular resolution, Dally-YFP signal was detected in both the basolateral and apical compartment of wing disc cells (Figure 4.12). Dally-YFP distributes uniformly within the basolateral compartment and is enriched at the apical compartment of the wing disc cells (Figure 4.12B, B', C, C'). Dally-YFP localizes above the SJs, marked by Dlg (Figure 4.12B'') and at the same level of Crb (Figure 4.12C'', C''').

In conclusion, Dally-YFP is present in both the basolateral and the apical compartments of the wing disc pouch cells.

Dlp-YFP is broadly expressed in the wing disc, with higher levels towards the anterior side of the disc and in the wing pouch (Figure 4.13A). In the notum, Dlp-YFP is expressed at higher levels in a group of anterior cells (Figure 4.13A). In the wing pouch, Dlp-YFP is strongly upregulated in the dorsal-anterior region and is downregulated at the D/V boundary (Figure 4.13C, C'). The high Dlp-YFP levels observed in the anterior compartment are due to upregulation by Hh signalling (Gallet et al., 2008), whereas the downregulation along the D/V boundary was reported to be the consequence of Wg signalling (Han, 2005) (see chapter 1.3.3.5).

This specific Dlp-YFP expression pattern is evident in the lateral regions of the wing imaginal disc cells (Figure 4.13D). Indeed, when analysed with high resolution, the lateral fraction of Dlp-YFP was observed as the most prominent one (Figure 4.14B, B'). Dlp-YFP uniformly distributes and localizes at high levels to the basolateral compartment, but is partially excluded from

the SJs (Figure 4.14B, B''). Dlp-YFP signal was detected also in the apical compartment of wing disc cells, as shown by α-GFP signal detected above the SJs, marked by Dlg (Figure 4.14B', B'', B''').

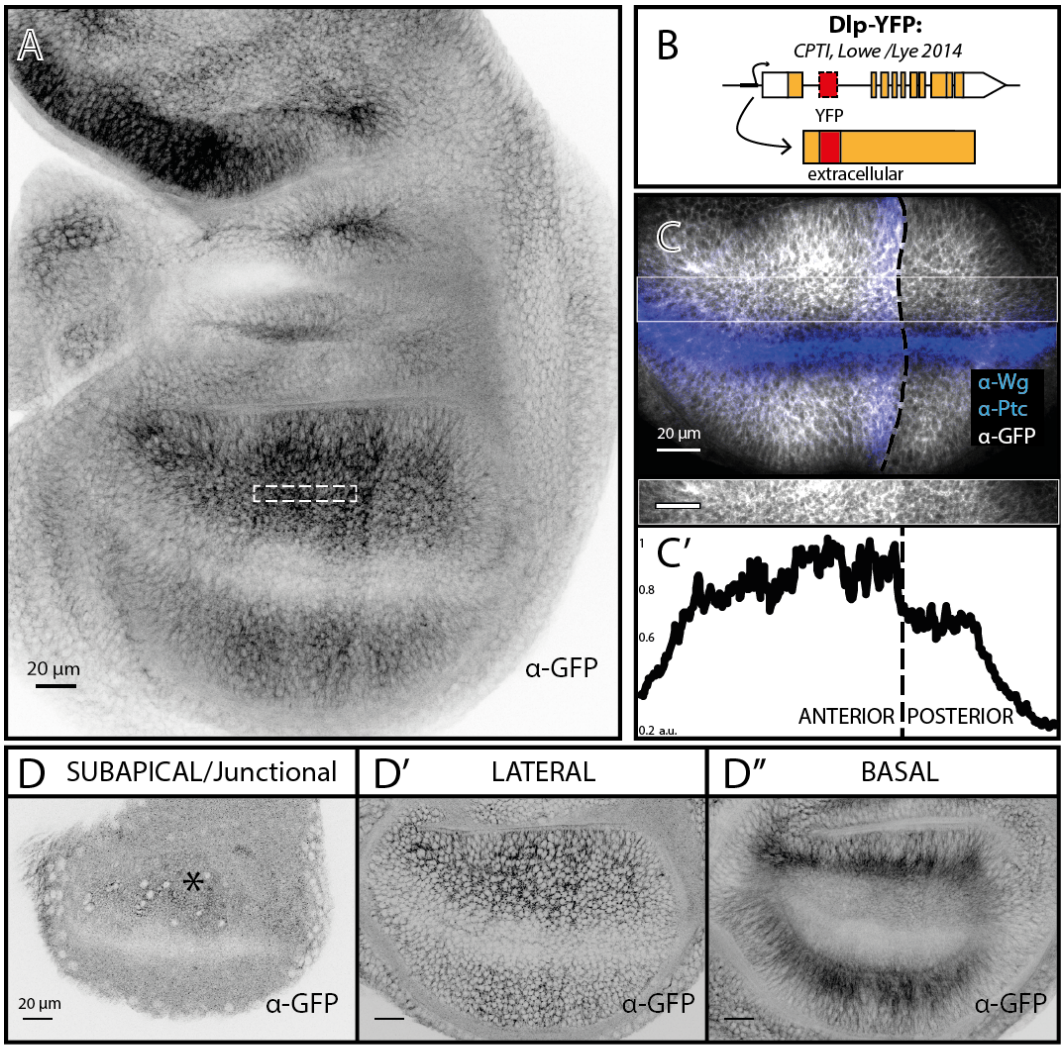

Figure 4.13 The expression pattern of Dlp-YFP in the wing disc. A. Dlp-YFP is upregulated towards the anterior side of the wing disc, with peaks of expression in a anterior notum region and in the dorsal anterior pouch. The white dotted square outlines a representative dorsal-anterior region, shown in **Figure 4.14**. **B.** Dlp-YFP is a protein trap line, generated in the Cambridge Protein Trap Insertions project (CPTI). The *dlp* locus is modified by insertion of an artificial YFP exon in the first intron. Extracellular=orange. YFP tag=red. **C.** Dlp-YFP is expressed at higher levels in the dorsal-anterior pouch region, but is repressed along the D/V border. Wg and Ptc are used as markers for A/P and D/V borders. **C'.** Dlp-YFP is expressed at higher levels in the anterior region of the wing pouch. The area used for the intensity plot is indicated by the white box in (C). a.u.= arbitrary units. **D.** Z-projections of a Dlp-YFP wing disc at the subapical, lateral or basal regions of the disc pouch.

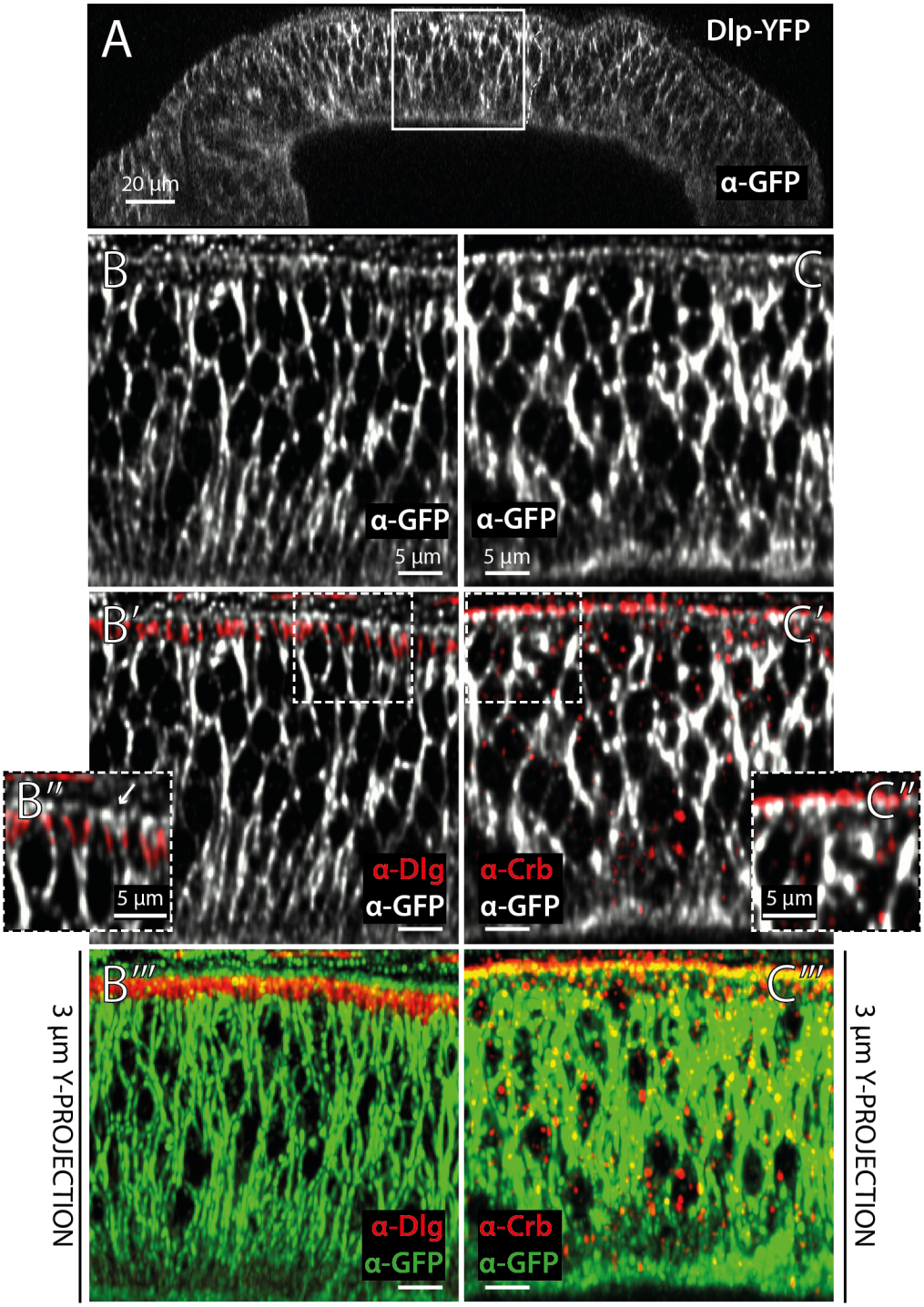

Figure 4.14 Subcellular localization of Dlp-YFP. A. Transversal cut of the dorsal compartment of Dlp-YFP wing disc. The white square outlines a representative anterior region, as those shown in (B) and (C)**.** The white dotted line indicates the A/P compartment boundary. **B.** Dlp-YFP (grey) strongly localizes to the basolateral compartment and localizes above Dlg (red). **B′′** is a magnification of the inset in (B′). **B′′′** A 3 µm Y-projection shows that Dlp-YFP (green) localizes above Dlg (red) and partially localizes at the SJs (yellow). **C.** Dlp-YFP (grey) localizes at the same level of Crb (red). **C′′** is a magnification of the inset in (C′). **C′′′** A 3 µm Y-projection shows that Dlp-YFP (green) localizes at the same level of Crb (red) and partially colocalizes with Crb (yellow).

Dlp-YFP localizes at the same level of the subapical marker Crb (Figure 4.14C, C', C'') and showing extensive colocalization at the subapical region (Figure 4.14C'''').

In conclusion, Dlp-YFP localizes to both the apical and the basolateral compartment of the wing disc pouch. These results recapitulate previous reports (Gallet et al., 2008), where extracellular α-Dlp staining was used to visualize the apical Dlp fraction.

4.1.7 Summary

Taken together, these results show that receptors and co-receptors belonging to the TGF-β superfamily are differentially localized along the apical/basolateral axis (Figure 4.15).

The type-I receptors belonging to the BMP branch, Tkv and Sax, are present in both compartments of the wing pouch epithelial cells. In contrast, the type-I receptor Babo, associated with the TGF-β/Activin branch, shows a subcellular bias towards the basolateral side and appears to be excluded from the apical compartment (Figure 4.15A, A').

Punt, one of the type-II receptors, is excluded from the apical compartment and is only observed basolateral. In contrast, the other type-II receptor Wit shows apically enrichment, but is also present in the basolateral compartment (Figure 4.15 B, B').

The glypicans Dally and Dlp are present in both compartments, localizing to both apical and basolateral sides (Figure 4.15C, C'). However, while apical Dally levels are enriched, Dlp localizes more prominently to the basolateral compartment.

In summary, I have investigated the subcellular localization of all Drosophila TGF-β receptors in a systematic manner. I have shown that TGF-β receptors and co-receptors localize to different subcellular compartments.

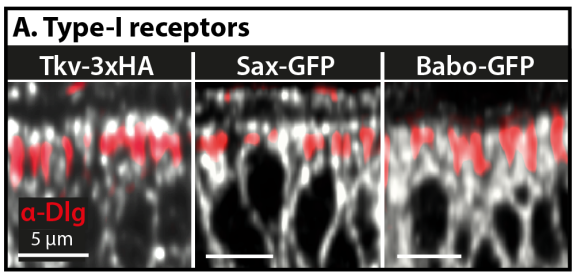

A′. Type-I receptors localization table

Type-I r.	Apical	Basolateral
Tkv-3xHA	✔	✔
Sax-GFP	✔	✔
Babo-GFP	✖	✔

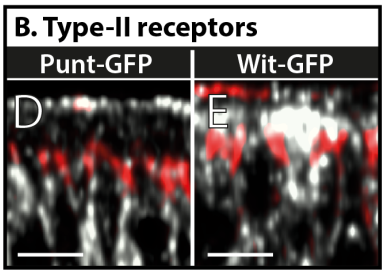

B′. Type-II receptors localization table

Type-II r.	Apical	Basolateral
Punt-GFP	✖	✔
Wit-GFP	✔	✔

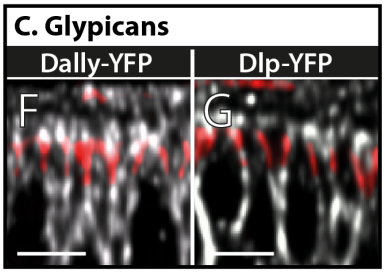

C′. Glypicans localization table

Glypicans	Apical	Basolateral
Dally-YFP	✔	✔
Dlp-YFP	✔	✔

Figure 4.15 The subcellular localization of the TGF-β receptors and the glypicans Dally and Dlp. (Left) Distribution of the TGF-β type-I (**A**) and type-II (**B**) receptors and of the glypicans Dally and Dlp (**C**) in a representative portion of the wing disc epithelium. The border between apical and basolateral compartment is labeled by Dlg (red), marking the SJs. **(Right)** Tables summarizing the subcellular localization of type-I (**A′**) and type-II receptors (**B′**) and of the glypicans (**C**).

In the following section, I will test approaches to mislocalize these receptors along the apical-basal axis in order to understand the function of the observed localization bias.

4.2 Scaffold-bound nanobodies as a tool for mislocalizing transmembrane proteins

A nanobody specific to GFP (vhhGFP4, Rothbauer et al., 2006) has been extensively used for cell and developmental biology applications. Importantly, vhhGFP4 retains its activity and specificity *in vivo* when fused to other proteins (Rothbauer et al., 2007). We attempted to functionalize vhhGFP4 by fusing it with different protein domains, in order to degrade (Caussinus et al., 2012), trap (Harmansa et al., 2015), phosphorylate (Roubinet and Caussinus, unpublished) or mislocalize GFP-tagged proteins.

S. Harmansa and E. Caussinus have generated scaffold-bound nanobodies (SBNs) that localize to specific domains along the apical-basal axis. In order to selectively localize the nanobody to either the apical or the basolateral membrane, vhhGFP4 was fused to scaffold-proteins of known subcellular localization, resulting in differential and specific targeting of the membrane-bound anti-GFP nanobody. In the following, I want to investigate the potential of these polarized SBNs in mislocalizing GFP/YFP-tagged transmembrane proteins.

In order to investigate the mislocalization potential of these tools, I combined the SBNs with different GFP/YFP-tagged transmembrane proteins that distribute in a polarized fashion, and screened for mislocalization along the apical-basal axis. I will show that SBNs can interact and change the localization of the uniformly distributed membrane-bound PH-GFP, of the basolateral protein Nrv1 and of the apical determinant Crb. Moreover, in the context of this thesis the purpose of using SBNs is to obtain mislocalization of the TGF-β receptors and co-receptors along the apical-basal axis. In particular, I will show the results I obtained with Tkv-YFP, Punt-GFP and Dally-YFP. The results shown are preliminary and further experiments are required to conclusively interpret the data obtained.

4.2.1 The scaffold-bound nanobodies toolset

S. Harmansa and E. Caussinus originally developed the SBNs in order to study the role of morphogen dispersal along the apical-basal axis of polarized epithelial tissues. To choose the scaffold, proteins that exhibit a strong polarization and that have a simple topology (only one transmembrane domain) were considered as best candidates. Additionally, the overexpression of the scaffold protein shouldn't affect development or tissue polarity – since the SBNs will be expressed at high levels using the UAS/Gal4 system (A. H. Brand & Perrimon, 1993). Therefore, polarity determinants were excluded as possible candidates, based on the fact that most of them exhibit a clear overexpression phenotype, as they influence the development of epithelial polarization.

The toolset generated consists of three different SBNs: (1) one with uniform, non-biased distribution along the apical/basolateral membranes (vhhGFP4::CD8, or SBN-AB_extra), (2) one apically enriched (vhhGFP4::T48-Baz, or SBN-A_extra), (3) one exclusively basolateral (vhhGFP4::Nrv1, or SBN-B_extra) (Figure 4.16). These three SBNs are characterized by a specific membrane topology with the anti-GFP nanobody exposed to the extracellular space (SBN_extra) and an intracellular mCherry tag used to visualize the tool (Figure 4.16B, C, D). SBN-A was generated in an additional version with reverse topology, so that the anti-GFP nanobody is present and works intracellularly. I will refer to this tool as SBN-A_intra (Figure 4.16A). I will shortly describe the generation and subcellular localization the SBNs toolset in the following chapter.

4.2.1.1 Choice of scaffold proteins for the SBNs

The SBNs where initially generated to trap secreted proteins. A membrane-bound anti-GFP nanobody with uniform distribution along the

apical/basolateral axis (SBN-AB_extra) was the first SBN successfully used to block morphogen spreading *in vivo* (Harmansa et al., 2015). SBN-AB_extra was generated by fusing vhhGFP4 to the coding region of the mouse CD8 transmembrane protein (Figure 4.16C). This construct localizes uniformly along the apical and basolateral membrane and it reaches above the SJs (Figure 4.16C, C').

In order to obtain SBN-A, vhhGFP4 was initially fused to the T48 protein (Figure 4.16A, B). T48 is a transmembrane protein that localizes to the apical membrane in the blastoderm cells of *D. melanogaster* embryo and is involved in mediating cell shape changes by recruiting Rho-GEF to the apical membrane (Kölsch, Seher, Fernandez-Ballester, Serrano, & Leptin, 2007). Overexpression of T48-HA was shown to result in precise apical localization in blastoderm cells (Kölsch et al., 2007). To further improve apical localization, the minimal apical localization sequence of Bazooka (Krahn, Klopfenstein, Fischer, & Wodarz, 2010) was C-terminally attached. Upon overexpression of both constructs, SBN-A_intra and SBN-A_extra show apical enrichment (Figure 4.16A', B'). However, a fraction of SBN-A localizes to the basolateral domain (Figure 4.16A', B'). Thus, SBN-A_intra and SBN-A_extra do not show exclusive apical localization, but are strongly enriched in the apical compartment (Figure 4.16A', B').

To obtain SBN-B_extra, vhhGFP4 was fused to the C-terminal portion (extracellular) of the Nrv1 protein and a blue fluorescent protein, (TagBFP, Evrogen) was inserted in the intracellular domain (Figure 4.16D). Nrv1 is the β subunit of the Na^+/K^+ ATPase, a heteromultimer composed by α/β subunits. The α subunit contains the Na^+ and K^+ channels, whereas the β subunit is required for the regulation of the transport and affinity of the α subunit for Na^+ and K^+ (Geering et al., 1996; Hasler et al., 1998).

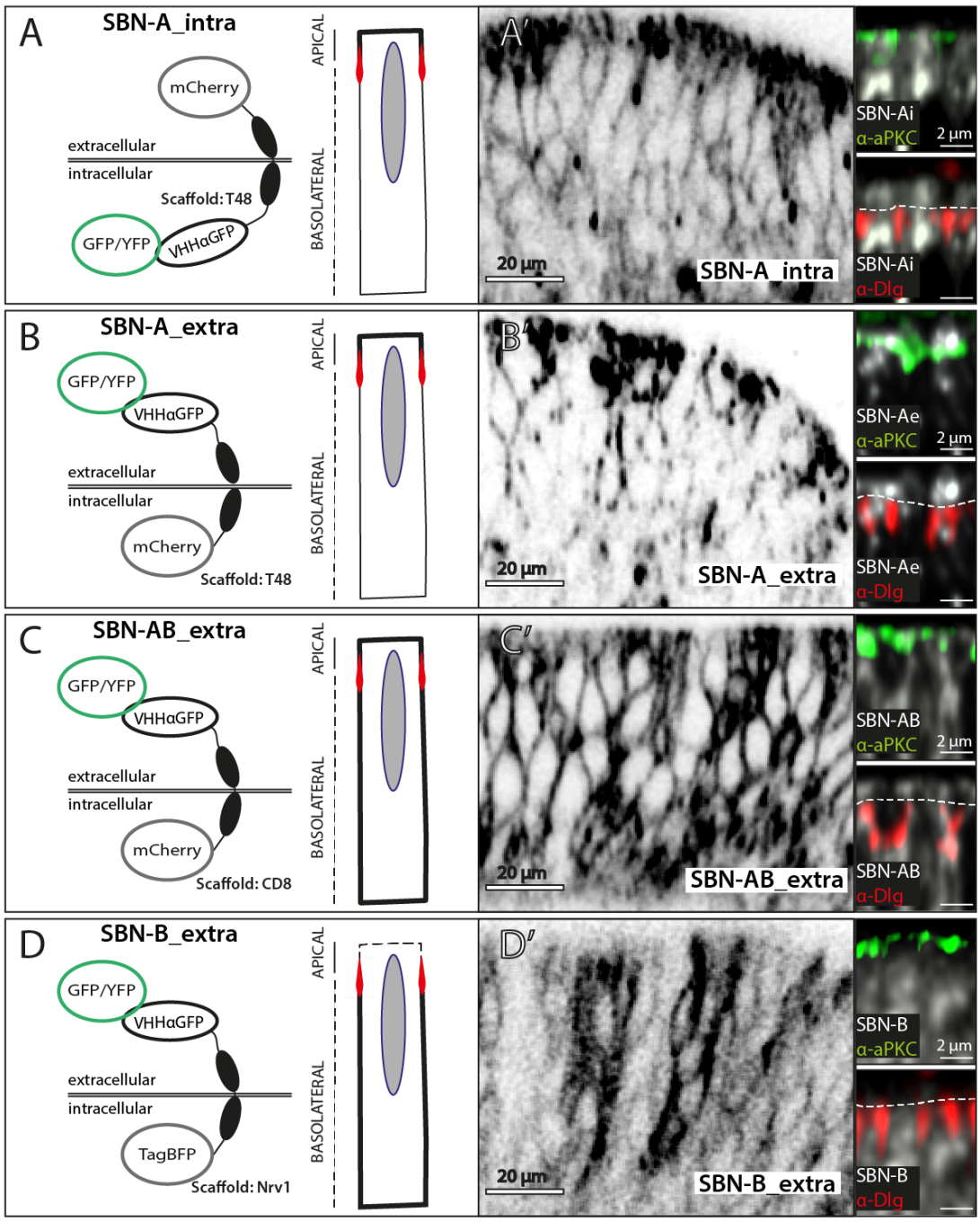

Figure 4.16 The SBNs toolset. A,B,C,D. Schematic of SBNs topology. In the SBN-A_intra the anti-GFP nanobody (VHHαGFP) localizes intracellularly, whereas in all the other SBNs the VHHαGFP faces extracellular. SBNs are fused with mCherry or TagBFP for visualization. The SBNs are made of different scaffold proteins and therefore localize differentially along the apical-basal axis. **A',B',C',D'. (left panel)** Computed cross-section of wing pouch cells expressing SBNs (apical to the top). The SBNs distribute differentially throughout the apical-basal axis of wing disc cells. Note that the SBNs-A (intra/extra) are enriched at the apical compartment, however they retain a basolateral fraction. **(right panel)** Magnification of the apical portion of wing disc cells expressing the SBNs. Note that SBN-A_intra, SBN-A_extra and SBN_AB-extra localize apically above the SJs (Dlg in red) and at the same level of the apical protein aPKC (green). SBN-B_extra is excluded from the apical compartment of wing disc cells.

In *D. melanogaster* three genes encode for the β subunits (*nrv1, nrv2, nrv3*) and they appear to have tissue-specific functions (Paul, 2003).

Nrv1 has a single transmembrane domain structure and has been implicated in the development of the nervous and the tracheal system (Genova, 2003; Paul, Palladino, & Beitel, 2007). Nrv1 is reported to localize basolaterally, and is excluded from the SJs (Paul et al., 2007). The basolateral Nrv1 localization is maintained in the system used in this study, the wing imaginal disc (Nrv1-YFP in Figure 4.18). In overexpression conditions, Nrv1 is still basolaterally localized (Genova, 2003). As expected, SBN-B_extra localizes specifically and exclusively to the basolateral domain (Figure 4.16D'). Moreover, SBN-B_extra is expressed in a patchy fashion, as different cells appear to express different levels of SBN-B_extra (Figure 4.16D').

4.2.2 Testing the potential of SBNs in a mislocalizing GFP/YFP-tagged transmembrane proteins

The extracellular position of vhhGFP4 in SBN-AB made it possible to successfully trap a GFP-tagged secreted molecule, the Dpp ligand (Harmansa et al., 2015). However, it is has not been investigated whether SBNs could bind and even mislocalize transmembrane proteins tagged with GFP (or GFP fluorescent derivatives) and if so, if the orientation of the nanobody would be relevant. In order to probe the mislocalization potential of this toolset, I coexpressed the SBNs together with GFP/YFP-tagged transmembrane proteins. In particular, since SBNs are Gal4-inducible transgenes, I used *hh-Gal4* (see chapter 2.1) to drive SBNs expression in the posterior compartment of the wing imaginal disc. The anterior compartment served as an internal control to monitor the unaltered GFP/YFP-tagged protein localization. Here, I report the results obtained by using SBNs to mislocalize transmembrane proteins.

4.2.2.1 The effect of SBNs on the uniformly distributed PH-GFP

First, I wanted to understand how the localization of the GFP tag, either intracellular or extracellular, influences the effect of the SBNs. All SBNs are available in a version where vhhGFP4 is exposed to the extracellular surface of the expressing cells (Figure 4.16B, C, D). SBN-A is also available in an additional version in which vhhGFP4 is intracellular (Figure 4.16A). Since the topology of transmembrane proteins is established during cotranslational translocation into the ER, SBNs with extracellularly facing vhhGFP4 should not affect proteins with a cytosolic GFP-tag. To test this hypothesis, I used PH-GFP, a uniformly distributed, intracellular GFP-fusion protein (flybase FBtp0020840, generated in Zelhof & Hardy, 2004). In PH-GFP the pleckstrin homology (PH) domain of the PLC-δ protein is fused to GFP. The PH domain binds specifically to apical membranes rich in PtdIns-4,5-bisphosphate (see chapter 1.1). However, when overexpressed, the apical specificity is reduced and PH-GFP localizes uniformly along the apical-basal axis of the membrane.

PH-GFP uniformly localizes to the apical and the basolateral side of the columnar cells of the wing disc pouch (Figure 4.17A, A'). When PH-GFP was coexpressed with the SBNs, only SBN-A_intra induced relocalization of a considerable fraction of PH-GFP to the apical compartment (Figure 4.17B). In this condition, PH-GFP appeared apically enriched, not only because of increase of fluorescence to the apical compartment, but also because of a reduction in the basolateral signal (Figure 4.17B). This could mean that SBN-A_intra mislocalized part of the basolateral PH-GFP fraction to the apical side of the wing disc cells. As expected, the SBN-A_extra, as wells as SBN-AB_extra and SBN-B_extra, did not cause significant changes in the PH-GFP distribution (Figure 4.17C, D, E).

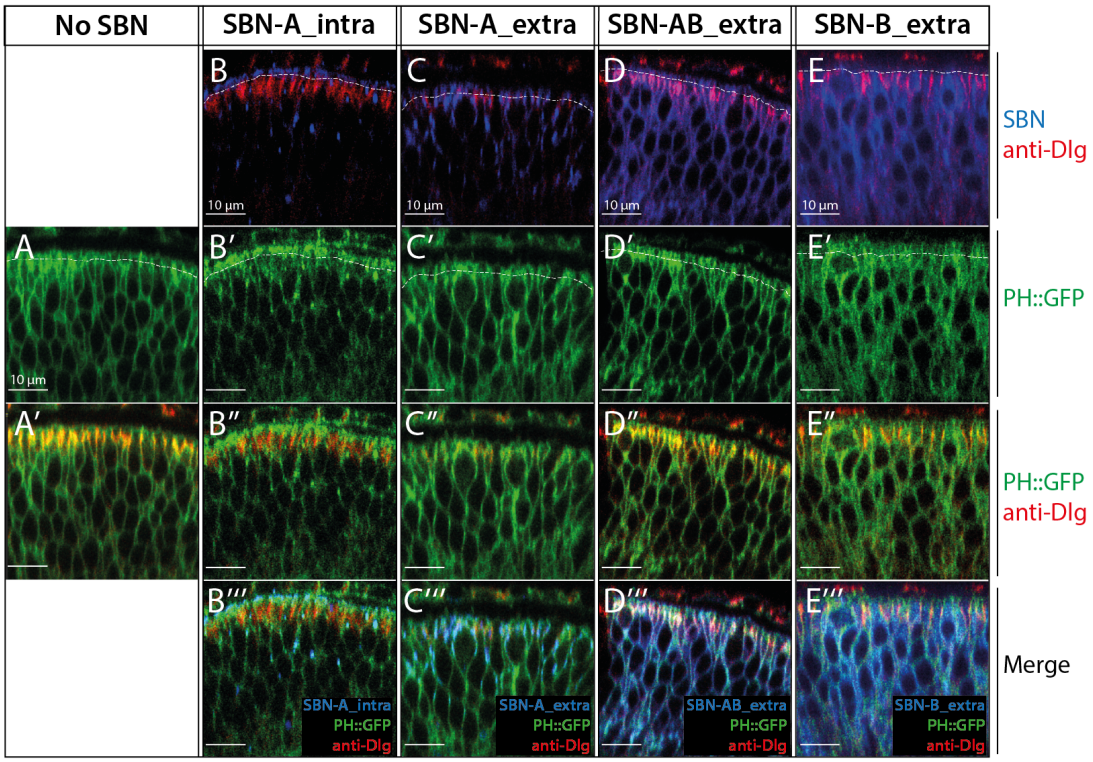

Figure 4.17 Effect of SBNs expression on PH-GFP localization. A. PH-GFP is uniformly localized at the membrane of wing disc pouch cells, when overexpressed in the posterior compartment (*hh-Gal4*). **B.** The coexpression of PH-GFP and SBN-A_intra results in a strong enrichment of the apical fractions (signal above Dlg, red, in B'') of PH-GFP and a reduction of the basolateral fraction. **C-E.** SBN-A_extra (C), SBN-AB_extra (D), SBN-B_extra (E) do not affect the distribution of PH-GFP. SBNs and PH-GFP constructs are expressed under the control of *hh-Gal4* (chapter 2.1). The dotted line indicates the apical border of the Dlg signal (red). All scale bars are 10 µm.

Moreover, the expression levels of PH-GFP affect the mislocalization efficiency of SBN-A_intra, since the PH-GFP apical enrichment seems more pronounced in discs with lower expression (data not shown). These results suggest that the orientation (extracellular or intracellular) of the GFP tag is critical for the binding and the interaction of the SBNs and the target protein.

4.2.2.2 The effect of SBNs on the basolateral protein Nrv1

Next, I assessed the effect of SBN-A_intra on the localization of the basolateral protein Nrv1-YFP. Nrv1 is a subunit of the Na^+/K^+ ATPase, described in chapter 4.2.1.1 and used as a scaffold for SBN-B_extra.

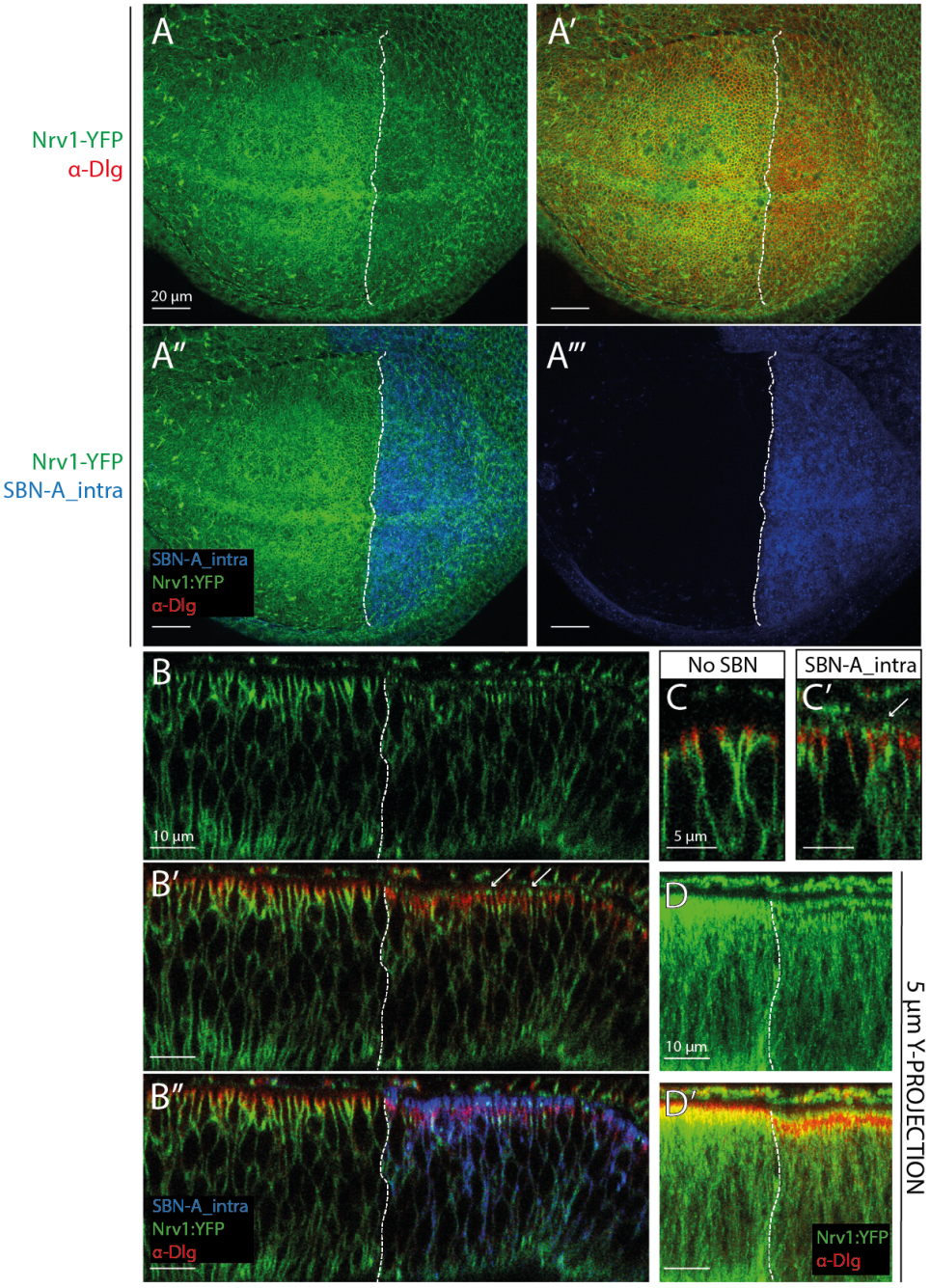

Figure 4.18 SBN-A_intra mislocalizes Nrv1-YFP to the apical compartment. A. Maximum projection of an Nrv1-YFP (green) heterozygous wing disc pouch expressing SBN-A_intra in the posterior compartment. **B.** Cross-section of the wing disc shown in (A). In the anterior compartment (left, control), Nrv1-YFP localizes exclusively to the basolateral compartment, up to the SJs marked by Dlg (red). In the posterior compartment (right), the coexpression of SBN-A_intra (blue) with Nrv1-YFP causes the gain of an apical Nrv1-YFP fraction (arrows in B′). **C.** Magnification of a representative portion of a Nrv1-YFP heterozygous wing disc epithelium, in control conditions (C) or expressing SBN-A_intra (C′). The arrow indicates the apical fraction in (C′). **D.** A 5 µm Y-projection of a Nrv1-YFP wing disc expressing SBN-A_intra in the posterior compartment. SBN-A_intra is expressed under the control of *hh-Gal4* (chapter 2.1). The dotted line indicates the border of expression of the SBNs.

Nrv1-YFP is a protein trap line (CPTI collection, Lowe et al., 2014; Lye et al., 2014), carrying an artificial YFP exon in the first intron of the *nrv1* locus. This leads to YFP insertion at the intracellular side of the Nrv1 protein.

Nrv1-YFP localizes only to the basolateral side of the wing imaginal disc, were it reaches up to the SJs and is partially excluded from the junctions (Figure 4.18B, C, D). In presence of SBN-A-intra, a portion of Nrv1-YFP is mislocalized to the apical membrane compartment (Figure 4.18B, C', D). In particular, the apical enrichment induced by SBN-A_intra is associated with a reduction of basolateral Nrv1-YFP signal (Figure 4.18B, D).

The mislocalization of Nrv1-YFP leads to a shift in the position of the SJs (marked by Dlg in Figure 4.18D). The SJs localize further to the basal side in cells coexpressing Nrv1-YFP and SBN-A_intra, likely indicating a reduction of the basolateral compartment size (Figure 4.18D). Moreover, Nrv1-YFP is still excluded from the SJs after mislocalization (Figure 4.18D).

In conclusion, SBN-A_intra affects Nrv1-YFP localization, showing that SBNs are potential tools for the mislocalization of basolateral proteins.

4.2.2.3 The effect of the SBNs on the apical determinant Crb

To evaluate the potential of the SBNs as tools to mislocalize apical proteins, I characterized their action on a Crb-GFP endogenous fusion proteins (Crb-GFP-A, (J. Huang et al., 2009), chapter 2.1). The Crb-GFP flies are homozygous viable and they retain an extracellular GFP tag. In the wing imaginal disc, Crb-GFP localizes to the subapical region, above the SJs (Figure 4.19A'', B'', C'' left). Expression of the SBNs in the posterior compartment of Crb-GFP heterozygous wing discs led to alterations in the Crb-GFP expression pattern. Posterior expression of SBN-A_extra caused an increase in the intensity of the apical fraction of Crb-GFP (Figure 4.19A).

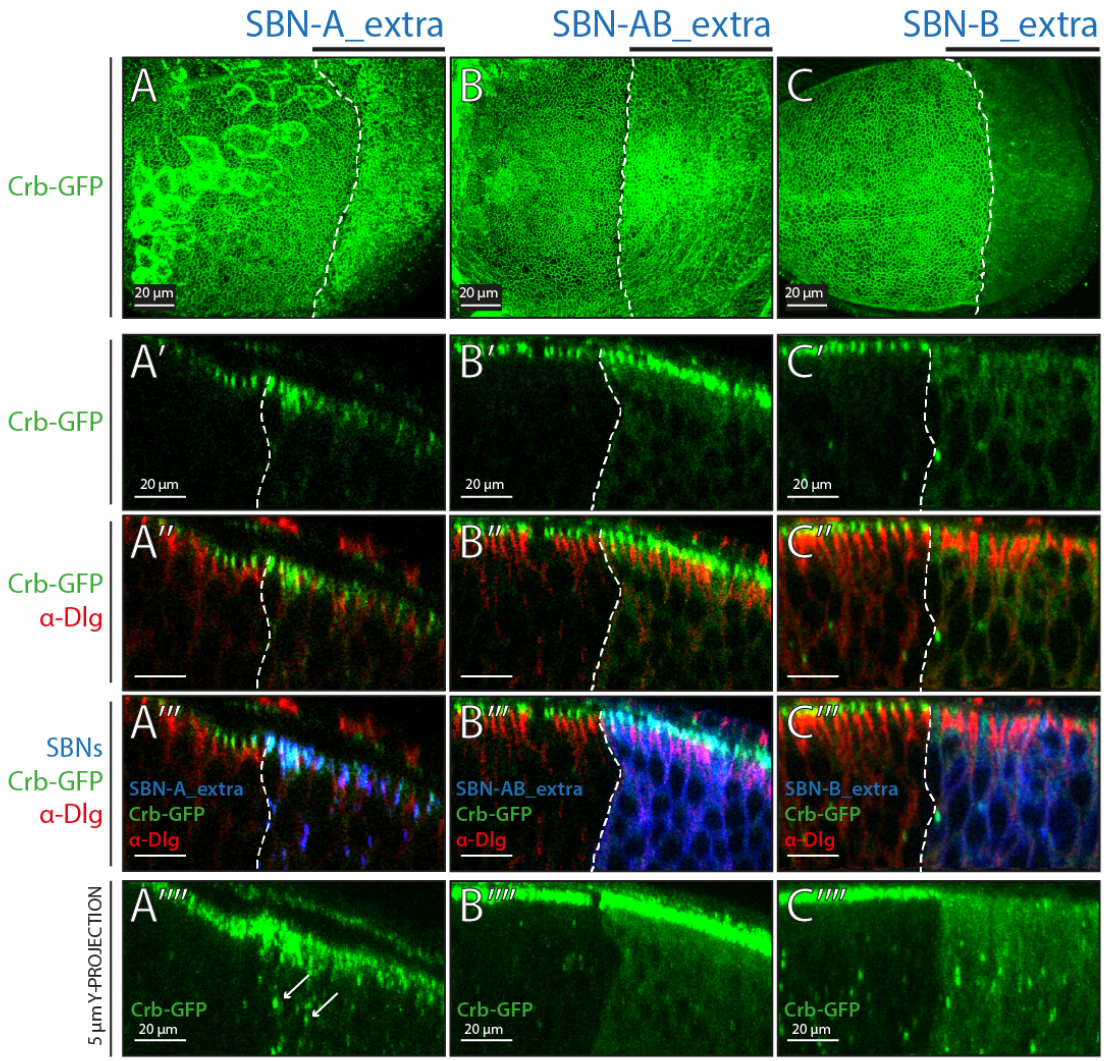

Figure 4.19 The effect of the SBNs on Crb-GFP distribution in Crb-GFP heterozygous wing disc. A-C. Crb-GFP heterozygous wing discs expressing SBNs in the posterior compartment, while the anterior compartment serves as internal control. **A** SBN-A_extra enhances the fluorescence of Crb-GFP at the apical side as seen in the maximum projection (A) and in the cross-section (A', A'', A'''). A small fraction of Crb-GFP is mislocalized to the basolateral compartment (arrows in A''''). **B.** Crb-GFP fluorescence is enhanced at the apical side of a Crb-GFP heterozygous wing pouch expressing SBN-AB_extra. In addition, Crb-GFP gains a uniform basolateral fraction (B, B''''). **C.** SBN-B_extra expression results in Crb-GFP mislocalization. While apical signal is lost, Crb-GFP gains a basolateral fraction (C', C'', C''', C''''). All SBNs are under the control of *hh-Gal4* (chapter 2.1). The dotted line indicates the border of expression of the SBNs.

The SBN-A_extra also caused mislocalization of a small fraction of Crb-GFP to the basolateral compartment (Figure 4.19A'''', arrows). The same was observed when expressing SBN-AB_extra in posterior cells. SBN-AB_extra enhanced the apical fraction of Crb-GFP and caused the gain of a weak and

uniform basolateral fraction (Figure 4.19B). In the previously mentioned experiments, Crb-GFP maintained its physiological position at the apical compartment of the wing disc.

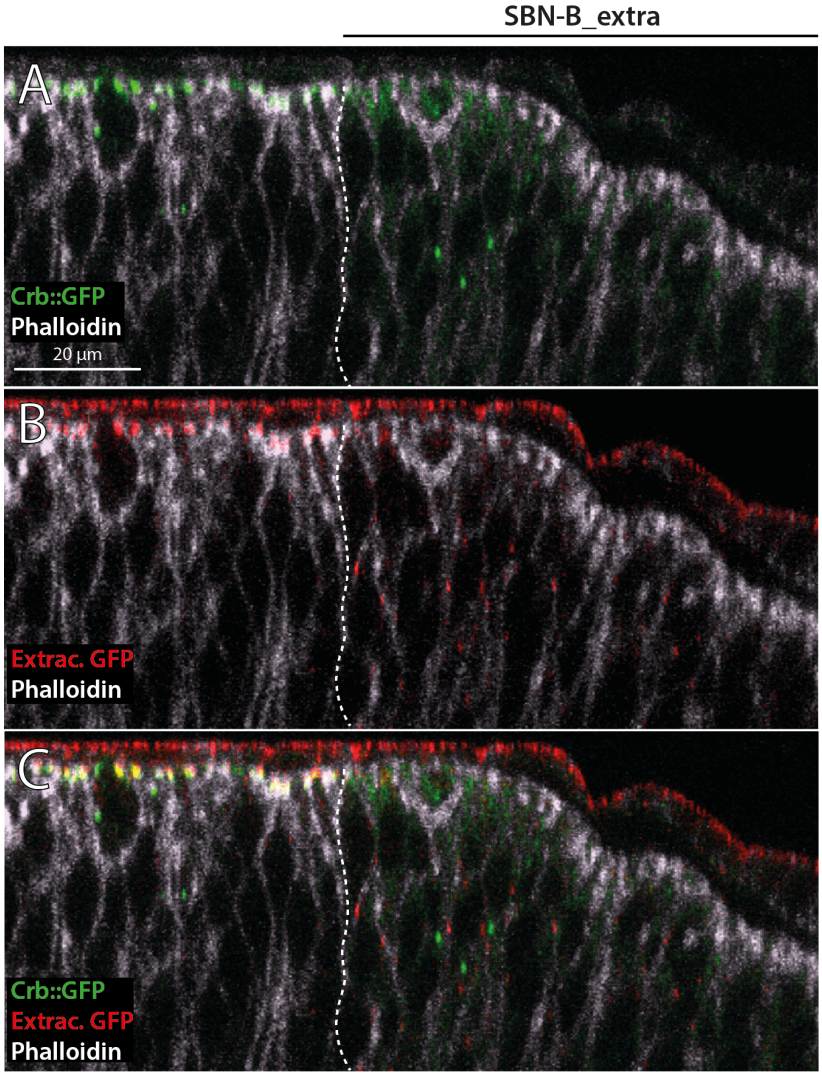

Figure 4.20 SBN-B partially mislocalizes Crb-GFP to the basolateral membrane. A-C. Cross-section of a Crb-GFP heterozygous wing disc expressing SBN-B_extra in the posterior compartment (right of the dotted line). **A.** The GFP signal (green) is detected in the apical compartment of the anterior side of the wing disc (control, left of the dotted line). In the posterior compartment (+ SBN-B_extra) the GFP signal is mostly intracellular, when compared to the cortical F-actin signal (detected by a Phalloidin-dye). **B.** Staining for extracellular GFP (grey) reveals that SBN-B expression results in gain of a membranous, basolateral fraction of Crb-GFP. **C.** The GFP signal and the extracellular α-GFP staining colocalize in the apical compartment of the anterior side of the wing disc pouch (control). The dotted line indicates the border of SBN expression (SBN-B_extra is expressed in the posterior compartment, under the control of *hh-Gal4* (chapter 2.1).

However, when SBN-B_extra was coexpressed in a Crb-GFP heterozygous background the apical Crb-GFP localization was lost and Crb-GFP localization to the basolateral compartment was observed (Figure 4.19C).

In order to understand if SBN-B_extra induces Crb-GFP insertion into the basolateral membrane, I performed an extracellular α-GFP staining on wing discs coexpressing Crb-GFP and SBN-B_extra in the posterior compartment. The outline of the plasma membrane of columnar cells was visualized using a Phalloidin-dye labelling cortical F-actin (see Figure 1.3 and chapter 1.2.3). Indeed, we observed extracellular GFP signal along the basolateral surface of posterior cells, suggesting that SBN-B_extra can relocalize Crb-GFP to the basolateral plasma membrane (Figure 4.20, red signal). Only a portion of basolateral Crb-GFP was found internalized (Figure 4.20, green signal).

Crb is a type-I transmembrane protein that specifies the apical domain of many epithelia, by recruiting polarity determinants to the apical cortex, through its cytoplasmic tail (Izaddoost, Nam, Bhat, Bellen, & Choi, 2002; Klebes & Knust, 2000; Médina et al., 2002; Sotillos, Díaz-Meco, Caminero, Moscat, & Campuzano, 2004). One of the components that Crb recruits is PatJ, that indirectly binds Crb through Std (Bulgakova & Knust, 2009; Roh et al., 2002). PatJ was reported to be reduced in *crb* mutant clones, however this reduction does not compromise epithelial polarity *per se* (C.-L. Chen et al., 2010; Hamaratoglu et al., 2009; W. Zhou & Hong, 2012). To characterize the functional implication of the basolateral mislocalization of Crb-GFP, I compared the localization of PatJ in the absence and in the presence of SBN-B_extra in Crb-GFP heterozygous wing discs. A reduction of apical PatJ staining is observed in conditions of Crb-GFP mislocalization (Figure 4.21).

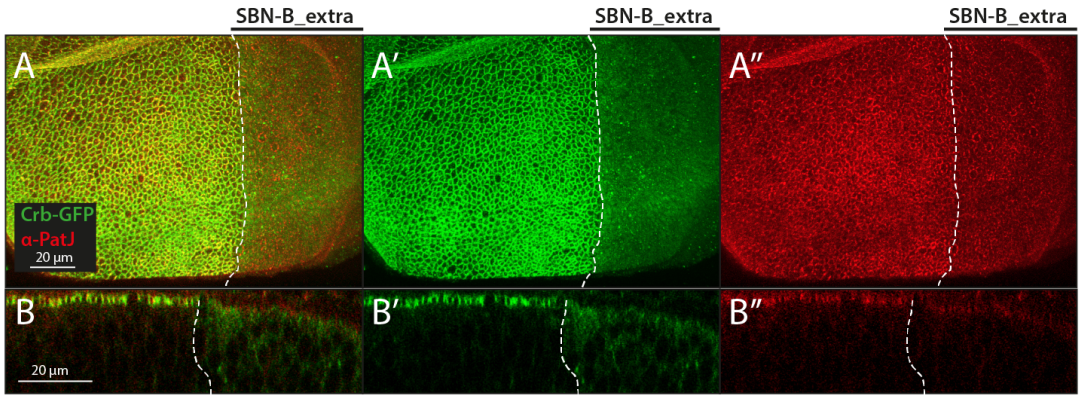

Figure 4.21 Apical PatJ is reduced when Crb-GFP is mislocalized by SBN-B_extra. A. Crb-GFP (green) and PatJ (red) colocalize in in the apical compartment of a Crb-GFP heterozygous wing imaginal disc (control, anterior compartment). The loss of the apical Crb-GFP fraction in the posterior compartment (+ SBN-B_extra) causes a reduction in PatJ signal (A''). **B.** PatJ is reduced in the apical compartment of cells with mislocalized Crb-GFP. No gain of PatJ signal is observed in the basolateral compartment. The dotted line indicates the border of SBN-B_extra expression. SBN-B_Extra is under the control of *hh-Gal4* (chapter 2.1).

No clear PatJ basolateral signal is visible in response to the gain of a basolateral fraction of Crb-GFP, indicating that the basolateral Crb-GFP is not sufficient to induce PatJ relocalization. Furthermore, the untagged Crb should still be apically localized and sufficient to maintain partial apical localization of PatJ.

To address the potential physiological consequences of the mislocalization of Crb-GFP, I expressed the SBNs in Crb-GFP homozygous conditions. SBNs expression was driven in the anterior compartment by *ci-Gal4* (see chapter 2.1). When SBN-A_extra was expressed in Crb-GFP homozygous wing discs, the apical portion of Crb-GFP was strongly enhanced, as observed in Crb-GFP heterozygous (Figure 4.22B, C, D). In these conditions the apical enhancement was stronger in the first row of cells expressing SBN-A_extra in the anterior compartment (Figure 4.22B, B''', B''''). SBN-A_extra expression also caused a partial mislocalization of Crb-GFP to the basolateral side (Figure 4.22C). Moreover, the anterior compartment of Crb-GFP homozygous

wing discs expressing SBN-A_extra was bigger than the control compartment (anterior and posterior, respectively) (Figure 4.22A).

Expressing SBN-B_extra in Crb-GFP homozygous wing discs caused loss of Crb-GFP from the apical compartment and gain of a basolateral fraction (Figure 4.23B, C, D). However, this effect was not uniform through the SBN-B_extra expression domain, but directly correlates with the expression levels of SBN-B_extra (Figure 4.23B, B''', B''''). Indeed, SBN-B_extra is characterized by a "patchy" expression (Figure 4.16D') and only cells that expressed SBN-B_extra at high levels showed a loss of apical Crb-GFP (Figure 4.23B). Since this effect was not seen in Crb-GFP heterozygous conditions, these results suggest that the expression ratio of the GFP-tagged protein and the SBN is directly influencing the mislocalization efficiency.

Finally, Crb-GFP homozygous wing discs were characterized by a fold at the anterior/posterior compartment border and variable cell shape size throughout the expression domain of SBN-B_extra (Figure 4.23B, C).

In conclusion, the SBNs are potential tools for protein mislocalization. Further analysis is required to understand the effect of the SBNs on the target protein function and how they achieve to mislocalize transmembrane proteins.

In the next chapter, I will characterize the SBNs as potential tools to study the function of the differential subcellular localization of TGF-β receptors along the apical-basal axis.

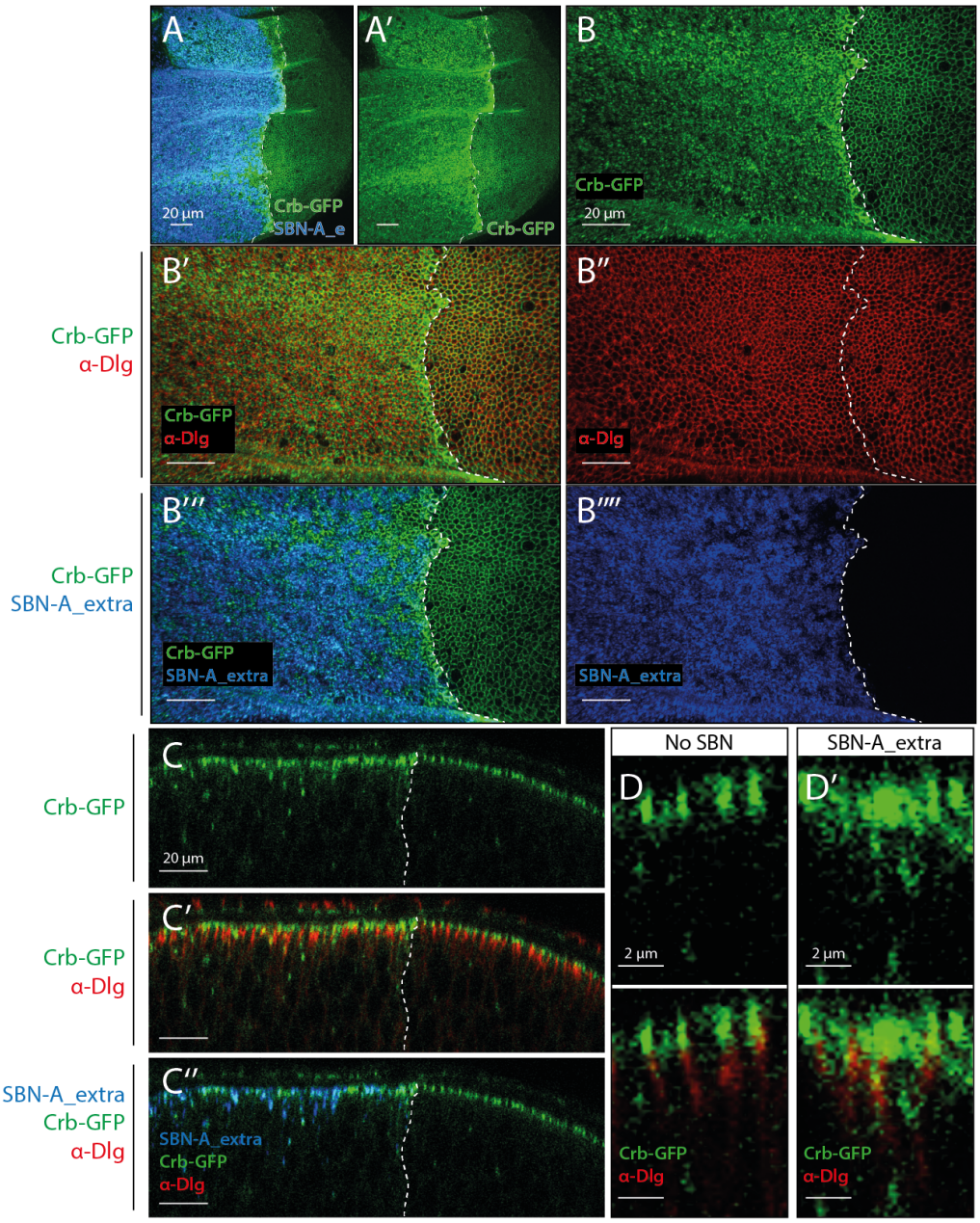

Figure 4.22 SBN-A_extra effect in Crb-GFP homozygous discs. A-B. Maximum projections of a Crb-GFP (green) homozygous wing disc expressing SBN-A_extra (blue) in the anterior compartment. Crb-GFP expression is enhanced in cells expressing SBN-A_extra. The first cell row expressing SBN-A_extra shows a stronger enhancement of Crb-GFP (B, B‴). **C.** Cross-section of a Crb-GFP homozygous wing pouch, expressing SBN-A_extra in the anterior compartment. SBN-A_extra causes Crb-GFP signal enhancement in the apical compartment (above Dlg, red) and a partial mislocalization to the basolateral compartment. **D.** Magnification of a representative portion of a Crb-GFP homozygous wing disc pouch epithelium, showing control cells (D) and cell expressing SBN-A_extra (D′). The apical Crb-GFP signal is enhanced in presence of SBN-A_extra (D′). The dotted line indicates the border of expression of the SBN. SBN-A_extra is expressed under the control of *ci-Gal4* (chapter 2.1).

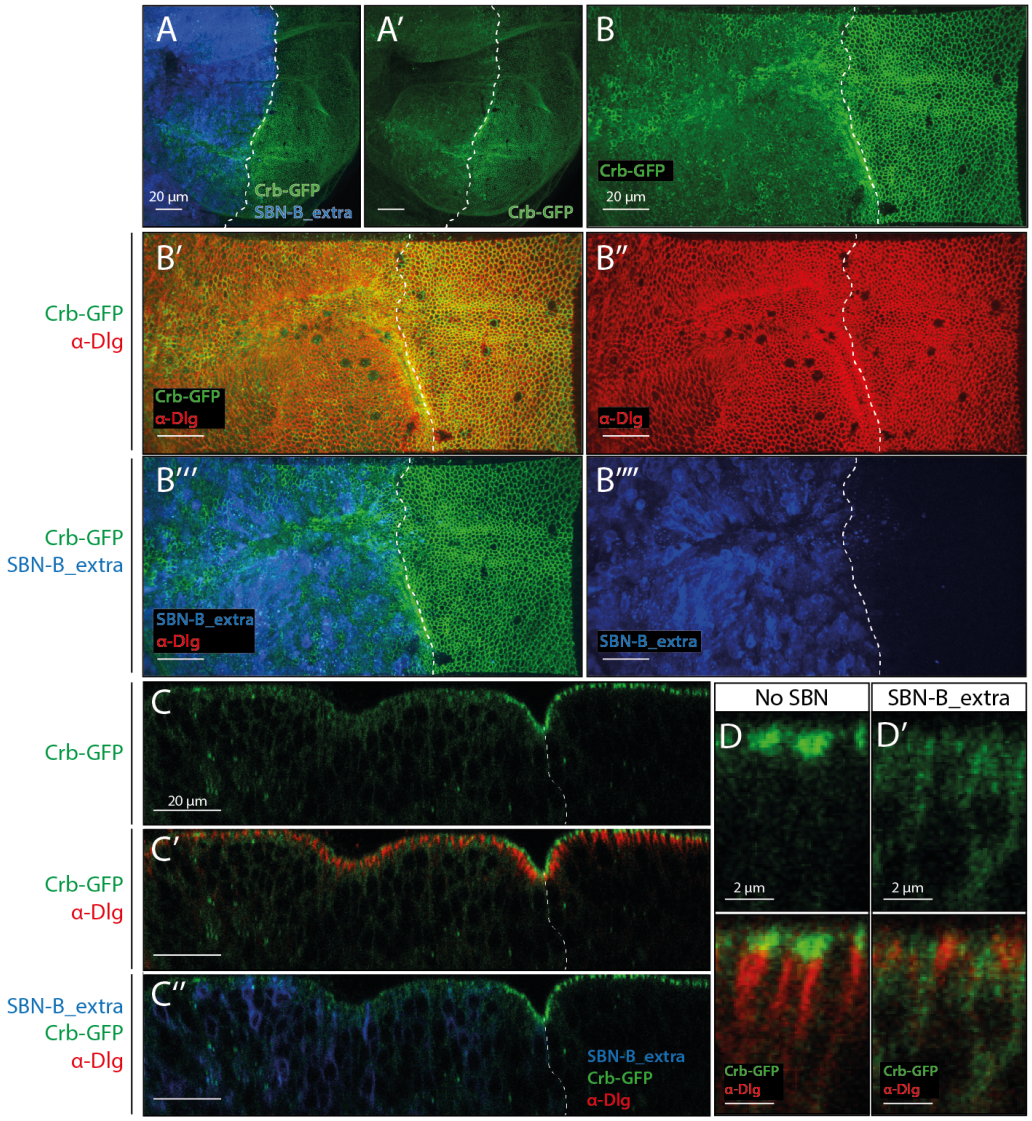

Figure 4.23 SBN-B_extra effect in Crb-GFP homozygous wing discs. A-B. Maximum projections of a Crb-GFP (green) homozygous wing disc expressing SBN-B_extra (blue) in the anterior compartment. Crb-GFP loses apical signal in some patches of cells expressing high levels of SBN-B_extra (B, B‴, B⁗). A fold is present at the border (dotted line) between Crb-GFP cells expressing SBN-B-extra and control cells. **C.** Cross-section of a Crb-GFP homozygous wing pouch, expressing SBN-B_extra in the anterior compartment. SBN-B_extra causes loss of apical Crb-GFP signal (above Dlg, red) and mislocalization to the basolateral compartment. **D.** Magnification of a representative portion of a Crb-GFP homozygous wing pouch epithelium, showing control cells (D) and cell expressing SBN-B_extra (D′). The dotted line indicates the border of expression of the SBN. SBN-B_extra is expressed under the control of *ci-Gal4* (chapter 2.1).

4.2.3 Characterization of the effect of SBNs on TGF-β receptors localization

4.2.3.1 The effect of the SBNs on Tkv-YFP

To understand the function of the different subcellular fractions of Tkv, I attempted to alter the distribution of Tkv along the apical-basal axis using SBNs. In order to use the SBNs toolset, the target protein has to be tagged with GFP or derivatives in the extracellular domain. Since we have not yet succeeded in inserting a GFP coding sequence into the endogenous tkv locus, I made use of a Tkv-YFP protein trap line (CPTI, Lowe et al., 2014; Lye et al., 2014) to investigate receptor mislocalization by the SBNs. Tkv-YFP carries an artificial YFP exon which is inserted in the second last common intron of the *tkv* locus, tagging the extracellular domain of the receptor (see chapter 4.5.1). While Tkv-3xHA was localized to the apical and basolateral cell surface (see chapter 4.1.1), Tkv-YFP did not show apical localization and was exclusively found basolateral (Figure 4.24A). This discrepancy could be due to the insertion of the large YFP tag, which potentially disrupts parts of an apical targeting domain. Furthermore, there is the possibility that the YFP-tag is not retained into all *tkv* transcripts, such that apical Tkv is not visualized with this tool. These alternative hypotheses will be discussed in chapter 5. Despite these drawbacks, Tkv-YFP was used for this pilot-study to provide a proof of concept for the effect of SBNs on receptor localization. Future approaches will aim to use SBNs to modify endogenous Tkv localization, using the tools described in chapter 4.3 to manipulate *tkv* locus.

All SBNs were expressed in the posterior compartment of the wing imaginal disc using *hh-Gal4* (see chapter 2.1). The localization of Tkv-YFP was perturbed by all SBNs tested (Figure 4.24). In particular, Tkv-YFP gains an apical fraction in condition of coexpression with SBN-A_extra or SBN-AB_extra (Figure 4.24B, C). With SBN-B the basolateral fraction of Tkv-YFP is

enhanced (Figure 4.24D). To assess if the change in Tkv-YFP distribution along the apical-basal axis has functional consequence, I analysed the Dpp signalling profiles using a P-Mad antibody. No clear change in the P-Mad profiles was observed in presence of the SBNs in Tkv-YFP heterozygous wing discs (data not shown). However, in these conditions parts of the Tkv population is untagged and hence unmodified, suggesting that it can activate P-Mad at physiological levels. Therefore, I repeated this experiment in Tkv-YFP homozygous conditions to increase the fraction of mislocalized Tkv protein.

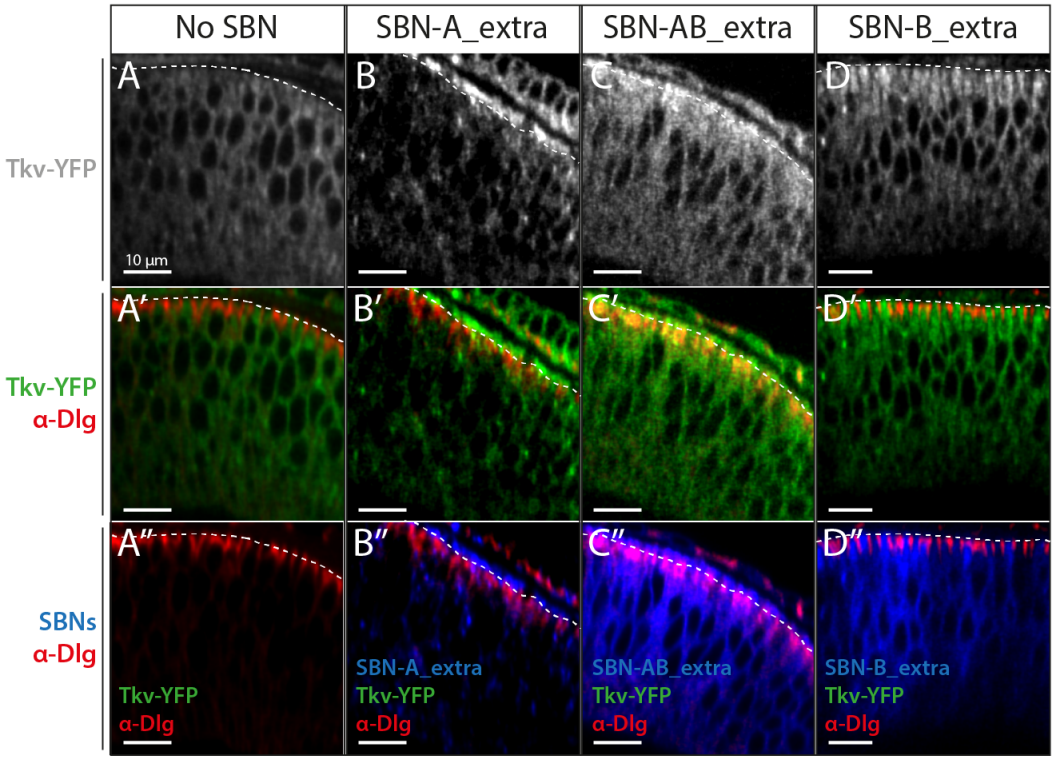

Figure 4.24 The SBNs affect Tkv-YFP localization in Tkv-YFP heterozygous wing discs. A. Tkv-YFP (green) localizes exclusively to the basolateral side of the wing disc epithelium (below Dlg, (red) in absence of SBNs. **B.** Tkv-YFP localizes to the apical side of the wing disc epithelium (signal above Dlg) when coexpressed with SBN-A_extra (blue). The basolateral Tkv-YFP signal appear reduced. **C.** Tkv-YFP gains an apical fraction of the wing disc epithelium (above Dlg) when coexpressed with SBN-AB_extra (blue). **D.** Tkv-YFP localizes exclusively to the basolateral side of the wing disc epithelium (signal below Dlg) in presence of SBN-B_extra (blue). The dotted line indicates the level of the SJs (Dlg, in red). SBNs where expressed under the control of *hh-Gal4* (chapter 2.1).

In this setup, I used SBN-A_extra and SBN-B_extra, which in Tkv-YFP heterozygous caused partial apical enrichment and enhancement of the basolateral localization, respectively. In Tkv-YFP homozygous wing discs, both SBN-A_extra and SBN-B_extra induced an increase in Tkv-YFP signal in the regions of SBN expression (Figure 4.25B, D).

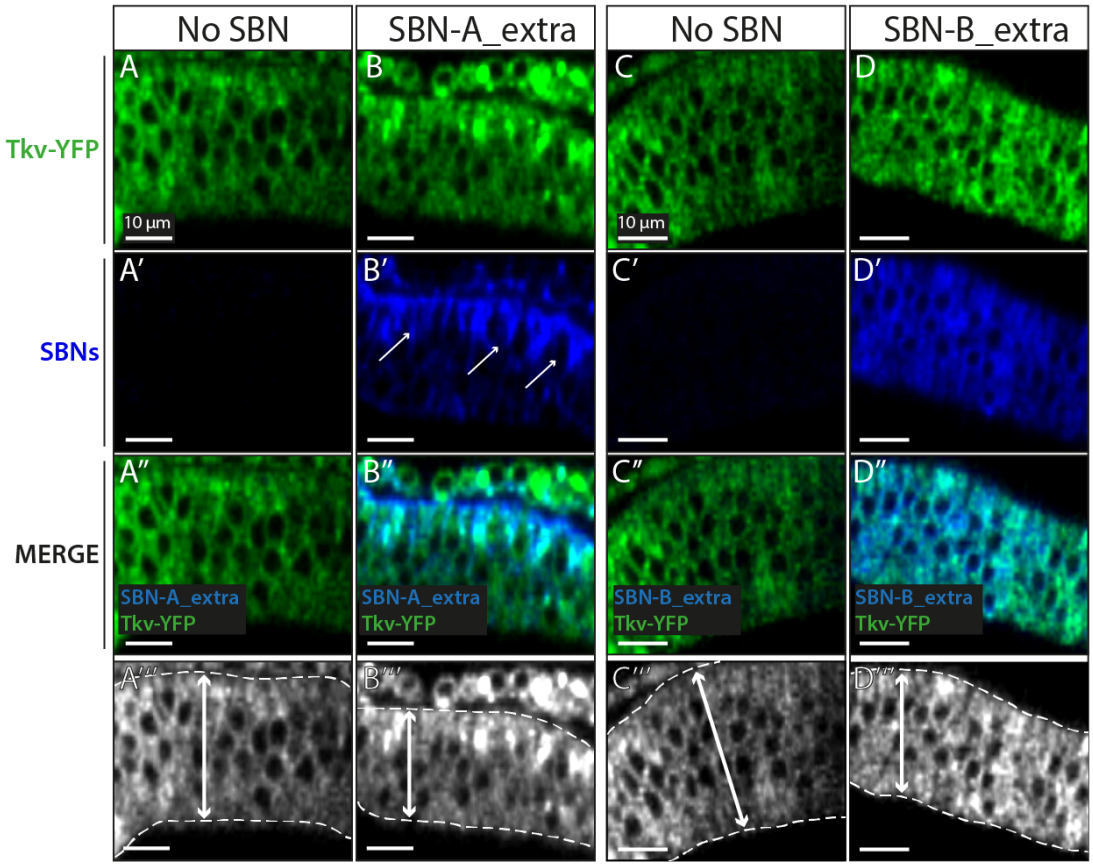

Figure 4.25 The effect of SBNs in Tkv-YFP homozygous wing discs. A-B. Cross-section of a Tkv-YFP (green) homozygous wing disc expressing SBN-A_extra (blue) (B) in the posterior compartment. Tkv-YFP signal is enhanced by SBN-A_extra (B, B''). SBN-A_extra acquires signal at the basolateral compartment (B', arrows). The epithelial thickness is reduced in the posterior compartment (B''') compared to the anterior control compartment (A'''). **C-D.** Cross-section of a Tkv-YFP (green) homozygous wing disc expressing SBN-B_extra (blue) (D) in the posterior compartment. Tkv-YFP signal is enhanced by SBN-A_extra (D, D''). The epithelial thickness is reduced in the posterior compartment (D'''). The dotted lines demarcate wing disc DP cells. SBNs where expressed under the control of *hh-Gal4* (chapter 2.1).

However, in Tkv-YFP homozygous condition the distribution of SBN-A_extra significantly changed, since increased localization of SBN-A_extra to the basolateral compartment was observed (Figure 4.25B'). Therefore, in Tkv-YFP homozygous wing discs SBN-A_extra did not cause a clear apical enrichment of Tkv-YFP (Figure 4.25B).

Another effect observed is a significant reduction in the epithelial thickness of cells expressing either SBN-A_extra or SBN-B_extra in Tkv-YFP homozygous wing discs (Figure 4.25B''' and D'''). A similar effect was observed when reducing Tkv levels using *tkvRNAi* (FBti0149846, chapter 2.1, data not shown). Collectively, these data suggest that SBN-binding inhibits Tkv receptor function. Therefore, I analysed BMP signalling activity in Tkv-YFP homozygous wing discs expressing either SBN-A_extra or SBN-B_extra.

Posterior P-Mad signal was severely reduced as a consequence of the expression of SBN-A_extra or SBN-B_extra in Tkv-YFP homozygous wing discs (Figure 4.26). The P-Mad reduction appeared to be more severe in SBN-A_extra expressing discs, whereas low basal P-Mad levels are still visible in cells expressing SBN-B_extra (Figure 4.26). P-Mad signal reduction was also observed in peripodial membrane cells expressing either SBN-A_extra or SBN-B_extra (Figure 4.27). Also here, expression of SBN-A_extra resulted in a stronger reduction of P-Mad levels compared to SBN-B_extra (Figure 4.27A versus B). The inhibition of the signal transduction function of Tkv-YFP, observed as a consequence of the coexpression with the SBNs, could have several reasons. P-Mad reduction could be explained by the requirement for TGF-β receptors to be endocytosed in order to mediate the signalling (see chapter 1.3.3.1) (Di Guglielmo, Le Roy, Goodfellow, & Wrana, 2003), a process potentially blocked by SBN-binding. Endocytosis defective cell clones showed autonomous reduction in P-Mad signalling in the wing disc (Belenkaya et al., 2004) (see chapter 1.3.3.1). Alternatively, binding of the

SBNs hinders the receptor during an essential step required for its signalling function (ligand binding, phosphorylation and activation of the kinase domain by the type-II receptor or phosphorylation of Mad; discussed in chapter 5).

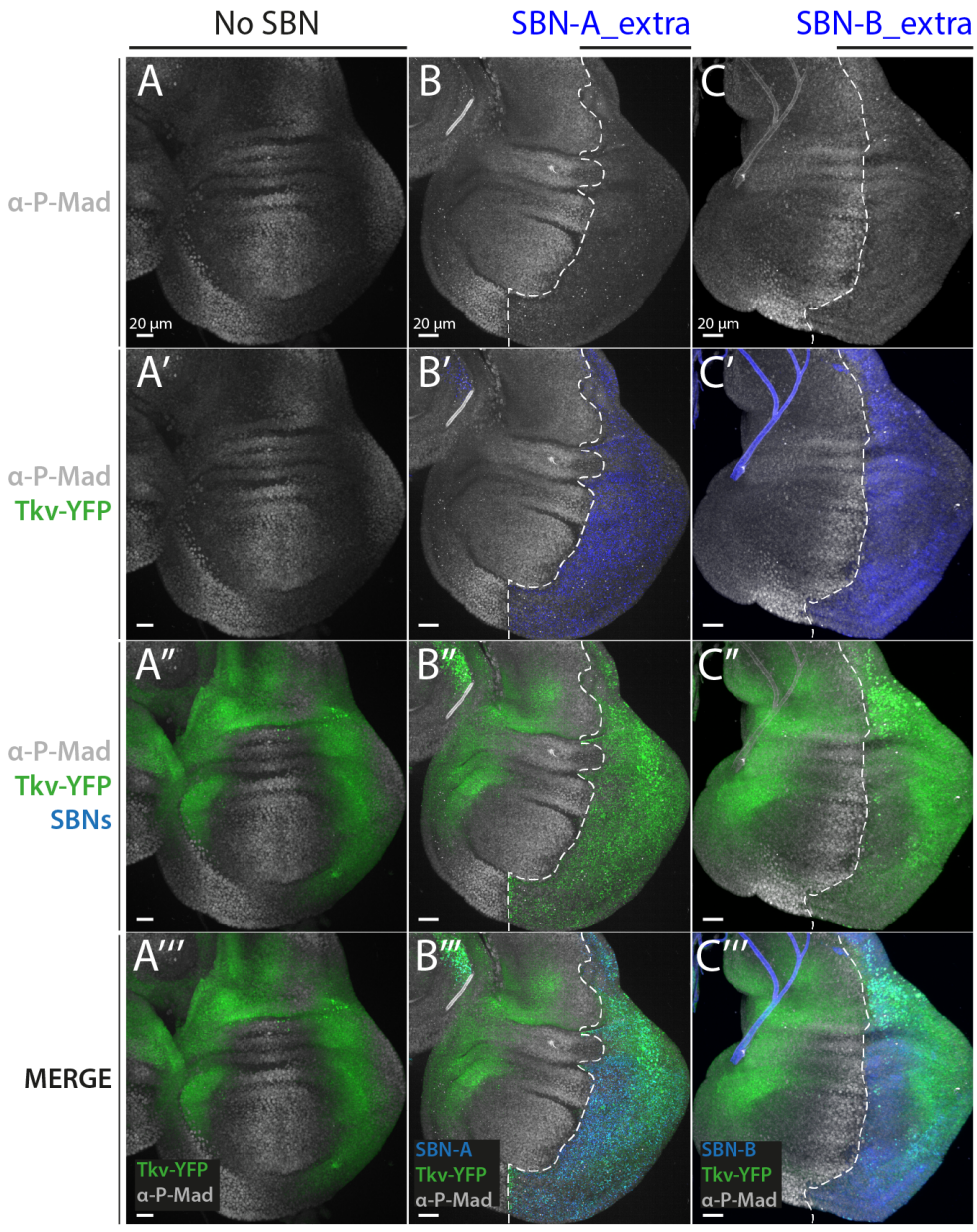

Figure 4.26 P-Mad levels are drastically reduced in cells coexpressing Tkv-YFP and SBNs. A. Control Tkv-YFP (green) homozygous wing disc (100 h AEL). **B.** Tkv-YFP homozygous wing disc expressing SBN-A_extra (blue) in the posterior compartment (100 h AEL). **C.** Tkv-YFP homozygous wing disc expressing SBN-B_extra (blue) in the posterior compartment (100 h AEL). The dotted line indicates the border of expression of the SBNs (A/P boundary). The SBNs are expressed under the control of *hh-Gal4* (chapter 2.1).

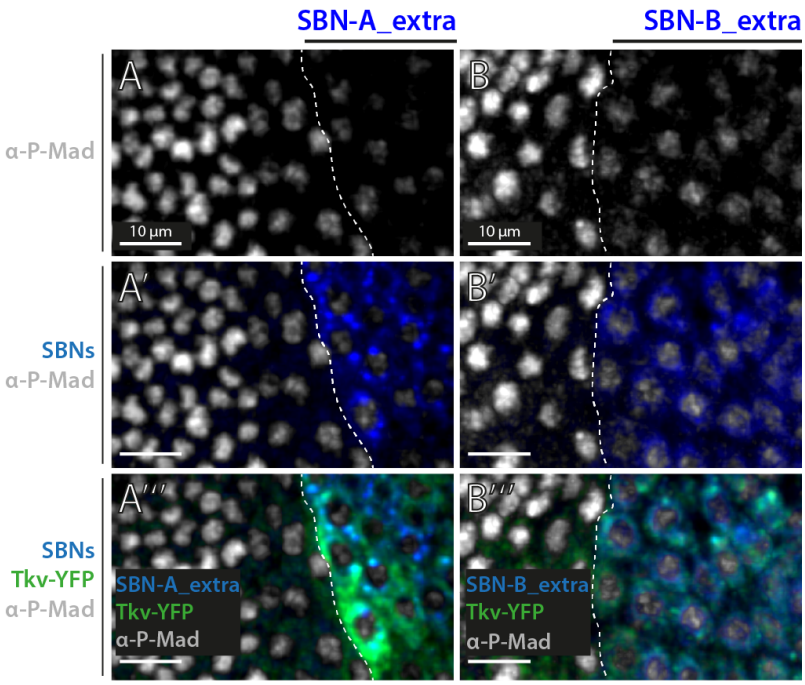

Figure 4.27 P-Mad is reduced in peripodial membrane cells expressing the SBNs. A. P-Mad is dramatically reduced in cells expressing SBN-A_extra. **B.** P-Mad is reduced in cells expressing SBN-B_extra. The dotted line indicates the border of expression of the SBNs. The SBNs are under the control of *hh-Gal4* (chapter 2.1).

These results suggest that the binding of SBNs affects Tkv receptor function. Therefore, I have used an alternative method to mislocalize Tkv, involving the manipulating of the endogenous Tkv protein. In this approach, I modified *tkv* at the endogenous locus and deleted a putative targeting domain in the *tkv* coding region (see chapter 4.3).

4.2.3.2 The effect of SBN-A_intra on Punt-GFP localization

Punt-GFP is the main type-II receptor associated with BMP signalling in the wing disc. In the first part of this thesis, I reported that Punt-GFP localizes exclusively to the basolateral side of the wing imaginal disc cells (see chapter 4.1.4). Therefore, it would be interest to observe the effect of Punt mislocalization to the apical compartment, where the type-I receptors Tkv and Sax localizes. The GFP-tag of Punt-GFP is placed at the C-terminal end,

which is intracellular (Figure 4.7B). Therefore, I used SBN-A_intra to mislocalize Punt-GFP to the apical compartment. Indeed, coexpression of SBN-A_intra with Punt-GFP (in heterozygous background) caused the appearance of a substantial apical Punt-GFP fraction (Figure 4.28).

Punt is a type-II receptor that mediates signal by activating type-I receptors. As mentioned before, the type-I receptors Tkv and Sax are localized at the apical and basolateral compartment of the wing disc (see chapters 4.1.1 and 4.1.2). Under physiological conditions, Punt cannot interact with the type-I receptors in the apical compartment of the wing disc. Thus, Punt-GFP mislocalization to the apical compartment should result in increased signalling activity due to the formation of new signalling complexes in the apical domain.

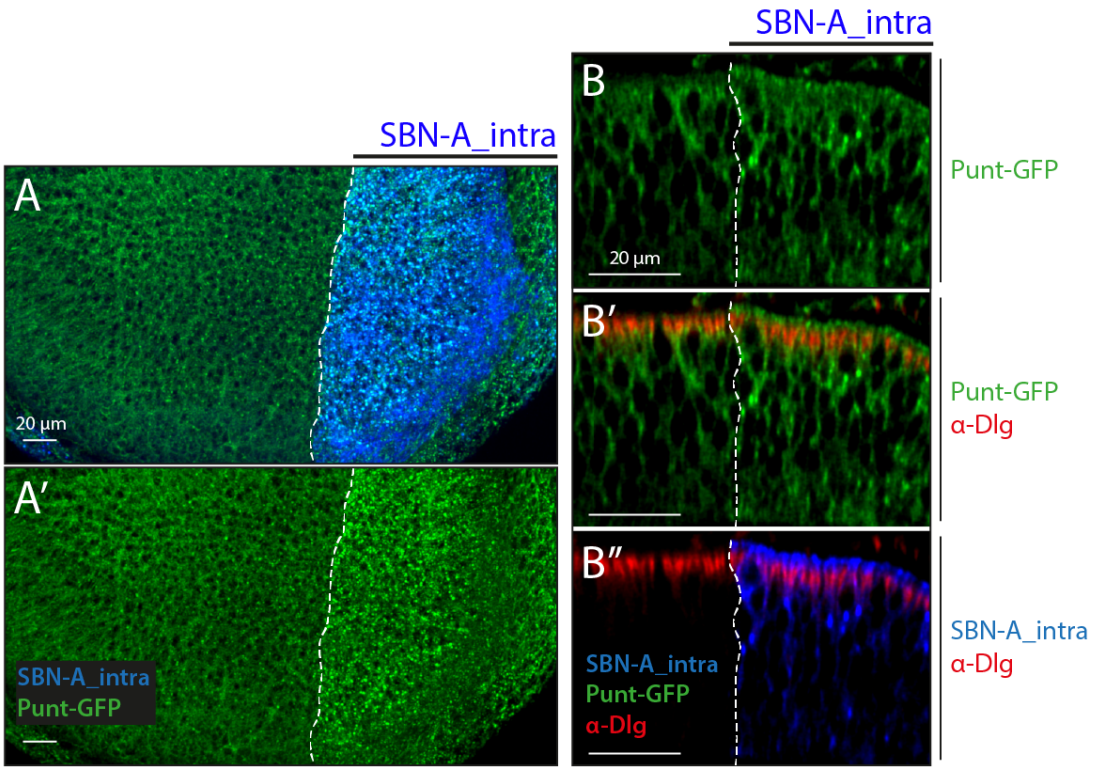

Figure 4.28 SBN-A_intra mislocalizes Punt-GFP to the apical compartment. A. Maximum projection of a Punt-GFP (green) heterozygous wing disc expressing SBN-A_intra (blue) in the posterior compartment. **B.** Cross-section of a Punt-GFP (green) heterozygous wing disc expressing SBN-A_intra (blue) in the posterior compartment. Punt-GFP gains an apical fraction (B′) in cells expressing SBN-A-intra (B′′). The dotted line indicates the border of expression of the SBN-A_intra. SBN-A_intra is expressed with *hh-Gal4* (chapter 2.1).

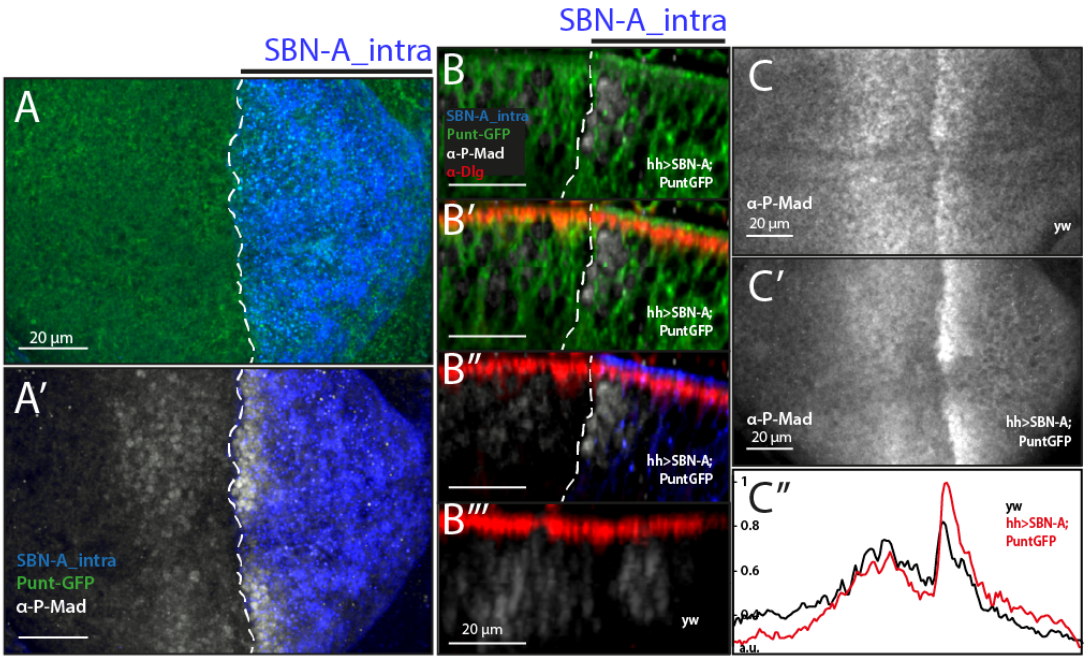

Figure 4.29 The gain of an apical Punt-GFP fraction leads to increased P-Mad signalling in the posterior compartment. A. Maximum projection of a Punt-GFP (green) heterozygous wing disc expressing SBN-A intra (blue) in the posterior compartment. P-Mad intensity in the posterior compartment is increased. **B.** Cross-section of a Punt-GFP heterozygous wing disc expressing SBN-A_intra in the posterior compartment. Cells expressing SBN-A_intra show increased P-Mad levels (B'') compared to control (B'''). **C.** P-Mad gradient of a representative yw wing disc (C, black line in C'') and of a representative Punt-GFP heterozygous wing disc expressing SBN-A_intra in the posterior compartment (C', red line in C''). The dotted line indicates the border of expression of SBN-A_intra. SBN-A_intra is expressed with *hh-Gal4* (chapter 2.1).

Indeed, when mislocalized to the apical side, Punt-GFP caused an increase in P-Mad intensity levels in the posterior compartment (Figure 4.29). This increase is accompanied by a decrease in the anterior P-Mad levels (Figure 4.29). These results suggest that, in contrast to what I observed with Tkv-YFP, the SBN-A_intra does not interfere with the function of the type-II receptor Punt. In conclusion, the gain of an apical fraction of Punt-GFP caused alteration of the P-Mad profile. Therefore, Punt exclusion from the apical compartment might play a role in modulating signalling from the apical compartment. These results and their implications will be discussed in chapter 5.

4.2.3.3 *The effect of SBN-B_extra on Dally-YFP*

Dally-YFP is present in both the apical and the basolateral compartments (chapter 4.1.6). In the attempt of enriching the basolateral fraction, I expressed SBN-B_extra in the posterior compartment of Dally-YFP heterozygous wing discs (*hh-Gal4*, chapter 2.1).

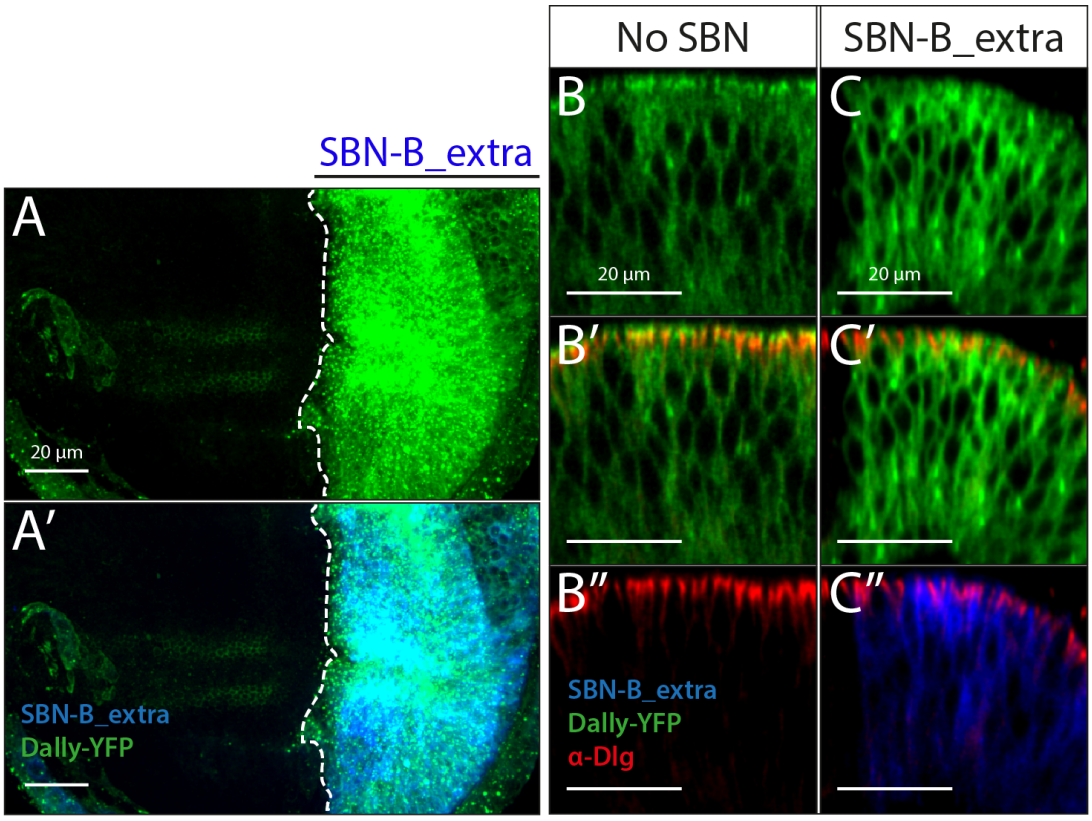

Figure 4.30 Dally-YFP is stabilized in the basolateral compartment by SBN-B_extra. A. Maximum projection of a Dally-YFP (green) heterozygous wing disc expressing SBN-B_extra (blue) in the posterior compartment. The fluorescence intensity was adapted to the high signal in the posterior compartment; therefore anterior compartment levels are underexposed and not representative. **B.** Cross-section of a representative area of the anterior compartment of a Dally-YFP heterozygous wing disc. Dally-YFP localizes to the apical (above Dlg, red) and basolateral compartment. **C.** Cross-section of a representative area of the posterior side of a Dally-YFP heterozygous wing disc expressing SBN-B_extra. Dally-YFP localizes only at the basolateral compartment (below Dlg, red). Please note that fluorescence levels have been adjusted and are not to be compared between (B) and (C). The dotted line indicates the border of expression of the SBN-B_extra. SBN-B_extra is expressed with *hh-Gal4* (chapter 2.1).

Upon coexpression with SBN-B_extra, Dally-YFP fluorescence levels were drastically enhanced (Figure 4.30A). Moreover, the subcellular distribution of Dally-YFP changed drastically when coexpressed with SBN-B_extra, as the apical fraction of Dally-YFP was lost and the basolateral levels were strongly enhanced (Figure 4.30B, C). Therefore, the observed increase in Dally-YFP fluorescence is due to a strong stabilization along the basolateral compartment.

To address the functional impact of the basolateral fraction of Dally-YFP, I analysed P-Mad in Dally-YFP heterozygous wing discs expressing SBN-B_extra. The preliminary results show a shrinking of the P-Mad gradient in the posterior compartment, accompanied by reduction in compartment size (Figure 4.31).

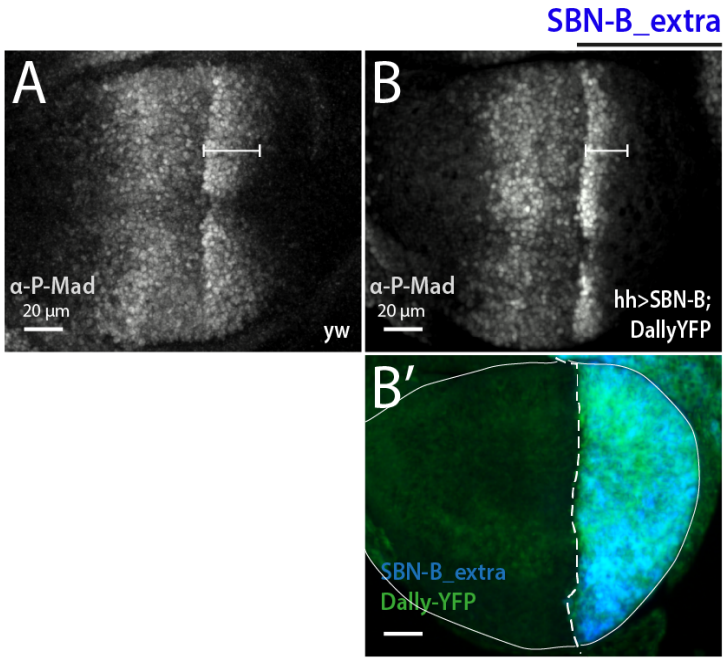

Figure 4.31 P-Mad gradient range is reduced upon basolateral enrichment of Dally-YFP. A. P-Mad (grey) gradient in a yw wing disc. **B.** P-Mad (grey) gradient in a Dally-YFP (green, B') heterozygous wing disc expressing SBN-B_extra in the posterior compartment (blue, B'). P-Mad range is restricted in the posterior compartment of (B). The posterior compartment size is reduced in (B'). Solid white line outlines the wing disc pouch in (B'). The dotted line indicates the border of expression of the SBN-B_extra. SBN-B_extra is expressed with *hh-Gal4* (chapter 2.1).

It will be interesting to further characterize the effect of the Dally-YFP basolateral enrichment on the spreading of the basolateral pool of Dpp ligand (discussed in chapter 5).

4.3 Manipulation of the endogenous Tkv locus using HR coupled with the CRISPR/Cas9 technology

In chapter 4.1, I showed that TGF-β receptors distribute differentially along the apical-basal axis of the wing disc epithelium. In order to gain insights into the physiological implications of these different subcellular distributions, it would be advantageous to modify receptors at their endogenous locus. Can mislocalized versions still fulfil normal receptor function? Are such modified receptors enough to support the complex developmental processes giving rise to an adult fly?

Because of its fundamental role during wing development, the Tkv receptor was chosen for genomic manipulation. First, I have aimed to generate a platform that allows modification of the endogenous *tkv* locus and Tkv protein tagging. Since tagging can affect protein function (Stadler et al., 2013), I generated two different versions of mCherry-tagged Tkv, where the tag is either extracellular or intracellular (C-terminal). By comparing these two lines, I will show that the position of the tag crucially influences receptor function. In a next step, I have deleted a basolateral targeting signal in the intracellular domain of Tkv and characterized the impact of this deletion on the subcellular localization and functionality of the Tkv receptor.

4.3.1 Strategy for tagging *tkv* at the endogenous locus

In order to manipulate the endogenous *tkv* locus, I have used a two-step approach (J. Huang et al., 2009), which relies on deleting the target gene and replacing it with a ΦC31-integration site (attP landing site) (Figure 4.33A). In the second step, I used this landing site to reintroduce modified target-gene DNA into the *tkv* locus, using re-entry vectors (Figure 4.33B).

The *tkv* locus extends over 60 kb and is therefore too large to be deleted and exchanged by HR. Four alternative splicing variants have been annotated

for the *tkv* gene, which differ in their extracellular domains (Figure 4.32A). All four splicing variants are characterized by two common exons at the C-terminal end, encoding for a part of the extracellular domain (113 aa), the transmembrane and intracellular domains (Figure 4.32B, C).

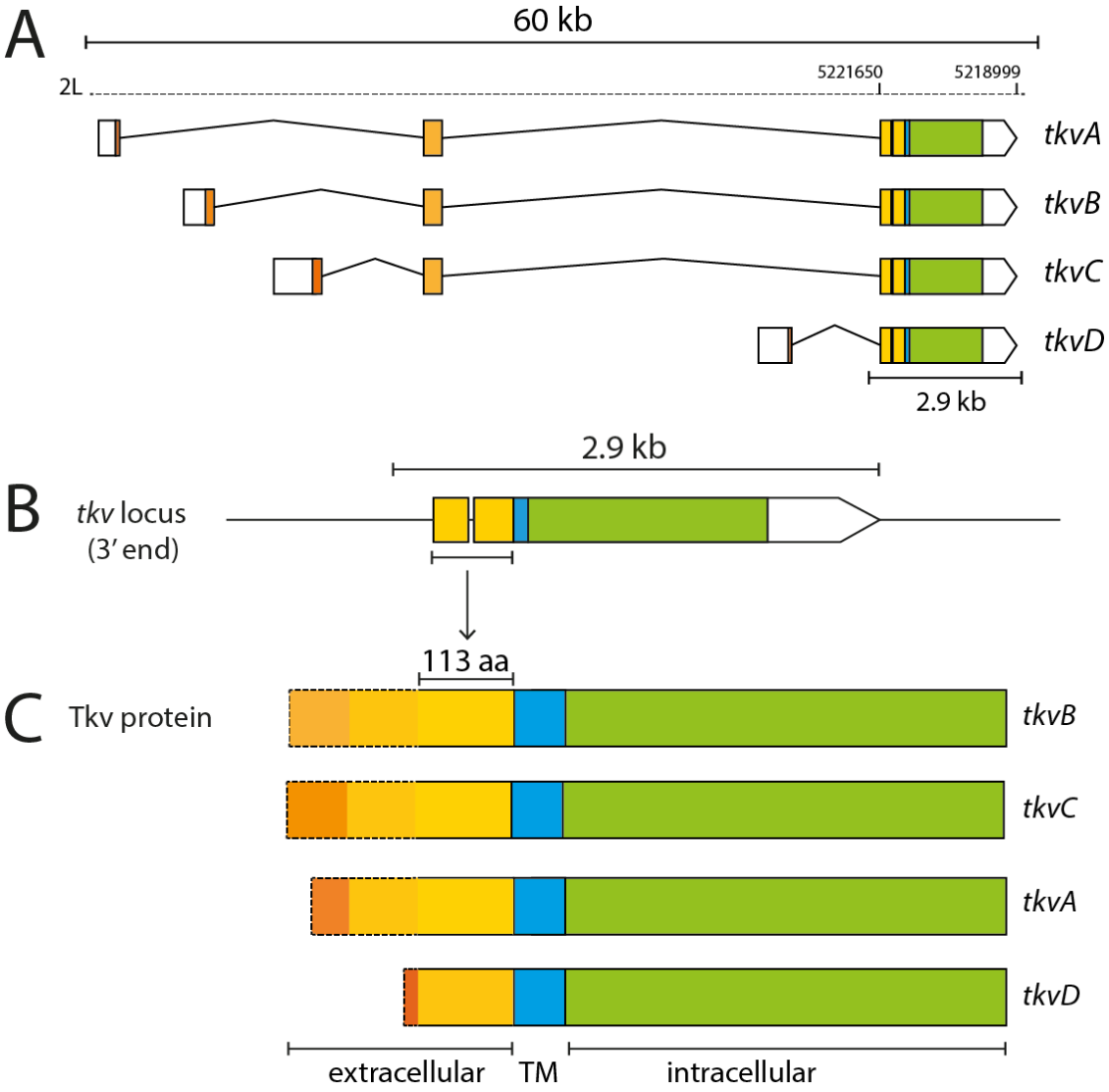

Figure 4.32 Schematic representation of the tkv locus. A. The *tkv* locus encompasses a region of 60 kb. The *tkv* gene has four splicing variants. The common region of all splicing isoforms consists of the last two exons at the 3'end. **B.** Schematic representation of the last two exons at the 3' end of the *tkv* locus. This region encodes the intracellular, the TM and a portion of the extracellular domain (113 aa). **C.** The different translated splicing variants differ in their extracellular domain (113 aa are common). The transmembrane domain and intracellular domain are shared by all splicing isoforms. White boxes=UTR. Orange=coding for an extracellular portion. Green=coding for an intracellular portion. Blue= coding for the transmembrane portion.

The common last two exons cover a region of approximately 2.9 kb and every modification of this region will be retained by all splicing isoforms.

Therefore, I aimed to replace the last two exons of *tkv* with a landing site and a screening marker, using ends-out gene targeting (Gong & Golic, 2003; J. Huang et al., 2009). The screening marker I used consists of the *mini-white (w^{+})* gene, driven by the Hsp70 promoter. This screening cassette is removable, since it is flanked by *loxP* sites (floxed) and can be precisely excised by Cre recombinase.

In *D. melanogaster* target-specific HR efficiency can be extremely variable depending on the locus (from 2.8x10^{-6}% to 0.5% of targeting efficiency) (J. Huang, Zhou, Watson, Jan, & Hong, 2008; Jones, Cayirlioglu, Grunwald Kadow, & Vosshall, 2006). Coupling DSBs with HR, can dramatically increase the efficiency of gene targeting (up to 7% of targeting efficiency, chapter 1.6.1) (L. A. Baena-Lopez et al., 2013; Beumer et al., 2008; Gratz et al., 2014a; Katsuyama et al., 2013). Thus, to increase the efficiency of HR, I have used the CRISPR/Cas9 technology to induce a DSB (L. A. Baena-Lopez et al., 2013). This approach has recently been named "homology-directed repair" (HDR, Gratz et al., 2014a). In order to generate a *tkv* null allele and insert an *attP* landing site in the *tkv* locus (Figure 4.33A), I designed the 5' and 3' homologous arms required for swapping the target region with a 50-bp attP phage recombination site and a floxed *mini-white*$^{+}$ screening marker and cloned them into the targeting vector (J. Huang et al., 2009). Importantly, the homologous arms contain the sequence immediately adjacent to the Cas9 cleavage sites (Gratz et al., 2014a). I have injected the targeting vector, together with two gRNAs, into flies expressing Cas9 in the germline (*vasa-Cas9*; see chapter 2.1). The two gRNAs are designed to induce DSB at the edges of the region of exchange (last two exons) in the *tkv* locus (Figure 4.33A).

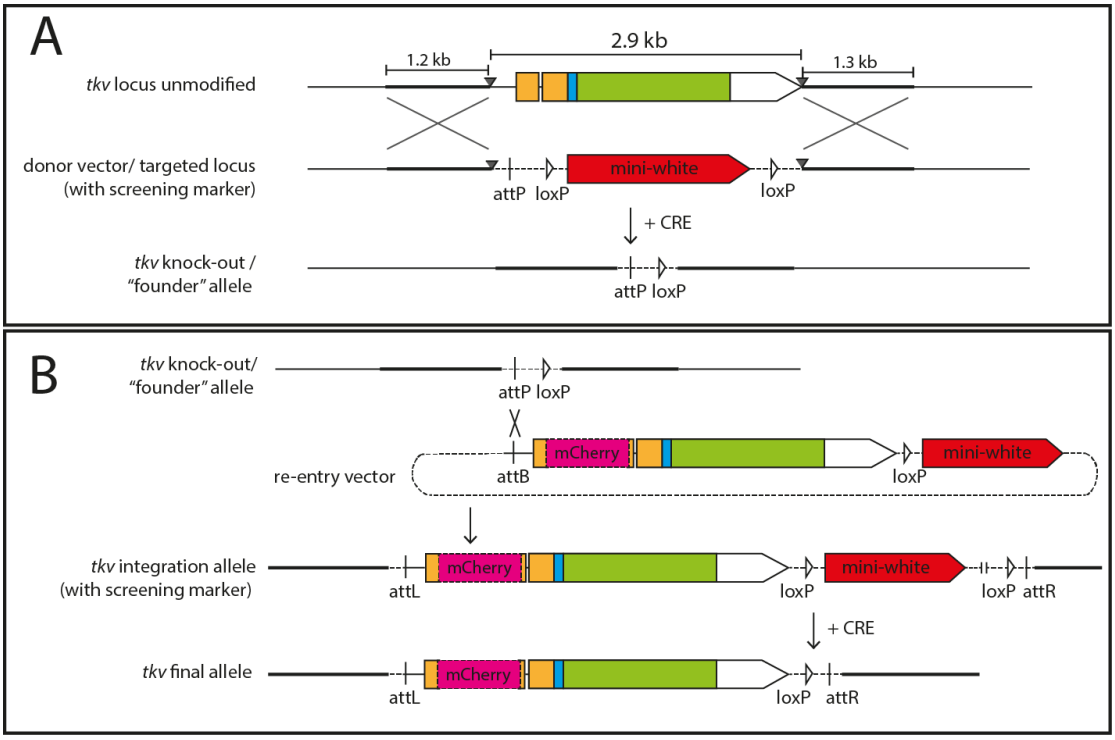

Figure 4.33 Targeting of the *tkv* gene. A. A founder knock-out allele is generated by inducing a double-strand break with a gRNA couple (arrows), which improves HR-mediated ends-out replacement. The donor vector used contains an attP landing site and the removable mini-white (red) screening marker, flanked by 5' and 3' homology arms (thicker black lines). Subsequently, the marker is removed by Cre-mediated excision. **B.** The engineered *tkv* allele is modified by using a re-entry vector containing an attB site. The ΦC31-mediated recombination of attP and attB sites leads to the incorporation of the whole re-entry vector into the *tkv* locus. The re-entry vector carries a mini-white marker, which can be removed together with the rest of the vector sequence, thanks to Cre-mediated excision. In the case depicted, Tkv is tagged at the extracellular domain with the fluorescent protein mCherry.

4.3.2 Choice of gRNAs and homologous arms

In order to obtain high targeting efficiency and to avoid off-targets, I used the web-based tool FlyCRISPR Optimal Target Finder for the gRNAs design (developed in Gratz et al., 2014a). This web-tool recognizes and classifies CRISPR target sites, based on their specificity (potential for off-target cleavage). During injections, I have tested two different CRISPR gRNAs couples to target the *tkv* locus. Hence, donor vectors with different homology arms were used for each gRNA couple. I was able to recover recombinant flies only with one of the couples injected. This result correlated

with the data obtained using the CRISPR Efficiency Evaluator tool (Housden et al., 2015). This tool scores gRNAs for the predicted efficiency of their nucleotide sequence based on experimental data. The recommended score has to be higher than 7, which was only true for the successful gRNA couple (8 versus 5.7). All the CRISPR gRNAs injected had no predicted off-targets.

4.3.3 Generation of a *tkv* knock-out allele and insertion of a landing site

I have used two different CRISPR gRNAs couples (therefore two donor vectors with different homology arms) and injected over 11,000 embryos (of which around 3,600 for the first gRNAs couple and 7,400 for the second gRNAs couple). The survival rate of the injected embryos was approximately 8.4%, similar than what observed for these same *vasa-Cas9* fly line (10%, Gratz et al., 2014a). The second gRNAs couple injected was successful, with a very low percentage of germline transmission 1/620 (1 founder male out of 620 crosses), meaning 0.16% of germline transmission. This founder male gave 4 transgenic flies out of 30 total flies of its progeny, meaning 13% HDR progeny per founder. These frequencies of germline transmission are low, when compared to what was observed with similar approaches (1/500 injected embryos (L. A. Baena-Lopez et al., 2013), 3-18% germline transmission Gratz et al., 2014a). However, as mentioned above, HR efficiency can be extremely variable, depending on the targeted locus.

I established 3 stocks out of the 4 transgenic flies obtained (1 male was sterile) and analysed and confirmed the integration by PCR and sequencing (Figure 4.34A). I have obtained a 2.9 kb deletion and introduced an attP landing site and a removable *mini-white*$^{+}$ (w^{+}) gene marker (Figure 4.33A). The line generated is here referred to as *tkvKO-attP(1)* and is homozygous lethal, as known for previously characterized *tkv* mutants (Nellen et al., 1994; Penton et al., 1994). Nevertheless, *tkvKO-attP(1)* heterozygous flies are viable

and develop wings that are slightly smaller and more round when compared to wild-type flies (Figure 4.33B, C). Unfortunately, the *tkvKO-attP(1)* heterozygous flies have low fertility and they could not produce the amount of embryos required for injections.

At the same time, the Pyrowolakis laboratory generated a similar *tkvKO-attP* allele, named here *tkvKO-attP(2)*. These flies were also generated through HR-based gene targeting, but without using the CRISPR/Cas9 system. The *tkvKO-attP(1)* and *tkvKO-attP(2)* alleles are functionally the same, since they both contain an *attP* landing site at the *tkv* locus, replacing the coding region of the last two exons of *tkv* (Figure 4.33A). However, the break points of HR-exchange differ between the two alleles (see chapter 2.5). The main difference between the two alleles consists in the 3'UTR region of tkv, that is deleted in *tkvKO-attP(1)* allele, but still intact in the *tkvKO-attP(2)* allele.

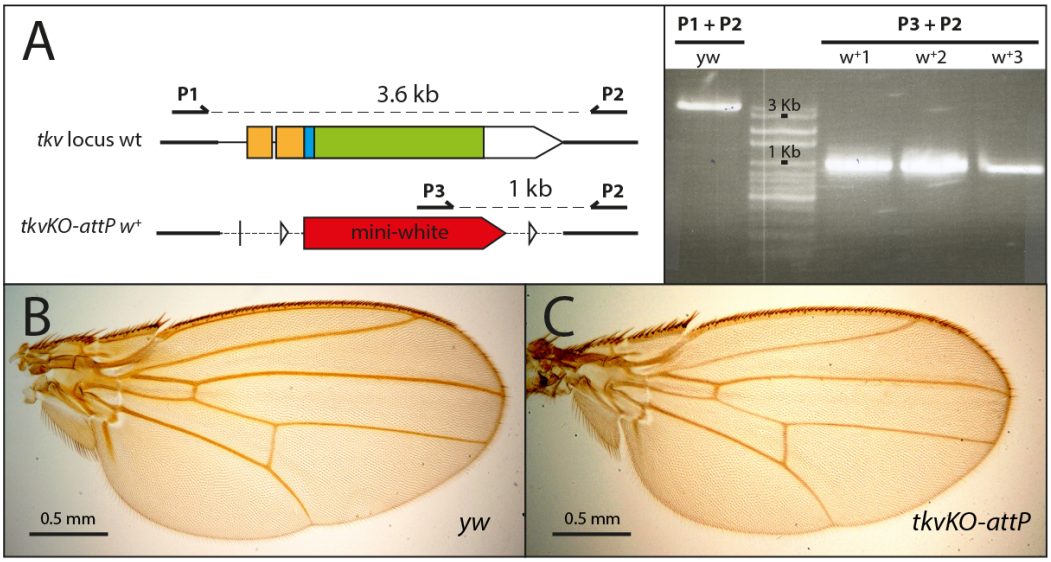

Figure 4.34 Isolation of *tkvKO-attP(1)* flies. A. PCR screening of *tkvKO-attP(1)* flies reveals the isolation of three identical *tkvKO-attP(1)* alleles. The primer couple P1 and P2 was used to detect the wild-type allele, whereas P3 is specific to the mini-white gene and was used to screen the targeted insertion. Primers external to the homology regions where used for sequencing and confirmed the generation of the *tkvKO-attP(1) w+* allele. **B.** Representative adult wing of yw (wild-type) female fly. **C.** Representative adult wing of *tkvKO-attP(1)* heterozygous female fly. For primer sequence see **Table 6**.

Interestingly, the *tkvKO-attP(2)* heterozygous fly line has higher fertility compared to the *tkvKO-attP(1)* heterozygous fly line. The reason for this difference is not clear and will be discussed in chapter 5. For the above mentioned reasons, the *tkvKO-attP(2)* heterozygous fly line was used for injection of the re-entry vectors, presented in the following section.

4.3.4 Re-entry vectors design and injection

The aforementioned *tkvKO-attP(2)* founder line was used to generate engineered *tkv* alleles by ΦC31-mediated integration (Figure 4.33B, chapter 2.5). The observed integration efficiencies were 5.5% on average, comparable to the integration rates observed in (J. Huang et al., 2009). However the survival rates of injected embryos were low (with an average of 2%, compared to an average of 20.5% observed in J. Huang et al., 2009).

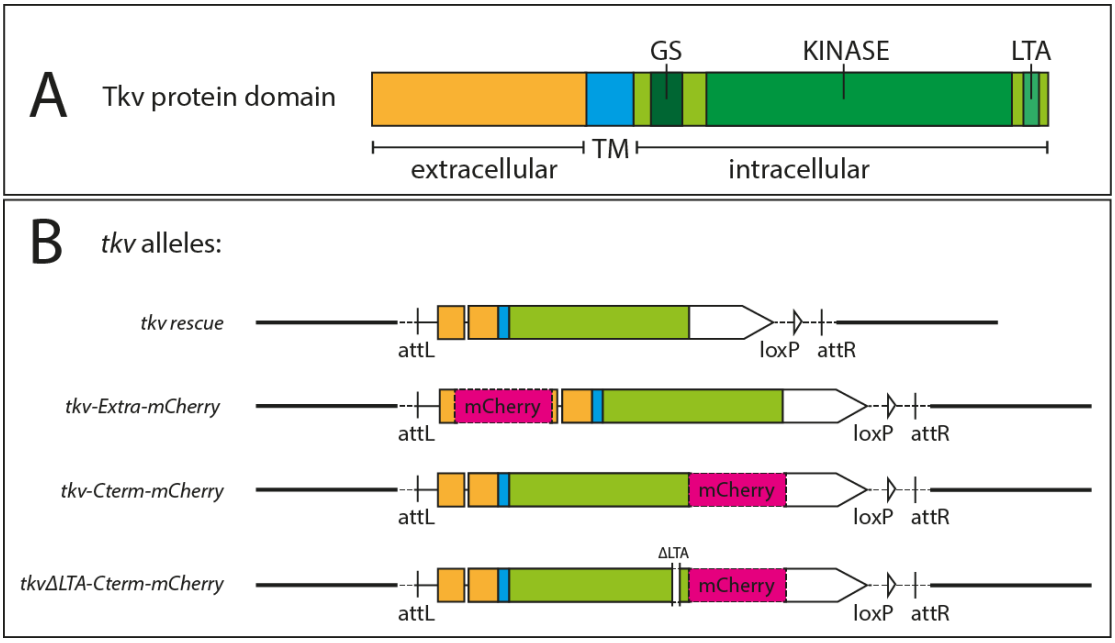

Figure 4.35 Schematic representation of the engineered *tkv* alleles generated. A. Protein domains of Tkv. The GS domain is phosphorylated by the type-II receptor and the kinase domain is responsible for pathway transduction. LTA is a putative targeting domain. **B.** Different *tkv* alleles generated using the *tkvKO-attp(2)* fly line. Extracellular = orange. Intracellular = green. TM = Blue.

The *tkv* alleles generated with this approach are depicted in (Figure 4.35B). I generated three different *tkv* alleles and a wild-type rescue as control (Figure 4.35B). With the *tkv-rescue* allele, I reintroduced the targeted region of the *tkv* locus without any modification. The other alleles generated encode endogenously tagged version of the Tkv protein. As mentioned above, the targeted region of the *tkv* locus includes the last two *tkv* exons that code for a large portion of the protein (Figure 4.32). This allows a very flexible design regarding the position of the tag, since both the extracellular and the intracellular domains of Tkv can be modified. Thus, I generated different *tkv* alleles inserting a fluorescent protein tag in either the extracellular domain (*tkv-Extra-mCherry* allele) or at the C-terminal end of Tkv (*tkv-Cterm-mCherry* allele) (Figure 4.35B). I used the fluorescent protein mCherry to tag Tkv, since it is monomeric, highly photostable and with fast maturation (Shaner, Steinbach, & Tsien, 2005). Furthermore, I have generated a mutant version of the C-terminally tagged Tkv-mCherry, in which a putative targeting sequence was deleted from the *tkv* coding region (Figure 4.35B). The recovered transgenic flies are characterized in the following section.

4.4 Characterization of the generated Tkv alleles

I have generated engineered *tkv* alleles by ΦC31-mediated integration into the *tkvKO-attP(2)* fly line (see chapter 4.3). Here, I report the characterization of these *tkv* alleles, with focus on the subcellular localization and on the receptor function of their different protein product.

4.4.1 Characterization of the *tkv-rescue* allele

To confirm that the manipulation of the *tkv* locus does not disturb the function of Tkv, I generated the *tkv-rescue* allele by reintroduction of the last two exons of *tkv* (Figure 4.35).

The *tkv-rescue* allele was recovered based on the w^+ marker expression and was subsequently confirmed by PCR and sequencing (Figure 4.36A).

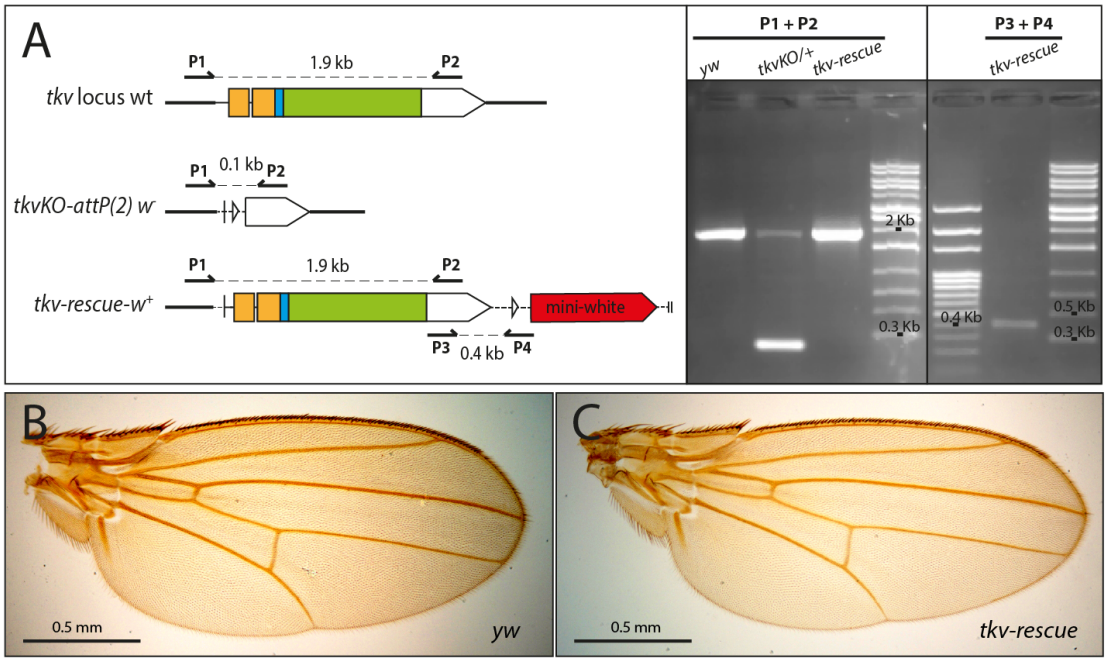

Figure 4.36 Generation of the *tkv-rescue* allele. A. PCR screening strategy for the isolation of *tkv-rescue-w*$^+$ flies. The primer couple P1 and P2 was used to amplify 1.9 Kb in *yw* and *tkv-rescue-w*$^+$, which was reduced to only 0.1 Kb by the deletion in the *tkvKO-attP(2)* mutant allele. The P4 primer binds to the exogenous regions introduced with the *tkv-rescue-w*$^+$ allele, giving a specific band of 0.4 kb indicating successful insertion. **B.** Adult wing of yw (wild-type) female fly. **C.** Adult wing of *tkv-rescue-w*$^+$ homozygous female fly. See **Table 7** for primers sequence.

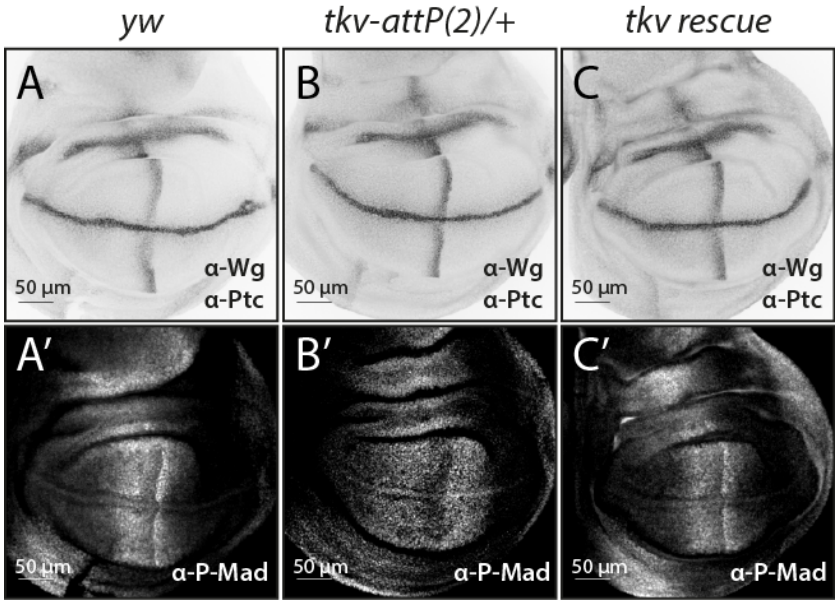

Figure 4.37 P-Mad gradient is comparable to wild type in *tkv-rescue* homozygous wing discs. A. A representative yw (wild type) wing disc, stained for Wg and Ptc (A) and P-Mad (A'). **B.** A representative *tkv-attP(2)* heterozygous wing disc, stained for Wg and Ptc (B) and P-Mad (B'). P-Mad range is broader and the gradient is clearly altered by the loss of *tkv*. **C.** A representative *tkv-rescue* homozygous wing disc, stained for Wg and Ptc (C) and P-Mad (C'). P-Mad appear comparable to wild type.

The allele is homozygous viable and the adult wings of *tkv-rescue* homozygous flies do not show detectable defects (Figure 4.36C). Moreover, no evident alteration of the P-Mad gradient is visible in *tkv-rescue* homozygous wing discs (Figure 4.37C'). Note that P-Mad gradient is severely altered in tkv-attP(2) heterozygous, consistent to what reported for tkv^{a12} heterozygous mutants in (Ogiso et al., 2011).

4.4.2 Characterization of Tkv-Extra-mCherry

Tkv-Extra-mCherry flies were recovered based on the w^+ marker and confirmed by PCR and sequencing (see chapter 2.5). These flies carry a mCherry tag in the extracellular domain of Tkv (64 aa before the transmembrane domain) (Figure 4.38B, chapter 2.5).

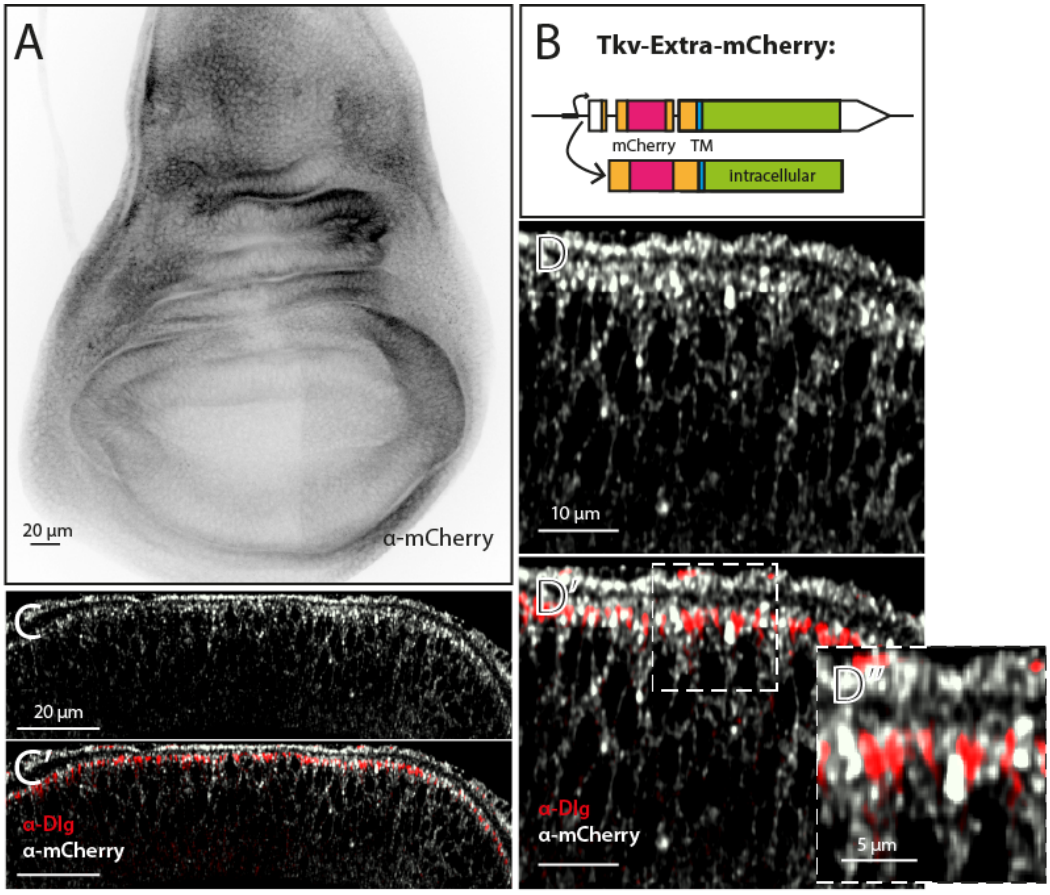

Figure 4.38 The localization of Tkv-Extra-mCherry in the wing imaginal disc. **A.** The expression pattern of Tkv-Extra-mCherry in the wing disc. **B.** Tkv-Extra-mCherry is an endogenous protein tag (mCherry, in the extracellular domain of Tkv). Extracellular = orange. Intracellular = green. TM = blue. mCherry tag = pink. **C.** Cross-section of an heterozygous Tkv-Extra-mCherry wing disc, stained for mCherry (grey) and Dlg (red). **D.** Magnification of an area of the posterior compartment of the cross-section in (C). Tkv-Extra-mCherry is present in the apical (above Dlg, D') and basolateral compartment of the wing disc. The apical fraction appears reduced in several regions of the wing disc (D'').

Tkv-Extra-mCherry was expressed at low levels in the central region of the wing pouch and high laterally, with higher basal levels in the posterior medial region, recapitulating the expected *tkv* expression pattern (Figure 4.38A). Tkv-Extra-mCherry was localized in the apical and basolateral compartment of the wing disc cells (Figure 4.38C, D), as observed for Tkv-3xHA (chapter 4.1.1). However, the apical fraction was reduced in several regions of the wing disc (Figure 4.38D''). The *tkv-Extra-mCherry* allele was not homozygous

viable, probably due to the fact that the extracellular tag influence the signalling ability of Tkv (see chapter 4.4.5).

4.4.3 Characterization of Tkv-Cterm-mCherry

The isolation of *Tkv-Cterm-mCherry* allele was based on the w^+ marker expression and confirmed by PCR and sequencing (see chapter 2.5).

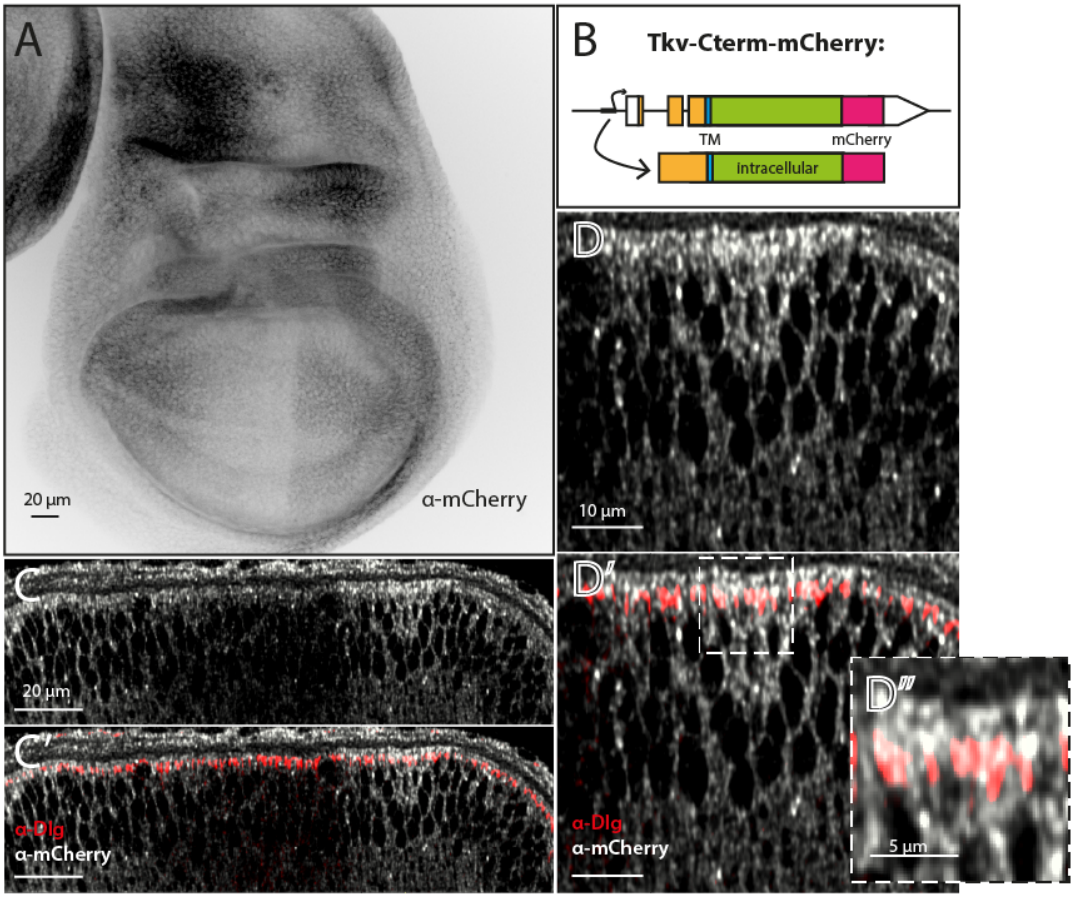

Figure 4.39 The localization of Tkv-Cterm-mCherry in the wing disc. A. The expression pattern of Tkv-Cterm-mCherry in the wing disc. **B.** Tkv-Cterm-mCherry is an endogenous protein tag (mCherry at the C-terminal end of Tkv). Extracellular = orange. Intracellular = green. TM = blue. mCherry tag = pink. **C.** Cross-section of an heterozygous Tkv-C-term-mCherry wing disc, stained for mCherry (grey) and Dlg (red) . **D.** Magnification of an area of the posterior compartment of the cross-section shown in (C). Tkv-Cterm-mCherry is present in the apical (above Dlg, D', D'') and the basolateral compartment of the wing disc.

The *Tkv-Cterm-mCherry* flies carry a mCherry tag at the C-terminal end of Tkv (Figure 4.39B) and showed the expected *tkv* expression pattern (Figure 4.39A). When analysed with subcellular resolution, Tkv-Cterm-mCherry signal was detected in the apical and basolateral compartment of the wing imaginal disc (Figure 4.39C, D). The subcellular distribution of Tkv-Cterm-mCherry was comparable to Tkv-3xHA (chapter 4.1.1), suggesting that the mCherry does not disturb Tkv localization. The *tkv-Cterm-mCherry* heterozygous flies displayed normal P-Mad signalling activity in the wing disc pouch (see chapter 4.4.5, discussed in chapter 5). However, the *tkv-Cterm-mCherry* allele was not homozygous viable.

4.4.4 Characterization of TkvΔLTA-Cterm-mCherry

TkvΔLTA-Cterm-mCherry flies were successfully recovered, as confirmed by PCR and sequencing (see chapter 2.5). These flies carry a mCherry tag at the C-terminal end of Tkv. Moreover, a putative basolateral targeting signal, named LTA (Figure 4.35, Figure 2.1, 11 aa) for its homology with the LTA domain found in the TGF-β type-II receptor (Murphy et al., 2007), see chapter 1.5.1), was deleted from the *tkv* coding region (Figure 4.40B).

TkvΔLTA-Cterm-mCherry recapitulated the expected *tkv* expression pattern in the wing imaginal disc (Figure 4.40A).

The LTA signal of the TGF-β type-II receptor is required for basolateral retention and its deletion caused gain of apical signal (Murphy et al., 2007). Accordingly, TkvΔLTA-Cterm-mCherry showed a clear enrichment in the apical compartment, but still retained a basolateral fraction (Figure 4.40C, D). A portion of the TkvΔLTA-Cterm-mCherry heterozygous wing discs displayed additional folding of the wing disc epithelium (Figure 4.40A).

In the next section, I will characterize the influence of the position of the tag and the mutation of the LTA signal on the function of Tkv.

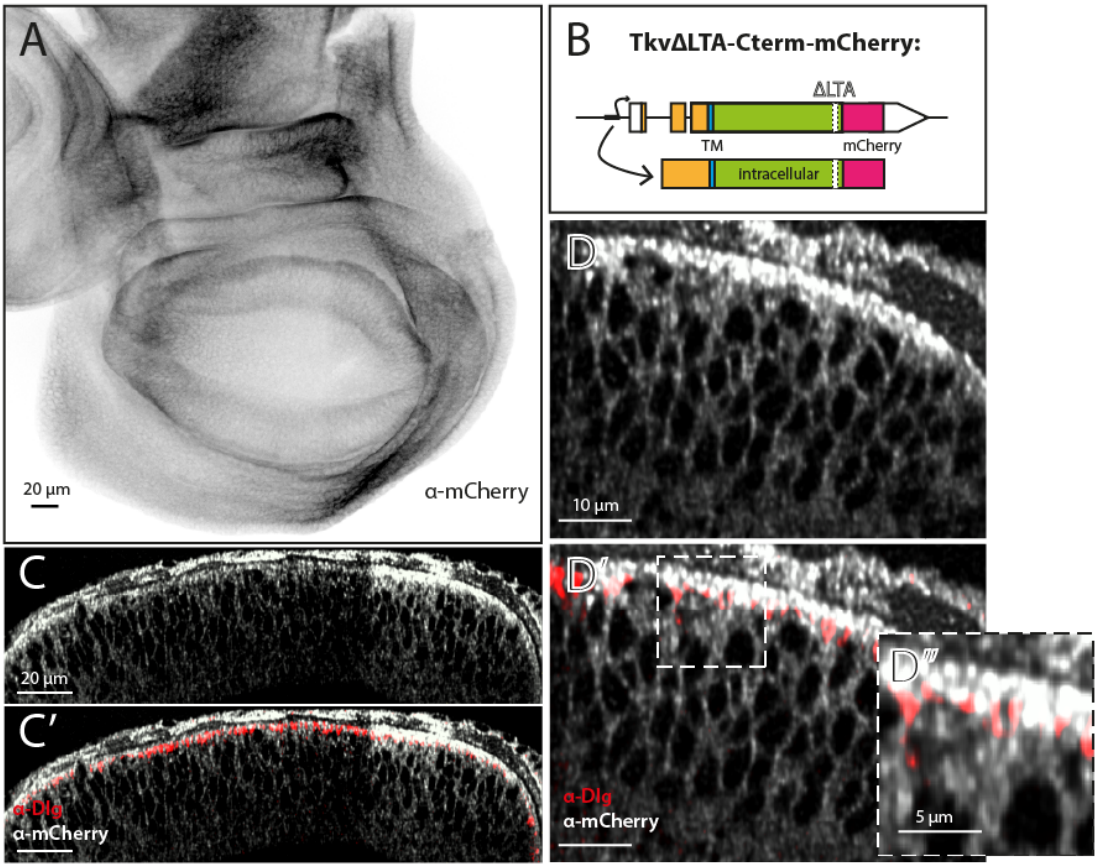

Figure 4.40 The localization of TkvΔLTA-Cterm-mCherry in the wing disc. A. The expression pattern of TkvΔLTA-Cterm-mCherry in the wing disc. **B.** In TkvΔLTA-Cterm-mCherry the basolateral LTA signal is deleted and mCherry tag inserted at the C-terminal end. Extracellular = orange. Intracellular = green. TM = blue. mCherry tag = pink. **C.** Cross-section of an heterozygous TkvΔLTA-Cterm-mCherry wing disc, stained for mCherry (grey) and Dlg (red) . **D.** Magnification of an area of the posterior compartment of the cross-section in (C). TkvΔLTA-Cterm-mCherry is enriched in the apical compartment (above Dlg, D′, D′′) and present in the basolateral compartment of the wing disc. The apical enrichment is more evident in the posterior compartment of the wing disc.

4.4.5 Tkv function is altered by tagging in a position-dependent manner and by mutation of the LTA signal

The function of Tkv in the wing imaginal disc is to mediate Mad phosphorylation in response of BMP ligand interaction (chapter 1.3.3.1). Thus, I analysed P-Mad gradients in wing discs heterozygous for the *tkv-Extra-mCherry*, *tkv-Cterm-mCherry* and *tkvΔLTA-Cterm-mCherry* alleles and compared them to wild-type (yw).

In wild-type wing discs, P-Mad distributes into a bidirectional gradient in the anterior and posterior compartment (Figure 4.41A''). Because of higher Tkv levels, in the posterior compartment the P-Mad gradient has a higher peak of intensity and a steeper slope (see chapter 1.3.2.1 and 1.3.3.1). Moreover, P-Mad levels are low in the Dpp source (anterior side of the A/P boundary), because in these cells Tkv is strongly downregulated by Hh (Tanimoto et al., 2000). The *tkv-Cterm-mCherry* heterozygous wing discs showed similar P-Mad gradient to wild-type wing discs (Figure 4.41C'').

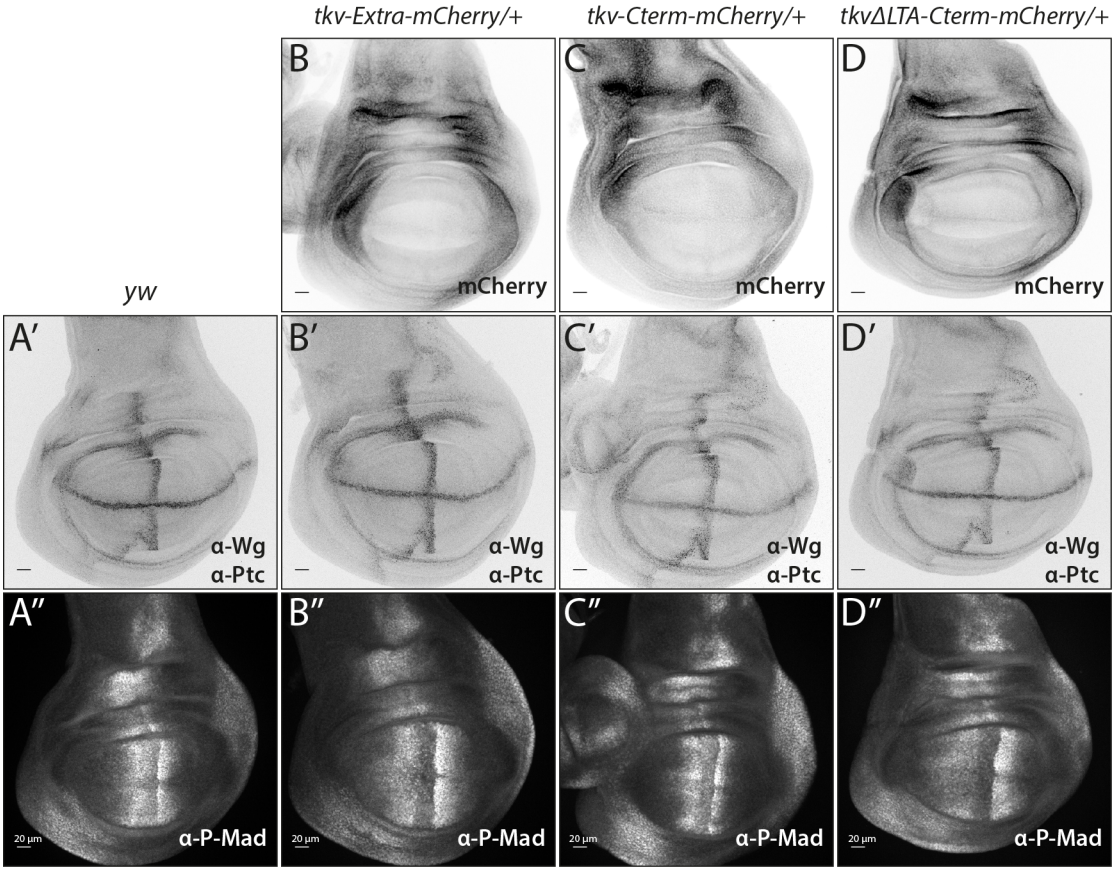

Figure 4.41 P-Mad gradient is broader in *tkv-Extra-mCherry* and *tkvΔLTA-Cterm-mCherry* heterozygous wing discs. A. A representative wild-type (yw) wing disc, stained with α-Wg and α-Ptc (A') and α-P-Mad antibodies (A''). **B.** A representative *tkv-Extra-mCherry* heterozygous wing disc, showing mCherry signal in (B) and stained for Wg and Ptc (B') and P-Mad (B''). **C.** A representative *tkv-Cterm-mCherry* heterozygous wing disc, showing mCherry signal in (C) and stained for Wg and Ptc (C') and P-Mad (C''). **D.** A representative *tkvΔLTA-Cterm-mCherry* heterozygous wing disc, showing mCherry signal in (D) and stained for Wg and Ptc (D') and P-Mad (D''). Scale bars = 20 µm.

In contrast, Tkv-Extra-mCherry showed a broader P-Mad gradient and a wider repression domain along the A/P boundary (Figure 4.41B''). The *tkv-Cterm-mCherry* heterozygous wing discs showed a wild-type P-Mad profile. However, when the LTA domain was deleted from the coding region of Tkv (*tkvΔLTA-Cterm-mCherry* heterozygous), P-Mad gradient range was increased (Figure 4.41D''). Moreover, in absence of the LTA domain, the repression domain of the P-Mad gradient located along the A/P boundary was broader and the intensity levels of P-Mad appeared lower than in wild-type and *tkv-Cterm-mCherry* heterozygous wing discs (Figure 4.41D'').

The alterations of the P-Mad gradient observed in *tkv-Extra-mCherry* and *tkvΔLTA-Cterm-mCherry* heterozygous were similar, but could have different reasons. Similar effects were observed in tkv^{a12} heterozygous mutants (Ogiso et al., 2011) and will be discussed in chapter 5.

4.5 Additional results

4.5.1 Characterization of the YFP exon skipping in Tkv-YFP flies

In chapter 4.2.3.1, I made use of an endogenously tagged Tkv-YFP line, retrieved from the Cambridge Protein Trap Insertion collection (Lowe et al., 2014; Lye et al., 2014). The CPTI lines were generated using a piggyBac transposition vector that carries an artificial YFP-Venus exon and that randomly integrated into the genome. Tkv-YFP is the result of an integration event happened in position 5223813 of chromosome 2L, corresponding to the second-last and largest intron of the *tkv* gene (Figure 4.43A). This integration was fortunate since this intron is common to all four splicing isoforms of *tkv*. The *tkv-YFP* allele is homozygous viable and the YFP signal can be detected in different tissues from stage 5 of embryogenesis to adulthood (see annotation from the CPTI consortium, flAnnotator). During larval stage, Tkv-YFP is expressed in all imaginal discs (data not shown), and it is expressed at high levels in the wing disc, where it recapitulates the expected *tkv* expression pattern (Figure 1.13). However, Tkv-YFP flies are characterized by a different subcellular localization, when compared to Tkv-3xHA flies (discussed in 4.2.3.1). Moreover, the wings of *tkv-YFP* homozygous flies reveal some patterning defects: the posterior cross vein (PCV) is thicker and there are some additional bristles in the longitudinal veins (LV) (data not shown). In addition to this, P-Mad gradient in *tkv-YFP* homozygous flies is broader, when compared to *tkv-YFP* heterozygous (Figure 4.42), as would be expected due to alterations of *tkv* function (Figure 4.37, Ogiso et al., 2011). I also observed that *tkv-YFP* homozygous larvae develop slower compared to *tkv-YFP* heterozygous. From the aforementioned data, it appears that Tkv-YFP is not fully functional. Nevertheless, the *tkv-YFP* allele is homozygous viable. This could be due to the fact that the receptor function of Tkv-YFP is not perturbed dramatically enough to drastically disturb fly development.

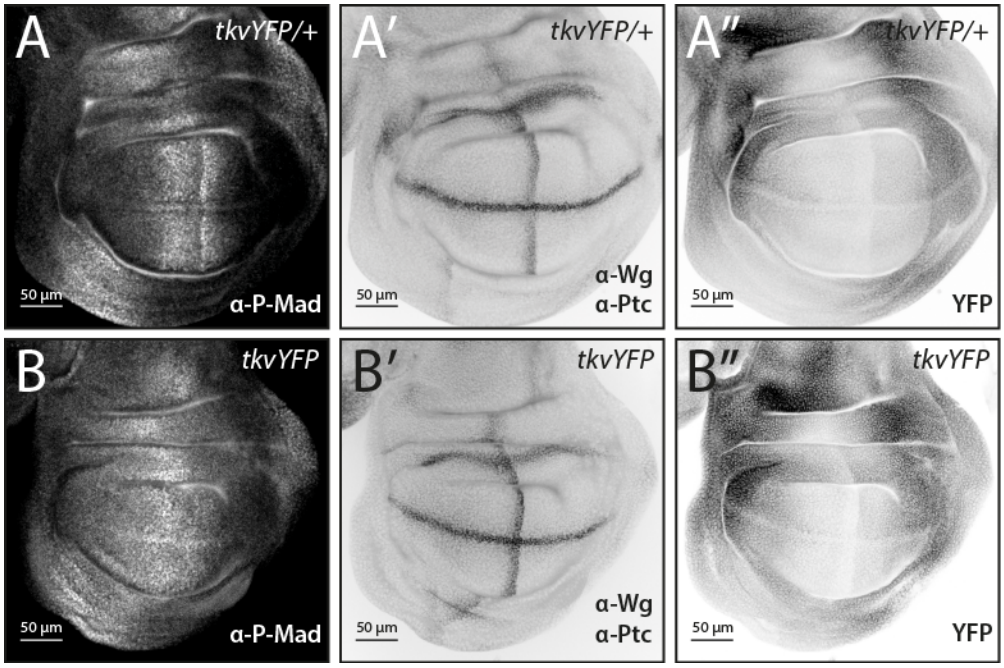

Figure 4.42 Tkv-YFP homozygous show altered P-Mad gradient. A. A representative Tkv-YFP heterozygous wing disc (100 AEL). The P-Mad gradient appears comparable to wild type. **B.** A representative Tkv-YFP homozygous wing disc (100 AEL). P-Mad is broader when compared to Tkv-YFP heterozygous. Moreover, the disc appears smaller as they would belong to an earlier developmental stage (B′, B′′).

Alternatively, it could be that a significant portion of Tkv is left untagged and it is the one able to fulfil the physiological receptor functions. Considering this, I addressed the issue of YFP exon skipping.

The generation of a protein trap relies on the integration of a transposable element into the intron of a coding region. The transposable element carries an engineered exon, made of a tag flanked by strong splicing donor and acceptor sites. In the case of Tkv-YFP, the splicing donor and acceptor sites of the Myosin Heavy Chain locus were used to flank the YFP-Venus exon. The artificial splicing acceptor and donor are supposed to be strongly recognized by the splicing machinery, however they compete with the endogenous sites. Especially in cases where the trapped protein is not fully functional, the cellular machinery could use exon skipping as a rescue mechanism. To estimate trapping efficiency I used semi-quantitative (semi-q) and quantitative (q) RT-PCR (Real-time PCR) (Figure 4.43B).

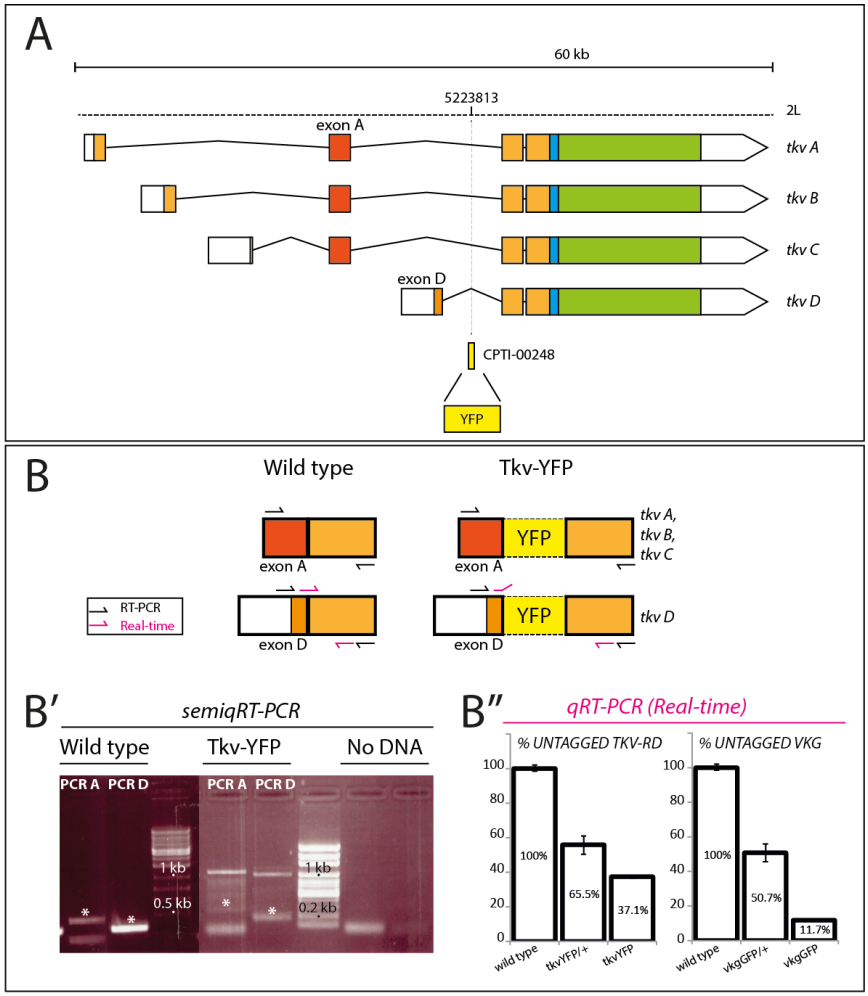

Figure 4.43 The YFP exon is not retained in all tkv transcripts of Tkv-YFP flies. A. Schematic representation of the *tkv* locus, with the four *tkv* splicing isoforms and the insertion site of the exogenous YFP exon that results in the generation of Tkv-YFP. **B.** The YFP exon is skipped in a portion of *tkv* transcripts. The exon skipping was observed with semi-quantitative RT-PCR (B'). In wild type a 388 bp band corresponds to the *tkv-A/B/C* isoforms (*, PCR A), and a 160 bp band to tkv-D (*, PCR D). Those bands (*) are still present in Tkv-YFP homozygous wing discs, indicating that exon skipping is not restricted to a specific splicing isoform. However, the majority of the exon skipping happens for the *tkv-D* isoform (B'). The incorporation of the YFP exon is visible as a shift in the wild type band (1.3 and 1.1 kb for PCR A and PCR D, respectively) (B'). When quantified, 37.1% of the *tkv-D* isoform revealed to be untagged in Tkv-YFP homozygous wing discs. The vkg-GFP RNA was used as a control for the Real-time PCR strategy **(Pastor-Pareja & Xu, 2011)**.

For semi-qRT-PCR I designed primers binding the exons flanking the YFP exon (Figure 4.43B, B'). For Real-time PCR, I used primers binding the exon junction and the exon flanking the YFP exon: in this way, the integration of the YFP exon is negatively detected, since the primer cannot bind to the exon junction in presence of the YFP coding region (Figure 4.43B, B''). Using

both methods, I detected the presence of an untagged fraction of Tkv in Tkv-YFP homozygous wing discs (Figure 4.43B', B''). The YFP exon skipping is not restricted to a specific splicing isoform of *tkv*, however is more relevant for the *tkv-D* isoform, that is also the most abundantly expressed isoform in wing discs and adults (FlyBase annotated transcripts, data not shown). YFP exon skipping was detected in 65% of the *tkv-D* transcripts in *tkv-YFP* heterozygous flies and 37% in the *tkv-YFP* homozygous flies (Figure 4.43B''). This indicates that only 63% of *tkv-D* transcripts are YFP-tagged in *tkv-YFP* homozygous flies. As a control, I used the *vkg-GFP* (*viking*) flies, for which trapping efficiency has been estimated with this same technique in (Pastor-Pareja & Xu, 2011). The results obtained for *vkg-GFP* were similar to what previously reported and indicated that around 90% of the *vkg* transcripts retain the GFP exon in *vkg-GFP* homozygous (5-10% variation compared to (Pastor-Pareja & Xu, 2011) FIG. S1).

Overall, these results reveal the flaws of the Tkv-YFP protein trap line and support the evidence for the need of modifying the endogenous *tkv* locus using precise gene targeting techniques (chapter 4.3).

5 DISCUSSION

5.1 Subcellular localization of TGF-β receptors

The TGF-β superfamily in *D. melanogaster* comprises seven different ligands and five receptors. Thus, a certain level of redundancy has to play a role in ligand-receptor recognition. Hence, subcellular restriction of the localization of TGF-β superfamily ligands and receptors could serve as an important level of regulation, in order to achieve pathway and tissue-specificity.

However, the subcellular distribution of TGF-β superfamily receptors and ligands in the wing disc is not well understood. Two different versions of Dpp-GFP were described to spread through the basolateral and apical domain of the wing imaginal disc (Entchev et al., 2000; Gibson et al., 2002; Teleman & Cohen, 2000). However, this analysis should be repeated with higher resolution and better tools, which would allow the visualization of the endogenous protein. The spreading of Gbb has not been characterized with subcellular resolution. Nevertheless, an anti-Gbb antibody (DSHB, Yowa) and a BAC insertion containing Gbb-GFP fusion are available (Ray, 2015) and could be used for this analysis. No tools are available to characterize TGF-β/Activin ligands distribution.

In contrast, endogenous protein tags and third copy reporter alleles became available during the last years for all five TGF-β superfamily receptors and for the two glypicans Dally and Dlp. Using these tools, I systematically characterized the subcellular distribution of the TGF-β superfamily receptors and the glypicans in the wing imaginal disc.

5.1.1 The TGF-β receptors are differentially localized along the apical-basal axis

I found that the *D. melanogaster* TGF-β superfamily type-I receptors have different subcellular localizations: while the BMP receptors Tkv and Sax localize in both the apical and the basolateral compartment of the wing disc epithelial cells, the TGF-β/Activin receptor Babo localizes preferentially basolateral. Furthermore, also the TGF-β type-II receptors Punt and Wit show different subcellular localization. While Punt is localized exclusively to the basolateral compartment, Wit is not only present, but also enriched in the apical compartment of the wing disc epithelium. The glypicans Dally and Dlp are localized to apical and basolateral compartments, as previously reported (Ayers et al., 2010; Gallet et al., 2008). However, Dlp is enriched along the basolateral side of the wing disc epithelium.

5.1.2 The potential function of the differential subcellular localization of TGF-β receptors

I have shown that the TGF-β receptors localize differentially along the apical-basal axis of wing disc cells. These findings raise the question whether restricted receptor localization results in pathway activation from specific cell poles (polarized signalling). Polarized signalling was initially postulated to explain the finding that many signalling receptors localize basolaterally in epithelial cells (reviewed in S. K. Kim, 1997). Differential receptor localization was suggested as a mechanism to provide different layers of regulation in the activation of signalling pathways. As reported in chapter 1.4.1, restricted subcellular localization of receptors can be required to prevent unwanted pathway activation (Murphy et al., 2004; Sotillos et al., 2008) or to mediate distinct downstream responses to the same ligand (Wu et al., 2004). Therefore, receptor localization can actively control signalling output.

In this thesis, I showed that TGF-β type-I receptors have different subcellular localizations. The type-I receptor Babo, which belongs to the TGF-β/Activin branch, is excluded from the apical side of wing disc cells, whereas Tkv and Sax, belonging to the BMP branch, are present at both apical and basolateral compartments of the wing disc epithelium. These data suggest that the ability of Babo to bind and traduce signals from any TGF-β ligand is restricted to the basolateral side of the wing disc epithelium. Thus, signalling input perceived from the apical side would exclusively originate from the BMP branch. The segregation of TGF-β/Activin and BMP branches into distinct cellular compartments was previously observed in the NMJ system (M.-J. Kim & O'Connor, 2014) and in MDCK epithelial cells (Saitoh et al., 2012). In these systems, the differential localization of the TGF-β receptors was proposed to be responsible for the activation of distinct signalling inputs, namely Mad (Smad1/5/8) from the BMP branch and Smad2 for the TGF-β/Activin branch. Thus, the segregation of the TGF-β superfamily receptors into distinct membrane domains could serve to regulate pathway specificity also in the wing imaginal disc.

Furthermore, TGF-β signal transduction requires the presence of type-I and type-II receptors. Interestingly, the two TGF-β type-II receptors of *D. melanogaster* are both expressed in the wing imaginal disc and localize in a complementary pattern along the apical-basal axis. Punt is excluded from the apical domain, while Wit is enriched in the apical domain. Therefore, the activation of the type-I receptors Tkv and Sax in the apical domain (therefore the apical BMP signal transduction) would depend exclusively on the type-II receptor Wit. However, this hypothesis is challenged by several observations. First, *wit* is dispensable for wing development (see chapter 1.3.3.4, Marqués et al., 2002). Secondly, I did not observe any alteration in the P-Mad gradient when I overexpressed Wit in the wing imaginal disc (data not shown). Finally,

Punt is the main type-II receptor responsible for BMP signal transduction (Letsou et al., 1995; Nellen et al., 1996; Ruberte et al., 1995). The overexpression of *punt* indeed causes activation of P-Mad independently of ligand binding (data not shown, Nellen et al., 1996; Schwank, Dalessi, et al., 2011a). Since TGF-β type-II receptors are constitutively active kinases, it is expected that their overexpression causes constitutive pathway activation (Persson et al., 1997). In summary, these data suggest that Wit might not be competent to mediate BMP signalling in the wing imaginal disc. Wit is in principle able to activate Tkv and Sax, since it mediates BMP signalling in motor neurons and in follicle cells (Marmion et al., 2013; Marqués, 2003; Marqués et al., 2002; McCabe et al., 2003). However, in the wing disc: (1) the apical pool of BMP ligands could be too low or not existent (in contrast to what previously observed in Gibson et al., 2002), (2) an uncharacterized protein that prevents TGF-β pathway activation could be present in the apical domain, or (3) apical BMP ligands are being transcytosed to the basolateral side prior to signalling (as suggested for Wg, see Gallet et al., 2008; Yamazaki et al., 2016). It could also be that (4) a cofactor that Wit needs to mediate Mad activation is missing in the wing disc (and present in motor neurons). Finally, the function of Wit in the wing imaginal disc could be to mediate non-canonical TGF-β signalling acting from the apical side of wing disc cells, as showed for the activation of LIM kinase during NMJ growth (B. A. Eaton & Davis, 2005). Therefore, canonical and non-canonical TGF-β signalling could be uncoupled by segregating receptors into different membrane compartments.

If not signal transduction, what could be the function of the type-I receptors Tkv and Sax in the apical compartment? As mentioned above, the type-II receptor Punt is excluded from the apical compartment of wing imaginal disc cells. If Wit is not capable of carrying out the type-II receptor function, then

Tkv and Sax are not able to transduce signals from the apical surface. However, Tkv and Sax could still be required to control ligand spreading and endocytosis from the apical side of the wing disc epithelium. Tkv was shown to bind the Dpp ligand with higher affinity than Gbb and Tkv levels are crucial to fine-tune the range of Dpp spreading (see chapter 1.3.3.1). In contrast, Sax was shown to preferentially bind Gbb and also interacts with Dpp when bound by Tkv (see chapter 1.3.3.2). Thus, I am tempted to speculate that the major function of Tkv and Sax in the apical compartment are the control of apical BMP ligands spreading and stability. Moreover, the type-I receptors – acting together with the glypican Dally – could mediate BMP ligands transcytosis from the apical to the lateral side of the wing disc, as observed for Hh and Wg (D'Angelo et al., 2015; Gallet et al., 2008; Yamazaki et al., 2016) (see chapter 1.4.2).

The glypicans Dally and Dlp also showed different enrichment along the apical-basal axis. It was shown that Dally can bind both Dpp and Gbb and is reported to influence Dpp spreading and signalling, whereas Dlp can bind only Gbb (Dejima et al., 2011). The two glypicans show a complementary subcellular bias, since Dally is enriched in the apical compartment, whereas Dlp is enriched at the basolateral side. Thus, the functions of Dally and Dlp would be more prominent at the apical or lateral side of the wing disc epithelium, respectively. Interestingly, Dlp overexpression was shown to increase Wg stability in the lateral compartment, supporting this hypothesis (Gallet et al., 2008). The increase in Wg stability in the lateral compartment was accompanied by a reduction in the apical Wg fraction, suggesting that Dlp is involved in shuttling Wg ligands between different cell compartments. As mentioned above, a similar mechanism could also apply to TGF-β ligands.

In conclusion, the apical and the basolateral compartment of the wing imaginal disc epithelium are characterized by a different composition of

receptors and might have different properties concerning the control of ligand spreading and signalling transduction.

Further studies are necessary to understand the function of receptor localization concerning TGF-β ligands spreading and signalling.

5.2 Nanobodies as tools for transmembrane protein mislocalization

In order to understand the function of receptor localization, I investigated ways to mislocalize transmembrane proteins along the apical-basal axis. Conventionally, protein mislocalization could be achieved by altering trafficking of the whole cell. However, these methods are unspecific and provide results that are difficult to interpret because of the unphysiological conditions generated and the vast array of factors that are modified. Studying protein function in a specific membrane compartment could also be achieved by depletion or overexpression of the protein of interest. However, this approach does not investigate the specific relevance of protein localization, but rather the general function of the protein itself and can be used only for proteins with exclusive localization to one membrane compartment. Another way to change the localization of a specific protein consists of mutating targeting domains present in the protein sequence. This causes missorting of the target protein that is directed to the inappropriate cell compartment. This last approach is very valuable, since it allows interfering with the localization of a specific target protein without disturbing the overall cellular environment (discussed in chapter 5.3.2).

In this thesis, I used scaffold bound anti-GFP nanobodies (SBNs) as novel tools for protein mislocalization along the apical-basal axis. SBNs have the advantages to: (1) provide a general and convenient framework to specifically mislocalize proteins, since large collections of GFP-tagged protein are

available in *D. melanogaster* (Lowe et al., 2014; Lye et al., 2014; Nagarkar-Jaiswal et al., 2015; Sarov et al., 2015); (2) induce protein mislocalization in a tissue-specific and temporally-controlled manner, since SBNs can be expressed under the control of the UAS/Gal4 system.

I used SBNs that localize to specific domains along the apical-basal axis: uniformly localized (SBN-AB_extra), apically enriched (SBN-A_extra/intra) or exclusively basolateral (SBN-B_extra) (Figure 4.16). The SBNs are characterized by a specific membrane topology, where the anti-GFP nanobody is presented along the extracellular cell surface (SBN_extra) (Figure 4.16B, C, D). Additionally, the apically enriched SBN-A was generated in a version with reverse topology, where the anti-GFP nanobody faces the cytosol (SBN-A_intra). These two designs allow the modification of extracellular and intracellular GFP-tagged proteins, respectively.

When coexpressing SBNs with GFP/YFP-tagged proteins, I observed efficient mislocalization of several of these target proteins along the apical-basal axis of the wing imaginal disc. In particular, SBNs changed the localization of the uniformly distributed PH-GFP, of the basolateral protein Nrv1 and of the apical determinant Crb. These results indicate that SBNs can be used for protein mislocalization to both the apical and the basolateral compartment. Moreover, only SBN-A_intra could mislocalize intracellular, membrane bound PH-GFP. This indicates that the toolset only works if the nanobody and the GFP tag are both presented to the same side of the cell membrane. The exact mechanism of SBNs action is not entirely clear. If SBNs interact with the target protein during trafficking, they would need to be contained in the same trafficking vesicles as the target protein, which usually does not happen for proteins with different subcellular localization (Carmosino et al., 2012). Further analysis is needed to characterize the molecular mechanisms responsible for the SBNs-induced mislocalization.

Of particular interest was the mislocalization of Crb-GFP obtained with the SBN-B_extra. The coexpression of Crb-GFP with SBN-B_extra led not only to a loss of the apical Crb signal, but also to the gain of a significant basolateral fraction of Crb (Figure 4.19 and Figure 4.23). The basolaterally-mislocalized fraction of Crb was at least partially membranous, suggesting that Crb might still be functional in this membrane compartment (Figure 4.20). As a result of Crb mislocalization, the apical protein PatJ was strongly reduced in the apical compartment of wing disc cells (Figure 4.21). When SBN-B_extra was expressed in the posterior compartment of Crb-GFP homozygous wing discs, only cells with high expression levels of SBN-B_extra showed efficient Crb-GFP mislocalization (Figure 4.23). This indicates that the expression ratio of SBN/target protein correlates with the efficiency of mislocalization. Moreover, cells in which Crb-GFP was effectively mislocalized (Crb-GFP homozygous) showed variable shape and size along the apical-basal axis, as well as a visible fold along the border of SBN-B_extra expression domain (Figure 4.23). More experiments will be needed to understand the reason for these alterations. For example, it will be necessary to induce clones expressing SBN-B-extra in Crb-GFP homozygous conditions and quantitatively analyse their distribution, size and shape to understand the functional effect of Crb mislocalization. Crb is required for the localization of many apical proteins in the wing imaginal disc and for controlling apical domain size (see chapter 1.1.2) (Genevet et al., 2009; Hamaratoglu et al., 2009; Pellikka et al., 2002). Furthermore, both *crb* loss and *crb* overexpression were reported to induce Hippo-dependent overgrowth (C.-L. Chen et al., 2010; Grzeschik et al., 2010; Ling et al., 2010; Lu & Bilder, 2005; Robinson et al., 2010). Thus, further experiments should aim to characterize the alteration of apical protein and Hippo pathway component distribution, induced by the mislocalization of Crb in Crb-GFP homozygous condition. This will help to understand the

functional relevance of Crb mislocalization and the impact of ectopic basolateral Crb on wing disc cells.

5.2.1 SBNs as tools for receptors mislocalization and stabilization

In the work presented in this thesis, I used SBNs to mislocalize TGF-β receptors and co-receptors along the apical-basal axis. In particular, I attempted to mislocalize Tkv-YFP, Punt-GFP and Dally-YFP to investigate the function of their localization. The results shown are preliminary and further experiments are required to conclusively interpret the data obtained.

In Tkv-YFP heterozygous conditions, the expression of the SBNs led to a clear relocalization of Tkv-YFP (Figure 4.24). However, when these experiments were repeated in Tkv-YFP homozygous conditions, the mislocalization became less effective and SBN-A_extra was itself partially mislocalized to the lateral compartment (Figure 4.25). This effect is likely due to the increase in the dose of Tkv-YFP, since the expression ratio of SBNs to target protein importantly influences SBNs efficiency (as mentioned above for Crb-GFP). In addition, the mislocalization of SBN-A_extra might be explained by a stronger tendency of Tkv to localize basolateral, than the SBNs tendency to localize apical.

The coexpression of SBNs in Tkv-YFP homozygous wing discs also caused loss of P-Mad signalling and a reduction of epithelial thickness, a phenotype reminiscent of a loss of *tkv*/Dpp signalling (Nellen et al., 1996; Schwank, Tauriello, et al., 2011b; Widmann & Dahmann, 2009a). These results could be explained by several interpretations. Firstly, SBNs could prevent Tkv endocytosis, which was suggested to be a requirement for the signalling function of Tkv (Belenkaya et al., 2004; Entchev et al., 2000; Teleman & Cohen, 2000). Secondly, the interaction of the SBNs with Tkv-YFP could interfere with one of the steps required for Tkv activation. For example, SBNs could interfere with ligand binding. Analysing whether Tkv-YFP is still

sensitive to Dpp overexpression when bound to SBNs, could test this hypothesis. It is also possible that SBNs interfere with the formation of the receptor complex. In that case, Tkv-YFP bound to SBNs should be insensitive to the activation induced by Punt overexpression. Furthermore, this hypothesis could be tested by using SBNs together with a constitutively active version of Tkv-YFP/GFP (TkvQ253D-YFP/GFP). If constitutively active Tkv bound to SBNs cannot mediate Mad phosphorylation, then the SBNs could interfere with the activation of Mad, for example by masking the Tkv kinase domain or hindering the interaction of Tkv with Mad. Eventually, Tkv-YFP may not represent suitable tool, since it does not recapitulate the observed localization of Tkv-3xHA, lacking the apical fraction. Moreover, the YFP is not retained in all *tkv* transcripts, as shown in chapter 4.5.1.

I also used the SBNs to mislocalize another TGF-β receptor, Punt-GFP. Mislocalization of Punt is crucial to understand the function of the polarized localization of TGF-β receptors, since Punt is excluded from the apical domain and it is unclear whether the apical type-II receptor Wit can sustain signalling function in the apical domain. Indeed, an increase in P-Mad was observed when Punt-GFP was mislocalized to the apical side of the wing disc cells. This result suggests that signal activation can happen from the apical compartment. However, further analysis and controls are missing to conclusively interpret this data. It would be very valuable to attempt to mislocalize endogenous Punt protein by modifying the *punt* locus, as will be discussed for Tkv in the following section.

Finally, I attempted to modify Dally-YFP localization with SBN-B_extra. Remarkably, SBN-B_extra changed the subcellular localization of Dally-YFP, leading to a loss of apical signal and a strong stabilization of the basolateral fraction. The alteration of Dally-YFP localization resulted in a shrinking of the P-Mad gradient, accompanied by a size reduction of the modified wing disc

compartment (Figure 4.31). Dally regulates both Dpp spreading and signalling (Crickmore & Mann, 2007; Fujise et al., 2003) (chapter 1.3.3.5). Shortening of the P-Mad range was observed with both *dally* overexpression in the *dpp* stripe and with *dally* loss of function (Crickmore & Mann, 2007; Fujise et al., 2003). However, *dally* overexpression in the posterior compartment caused broadening of the P-Mad gradient (Hufnagel et al., 2007). Therefore, the observed reduction in P-Mad range when mislocalizing Dally-YFP could be the result of two effects: (1) the absence of Dally-YFP in the apical compartment could block apical Dpp signaling, e.g. by preventing Dpp endocytosis from the apical side (discussed in 5.1.2). Moreover, (2) the strong increase in basolateral Dally-YFP levels might interfere with the spreading of the lateral pool of Dpp. Thus, it will be crucial to characterize the effect of Dally-YFP mislocalization on Dpp spreading. This can be done by performing extracellular stainings against Dpp and observe the alterations of the apical and basolateral Dpp fractions. Additionally, if Dally-YFP acts as a co-receptor in the apical compartment, apical signalling could be lost due to Dally-YFP mislocalization.

In conclusion, further analyses are required to assess whether the binding of SBNs to the target protein leaves the protein function intact.

5.3 Manipulation of the endogenous *tkv* locus

In order to study the localization and function of the endogenous Tkv protein, I have attempted to manipulate the endogenous *tkv* locus. Using the CRISPR/Cas9 technology, I deleted the two major coding exons of *tkv* and replaced them with a landing site. Ultimately, this approach allowed me to reintroduce either wild type or mutated versions of the *tkv* coding sequence and thereby test the function of the Tkv protein *in vivo*.

Initially, I used TALENs to generate the DSBs required for enhancing HR, together with the pTV-Cherry plasmid developed in (L. A. Baena-Lopez et al., 2013). Unfortunately, this strategy was not successful. TALENs technology has now been largely replaced by the CRISPR/Cas9 technology, probably due to differences in time and bench work required for the production.

In a second approach, I used the CRISPR/Cas9 system to generate the DBS together with a targeting vector (J. Huang et al., 2009). The targeting efficiency I obtained was low when compared to similar approaches (0.16% versus 3-18% of germline transmission). However, the targeting efficiency can vary greatly depending on the locus and on the target sites chosen (chapter 1.6.1).

The *tkvKO-attP(1)* heterozygous flies I generated showed low fertility and they could not produce the amount of embryos required for integration of the re-entry vectors. For this reason, I used the *tkvKO-attP(2)* allele generated in the Pyrowolakis laboratory.

There are two main differences between the *tkvKO-attP(1)* and the *tkvKO-attP(2)* alleles, which could account for their different phenotypes.

First, the break points of HR-exchange differ between the two alleles (see chapter 2.5). The *tkvKO-attP(1)* allele carries a bigger deletion of the *tkv* locus, deleting the 3'UTR of *tkv*, which is still present in the *tkvKO-attP(2)* allele. The 3'UTR of *tkv* overlaps with 50 bp of the 3'UTR of the neighbouring gene *tpnC25D* (*troponin C* located at the 25D chromosome subdivision), which were deleted in the *tkvKO-attP(1)* allele. Thus, the function of the *tpnC25D* gene could be compromised in *tkvKO-attP(1)* flies and cause fertility defects. However, *tpnC25* mutant allele are viable, since five genes encode for Troponin C in *D. melanogaster* and have redundant functions (Herranz et al., 2004). Moreover, no amelioration of the fertility defects was

observed when an additional copy of *tpnC25D* was supplied to the *tkvKO-attP(1)* flies (using the chromosomal duplication *Dp(2;3)tkv3*, chapter 2.1).

The second major difference between the *tkvKO-attP(1)* and the *tkvKO-attP(2)* alleles concerns their generation. The *tkvKO-attP(1)* allele was produced by using CRISPR/Cas9, whereas the *tkvKO-attP(2)* allele was generated with conventional gene targeting. The use of the CRISPR/Cas9 system could have caused off-target mutations in the *tkvKO-attP(1)* flies, even though no off-targets were predicted for the gRNAs used. Thus, the difference in fertility of *tkvKO-attP(1)* and *tkvKO-attP(2)* flies remains unclear.

Re-integration of the complete *tkv* wild type sequence (*tkv-rescue*) as well as a wild type sequence tagged with an HA-tag (*tkv-3x-HA*) into the attP landing site completely rescued the *tkv* phenotypes and resulted in viable and fertile flies, validating *tkvKO-attP(2)* as invaluable tool to study endogenous Tkv function.

5.3.1 The position of the tag influences Tkv function

In order to visualize endogenous Tkv and gain insights into the physiological implications of the subcellular distribution of Tkv, I generated different endogenously tagged versions of the Tkv protein. Since the position of the tag can affect protein function, I generated two different versions of mCherry-tagged Tkv, one with an extracellular tag (Tkv-Extra-mCherry) and one with a C-terminal tag (Tkv-Cterm-mCherry). The *tkv-Extra-mCherry* heterozygous wing discs showed alterations of the BMP signalling, with a broader P-Mad gradient, similar to what was observed in tkv^{a12} heterozygous mutants (chapter 4.4.5, Ogiso et al., 2011). Therefore, these results suggest that the chosen site for mCherry insertion affects Tkv function. In contrast, the *tkv-Cterm-mCherry* heterozygous wing discs displayed a wild-type P-Mad profile (chapter 4.4.5). However, in contrast to the wild type *tkv-rescue* and to

the *tkv-3xHA* alleles, both *tkv-Extra-mCherry* and *tkv-Cterm-mCherry* alleles were not homozygous viable. These results suggest that not only the position of the tag, but also the size of the tag is an important factor to consider in order to avoid altering protein function (27 aa for 3xHA versus 256 aa for mCherry). Thus, these results suggest that small epitope tags should in general be preferred to bigger tags.

5.3.2 The functional requirements for proper Tkv localization

I also generated tagged versions of Tkv in which putative targeting domains required for protein localization have been mutated or deleted. The ultimate goal of this approach was to test if mislocalized versions of the Tkv receptor can still function *in vivo* and if different subcellular fractions of Tkv might be involved in different properties/functions.

In order to understand the function of Tkv localization, I mutated a putative basolateral-targeting signal (LTA, Figure 2.1). The LTA signal was originally discovered and characterized in the TGF-β type-II receptor and is required for basolateral retention, since its deletion causes gain of apical localization (Murphy et al., 2007). Accordingly, TkvΔLTA-Cterm-mCherry showed a clear apical enrichment when compared to Tkv-Cterm-mCherry (and Tkv-3xHA) (Figure 4.40). However, the basolateral fraction of TkvΔLTA-Cterm-mCherry was still present and did not appear to be reduced. In response to this shift in Tkv subcellular localization, the P-Mad gradient expanded in range and was repressed in a larger region along the A/P boundary (*tkvΔLTA-Cterm-mCherry* heterozygous, Figure 4.41). As reported above, a similar alteration of the P-Mad gradient was observed in *tkv-Extra-mCherry* and tkv^{a12} heterozygous (Figure 4.41, Ogiso et al., 2011).

Assuming that the mutation of the LTA signal alters only Tkv distribution along the apical-basal axis, it appears that increasing Tkv levels in the apical

compartment caused an increase in Dpp spreading (seen by a broader P-Mad gradient). This could be explained by speculating that the apical Tkv fraction supports Dpp spreading, either by altering the movement of the apical Dpp pool or by mediating a hypothetical apical Dpp transcytosis to the lateral side. Alternatively, mutating the LTA could lead to alteration of Tkv function (such as ligand binding or receptor complex formation or kinase activity) or stability. This different hypothesis will be discussed in the following chapter.

5.3.3 The role of Tkv function and stability in shaping the Dpp signalling response

The described endogenous alterations of the *tkv* locus strongly impacted the observed Dpp signalling pattern (visualized by P-Mad) (Figure 4.41). Since these alterations affect different domains and therefore potentially different functions of the Tkv protein, there might be different explanations for the observed changes in P-Mad gradient shape.

Tkv was shown to have a dual action on the P-Mad gradient: high levels of Tkv were shown to both sensitize cells to Dpp signalling and at the same time limit Dpp spreading (Crickmore & Mann, 2006; Lecuit & Cohen, 1998; Tanimoto et al., 2000). Therefore, reduction of Tkv function should result in the opposite effect, increasing the spreading range of Dpp and decreasing its signalling strength. This can explain the broadening of the P-Mad gradient observed in the *tkv* heterozygous mutant conditions - using tkv^{a12} or the *tkv-attP(2)* allele (Figure 4.37). Interestingly, tkv^{a12} mutants lack 34 aa at the C-terminal portion of the receptor, deleting part of the kinase domain, arguing that this mutation interferes with the signalling function of the Tkv receptor (tkv^{a12} is also known as *tkv4*) (Lecuit & Cohen, 1997; Nellen et al., 1996; Penton et al., 1994; Terracol & Lengyel, 1994). Thus, inhibiting the signalling

function of Tkv, without modifying the extracellular domain, also results in increased Dpp spreading. These results could indicate that it is not the actual Tkv levels that (directly) regulate Dpp spreading, but rather that the signal transduction function of Tkv is required to indirectly regulate Dpp ligand spreading. For example, Dpp signalling is known to transcriptionally regulate target genes required to modify Dpp ligand spreading, such as the secreted factor Pent (Vuilleumier et al., 2010) and the glypican Dally (Fujise et al., 2003).

A broadening of the P-Mad gradient was also observed in *tkv-Extra-mCherry* heterozygous wing discs. This suggests that the extracellular mCherry tag interferes with Tkv functions. In particular, the extracellular tag could alter the ligand binding properties of Tkv, which would explain the broader P-Mad gradient (Dpp spreading is increased because Dpp is not bound and restricted by Tkv). The case of tkv^{a12} and *tkvΔLTA-Cterm-mCherry* heterozygous flies could be different. Both alleles leave the extracellular domain of Tkv intact, suggesting that the alteration of Dpp spreading observed (P-Mad range increase) depends on other properties of the Tkv receptor than ligand binding. As mentioned above, the signalling function of Tkv receptor could be impaired in tkv^{a12} and *tkvΔLTA-Cterm-mCherry* alleles. Alternatively, these mutations could change the protein stability and turnover properties of Tkv, and alter important cellular processes, such as Tkv endocytosis. Tkv endocytosis is required for BMP signalling in the wing disc and was suggested to involve internalization of the Dpp ligand, which would considerably impact the range of the extracellular Dpp gradient (Belenkaya et al., 2004; Miaczynska, Pelkmans, & Zerial, 2004).

The results shown are preliminary and a conclusive interpretation will require further analysis. In particular, it will be interesting to investigate how the extracellular Dpp gradient is altered in different *tkv* alleles. Characterization

of Dpp target genes like Sal, Omb and Brk in the different *tkv* alleles will help to understand how patterning is affected by Tkv alteration. Finally, the role of Dpp signalling in growth is still disputed (Akiyama & Gibson, 2015; Harmansa et al., 2015), therefore it will be interesting to quantitatively analyse the effect of Tkv mislocalization on the growth properties of the wing imaginal disc.

In conclusion, the work presented in my thesis provides evidence that TGF-β receptor levels and subcellular localization is of major importance in regulating *D. melanogaster* wing development. Furthermore, my results highlight the importance of studying protein function at the endogenous levels, thereby avoiding artefacts due to overexpression or altered spatial-temporal regulation. Finally, in this thesis I showed the potentials and the limitations of SBNs as novel tools to study and disturb the subcellular distribution of transmembrane proteins. With the characterization of both, endogenous protein modification and the SBNs toolset, I am providing a novel platform for future studies to better investigate the role of TGF-β receptors in *D. melanogaster* development.

6 LIST OF ABBREVIATIONS

aa	amino acids
ACV	Anterior cross vein
AJs	Adherens junctions
Ap	Apterous
aPKC	atypical Protein Kinase C
BAC	Bacterial Artificial Chromosome
Baz	Bazooka
BMP	Bone Morphogenetic Protein
Ci	Cubitus Interruptus
Crb	Crb
dAct	*Drosophila* Activin
Dad	Daughters against Dpp
Dally	Divisions abnormally delayed
Daw	Dawdle
Dlp	Dally-like protein
DP	Disc proper
Dpp	Decapentaplegic
EGFR	Epidermal Growth Factor Receptor
En	Engrailed
FP	Fluorescent Protein
Gbb	Glass bottom boat
GFP	Green Fluorescent Protein
GOI	Gene of interest
HDR	Homology-directed repair
Hh	Hedgehog
HR	Homologous Recombination

Hth	Homothorax
IF	Immunofluorescence
Iro-C	Iroquois-complex
kb	kilobase pairs
Lgl	Lethal Giant Larvae
LV	Longitudinal Vein
Mav	Maverick
Msh	Muscle segment homeodomain
Myo	Myoglianin
NMJ	Neuromuscular Junction
Nrv1/2	Nervana1/2
nts	nucleotides
Nub	Nubbin
PATJ	PALS1-associated tight-junction
PCV	Posterior Cross Vein
Pent	Pentagone
PM	Peripodial Membrane
POI	Protein of interest
Put	Punt
Rd	Rotund
Sax	Saxophone
SBN-A	Apically enriched SBN
SBN-AB	SBN uniformly localized (apical/basolateral)
SBN-B	Basolateral only SBN
SBNs	Scaffold-bound nanobodies
Scw	Screw
sGFP	Superfolder Green Fluorescent Protein
SJs	Septate Junctions

Sqh	Spaghetti squash
Std	Stardust
TGF-β	Transforming Growth Factor-β
Tkv	Thickveins
Tkv-EmCh	Tkv-mCherry (extracellular tag)
Tsh	Teashirt
TpnC25D	Troponin C on 25D
Ubx	Ultrabithorax
VEGF	Vascular Endothelia Growth Factor
Vg	Vestigial
Vkg	Viking
Wg	Wingless
Wit	Wishfulthinking
YFP	Yellow Fluorescent Protein
α	Anti

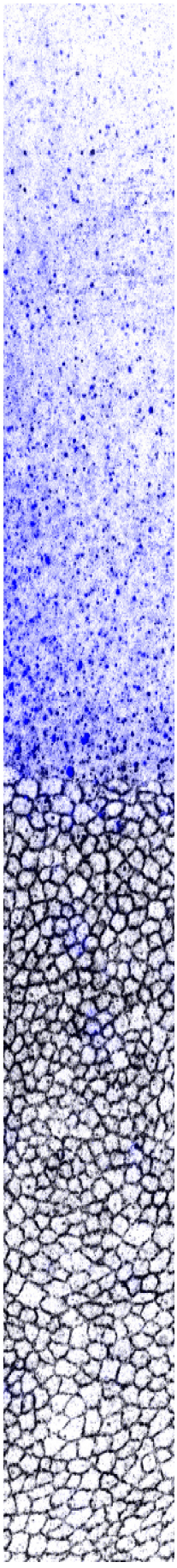

7 ACKNOWLEDGMENTS

"Everything should be made as simple as possible, but not simpler."

R. Session, A. Einstein

First of all, my gratitude goes to Professor Markus Affolter for giving me the opportunity to work in his great lab and for supporting me during these four years of PhD. I truly appreciate your scientific enthusiasm and knowledge and your drive towards high quality data. Also, thanks for patiently waiting and pushing me to finish this thesis.

I thank the members of my scientific committee, Giorgos Pyrowolakis and Konrad Basler for their time and scientific input. I would like to thank Giorgos for his generosity in sharing reagents with me from the beginning until the end of my PhD. Many thanks to Jennifer Gawlik for sharing the precious endogenous *tkv* tag and the *tkv* landing site.

Thanks to the former and present members of the Affolter lab. In particular, my biggest thank goes to Stefan B. Harmansa for being a great friend and scientist. Also, I want to sincerely thank him for proofreading and suffering with me on this thesis. I wish you all the success that you deserve in science and life. I also want to thank Shinya Matsuda PhD, for teaching me the real – but secret – meaning of the word Dpp. I want to thank Dimi and Mario for their friendship and for our Californian adventure. I will not forget how much you mistrusted my driving skills. And how

much fun we had. Grazie Ale, per i nostri caffè e le chiacchierate! Thanks to Amanda and Fisun for their support and encouragement, even after they left the lab. In particular, thank you Fisun for taking time to read my thesis in your busy PI+mum days. Many thanks to our first lady Helen, for taking care of all of us and for her constant kindness and patience.

Un grande ringraziamento a Gina, Karin e Bernadette. Per le nostre chiacchierate e per tutta la polenta che avete sfornato in questi anni per le mie moschine affamate. Thanks to Oliver, Alexia, Niko and Wolf of the IMCF facility for their help and excellent job.

The greatest thank goes to my family and friends.

To my splendid friends, Anna, Anjana, Pavlina, Dani, Vanja, JD and Andrea, I am so lucky to have you! Gloria, Ileana, Maria, che mondo sarebbe senza di voi? I hope you know how much I value you and your friendship.

I want to thank my family, to whom this thesis is dedicated. Alla mia mamma, il cui supporto è stato fondamentale negli ultimi mesi come per il resto della mia vita, grazie per essere la donna forte, intelligente e in gamba che sei. Ti ammiro molto e spero di diventare determinata e forte come te.

Alla mia sorellina, grazie per essere tu, per le tante cose che ti rendono speciale e che mi hai insegnato, per essere sempre felice per me, perché parliamo la stessa lingua (anche se il mio italiano sta peggiorando…). E grazie a Chiara, for being a great and very special cognatina and a knowledgeable perfume lover!

Last but not least, the final thank goes to Loïc for being an awesome boyfriend (and neat former desk mate) and for being smart and full of surprises. He supported me during these last months in many ways, from proofreading my thesis to cooking dinner and offering (or being obliged to offer) psychological counselling. I am so happy to have you in my life ;)

8 REFERENCES

Aberle, H., Haghighi, A. P., Fetter, R. D., McCabe, B. D., Magalhães, T. R., & Goodman, C. S. (2002). wishful thinking encodes a BMP type II receptor that regulates synaptic growth in Drosophila. *Neuron*, *33*(4), 545–558.

Affolter, M., & Basler, K. (2007). The Decapentaplegic morphogen gradient: from pattern formation to growth regulation. *Nature Reviews Genetics*, *8*(9), 663–674. http://doi.org/10.1038/nrg2166

Akhurst, R. J., & Padgett, R. W. (2015). Matters of context guide future research in TGFβ superfamily signaling. *Science Signaling*, *8*(399), re10. http://doi.org/10.1126/scisignal.aad0416

Akiyama, T., & Gibson, M. C. (2015). Decapentaplegic and growth control in the developing Drosophila wing. *Nature*, *527*(7578), 375–378. http://doi.org/10.1038/nature15730

Akiyama, T., Kamimura, K., Firkus, C., Takeo, S., Shimmi, O., & Nakato, H. (2008). Dally regulates Dpp morphogen gradient formation by stabilizing Dpp on the cell surface. *Developmental Biology*, *313*(1), 408–419. http://doi.org/10.1016/j.ydbio.2007.10.035

Alberto Baena-Lopez, L., Rodriguez, I., & Baonza, A. (2008). The tumor suppressor genes dachsous and fat modulate different signalling pathways by regulating dally and dally-like. *Proceedings of the National Academy of Sciences of the United States of America*, *105*(28), 9645–9650. http://doi.org/10.1073/pnas.0803747105

Alexandre, C., Baena-Lopez, A., & Vincent, J.-P. (2014). Patterning and growth control by membrane-tethered Wingless. *Nature*, *505*(7482), 180–. http://doi.org/10.1038/nature12879

Allan, D. W., Pierre, S., Miguel-Aliaga, I., & Thor, S. (2003). Specification of Neuropeptide Cell Identity by the Integration of Retrograde BMP Signaling and a Combinatorial Transcription Factor Code. *Cell*.

Arora, K., Dai, H., Kazuko, S. G., Jamal, J., & O'Connor, M. B. (1995). The drosophila schnurri gene acts in the Dpp/TGFβ signaling pathway and encodes a transcription factor homologous to the human MBP family. *Cell*.

Arora, K., Levine, M. S., & O'Connor, M. B. (1994). The screw gene encodes a ubiquitously expressed member of the TGF-beta family required for specification of dorsal cell fates in the Drosophila embryo. *Genes & Development*, *8*(21), 2588–2601. http://doi.org/10.1101/gad.8.21.2588

Ashe, H. L., Ashe, H. L., Levine, M., & Levine, M. (1999). Local inhibition and long-range enhancement of Dpp signal transduction by Sog. *Nature*.

Awasaki, T., Huang, Y., O'Connor, M. B., & Lee, T. (2011). Glia instruct developmental neuronal remodeling through TGF-β signaling. *Nature*

Neuroscience, *14*(7), 821–823. http://doi.org/10.1038/nn.2833
Ayala-Camargo, A., Anderson, A. M., Amoyel, M., Rodrigues, A. B., Flaherty, M. S., & Bach, E. A. (2013). JAK/STAT signaling is required for hinge growth and patterning in the Drosophila wing disc. *Developmental Biology*, *382*(2), 413–426. http://doi.org/10.1016/j.ydbio.2013.08.016
Ayers, K. L., Gallet, A., Staccini-Lavenant, L., & Thérond, P. P. (2010). The Long-Range Activity of Hedgehog Is Regulated in the Apical Extracellular Space by the Glypican Dally and the Hydrolase Notum. *Developmental Cell*.
Ayyaz, A., Li, H., & Jasper, H. (2015). Haemocytes control stem cell activity in the Drosophila intestine. *Nature Cell Biology*, *17*(6), 736–748. http://doi.org/10.1038/ncb3174
Azpiazu, N., & Morata, G. (2000). Function and regulation of homothorax in the wing imaginal disc of Drosophila. *Development (Cambridge, England)*, *127*(12), 2685–2693.
Baena-Lopez, L. A., Alexandre, C., Mitchell, A., Pasakarnis, L., & Vincent, J.-P. (2013). Accelerated homologous recombination and subsequent genome modification in Drosophila. *Development (Cambridge, England)*, *140*(23), 4818–4825. http://doi.org/10.1242/dev.100933
Bai, H., Kang, P., Hernandez, A. M., & Tatar, M. (2013). Activin signaling targeted by insulin/dFOXO regulates aging and muscle proteostasis in Drosophila. *PLoS Genetics*, *9*(11), e1003941. http://doi.org/10.1371/journal.pgen.1003941
Ballard, S. L., Jarolimova, J., & Wharton, K. A. (2010). Gbb/BMP signaling is required to maintain energy homeostasis in Drosophila. *Developmental Biology*.
Bangi, E., & Wharton, K. (2006a). Dpp and Gbb exhibit different effective ranges in the establishment of the BMP activity gradient critical for Drosophila wing patterning. *Developmental Biology*, *295*(1), 16–16. http://doi.org/10.1016/j.ydbio.2006.03.021
Bangi, E., & Wharton, K. (2006b). Dual function of the Drosophila Alk1/Alk2 ortholog Saxophone shapes the Bmp activity gradient in the wing imaginal disc. *Development (Cambridge, England)*, *133*(17), 3295–3303. http://doi.org/10.1242/dev.02513
Barrangou, R., Fremaux, C., Deveau, H., Richards, M., Boyaval, P., Moineau, S., et al. (2007). CRISPR Provides Acquired Resistance Against Viruses in Prokaryotes. *Science (New York, N.Y.)*, *315*(5819), 1709–1712. http://doi.org/10.1126/science.1138140
Barrio, R., & De Celis, J. F. (2004). Regulation of spalt expression in the Drosophila wing blade in response to the Decapentaplegic signaling pathway. *Proceedings of the National Academy of Sciences of the United States of America*, *101*(16), 6021–6026.

http://doi.org/10.1073/pnas.0401590101
Bassett, A. R., Tibbit, C., Ponting, C. P., & Liu, J. L. (2014). Mutagenesis and homologous recombination in Drosophila cell lines using CRISPR/Cas9. *Biology Open*, *3*(1), 42–49. http://doi.org/10.1242/bio.20137120
Bate, M., & Arias, A. M. (1991). The embryonic origin of imaginal discs in Drosophila. *Development (Cambridge, England)*, *112*(3), 755–761.
Belenkaya, T. Y. T., Han, C. C., Yan, D. D., Opoka, R. J. R., Khodoun, M. M., Liu, H. H., & Lin, X. X. (2004). Drosophila Dpp morphogen movement is independent of dynamin-mediated endocytosis but regulated by the glypican members of heparan sulfate proteoglycans. *Cell*, *119*(2), 231–244. http://doi.org/10.1016/j.cell.2004.09.031
Benton, R., & St Johnston, D. (2003). Drosophila PAR-1 and 14-3-3 inhibit Bazooka/PAR-3 to establish complementary cortical domains in polarized cells. *Cell*, *115*(6), 691–704.
Beumer, K. (2005). Efficient Gene Targeting in Drosophila With Zinc-Finger Nucleases. *Genetics*, *172*(4), 2391–2403. http://doi.org/10.1534/genetics.105.052829
Beumer, K. J., Trautman, J. K., Bozas, A., Liu, J. L., Rutter, J., Gall, J. G., & Carroll, D. (2008). Efficient gene targeting in Drosophila by direct embryo injection with zinc-finger nucleases. *Proceedings of the National Academy of Sciences of the United States of America*, *105*(50), 19821–19826. http://doi.org/10.1073/pnas.0810475105
Bibikova, M. (2003). Enhancing Gene Targeting with Designed Zinc Finger Nucleases. *Science (New York, N.Y.)*, *300*(5620), 764–764. http://doi.org/10.1126/science.1079512
Bibikova, M., Golic, M., Golic, K. G., & Carroll, D. (2002). Targeted Chromosomal Cleavage and Mutagenesis in Drosophila Using Zinc-Finger Nucleases. *Genetics*, *161*(3), 1169–1175.
Bilder, D., Li, M., & Perrimon, N. (2000). Cooperative regulation of cell polarity and growth by Drosophila tumor suppressors. *Science (New York, N.Y.)*, *289*(5476), 113–116.
Bischof, J., Bjorklund, M., Furger, E., Schertel, C., Taipale, J., & Basler, K. (2013). A versatile platform for creating a comprehensive UAS-ORFeome library in Drosophila. *Development (Cambridge, England)*, *140*(11), 2434–2442. http://doi.org/10.1242/dev.088757
Bischof, J., Maeda, R. K., & Hediger, M. (2007). An optimized transgenesis system for Drosophila using germ-line-specific φC31 integrases. Presented at the Proceedings of the ….
Bischoff, M., Gradilla, A.-C., Seijo, I., Andres, G., Rodriguez-Navas, C., Gonzalez-Mendez, L., & Guerrero, I. (2013). Cytonemes are required for the establishment of a normal Hedgehog morphogen gradient in Drosophila epithelia. *Nature Cell Biology*, *15*(11), 1269–U40.

http://doi.org/10.1038/ncb2856
Blair, S. S. (2007). Wing Vein Patterning in Drosophilaand the Analysis of Intercellular Signaling. *Annual Review of Cell and Developmental Biology*, *23*(1), 293–319. http://doi.org/10.1146/annurev.cellbio.23.090506.123606
Bornemann, D. J. (2004). Abrogation of heparan sulfate synthesis in Drosophila disrupts the Wingless, Hedgehog and Decapentaplegic signaling pathways. *Development (Cambridge, England)*, *131*(9), 1927–1938. http://doi.org/10.1242/dev.01061
Brand, A. H., & Perrimon, N. (1993). Targeted gene expression as a means of altering cell fates and generating dominant phenotypes. *Development (Cambridge, England)*.
Brouns, S. J. J., Jore, M. M., Lundgren, M., Westra, E. R., Slijkhuis, R. J. H., Snijders, A. P. L., et al. (2008). Small CRISPR RNAs Guide Antiviral Defense in Prokaryotes. *Science (New York, N.Y.)*, *321*(5891), 960–964. http://doi.org/10.1126/science.1159689
Brummel, T. J., Twombly, V., Marqués, G., Wrana, J. L., Newfeld, S. J., Attisano, L., et al. (1994). Characterization and relationship of Dpp receptors encoded by the saxophone and thick veins genes in Drosophila. *Cell*, *78*(2), 251–261.
Brummel, T., Abdollah, S., Haerry, T. E., Shimell, M. J., Merriam, J., Raftery, L., et al. (1998). The Drosophila activin receptor baboon signals through dSmad2 and controls cell proliferation but not patterning during larval development. *Genes & Development*, *13*(1), 98–111.
Bryant, P. J. (1979). Pattern formation in imaginal discs. *Genetics and Biology of Drosophila*.
Bryant, P. J., & Levinson, P. (1985). Intrinsic growth control in the imaginal primordia of Drosophila, and the autonomous action of a lethal mutation causing overgrowth. *Developmental Biology*.
Bujakowska, K., Audo, I., Mohand-Saïd, S., Lancelot, M.-E., Antonio, A., Germain, A., et al. (2012). CRB1 mutations in inherited retinal dystrophies. *Human Mutation*, *33*(2), 306–315. http://doi.org/10.1002/humu.21653
Bulgakova, N. A., & Knust, E. (2009). The Crumbs complex: from epithelial-cell polarity to retinal degeneration. *Journal of Cell Science*, *122*(15), 2587–2596. http://doi.org/10.1242/jcs.023648
Burke, R., & Basler, K. (1996). Dpp receptors are autonomously required for cell proliferation in the entire developing Drosophila wing. *Development (Cambridge, England)*, *122*(7), 2261–2269.
Buszczak, M., Paterno, S., Lighthouse, D., Bachman, J., Planck, J., Owen, S., et al. (2007). The carnegie protein trap library: a versatile tool for Drosophila developmental studies. *Genetics*, *175*(3), 1505–1531.

http://doi.org/10.1534/genetics.106.065961
Butler, M. J., Jacobsen, T. L., Cain, D. M., Jarman, M. G., Hubank, M., Whittle, J., et al. (2003). Discovery of genes with highly restricted expression patterns in the Drosophila wing disc using DNA oligonucleotide microarrays. *Development (Cambridge, England)*, *130*(4), 659–670. http://doi.org/10.1242/dev.00293
Callejo, A., Bilioni, A., Mollica, E., Gorfinkiel, N., Andres, G., Ibáñez, C., et al. (2011). Dispatched mediates Hedgehog basolateral release to form the long-range morphogenetic gradient in the Drosophila wing disk epithelium. *Proceedings of the National Academy of Sciences of the United States of America*, *108*(31), 12591–12598. http://doi.org/10.1073/pnas.1106881108
Campbell, G., & Tomlinson, A. (1999). Transducing the Dpp Morphogen Gradient in the Wing of Drosophila: Regulation of Dpp Targets by brinker. *Cell*.
Campbell, K., Knust, E., & Skaer, H. (2009). Crumbs stabilises epithelial polarity during tissue remodelling. *Journal of Cell Science*. Retrieved from http://jcs.biologists.org/content/122/15/2604
Cao, X., Surma, M. A., & Simons, K. (2012). Polarized sorting and trafficking in epithelial cells. *Cell Research*, *22*(5), 793–805. http://doi.org/10.1038/cr.2012.64
Capdevila, J., & Guerrero, I. (1994). Targeted expression of the signaling molecule decapentaplegic induces pattern duplications and growth alterations in Drosophila wings. *The EMBO Journal*, *13*(19), 4459–4468.
Carmosino, M., Valenti, G., Caplan, M., & Svelto, M. (2012). Polarized traffic towards the cell surface: how to find the route. *Biology of the Cell*, *102*(2), 75–91. http://doi.org/10.1042/BC20090134
Carvajal-Gonzalez, J. M., Gravotta, D., Mattera, R., Diaz, F., Bay, A. P., Roman, A. C., et al. (2012). Basolateral sorting of the coxsackie and adenovirus receptor through interaction of a canonical YXX motif with the clathrin adaptors AP-1A and AP-1B, *109*(10), 3820–3825. http://doi.org/10.1073/pnas.1117949109
Casares, F., & Mann, R. S. (2000). A dual role for homothorax in inhibiting wing blade development and specifying proximal wing identities in Drosophila. *Development (Cambridge, England)*, *127*(7), 1499–1508.
Caussinus, E., Kanca, O., & Affolter, M. (2012). Fluorescent fusion protein knockout mediated by anti-GFP nanobody. *Nature Structural & Molecular Biology*, *19*(1), 117–121. http://doi.org/10.1038/nsmb.2180
Cavodeassi, F., Rodriguez, I., & Modolell, J. (2002). Dpp signalling is a key effector of the wing-body wall subdivision of the Drosophila mesothorax. *Development (Cambridge, England)*, *129*(16), 3815–3823.
Chang, C., Holtzman, D. A., Chau, S., Chickering, T., Woolf, E. A., Holmgren,

L. M., et al. (2001). Twisted gastrulation can function as a BMP antagonist : Abstract : Nature. *Nature*, *410*(6827), 483–487. http://doi.org/10.1038/35068583

Chen, C.-L., Gajewski, K. M., Hamaratoglu, F., Bossuyt, W., Sansores-Garcia, L., Tao, C., & Halder, G. (2010). The apical-basal cell polarity determinant Crumbs regulates Hippo signaling in Drosophila. *Proceedings of the National Academy of Sciences of the United States of America*, *107*(36), 15810–15815. http://doi.org/10.1073/pnas.1004060107

Chenna, R., Sugawara, H., Koike, T., Lopez, R., Gibson, T. J., Higgins, D. G., & Thompson, J. D. (2003). Multiple sequence alignment with the Clustal series of programs. *Nucleic Acids Research*, *31*(13), 3497–3500.

Crickmore, M. A., & Mann, R. S. (2006). Hox control of organ size by regulation of morphogen production and mobility. *Science (New York, N.Y.)*, *313*(5783), 63–68. http://doi.org/10.1126/science.1128650

Crickmore, M. A., & Mann, R. S. (2007). Hox control of morphogen mobility and organ development through regulation of glypican expression. *Development (Cambridge, England)*, *134*(2), 327–334. http://doi.org/10.1242/dev.02737

D'Angelo, G., Matusek, T., Pizette, S., & Thérond, P. P. (2015). Endocytosis of Hedgehog through Dispatched Regulates Long-Range Signaling. *Developmental Cell*, *32*(3), 290–303. http://doi.org/10.1016/j.devcel.2014.12.004

Das, P., Inoue, H., Baker, J. C., Beppu, H., Kawabata, M., Harland, R. M., et al. (1999). Drosophila dSmad2 and Atr-I transmit activin/TGFbeta signals. *Genes to Cells*, *4*(2), 123–134. http://doi.org/10.1046/j.1365-2443.1999.00244.x

David, D. J. V., Tishkina, A., & Harris, T. J. C. (2010). The PAR complex regulates pulsed actomyosin contractions during amnioserosa apical constriction in Drosophila. *Development (Cambridge, England)*, *137*(10), 1645–1655. http://doi.org/10.1242/dev.044107

De Celis, J. F., & Diaz-Benjumea, F. J. (2003). Developmental basis for vein pattern variations in insect wings. *The International Journal of Developmental Biology*, *47*(7-8), 653–663.

Dejima, K., Kanai, M. I., Akiyama, T., Levings, D. C., & Nakato, H. (2011). Novel contact-dependent bone morphogenetic protein (BMP) signaling mediated by heparan sulfate proteoglycans. *The Journal of Biological Chemistry*, *286*(19), 17103–17111. http://doi.org/10.1074/jbc.M110.208082

Demontis, F., & Dahmann, C. (2007). Apical and lateral cell protrusions interconnect epithelial cells in live Drosophila wing imaginal discs. *Developmental Dynamics : an Official Publication of the American Association of Anatomists*, *236*(12), 3408–3418.

http://doi.org/10.1002/dvdy.21324
Denef, N., Neubüser, D., Perez, L., & Cohen, S. M. (2000). Hedgehog induces opposite changes in turnover and subcellular localization of patched and smoothened. *Cell*, *102*(4), 521–531.
Di Guglielmo, G. M., Le Roy, C., Goodfellow, A. F., & Wrana, J. L. (2003). Distinct endocytic pathways regulate TGF-β receptor signalling and turnover. *Nature Cell Biology*, *5*(5), 410–421. http://doi.org/10.1038/ncb975
Diaz-Benjumea, F. J., & Cohen, S. M. (1993). Interaction Between Dorsal and Ventral Cells in the Imaginal Disc Directs Wing Development in Drosophila. *Cell*, *75*(4), 741–752. http://doi.org/10.1016/0092-8674(93)90494-B
Diaz-Benjumea, F. J., & Cohen, S. M. (1995). Serrate signals through Notch to establish a Wingless-dependent organizer at the dorsal/ventral compartment boundary of the Drosophila wing. *Development (Cambridge, England)*, *121*(12), 4215–4225.
Doherty, D., Feger, G., YoungerShepherd, S., Jan, L. Y., & Jan, Y. N. (1996). Delta is a ventral to dorsal signal complementary to Serrate, another Notch ligand in Drosophila wing formation. *Genes & Development*, *10*(4), 421–434.
Eaton, B. A., & Davis, G. W. (2005). LIM Kinase1 Controls Synaptic Stability Downstream of the Type II BMP Receptor. *Neuron*, *47*(5), 695–708. http://doi.org/10.1016/j.neuron.2005.08.010
Eaton, S., & Kornberg, T. B. (1990). Repression of Ci-D in Posterior Compartments of Drosophila by Engrailed. *Genes & Development*, *4*(6), 1068–1077.
Ehrlich, M. (2015). Endocytosis and trafficking of BMP receptors: Regulatory mechanisms for fine-tuning the signaling response in different cellular contexts. *Cytokine & Growth Factor Reviews*. http://doi.org/10.1016/j.cytogfr.2015.12.008
Ejsmont, R. K., Sarov, M., Winkler, S., Lipinski, K. A., & Tomancak, P. (2009). A toolkit for high-throughput, cross-species gene engineering in Drosophila. *Nature Methods*, *6*(6), 435–437. http://doi.org/10.1038/nmeth.1334
Entchev, E. V., Schwabedissen, A., & González-Gaitán, M. (2000). Gradient formation of the TGF-beta homolog Dpp. *Cell*, *103*(6), 981–991.
Feng, X.-H., & Derynck, R. (2005). Specificity and versatility in tgf-beta signaling through Smads. *Annual Review of Cell and Developmental Biology*, *21*, 659–693. http://doi.org/10.1146/annurev.cellbio.21.022404.142018
Ferguson, E. L., & Anderson, K. V. (1992). decapentaplegic acts as a morphogen to organize dorsal-ventral pattern in the Drosophila embryo.

Cell.

Fleming, R. J., Gu, Y., & Hukriede, N. A. (1997). Serrate-mediated activation of Notch is specifically blocked by the product of the gene fringe in the dorsal compartment of the Drosophila wing imaginal disc. *Development (Cambridge, England)*, *124*(15), 2973–2981.

Foletta, V. C., Lim, M. A., Soosairajah, J., Kelly, A. P., Stanley, E. G., Shannon, M., et al. (2003). Direct signaling by the BMP type II receptor via the cytoskeletal regulator LIMK1. *The Journal of Cell Biology*, *162*(6), 1089–1098. http://doi.org/10.1083/jcb.200212060

Francois, V., Solloway, M., O'Neill, J. W., Emery, J., & Bier, E. (1994). Dorsal-ventral patterning of the Drosophila embryo depends on a putative negative growth factor encoded by the short gastrulation gene. *Genes & Development*, *8*(21), 2602–2616. http://doi.org/10.1101/gad.8.21.2602

Fristrom, D., & Fristrom, J. W. (1993). The metamorphic development of the adult epidermis. The ….

Fujise, M., Izumi, S., Selleck, S. B., & Nakato, H. (2001). Regulation of dally, an integral membrane proteoglycan, and its function during adult sensory organ formation of Drosophila. *Developmental Biology*, *235*(2), 433–448. http://doi.org/10.1006/dbio.2001.0290

Fujise, M., Takeo, S., Kamimura, K., Matsuo, T., Aigaki, T., Izumi, S., & Nakato, H. (2003). Dally regulates Dpp morphogen gradient formation in the Drosophila wing. *Development (Cambridge, England)*, *130*(8), 1515–1522.

Funakoshi, Y., Minami, M., & Tabata, T. (2001). mtv shapes the activity gradient of the Dpp morphogen through regulation of thickveins. *Development (Cambridge, England)*, *128*(1), 67–74.

Gallet, A., Staccini-Lavenant, L., & Thérond, P. P. (2008). Cellular trafficking of the glypican Dally-like is required for full-strength Hedgehog signaling and wingless transcytosis. *Developmental Cell*, *14*(5), 712–725. http://doi.org/10.1016/j.devcel.2008.03.001

Gao, S., Steffen, J., & Laughon, A. (2005). Dpp-responsive silencers are bound by a trimeric Mad-Medea complex. *The Journal of Biological Chemistry*, *280*(43), 36158–36164. http://doi.org/10.1074/jbc.M506882200

Garcia-Bellido, A. (1975). Genetic control of wing disc development in Drosophila. *Cell Patterning*.

Gasiunas, G., Barrangou, R., Horvath, P., & Siksnys, V. (2012). Cas9-crRNA ribonucleoprotein complex mediates specific DNA cleavage for adaptive immunity in bacteria, *109*(39), E2579–E2586. http://doi.org/10.1073/pnas.1208507109

Gassama-Diagne, A., Yu, W., Beest, ter, M., Martin-Belmonte, F., Kierbel, A., Engel, J., & Mostov, K. (2006). Phosphatidylinositol-3,4,5-trisphosphate

regulates the formation of the basolateral plasma membrane in epithelial cells. *Nature Cell Biology*, *8*(9), 963–970. http://doi.org/10.1038/ncb1461

Geering, K., Beggah, A., Good, P., Girardet, S., Roy, S., Schaer, D., & Jaunin, P. (1996). Oligomerization and maturation of Na,K-ATPase: functional interaction of the cytoplasmic NH2 terminus of the beta subunit with the alpha subunit. *The Journal of Cell Biology*, *133*(6), 1193–1204.

Genevet, A., Polesello, C., Blight, K., Robertson, F., Collinson, L. M., Pichaud, F., & Tapon, N. (2009). The Hippo pathway regulates apical-domain size independently of its growth-control function. *Journal of Cell Science*, *122*(Pt 14), 2360–2370. http://doi.org/10.1242/jcs.041806

Genova, J. L. (2003). Neuroglian, Gliotactin, and the Na+/K+ ATPase are essential for septate junction function in Drosophila. *The Journal of Cell Biology*, *161*(5), 979–989. http://doi.org/10.1083/jcb.200212054

Gesualdi, S. C., & Haerry, T. E. (2007). Distinct Signaling of Drosophila Activin/TGF-β Family Members. *Fly*, *1*(4), 212–221. http://doi.org/10.4161/fly.5116

Ghosh, A. C., & O'Connor, M. B. (2014). Systemic Activin signaling independently regulates sugar homeostasis, cellular metabolism, and pH balance in Drosophila melanogaster. *Proceedings of the National Academy of Sciences of the United States of America*, *111*(15), 5729–5734. http://doi.org/10.1073/pnas.1319116111

Gibson, M. C. (2005). Extrusion and Death of DPP/BMP-Compromised Epithelial Cells in the Developing Drosophila Wing. *Science (New York, N.Y.)*, *307*(5716), 1785–1789. http://doi.org/10.1126/science.1104751

Gibson, M. C., & Schubiger, G. (2001). Drosophila peripodial cells, more than meets the eye? *Bioessays*.

Gibson, M. C., Lehman, D. A., & Schubiger, G. (2002). Lumenal transmission of decapentaplegic in Drosophila imaginal discs. *Developmental Cell*, *3*(3), 451–460.

Giepmans, B. N. G., & van Ijzendoorn, S. C. D. (2009). Epithelial cell-cell junctions and plasma membrane domains. *Biochimica Et Biophysica Acta-Biomembranes*, *1788*(4), 820–831. http://doi.org/10.1016/j.bbamem.2008.07.015

Gleason, R. J., Akintobi, A. M., Grant, B. D., & Padgett, R. W. (2014). BMP signaling requires retromer-dependent recycling of the type I receptor. *Proc Natl Acad Sci USA*, *111*(7), 2578–2583. http://doi.org/10.1073/pnas.1319947111

Goldstein, B., & Macara, I. G. (2007). The PAR proteins: fundamental players in animal cell polarization. *Developmental Cell*, *13*(5), 609–622. http://doi.org/10.1016/j.devcel.2007.10.007

Gong, W. J., & Golic, K. G. (2003). Ends-out, or replacement, gene targeting in Drosophila. *Proceedings of the National Academy of Sciences of the*

United States of America, *100*(5), 2556–2561. http://doi.org/10.1073/pnas.0535280100

González-Gaitán, M. (2003). Signal dispersal and transduction through the endocytic pathway. *Nature Reviews Molecular Cell Biology*, *4*(3), 213–224. http://doi.org/10.1038/nrm1053

González-Gaitán, M., & Jäckle, H. (1999). The range of spalt-activating Dpp signalling is reduced in endocytosis-defective Drosophila wing discs. *Mechanisms of Development*, *87*(1-2), 143–151.

Goold, C. P., & Davis, G. W. (2007). The BMP ligand Gbb gates the expression of synaptic homeostasis independent of synaptic growth control. *Neuron*, *56*(1), 109–123. http://doi.org/10.1016/j.neuron.2007.08.006

Gradilla, A.-C., Gonzalez, E., Seijo, I., Andres, G., Bischoff, M., Gonzalez-Mendez, L., et al. (2014). Exosomes as Hedgehog carriers in cytoneme-mediated transport and secretion. *Nature Communications*, *5*, –5649. http://doi.org/10.1038/ncomms6649

Gratz, S. J., Cummings, A. M., Nguyen, J. N., Hamm, D. C., Donohue, L. K., Harrison, M. M., Wildonger, J., & O'Connor-Giles, K. M. (2013a). Genome Engineering of Drosophila with the CRISPR RNA-Guided Cas9 Nuclease. *Genetics*, *194*(4), 1029–1035. http://doi.org/10.1534/genetics.113.152710

Gratz, S. J., Cummings, A. M., Nguyen, J. N., Hamm, D. C., Donohue, L. K., Harrison, M. M., Wildonger, J., & O'Connor-Giles, K. M. (2013b). Genome engineering of Drosophila with the CRISPR RNA-guided Cas9 nuclease. *Genetics*. http://doi.org/10.1534/genetics.113.152710

Gratz, S. J., Ukken, F. P., Rubinstein, C. D., Thiede, G., Donohue, L. K., Cummings, A. M., & O'Connor-Giles, K. M. (2014a). Highly Specific and Efficient CRISPR/Cas9-Catalyzed Homology-Directed Repair in Drosophila. *Genetics*, *196*(4), 961–971. http://doi.org/10.1534/genetics.113.160713

Gratz, S. J., Wildonger, J., Harrison, M. M., & O'Connor-Giles, K. M. (2014b). CRISPR/Cas9-mediated genome engineering and the promise of designer flies on demand. *Fly*, *7*(4), 249–255. http://doi.org/10.4161/fly.26566

Grieder, N. C., Nellen, D., Burke, R., Basler, K., & Affolter, M. (1995). schnurri is required for drosophila Dpp signaling and encodes a zinc finger protein similar to the mammalian transcription factor PRDII-BF1. *Cell*.

Groth, A. C., Fish, M., Nusse, R., & Calos, M. P. (2004). Construction of transgenic Drosophila by using the site-specific integrase from phage phiC31. *Genetics*, *166*(4), 1775–1782.

Grzeschik, N. A., Parsons, L. M., Allott, M. L., Harvey, K. F., & Richardson, H. E. (2010). Lgl, aPKC, and Crumbs regulate the Salvador/Warts/Hippo

pathway through two distinct mechanisms. *Current Biology : CB*, *20*(7), 573–581. http://doi.org/10.1016/j.cub.2010.01.055

Guzman, A., Femiak, M. Z., Boergermann, J. H., Paschkowsky, S., Kreuzaler, P. A., Fratzl, P., et al. (2012). SMAD versus Non-SMAD Signaling Is Determined by Lateral Mobility of Bone Morphogenetic Protein (BMP) Receptors. *The Journal of Biological Chemistry*, *287*(47), 39492–39504. http://doi.org/10.1074/jbc.M112.387639

Haerry, T. E. (2010). The interaction between two TGF-beta type I receptors plays important roles in ligand binding, SMAD activation, and gradient formation. *Mechanisms of Development*, *127*(7-8), 358–370. http://doi.org/10.1016/j.mod.2010.04.001

Haerry, T. E., Khalsa, O., O'Connor, M. B., & Wharton, K. A. (1998). Synergistic signaling by two BMP ligands through the SAX and TKV receptors controls wing growth and patterning in Drosophila. *Development (Cambridge, England)*, *125*(20), 3977–3987.

Hamaratoglu, F., de Lachapelle, A. M., Pyrowolakis, G., Bergmann, S., & Affolter, M. (2011). Dpp signaling activity requires Pentagone to scale with tissue size in the growing Drosophila wing imaginal disc. *PLoS Biology*, *9*(10), e1001182. http://doi.org/10.1371/journal.pbio.1001182

Hamaratoglu, F., Gajewski, K., Sansores-Garcia, L., Morrison, C., Tao, C., & Halder, G. (2009). The Hippo tumor-suppressor pathway regulates apical-domain size in parallel to tissue growth. *Journal of Cell Science*, *122*(Pt 14), 2351–2359. http://doi.org/10.1242/jcs.046482

Hamers-Casterman, C., Atarhouch, T., & Muyldermans, S. (1993). Naturally occurring antibodies devoid of light chains. *Nature*.

Han, C. (2004). Distinct and collaborative roles of Drosophila EXT family proteins in morphogen signalling and gradient formation. *Development (Cambridge, England)*, *131*(7), 1563–1575. http://doi.org/10.1242/dev.01051

Han, C. (2005). Drosophila glypicans Dally and Dally-like shape the extracellular Wingless morphogen gradient in the wing disc. *Development (Cambridge, England)*, *132*(4), 667–679. http://doi.org/10.1242/dev.01636

Harmansa, S., Hamaratoglu, F., Affolter, M., & Caussinus, E. (2015). Dpp spreading is required for medial but not for lateral wing disc growth. *Nature*, *527*(7578), 317–322. http://doi.org/10.1038/nature15712

Hasler, U., Wang, X., Crambert, G., Béguin, P., Jaisser, F., Horisberger, J. D., & Geering, K. (1998). Role of beta-subunit domains in the assembly, stable expression, intracellular routing, and functional properties of Na,K-ATPase. *The Journal of Biological Chemistry*, *273*(46), 30826–30835.

Hassanzadeh-Ghassabeh, G., Devoogdt, N., De Pauw, P., Vincke, C., & Muyldermans, S. (2013). Nanobodies and their potential applications.

Nanomedicine (London, England), *8*(6), 1013–1026. http://doi.org/10.2217/nnm.13.86

Hassel, S., Schmitt, S., Hartung, A., Roth, M., Nohe, A., Petersen, N., et al. (2003). Initiation of Smad-dependent and Smad-independent signaling via distinct BMP-receptor complexes. *The Journal of Bone and Joint Surgery. American Volume*, *85-A Suppl 3*, 44–51.

Held, L. I., Jr, & Held, L. I., Jr. (2005). Imaginal Discs: The Genetic and Cellular Logic of Pattern Formation - Lewis I. Held, Jr., Lewis I. Held Jr - Google Books.

Helma, J., Cardoso, M. C., Muyldermans, S., & Leonhardt, H. (2015). Nanobodies and recombinant binders in cell biology. *The Journal of Cell Biology*, *209*(5), 633–644. http://doi.org/10.1083/jcb.201409074

Herranz, R., Díaz-Castillo, C., Nguyen, T. P., Lovato, T. L., Cripps, R. M., & Marco, R. (2004). Expression patterns of the whole troponin C gene repertoire during Drosophila development. *Gene Expression Patterns*, *4*(2), 183–190. http://doi.org/10.1016/j.modgep.2003.09.008

Hevia, C. F., & De Celis, J. F. (2013). Activation and function of TGFβ signalling during Drosophila wing development and its interactions with the BMP pathway. *Developmental Biology*, *377*(1), 138–153. http://doi.org/10.1016/j.ydbio.2013.02.004

Horikoshi, Y., Suzuki, A., Yamanaka, T., Sasaki, K., Mizuno, K., Sawada, H., et al. (2009). Interaction between PAR-3 and the aPKC-PAR-6 complex is indispensable for apical domain development of epithelial cells. *Journal of Cell Science*, *122*(10), 1595–1606. http://doi.org/10.1242/jcs.043174

Horton, A. C., & Ehlers, M. D. (2003). Neuronal Polarity and Trafficking. *Neuron*, *40*(2), 277–295. http://doi.org/10.1016/S0896-6273(03)00629-9

Housden, B. E., Valvezan, A. J., Kelley, C., Sopko, R., Hu, Y., Roesel, C., et al. (2015). Identification of potential drug targets for tuberous sclerosis complex by synthetic screens combining CRISPR-based knockouts with RNAi. *Science Signaling*, *8*(393), rs9–rs9. http://doi.org/10.1126/scisignal.aab3729

Hsiung, F., Ramirez-Weber, F.-A., Iwaki, D. D., & Kornberg, T. B. (2005). Dependence of Drosophila wing imaginal disc cytonemes on Decapentaplegic. *Nature*, *437*(7058), 560–563. http://doi.org/10.1038/nature03951

Huang, F., & Chen, Y. G. (2012). Regulation of TGF-b receptor activity. *Cell Biosci*.

Huang, J., Zhou, W., Dong, W., Watson, A. M., & Hong, Y. (2009). Directed, efficient, and versatile modifications of the Drosophila genome by genomic engineering. *Proceedings of the National Academy of Sciences of the United States of America*, *106*(20), 8284–8289. http://doi.org/10.1073/pnas.0900641106

Huang, J., Zhou, W., Watson, A. M., Jan, Y. N., & Hong, Y. (2008). Efficient Ends-Out Gene Targeting In Drosophila. *Genetics*, *180*(1), 703–707. http://doi.org/10.1534/genetics.108.090563

Huang, Y.-L., & Niehrs, C. (2014). Polarized Wnt Signaling Regulates Ectodermal Cell Fate in Xenopus. *Developmental Cell*, *29*(2), 250–257. http://doi.org/10.1016/j.devcel.2014.03.015

Hufnagel, L., Teleman, A. A., Rouault, H., Cohen, S. M., & Shraiman, B. I. (2007). On the mechanism of wing size determination in fly development. *Proceedings of the National Academy of Sciences of the United States of America*, *104*(10), 3835–3840. http://doi.org/10.1073/pnas.0607134104

Huminiecki, L., Goldovsky, L., Freilich, S., Moustakas, A., Ouzounis, C., & Heldin, C.-H. (2009). Emergence, development and diversification of the TGF-beta signalling pathway within the animal kingdom. *BMC Evolutionary Biology*, *9*, 28. http://doi.org/10.1186/1471-2148-9-28

Hunziker, W., & Fumer, C. (1994). A Di-Leucine Motif Mediates Endocytosis and Basolateral Sorting of Macrophage Igg Fc-Receptors in Mdck Cells. *The EMBO Journal*, *13*(13), 2963–2969.

Huse, M., Muir, T. W., Xu, L., Chen, Y. G., Kuriyan, J., & Massagué, J. (2001). The TGF beta receptor activation process: an inhibitor- to substrate-binding switch. *Molecular Cell*, *8*(3), 671–682.

Inaba, M., Buszczak, M., & Yamashita, Y. M. (2015). Nanotubes mediate niche-stem-cell signalling in the Drosophila testis. *Nature*, *523*(7560), 329–332. http://doi.org/10.1038/nature14602

Ishino, Y., Shinagawa, H., Makino, K., Amemura, M., & Nakata, A. (1987). Nucleotide sequence of the iap gene, responsible for alkaline phosphatase isozyme conversion in Escherichia coli, and identification of the gene product. *Journal of ….*

Izaddoost, S., Nam, S. C., Bhat, M. A., Bellen, H. J., & Choi, K. W. (2002). Drosophila Crumbs is a positional cue in photoreceptor adherens junctions and rhabdomeres. *Nature*, *416*(6877), 178–182. http://doi.org/10.1038/nature720

J J Sekelsky, S. J. N. L. A. R. E. H. C. W. M. G. (1995). Genetic Characterization and Cloning of Mothers against Dpp, a Gene Required for Decapentaplegic Function in Drosophila Melanogaster. *Genetics*, *139*(3), 1347.

Jansen, R., Embden, J. D. A. V., Gaastra, W., & Schouls, L. M. (2002). Identification of genes that are associated with DNA repeats in prokaryotes. *Molecular Microbiology*, *43*(6), 1565–1575. http://doi.org/10.1046/j.1365-2958.2002.02839.x

Jaźwińska, A., Kirov, N., Wieschaus, E., Roth, S., & Rushlow, C. (1999). The Drosophila gene brinker reveals a novel mechanism of Dpp target gene regulation. *Cell*, *96*(4), 563–573.

Jensen, P. A., Zheng, X., Lee, T., & O'Connor, M. B. (2009). The Drosophila Activin-like ligand Dawdle signals preferentially through one isoform of the Type-I receptor Baboon. *Mechanisms of Development*, *126*(11-12), 950–957. http://doi.org/10.1016/j.mod.2009.09.003

Jiang, Y., Nohe, A., Bragdon, B., Tian, C., Rudarakanchana, N., Morrell, N. W., & Petersen, N. O. (2011). Trapping of BMP receptors in distinct membrane domains inhibits their function in pulmonary arterial hypertension. *American Journal of Physiology-Lung Cellular and Molecular Physiology*, *301*(2), L218–L227. http://doi.org/10.1152/ajplung.00300.2010

Jinek, M., Chylinski, K., Fonfara, I., Hauer, M., Doudna, J. A., & Charpentier, E. (2012). A Programmable Dual-RNA-Guided DNA Endonuclease in Adaptive Bacterial Immunity. *Science (New York, N.Y.)*, *337*(6096), 816–821. http://doi.org/10.1126/science.1225829

Johnstone, K., Wells, R. E., Strutt, D., & Zeidler, M. P. (2013). Localised JAK/STAT Pathway Activation Is Required for Drosophila Wing Hinge Development. *PloS One*, *8*(5), –e65076. http://doi.org/10.1371/journal.pone.0065076

Jones, W. D., Cayirlioglu, P., Grunwald Kadow, I., & Vosshall, L. B. (2006). Two chemosensory receptors together mediate carbon dioxide detection in Drosophila. *Nature*, *445*(7123), 86–90. http://doi.org/10.1038/nature05466

Kamiya, Y., Miyazono, K., & Miyazawa, K. (2008). Specificity of the inhibitory effects of Dad on TGF-beta family type I receptors, Thickveins, Saxophone, and Baboon in Drosophila. *FEBS Letters*, *582*(17), 2496–2500. http://doi.org/10.1016/j.febslet.2008.05.052

Kamiyama, D., McGorty, R., Kamiyama, R., Kim, M. D., Chiba, A., & Huang, B. (2015). Specification of Dendritogenesis Site in Drosophila aCC Motoneuron by Membrane Enrichment of Pak1 through Dscam1. *Developmental Cell*, *35*(1), 93–106.

Katsuyama, T., Akmammedov, A., Seimiya, M., Hess, S. C., Sievers, C., & Paro, R. (2013). An efficient strategy for TALEN-mediated genome engineering in Drosophila. *Nucleic Acids Research*, *41*(17), e163. http://doi.org/10.1093/nar/gkt638

Kemphues, K. J., Priess, J. R., Morton, D. G., & Cheng, N. S. (1988). Identification of genes required for cytoplasmic localization in early C. elegans embryos. *Cell*, *52*(3), 311–320.

Khalsa, O., Yoon, J. W., Torres-Schumann, S., & Wharton, K. A. (1998). TGF-beta/BMP superfamily members, Gbb-60A and Dpp, cooperate to provide pattern information and establish cell identity in the Drosophila wing. *Development (Cambridge, England)*, *125*(14), 2723–2734.

Kicheva, A., Pantazis, P., Bollenbach, T., Kalaidzidis, Y., Bittig, T., Juelicher,

F., & González-Gaitán, M. (2007). Kinetics of morphogen gradient formation. *Science (New York, N.Y.)*, *315*(5811), 521–525. http://doi.org/10.1126/science.1135774

Kim, M.-J., & O'Connor, M. B. (2014). Anterograde Activin signaling regulates postsynaptic membrane potential and GluRIIA/B abundance at the Drosophila neuromuscular junction. *PloS One*, *9*(9), e107443. http://doi.org/10.1371/journal.pone.0107443

Kim, S. K. (1997). Polarized signaling: basolateral receptor localization in epithelial cells by PDZ-containing proteins. *Current Opinion in Cell Biology*, *9*(6), 853–859.

Klebes, A., & Knust, E. (2000). A conserved motif in Crumbs is required for E-cadherin localisation and zonula adherens formation in Drosophila. *Current Biology*.

Klein, T., & Arias, A. M. (1998). Interactions among Delta, Serrate and Fringe modulate Notch activity during Drosophila wing development. *Development (Cambridge, England)*, *125*(15), 2951–2962.

Knoblich, J. A. (2010). Asymmetric cell division: recent developments and their implications for tumour biology. *Nature Reviews Molecular Cell Biology*, *11*(12), 849–860. http://doi.org/10.1038/nrm3010

Kondo, S., & Ueda, R. (2013). Highly Improved Gene Targeting by Germline-Specific Cas9 Expression in Drosophila. *Genetics*, *195*(3), 715–721. http://doi.org/10.1534/genetics.113.156737

Koorman, T., Klompstra, D., van der Voet, M., Lemmens, I., Ramalho, J. J., Nieuwenhuize, S., et al. (2016). A combined binary interaction and phenotypic map of C. elegans cell polarity proteins. *Nature Cell Biology*. http://doi.org/10.1038/ncb3300

Kölsch, V., Seher, T., Fernandez-Ballester, G. J., Serrano, L., & Leptin, M. (2007). Control of Drosophila gastrulation by apical localization of adherens junctions and RhoGEF2. *Science (New York, N.Y.)*, *315*(5810), 384–386. http://doi.org/10.1126/science.1134833

Krahn, M. P., Klopfenstein, D. R., Fischer, N., & Wodarz, A. (2010). Membrane Targeting of Bazooka/PAR-3 Is Mediated by Direct Binding to Phosphoinositide Lipids. *Current Biology*, *20*(7), 636–642. http://doi.org/10.1016/j.cub.2010.01.065

Kruse, K., Pantazis, P., Bollenbach, T., Jülicher, F., & González-Gaitán, M. (2004). Dpp gradient formation by dynamin-dependent endocytosis: receptor trafficking and the diffusion model. *Development (Cambridge, England)*, *131*(19), 4843–4856. http://doi.org/10.1242/dev.01335

Kuo, W. J., Digman, M. A., & Lander, A. D. (2010). Heparan Sulfate Acts as a Bone Morphogenetic Protein Coreceptor by Facilitating Ligand-induced Receptor Hetero-oligomerization. *Molecular Biology of the Cell*, *21*(22), 4028–4041. http://doi.org/10.1091/mbc.E10-04-0348

Lander, A. D., Nie, Q., & Wan, F. (2002). Do Morphogen Gradients Arise by Diffusion? *Developmental Cell*.

Laprise, P., Lau, K. M., Harris, K. P., Silva-Gagliardi, N. F., Paul, S. M., Beronja, S., et al. (2009). Yurt, Coracle, Neurexin IV and the Na(+),K(+)-ATPase form a novel group of epithelial polarity proteins. *Nature*, *459*(7250), 1141–1145. http://doi.org/10.1038/nature08067

Lecuit, T. T., & Cohen, S. M. S. (1998). Dpp receptor levels contribute to shaping the Dpp morphogen gradient in the Drosophila wing imaginal disc. *Development (Cambridge, England)*, *125*(24), 4901–4907.

Lecuit, T., & Cohen, S. M. (1997). Proximall[ndash]ldistal axis formation in the Drosophila leg. *Nature*, *388*(6638), 139–145. http://doi.org/doi:10.1038/40563

Lecuit, T., Brook, W. J., Ng, M., Calleja, M., Sun, H., & Cohen, S. M. (1996). 2 Distinct Mechanisms for Long-Range Patterning by Decapentaplegic in the Drosophila Wing (Vol 381, Pg 387, 1996). *Nature*, *381*(6581), 387–393. Retrieved from http://www.cheric.org/research/tech/periodicals/view.php?seq=221631

Lee-Hoeflich, S. T., Causing, C. G., Podkowa, M., Zhao, X., Wrana, J. L., & Attisano, L. (2004). Activation of LIMK1 by binding to the BMP receptor, BMPRII, regulates BMP-dependent dendritogenesis. *The EMBO Journal*, *23*(24), 4792–4801. http://doi.org/10.1038/sj.emboj.7600418

Lee-Hoeflich, S. T., Zhao, X., Mehra, A., & Attisano, L. (2005). The Drosophila type II receptor, Wishful thinking, binds BMP and myoglianin to activate multiple TGFbeta family signaling pathways. *FEBS Letters*, *579*(21), 4615–4621. http://doi.org/10.1016/j.febslet.2005.06.088

Letsou, A., Arora, K., Wrana, J. L., Simin, K., Twombly, V., Jamal, J., et al. (1995). Drosophila Dpp signaling is mediated by the punt gene product: a dual ligand-binding type II receptor of the TGF beta receptor family. *Cell*, *80*(6), 899–908.

Levine, M., & Ashe, H. L. (1999). Local inhibition and long-range enhancement of Dpp signal transduction by Sog. *Nature*, *398*(6726), 427–431. http://doi.org/10.1038/18892

Li, C.-Y., Guo, Z., & Wang, Z. (2007). TGFbeta receptor saxophone non-autonomously regulates germline proliferation in a Smox/dSmad2-dependent manner in Drosophila testis. *Developmental Biology*, *309*(1), 70–77. http://doi.org/10.1016/j.ydbio.2007.06.019

Li, P., Mao, X., Ren, Y., & Liu, P. (2015). Epithelial Cell Polarity Determinant CRB3 in Cancer Development. *International Journal of Biological Sciences*, *11*(1), 31–37. http://doi.org/10.7150/ijbs.10615

Ling, C., Zheng, Y., Yin, F., Yu, J., Huang, J., Hong, Y., et al. (2010). The apical transmembrane protein Crumbs functions as a tumor suppressor that regulates Hippo signaling by binding to Expanded. *Proceedings of*

the National Academy of Sciences of the United States of America, *107*(23), 10532–10537. http://doi.org/10.1073/pnas.1004279107

Liu, J., Li, C., Yu, Z., Huang, P., Wu, H., Wei, C., et al. (2012). Efficient and specific modifications of the Drosophila genome by means of an easy TALEN strategy. *Journal of Genetics and Genomics = Yi Chuan Xue Bao*, *39*(5), 209–215. http://doi.org/10.1016/j.jgg.2012.04.003

Lo, P. C. H., & Frasch, M. (1999). Sequence and expression of myoglianin, a novel Drosophila gene of the TGF-β superfamily. *Mechanisms of Development*, *86*(1-2), 171–175. http://doi.org/10.1016/S0925-4773(99)00108-2

Lowe, N., Rees, J. S., Roote, J., Ryder, E., Armean, I. M., Johnson, G., et al. (2014). Analysis of the expression patterns, subcellular localisations and interaction partners of Drosophila proteins using a pigP protein trap library. *Development (Cambridge, England)*, *141*(20), 3994–4005. http://doi.org/10.1242/dev.111054

Lu, H., & Bilder, D. (2005). Endocytic control of epithelial polarity and proliferation in Drosophila. *Nature Cell Biology*, *7*(12), 1232–1239. http://doi.org/10.1038/ncb1324

Luo, L., Wang, H., Fan, C., Liu, Sen, & Cai, Y. (2015). Wnt ligands regulate Tkv expression to constrain Dpp activity in the Drosophila ovarian stem cell niche. *The Journal of Cell Biology*, *209*(4), 595–608. http://doi.org/10.1083/jcb.201409142.dv

Lye, C. M., Naylor, H. W., & Sanson, B. (2014). Subcellular localisations of the CPTI collection of YFP-tagged proteins in Drosophila embryos. *Development (Cambridge, England)*, *141*(20), 4006–4017. http://doi.org/10.1242/dev.111310

Mali, P., Aach, J., Stranges, P. B., Esvelt, K. M., Moosburner, M., Kosuri, S., et al. (2013). CAS9 transcriptional activators for target specificity screening and paired nickases for cooperative genome engineering. *Nature Biotechnology*, *31*(9), 833–838. http://doi.org/10.1038/nbt.2675

Marmion, R. A., Jevtic, M., Springhorn, A., Pyrowolakis, G., & Yakoby, N. (2013). The Drosophila BMPRII, wishful thinking, is required for eggshell patterning. *Developmental Biology*, *375*(1), 45–53. http://doi.org/10.1016/j.ydbio.2012.12.011

Marois, E., Mahmoud, A., & Eaton, S. (2006). The endocytic pathway and formation of the Wingless morphogen gradient. *Development (Cambridge, England)*, *133*(2), 307–317. http://doi.org/10.1242/dev.02197

Marqués, G. (2003). Retrograde Gbb signaling through the Bmp type 2 receptor Wishful Thinking regulates systemic FMRFa expression in Drosophila. *Development (Cambridge, England)*, *130*(22), 5457–5470. http://doi.org/10.1242/dev.00772

Marqués, G., Bao, H., Haerry, T. E., Shimell, M. J., Duchek, P., Zhang, B., & O'Connor, M. B. (2002). The Drosophila BMP type II receptor Wishful Thinking regulates neuromuscular synapse morphology and function. *Neuron*, *33*(4), 529–543.

Marqués, G., Musacchio, M., & Shimell, M. J. (1997). Production of a DPP Activity Gradient in the Early Drosophila Embryo through the Opposing Actions of the SOG and TLD Proteins. *Cell*.

Martin, F. A., Herrera, S. C., & Morata, G. (2009). Cell competition, growth and size control in the Drosophila wing imaginal disc. *Development (Cambridge, England)*, *136*(22), 3747–3756. http://doi.org/10.1242/dev.038406

Martin-Belmonte, F., Gassama, A., Datta, A., Yu, W., Rescher, U., Gerke, V., & Mostov, K. (2007). PTEN-mediated apical segregation of phosphoinositides controls epithelial morphogenesis through Cdc42. *Cell*, *128*(2), 383–397. http://doi.org/10.1016/j.cell.2006.11.051

Martín-Castellanos, C., & Edgar, B. A. (2002). A characterization of the effects of Dpp signaling on cell growth and proliferation in the Drosophila wing. *Development (Cambridge, England)*, *129*(4), 1003–1013.

Marty, T., Müller, B., Basler, K., & Affolter, M. (2000). Schnurri mediates Dpp-dependent repression of : brinker: transcription : Abstract : Nature Cell Biology. *Nature Cell Biology*, *2*(10), 745–749. http://doi.org/10.1038/35036383

Massagué, J. (2000). Transcriptional control by the TGF-beta/Smad signaling system. *The EMBO Journal*, *19*(8), 1745–1754. http://doi.org/10.1093/emboj/19.8.1745

Massagué, J. (2012). TGFβ signalling in context. *Nature Reviews Molecular Cell Biology*, *13*(10), 616–630. http://doi.org/10.1038/nrm3434

Matsuda, S., & Shimmi, O. (2012). Directional transport and active retention of Dpp/BMP create wing vein patterns in Drosophila. *Developmental Biology*, *366*(2), 153–162. http://doi.org/10.1016/j.ydbio.2012.04.009

Matsuda, S., Harmansa, S., & Affolter, M. (2015). BMP morphogen gradients in flies. *Cytokine & Growth Factor Reviews*.

Matter, K., Hunziker, W., & Mellman, I. (1992). Basolateral sorting of LDL receptor in MDCK cells: The cytoplasmic domain contains two tyrosine-dependent targeting determinants. *Cell*.

Matusek, T., Wendler, F., Polès, S., Pizette, S., D'Angelo, G., Fürthauer, M., & Thérond, P. P. (2014). The ESCRT machinery regulates the secretion and long-range activity of Hedgehog. *Nature*, *516*(7529), 99–103. http://doi.org/10.1038/nature13847

McCabe, B. D., Marqués, G., Haghighi, A. P., Fetter, R. D., Crotty, M. L., Haerry, T. E., et al. (2003). The BMP homolog Gbb provides a retrograde signal that regulates synaptic growth at the Drosophila neuromuscular

junction. *Neuron*, *39*(2), 241–254.
McClure, K. D., & Schubiger, G. (2005). Developmental analysis and squamous morphogenesis of the peripodial epithelium in Drosophila imaginal discs. *Development (Cambridge, England)*, *132*(22), 5033–5042. http://doi.org/10.1242/dev.02092
Meyer, E. J., Ikmi, A., & Gibson, M. C. (2011). Interkinetic Nuclear Migration Is a Broadly Conserved Feature of Cell Division in Pseudostratified Epithelia. *Current Biology : CB*, *21*(6), 485–491. http://doi.org/10.1016/j.cub.2011.02.002
Médina, E., Williams, J., Klipfell, E., Zarnescu, D., Thomas, G., & Le Bivic, A. (2002). Crumbs interacts with moesin and beta(Heavy)-spectrin in the apical membrane skeleton of Drosophila. *The Journal of Cell Biology*, *158*(5), 941–951. http://doi.org/10.1083/jcb.200203080
Miaczynska, M., Pelkmans, L., & Zerial, M. (2004). Not just a sink: endosomes in control of signal transduction. *Current Opinion in Cell Biology*, *16*(4), 400–406. http://doi.org/10.1016/j.ceb.2004.06.005
Michel, M., Raabe, I., Kupinski, A. P., Pérez-Palencia, R., & Bökel, C. (2011). Local BMP receptor activation at adherens junctions in the Drosophila germline stem cell niche. *Nature Communications*, *2*, 415. http://doi.org/10.1038/ncomms1426
Minami, M., Kinoshita, N., Kamoshida, Y., Tanimoto, H., & Tabata, T. (1999). brinker: is a target of Dpp in : Drosophila: that negatively regulates Dpp-dependent genes : Abstract : Nature. *Nature*, *398*(6724), 242–246. http://doi.org/10.1038/18451
Miranda, K. C., Khromykh, T., Christy, P., Le, T. L., Gottardi, C. J., Yap, A. S., et al. (2001). A dileucine motif targets E-cadherin to the basolateral cell surface in Madin-Darby canine kidney and LLC-PK1 epithelial cells. *The Journal of Biological Chemistry*, *276*(25), 22565–22572. http://doi.org/10.1074/jbc.M101907200
Miyazono, K. (2007). Regulation of TGF-β Family Signaling by Inhibitory Smads. *Cold Spring Harb Laboratory Press*, 363–387.
Morais-de-Sá, E., Mirouse, V., & St Johnston, D. (2010). aPKC phosphorylation of Bazooka defines the apical/lateral border in Drosophila epithelial cells. *Cell*, *141*(3), 509–523. http://doi.org/10.1016/j.cell.2010.02.040
Morata, G., & Lawrence, P. A. (1975). Control of compartment development by the engrailed gene in Drosophila. *Nature*, *255*(5510), 614–617.
Moustakas, A. (2005). Non-Smad TGF- signals. *Journal of Cell Science*, *118*(16), 3573–3584. http://doi.org/10.1242/jcs.02554
Moustakas, A., & Heldin, C. H. (2009). The regulation of TGF signal transduction. *Development (Cambridge, England)*, *136*(22), 3699–3714. http://doi.org/10.1242/dev.030338

Mueller, T. D., & Nickel, J. (2012). Promiscuity and specificity in BMP receptor activation. *FEBS Letters*, *586*(14), 1846–1859. http://doi.org/10.1016/j.febslet.2012.02.043

Muller, P., Rogers, K. W., Yu, S. R., Brand, M., & Schier, A. F. (2013). Morphogen transport. *Development (Cambridge, England)*, *140*(8), 1621–1638. http://doi.org/10.1242/dev.083519

Murphy, S. J., Dore, J., Edens, M., Coffey, R. J., Barnard, J. A., Mitchell, H., et al. (2004). Differential trafficking of transforming growth factor-beta receptors and ligand in polarized epithelial cells. *Molecular Biology of the Cell*, *15*(6), 2853–2862. http://doi.org/10.1091/mbc.E04-02-0097

Murphy, S. J., Shapira, K. E., Henis, Y. I., & Leof, E. B. (2007). A unique element in the cytoplasmic tail of the type II transforming growth factor-beta receptor controls basolateral delivery. *Molecular Biology of the Cell*, *18*(10), 3788–3799. http://doi.org/10.1091/mbc.E06-10-0930

Muyldermans, S. (2013). Nanobodies: Natural Single-Domain Antibodies. *Annual Review of Biochemistry, Vol 82*, *82*, 775–797. http://doi.org/10.1146/annurev-biochem-063011-092449

Müller, B., Hartmann, B., Pyrowolakis, G., Affolter, M., & Basler, K. (2003). Conversion of an extracellular Dpp/BMP morphogen gradient into an inverse transcriptional gradient. *Cell*, *113*(2), 221–233.

Nagarkar-Jaiswal, S., Lee, P.-T., Campbell, M. E., Chen, K., Anguiano-Zarate, S., Gutierrez, M. C., et al. (2015). A library of MiMICs allows tagging of genes and reversible, spatial and temporal knockdown of proteins in Drosophila. *Elife*, *4*, –. http://doi.org/10.7554/eLife.05338

Nellen, D. D., Affolter, M. M., & Basler, K. K. (1994). Receptor serine/threonine kinases implicated in the control of Drosophila body pattern by decapentaplegic. *Cell*, *78*(2), 225–237. http://doi.org/10.1016/0092-8674(94)90293-3

Nellen, D. D., Burke, R., Struhl, G., & Basler, K. (1996). Direct and Long-Range Action of a DPP Morphogen Gradient. *Cell*, *85*(3), 357–368. http://doi.org/10.1016/S0092-8674(00)81114-9

Neul, J. L., & Ferguson, E. L. (1998). Spatially restricted activation of the SAX receptor by SCW modulates DPP/TKV signaling in Drosophila dorsal-ventral patterning. *Cell*, *95*(4), 483–494.

Neumann, C. J., & Cohen, S. M. (1997). Long-range action of Wingless organizes the dorsal-ventral axis of the Drosophila wing. *Development (Cambridge, England)*, *124*(4), 871–880.

Nguyen, M., Park, S., Marqués, G., & Arora, K. (1998). Interpretation of a BMP Activity Gradient in Drosophila Embryos Depends on Synergistic Signaling by Two Type I Receptors, SAX and TKV. *Cell*, *95*(4), 495–506. http://doi.org/10.1016/S0092-8674(00)81617-7

Nguyen, M., Parker, L., & Arora, K. (2000). Identification of maverick, a novel

member of the TGF-beta superfamily in Drosophila. *Mechanisms of Development*, *95*(1-2), 201–206.
Nishihara, A., Watabe, T., Imamura, T., & Miyazono, K. (2002). Functional heterogeneity of bone morphogenetic protein receptor-II mutants found in patients with primary pulmonary hypertension. *Molecular Biology of the Cell*, *13*(9), 3055–3063. http://doi.org/10.1091/mbc.E02-02-0063
Nüsslein-Volhard, C., & Wieschaus, E. (1980). Mutations affecting segment number and polarity in Drosophila. *Nature*, *287*(5785), 795–801. http://doi.org/10.1038/287795a0
O'Brien, L. E., Jou, T. S., Pollack, A. L., Zhang, Q., Hansen, S. H., Yurchenco, P., & Mostov, K. E. (2001). Rac1 orientates epithelial apical polarity through effects on basolateral laminin assembly. *Nature Cell Biology*, *3*(9), 831–838. http://doi.org/10.1038/ncb0901-831
O'Connor-Giles, K. M., Ho, L. L., & Ganetzky, B. (2008). Nervous wreck interacts with thickveins and the endocytic machinery to attenuate retrograde BMP signaling during synaptic growth. *Neuron*, *58*(4), 507–518. http://doi.org/10.1016/j.neuron.2008.03.007
Ogiso, Y., Tsuneizumi, K., Masuda, N., Sato, M., & Tabata, T. (2011). Robustness of the Dpp morphogen activity gradient depends on negative feedback regulation by the inhibitory Smad, Dad. *Development, Growth & Differentiation*, *53*(5), 668–678. http://doi.org/10.1111/j.1440-169X.2011.01274.x
Ohata, S., Aoki, R., Kinoshita, S., Yamaguchi, M., Tsuruoka-Kinoshita, S., Tanaka, H., et al. (2011). Dual roles of Notch in regulation of apically restricted mitosis and apicobasal polarity of neuroepithelial cells. *Neuron*, *69*(2), 215–230. http://doi.org/10.1016/j.neuron.2010.12.026
Ozdamar, B., Bose, R., Barrios-Rodiles, M., Wang, H.-R., Zhang, Y., & Wrana, J. L. (2005). Regulation of the polarity protein Par6 by TGFbeta receptors controls epithelial cell plasticity. *Science (New York, N.Y.)*, *307*(5715), 1603–1609. http://doi.org/10.1126/science.1105718
Paladino, S., Lebreton, S., Tivodar, S., Campana, V., Tempre, R., & Zurzolo, C. (2008). Different GPI-attachment signals affect the oligomerisation of GPI-anchored proteins and their apical sorting. *Journal of Cell Science*, *121*(24), 4001–4007. http://doi.org/10.1242/jcs.036038
Pallavi, S. K., & Shashidhara, L. S. (2003). Egfr/Ras pathway mediates interactions between peripodial and disc proper cells in Drosophila wing discs. *Development (Cambridge, England)*, *130*(20), 4931–4941. http://doi.org/10.1242/dev.00719
Pallavi, S. K., & Shashidhara, L. S. (2005). Signaling interactions between squamous and columnar epithelia of the Drosophila wing disc | Journal of Cell Science. *Journal of Cell Science*.
Panganiban, G., Rashka, K. E., Neitzel, M. D., & Hoffmann, F. M. (1990).

Biochemical-Characterization of the Drosophila-Dpp Protein, a Member of the Transforming Growth-Factor-Beta Family of Growth-Factors. *Molecular and Cellular Biology*, *10*(6), 2669–2677.

Panin, V. M., Papayannopoulos, V., Wilson, R., & Irvine, K. D. (1997). Fringe modulates Notch-ligand interactions. *Nature*, *387*(6636), 908–912. http://doi.org/10.1038/43191

Parker, L., Ellis, J. E., Nguyen, M. Q., & Arora, K. (2006). The divergent TGF-beta ligand Dawdle utilizes an activin pathway to influence axon guidance in Drosophila. *Development (Cambridge, England)*, *133*(24), 4981–4991. http://doi.org/10.1242/dev.02673

Pastor-Pareja, J. C., & Xu, T. (2011). Shaping cells and organs in Drosophila by opposing roles of fat body-secreted Collagen IV and perlecan. *Developmental Cell*, *21*(2), 245–256. http://doi.org/10.1016/j.devcel.2011.06.026

Paul, S. M. (2003). The Na+/K+ ATPase is required for septate junction function and epithelial tube-size control in the Drosophila tracheal system. *Development (Cambridge, England)*, *130*(20), 4963–4974. http://doi.org/10.1242/dev.00691

Paul, S. M., Palladino, M. J., & Beitel, G. J. (2007). A pump-independent function of the Na,K-ATPase is required for epithelial junction function and tracheal tube-size control. *Development (Cambridge, England)*, *134*(1), 147–155. http://doi.org/10.1242/dev.02710

Pellikka, M., Tanentzapf, G., Pinto, M., Smith, C., McGlade, C. J., Ready, D. F., & Tepass, U. (2002). Crumbs, the Drosophila homologue of human CRB1/RP12, is essential for photoreceptor morphogenesis. *Nature*, *416*(6877), 143–149. http://doi.org/10.1038/nature721

Penton, A., Chen, Y., Staehling-Hampton, K., Wrana, J. L., Attisano, L., Szidonya, J., et al. (1994). Identification of two bone morphogenetic protein type I receptors in Drosophila and evidence that Brk25D is a decapentaplegic receptor. *Cell*, *78*(2), 239–250. http://doi.org/10.1016/0092-8674(94)90294-1

Persson, U., Souchelnytskyi, S., Franzén, P., Miyazono, K., Dijke, ten, P., & Heldin, C. H. (1997). Transforming growth factor (TGF-beta)-specific signaling by chimeric TGF-beta type II receptor with intracellular domain of activin type IIB receptor. *The Journal of Biological Chemistry*, *272*(34), 21187–21194.

Peterson, A. J., & O'Connor, M. B. (2012). You're Going to Need a Bigger (Glass Bottom) Boat. *Science Signaling*, *5*(218), pe14–pe14. http://doi.org/10.1126/scisignal.2002998

Peterson, A. J., & O'Connor, M. B. (2013). Activin receptor inhibition by Smad2 regulates Drosophila wing disc patterning through BMP-response elements. *Development (Cambridge, England)*, *140*(3), 649–659.

http://doi.org/10.1242/dev.085605
Peterson, A. J., Jensen, P. A., Shimell, M., Stefancsik, R., Wijayatonge, R., Herder, R., et al. (2012). R-Smad competition controls activin receptor output in Drosophila. *PloS One*, *7*(5), e36548. http://doi.org/10.1371/journal.pone.0036548
Prewitt, A. R., Ghose, S., Frump, A. L., Datta, A., Austin, E. D., Kenworthy, A. K., & de Caestecker, M. P. (2015). Heterozygous Null Bone Morphogenetic Protein Receptor Type 2 Mutations Promote SRC Kinase-dependent Caveolar Trafficking Defects and Endothelial Dysfunction in Pulmonary Arterial Hypertension. *The Journal of Biological Chemistry*, *290*(2), 960–971. http://doi.org/10.1074/jbc.M114.591057
Pyrowolakis, G., Hartmann, B., Müller, B., Basler, K., & Affolter, M. (2004). A simple molecular complex mediates widespread BMP-induced repression during Drosophila development. *Developmental Cell*, *7*(2), 229–240. http://doi.org/10.1016/j.devcel.2004.07.008
Raftery, L. A., Twombly, V., Wharton, K., & Gelbart, W. M. (1995). Genetic screens to identify elements of the decapentaplegic signaling pathway in Drosophila. *Genetics*, *139*(1), 241–254.
Ramirez-Weber, F. A., & Kornberg, T. B. (1999). Cytonemes: Cellular Processes that Project to the Principal Signaling Center in Drosophila Imaginal Discs. *Cell*.
Ray, R. (2015). gbb-GFP construct and insertions.
Ray, R. P., & Wharton, K. A. (2001). Context-dependent relationships between the BMPs gbb and dpp during development of the Drosophila wing imaginal disk. *Development (Cambridge, England)*, *128*(20), 3913–3925.
Ren, X., Sun, J., Housden, B. E., Hu, Y., Roesel, C., Lin, S., et al. (2013). Optimized gene editing technology for Drosophila melanogaster using germ line-specific Cas9. *Proceedings of the National Academy of Sciences of the United States of America*, *110*(47), 19012–19017. http://doi.org/10.1073/pnas.1318481110
Restrepo, S., Zartman, J. J., & Basler, K. (2014). Coordination of Patterning and Growth by the Morphogen DPP. *Current Biology : CB*, *24*(6), R245–R255. http://doi.org/10.1016/j.cub.2014.01.055
Richardson, E. C. N., & Pichaud, F. (2010). Crumbs is required to achieve proper organ size control during Drosophila head development. *Development (Cambridge, England)*, *137*(4), 641–650. http://doi.org/10.1242/dev.041913
Robinson, B. S., Huang, J., Hong, Y., & Moberg, K. H. (2010). Crumbs Regulates Salvador/Warts/Hippo Signaling in Drosophila via the FERM-Domain Protein Expanded. *Current Biology*.
Rodriguez-Boulan, E., & Macara, I. G. (2014). Organization and execution of

the epithelial polarity programme. *Nature Reviews Molecular Cell Biology*, *15*(4), 225–242. http://doi.org/10.1038/nrm3775

Rodríguez Dd, D. D. A., Terriente, J., Galindo, M. I., Couso, J. P., & Diaz-Benjumea, F. J. (2002). Different mechanisms initiate and maintain wingless expression in the Drosophila wing hinge. *Development (Cambridge, England)*, *129*(17), 3995–4004.

Roh, M. H., Makarova, O., Liu, C.-J., Shin, Lee, S., Laurinec, S., et al. (2002). The Maguk protein, Pals1, functions as an adapter, linking mammalian homologues of Crumbs and Discs Lost. *The Journal of Cell …*.

Rong, Y. S. (2000). Gene Targeting by Homologous Recombination in Drosophila. *Science (New York, N.Y.)*, *288*(5473), 2013–2018. http://doi.org/10.1126/science.288.5473.2013

Ross, J. J., Shimmi, O., Vilmos, P., Petryk, A., Kim, H., Gaudenz, K., et al. (2001). Twisted gastrulation is a conserved extracellular BMP antagonist : Abstract : Nature. *Nature*, *410*(6827), 479–483. http://doi.org/10.1038/35068578

Rothbauer, U., Zolghadr, K., Muyldermans, S., Schepers, A., Cardoso, M. C., & Leonhardt, H. (2007). A Versatile Nanotrap for Biochemical and Functional Studies with Fluorescent Fusion Proteins. *Molecular & Cellular Proteomics*, *7*(2), 282–289. http://doi.org/10.1074/mcp.M700342-MCP200

Rothbauer, U., Zolghadr, K., Tillib, S., Nowak, D., Schermelleh, L., Gahl, A., et al. (2006). Targeting and tracing antigens in live cells with fluorescent nanobodies. *Nature Methods*, *3*(11), 887–889. http://doi.org/10.1038/nmeth953

Roy, S., Hsiung, F., & Kornberg, T. B. (2011). Specificity of Drosophila cytonemes for distinct signaling pathways. *Science (New York, N.Y.)*, *332*(6027), 354–358. http://doi.org/10.1126/science.1198949

Roy, S., Huang, H., Liu, S., & Kornberg, T. B. (2014). Cytoneme-mediated contact-dependent transport of the Drosophila decapentaplegic signaling protein. *Science (New York, N.Y.)*, *343*(6173), 1244624. http://doi.org/10.1126/science.1244624

Ruberte, E., Marty, T., Nellen, D., Affolter, M., & Basler, K. (1995). An absolute requirement for both the type II and type I receptors, punt and thick veins, for dpp signaling in vivo. *Cell*, *80*(6), 889–897.

Saerens, D., Pellis, M., Loris, R., Pardon, E., Dumoulin, M., Matagne, A., et al. (2005). Identification of a universal VHH framework to graft non-canonical antigen-binding loops of camel single-domain antibodies. *Journal of Molecular Biology*, *352*(3), 597–607. http://doi.org/10.1016/j.jmb.2005.07.038

Saitoh, M., Shirakihara, T., Fukasawa, A., Horiguchi, K., Sakamoto, K., Sugiya, H., et al. (2012). Basolateral BMP signaling in polarized epithelial cells.

PloS One, *8*(5), e62659–e62659. http://doi.org/10.1371/journal.pone.0062659

Sander, V., Eivers, E., Choi, R. H., & De Robertis, E. M. (2010). Drosophila Smad2 opposes Mad signaling during wing vein development. *PloS One*, *5*(4), e10383. http://doi.org/10.1371/journal.pone.0010383

Sarov, M., Barz, C., Jambor, H., Hein, M. Y., Schmied, C., Suchold, D., et al. (2015). *A genome-wide resource for the analysis of protein localisation in Drosophila*. *BioRxiv*.

Schmierer, B., & Hill, C. S. (2007). TGFβ–SMAD signal transduction: molecular specificity and functional flexibility. *Nature Reviews Molecular Cell Biology*, *8*(12), 970–982. http://doi.org/10.1038/nrm2297

Schornack, S., Fuchs, R., Huitema, E., Rothbauer, U., Lipka, V., & Kamoun, S. (2009). Protein mislocalization in plant cells using a GFP-binding chromobody. *The Plant Journal*, *60*(4), 744–754. http://doi.org/10.1111/j.1365-313X.2009.03982.x

Schwank, G., Dalessi, S., Yang, S.-F., Yagi, R., de Lachapelle, A. M., Affolter, M., et al. (2011a). Formation of the long range Dpp morphogen gradient. *PLoS Biology*, *9*(7), e1001111. http://doi.org/10.1371/journal.pbio.1001111

Schwank, G., Restrepo, S., & Basler, K. (2008). Growth regulation by Dpp: an essential role for Brinker and a non-essential role for graded signaling levels. *Development (Cambridge, England)*, *135*(24), 4003–4013. http://doi.org/10.1242/dev.025635

Schwank, G., Tauriello, G., Yagi, R., Kranz, E., Koumoutsakos, P., & Basler, K. (2011b). Antagonistic growth regulation by Dpp and Fat drives uniform cell proliferation. *Developmental Cell*, *20*(1), 123–130. http://doi.org/10.1016/j.devcel.2010.11.007

Sebald, W., Nickel, J., Zhang, J.-L., & Mueller, T. D. (2004). Molecular recognition in bone morphogenetic protein (BMP)/receptor interaction. *Biological Chemistry*, *385*(8), 697–710. http://doi.org/10.1515/BC.2004.086

Sebo, Z. L., Lee, H. B., Peng, Y., & Guo, Y. (2014). A simplified and efficient germline-specific CRISPR/Cas9 system for Drosophilagenomic engineering. *Fly*, *8*(1), 52–57. http://doi.org/10.4161/fly.26828

Serpe, M., & O'Connor, M. B. (2006). The metalloprotease tolloid-related and its TGF-beta-like substrate Dawdle regulate Drosophila motoneuron axon guidance. *Development (Cambridge, England)*, *133*(24), 4969–4979. http://doi.org/10.1242/dev.02711

Shaner, N. C., Steinbach, P. A., & Tsien, R. Y. (2005). A guide to choosing fluorescent proteins. *Nature Methods*, *2*(12), 905–909. http://doi.org/10.1038/nmeth819

Shi, Y., & Massagué, J. (2003). Mechanisms of TGF-β Signaling from Cell

Membrane to the Nucleus. *Cell*, *113*(6), 685–700. http://doi.org/10.1016/S0092-8674(03)00432-X

Shimell, M. J., Ferguson, E. L., Childs, S. R., & O'Connor, M. B. (1991). The Drosophila dorsal-ventral patterning gene tolloid is related to human bone morphogenetic protein 1. *Cell*.

Shimmi, O. (2003). Physical properties of Tld, Sog, Tsg and Dpp protein interactions are predicted to help create a sharp boundary in Bmp signals during dorsoventral patterning of the Drosophila embryo. *Development (Cambridge, England)*, *130*(19), 4673–4682. http://doi.org/10.1242/dev.00684

Shimmi, O., Ralston, A., Blair, S. S., & O'Connor, M. B. (2005a). The crossveinless gene encodes a new member of the Twisted gastrulation family of BMP-binding proteins which, with Short gastrulation, promotes BMP …. *Developmental Biology*.

Shimmi, O., Umulis, D., Othmer, H., & O'Connor, M. B. (2005b). Facilitated Transport of a Dpp/Scw Heterodimer by Sog/Tsg Leads to Robust Patterning of the Drosophila Blastoderm Embryo. *Cell*, *120*(6), 873–886. http://doi.org/10.1016/j.cell.2005.02.009

Simin, K., Bates, E. A., Horner, M. A., & Letsou, A. (1998). Genetic analysis of punt, a type II Dpp receptor that functions throughout the Drosophila melanogaster life cycle. *Genetics*, *148*(2), 801–813.

Singer, M. A., Penton, A., Twombly, V., Hoffmann, F. M., & Gelbart, W. M. (1997). Signaling through both type I DPP receptors is required for anterior-posterior patterning of the entire Drosophila wing. *Development (Cambridge, England)*, *124*(1), 79–89.

Sivasankaran, R., Vigano, M. A., Müller, B., Affolter, M., & Basler, K. (2000). Direct transcriptional control of the Dpp target omb by the DNA binding protein Brinker. *The EMBO Journal*, *19*(22), 6162–6172. http://doi.org/10.1093/emboj/19.22.6162

Sotillos, S., Díaz-Meco, M. T., Caminero, E., Moscat, J., & Campuzano, S. (2004). DaPKC-dependent phosphorylation of Crumbs is required for epithelial cell polarity in Drosophila. *The Journal of Cell Biology*, *166*(4), 549–557. http://doi.org/10.1083/jcb.200311031

Sotillos, S., Díaz-Meco, M. T., Moscat, J., & Castelli-Gair Hombría, J. (2008). Polarized subcellular localization of Jak/STAT components is required for efficient signaling. *Current Biology : CB*, *18*(8), 624–629. http://doi.org/10.1016/j.cub.2008.03.055

Spencer, F. A., Hoffmann, F. M., & Gelbart, W. M. (1982). Decapentaplegic: A gene complex affecting morphogenesis in Drosophila melanogaster. *Cell*.

St Johnston, D., & Sanson, B. (2011). Epithelial polarity and morphogenesis. *Current Opinion in Cell Biology*, *23*(5), 540–546.

http://doi.org/10.1016/j.ceb.2011.07.005
St Pierre, S. E., Galindo, M. I., Couso, J. P., & Thor, S. (2002). Control of Drosophila imaginal disc development by rotund and roughened eye: differentially expressed transcripts of the same gene encoding functionally distinct zinc finger proteins. *Development (Cambridge, England)*, *129*(5), 1273–1281.
Stadler, C., Rexhepaj, E., Singan, V. R., Murphy, R. F., Pepperkok, R., Uhlén, M., et al. (2013). Immunofluorescence and fluorescent-protein tagging show high correlation for protein localization in mammalian cells. *Nature Methods*, *10*(4), 315–323. http://doi.org/10.1038/nmeth.2377
Staehling-Hampton, K., Laughon, A. S., & Hoffmann, F. M. (1995). A Drosophila protein related to the human zinc finger transcription factor PRDII/MBPI/HIV-EP1 is required for dpp signaling. *Development (Cambridge, England)*, *121*(10), 3393–3403.
Stein, von, W., Ramrath, A., Grimm, A., Müller-Borg, M., & Wodarz, A. (2005). Direct association of Bazooka/PAR-3 with the lipid phosphatase PTEN reveals a link between the PAR/aPKC complex and phosphoinositide signaling. *Development (Cambridge, England)*, *132*(7), 1675–1686. http://doi.org/10.1242/dev.01720
Strigini, M., & Cohen, S. M. (2000). Wingless gradient formation in the Drosophila wing. *Current Biology : CB*, *10*(6), 293–300. http://doi.org/10.1016/S0960-9822(00)00378-X
Sutherland, D. J. (2003). Stepwise formation of a SMAD activity gradient during dorsal-ventral patterning of the Drosophila embryo. *Development (Cambridge, England)*, *130*(23), 5705–5716. http://doi.org/10.1242/dev.00801
Suzuki, A. (2006). The PAR-aPKC system: lessons in polarity. *Journal of Cell Science*, *119*(6), 979–987. http://doi.org/10.1242/jcs.02898
Tabata, T., Eaton, S., & Kornberg, T. B. (1992). The Drosophila hedgehog gene is expressed specifically in posterior compartment cells and is a target of engrailed regulation. *Genes & Development*, *6*(12B), 2635–2645.
Tai, A. W., Chuang, J. Z., Bode, C., Wolfrum, U., & Sung, C. H. (1999). Rhodopsin's Carboxy-Terminal Cytoplasmic Tail Acts as a Membrane Receptor for Cytoplasmic Dynein by Binding to the Dynein Light Chain Tctex-1. *Cell*.
Takeda, M., Leser, G. P., Russell, C. J., & Lamb, R. A. (2003). Influenza virus hemagglutinin concentrates in lipid raft microdomains for efficient viral fusion. *Proceedings of the National Academy of Sciences of the United States of America*, *100*(25), 14610–14617. http://doi.org/10.1073/pnas.2235620100
Tanentzapf, G., & Tepass, U. (2003). Interactions between the : crumbs: , :

lethal giant larvae: and : bazooka: pathways in epithelial polarization : Abstract : Nature Cell Biology. *Nature Cell Biology*.

Tanimoto, H., Itoh, S., Dijke, ten, P., & Tabata, T. (2000). Hedgehog creates a gradient of DPP activity in Drosophila wing imaginal discs. *Molecular Cell*, *5*(1), 59–71. http://doi.org/10.1016/S1097-2765(00)80403-7

Teleman, A. A. A., & Cohen, S. M. S. (2000). Dpp Gradient Formation in the Drosophila Wing Imaginal Disc. *Cell*, *103*(6), 10–10. http://doi.org/10.1016/S0092-8674(00)00199-9

Tepass, U. (1996). Crumbs, a Component of the Apical Membrane, Is Required for Zonula Adherens Formation in Primary Epithelia ofDrosophila. *Developmental Biology*, *177*(1), 217–225. http://doi.org/10.1006/dbio.1996.0157

Tepass, U. (2012). The apical polarity protein network in Drosophila epithelial cells: regulation of polarity, junctions, morphogenesis, cell growth, and survival. *Annual Review of Cell and Developmental Biology*, *28*, 655–685. http://doi.org/10.1146/annurev-cellbio-092910-154033

Tepass, U., & Knust, E. (1990). Phenotypic and developmental analysis of mutations at thecrumbs locus, a gene required for the development of epithelia inDrosophila melanogaster. *Development Genes and Evolution*, *199*(4), 189–206. http://doi.org/10.1007/BF01682078

Tepass, U., Theres, C., & Knust, E. (1990). crumbs encodes an EGF-like protein expressed on apical membranes of Drosophila epithelial cells and required for organization of epithelia. *Cell*.

Terracol, R., & Lengyel, J. A. (1994). The thick veins gene of Drosophila is required for dorsoventral polarity of the embryo. *Genetics*, *138*(1), 165–178.

Torres-Vazquez, J., Warrior, R., & Arora, K. (2000). schnurri Is Required for dpp-Dependent Patterning of the Drosophila Wing. *Developmental Biology*, *227*(2), 388–402. http://doi.org/10.1006/dbio.2000.9900

Torroja, C., Gorfinkiel, N., & Guerrero, I. (2005). Mechanisms of Hedgehog gradient formation and interpretation. *Journal of Neurobiology*, *64*(4), 334–356. http://doi.org/10.1002/neu.20168

Tsuneizumi, K., Nakayama, T., Kamoshida, Y., Kornberg, T. B., Christian, J. L., & Tabata, T. (1997). Daughters against dpp modulates dpp organizing activity in Drosophila wing development. *Nature*, *389*(6651), 627–631. http://doi.org/10.1038/39362

Venken, K. J. T., Carlson, J. W., Schulze, K. L., Pan, H., He, Y., Spokony, R., et al. (2009). Versatile P[acman] BAC libraries for transgenesis studies in Drosophila melanogaster. *Nature Methods*, *6*(6), 431–434. http://doi.org/10.1038/nmeth.1331

Venken, K. J. T., Schulze, K. L., Haelterman, N. A., Pan, H., He, Y., Evans-Holm, M., et al. (2011). MiMIC: a highly versatile transposon insertion

resource for engineering Drosophila melanogaster genes. *Nature Methods*, *8*(9), 737–743. http://doi.org/10.1038/nmeth.1662

Vicente-Manzanares, M., Webb, D. J., & Horwitz, A. R. (2005). Cell migration at a glance. *Journal of Cell Science*, *118*(Pt 21), 4917–4919. http://doi.org/10.1242/jcs.02662

Vuilleumier, R., Springhorn, A., Patterson, L., Koidl, S., Hammerschmidt, M., Affolter, M., & Pyrowolakis, G. (2010). Control of Dpp morphogen signalling by a secreted feedback regulator. *Nature Cell Biology*, *12*(6), 611–617. http://doi.org/10.1038/ncb2064

Wang, S. H., Simcox, A., & Campbell, G. (2000). Dual role for Drosophila epidermal growth factor receptor signaling in early wing disc development. *Genes & Development*, *14*(18), 2271–2276.

Wartlick, O., Mumcu, P., Kicheva, A., Bittig, T., Seum, C., Jülicher, F., & González-Gaitán, M. (2011). Dynamics of Dpp signaling and proliferation control. *Science (New York, N.Y.)*, *331*(6021), 1154–1159. http://doi.org/10.1126/science.1200037

Weiss, A., Charbonnier, E., Ellertsdóttir, E., Tsirigos, A., Wolf, C., Schuh, R., et al. (2010). A conserved activation element in BMP signaling during Drosophila development. *Nature Structural & Molecular Biology*, *17*(1), 69–76. http://doi.org/10.1038/nsmb.1715

Weisz, O. A., & Rodriguez-Boulan, E. (2009). Apical trafficking in epithelial cells: signals, clusters and motors. *Journal of Cell Science*, *122*(23), 4253–4266. http://doi.org/10.1242/jcs.032615

Wharton, K. A., Ray, R. P., & Gelbart, W. M. (1993). An activity gradient of decapentaplegic is necessary for the specification of dorsal pattern elements in the Drosophila embryo. *Development (Cambridge, England)*, *117*(2), 807–822.

Whitworth, A. J., & Russell, S. (2003). Temporally dynamic response to Wingless directs the sequential elaboration of the proximodistal axis of the Drosophila wing. *Developmental Biology*, *254*(2), 277–288.

Widmann, T. J., & Dahmann, C. (2009a). Dpp signaling promotes the cuboidal-to-columnar shape transition of Drosophila wing disc epithelia by regulating Rho1. *Journal of Cell Science*, *122*(9), 1362–1373. http://doi.org/10.1242/jcs.044271

Widmann, T. J., & Dahmann, C. (2009b). Wingless signaling and the control of cell shape in Drosophila wing imaginal discs. *Developmental Biology*, *334*(1), 161–173. http://doi.org/10.1016/j.ydbio.2009.07.013

Wodarz, A., Grawe, F., & Knust, E. (1993). CRUMBS is involved in the control of apical protein targeting during Drosophila epithelial development. *Mechanisms of Development*, *44*(2-3), 175–187.

Wodarz, A., Hinz, U., Engelbert, M., & Knust, E. (1995). Expression of crumbs confers apical character on plasma membrane domains of ectodermal

epithelia of Drosophila. *Cell*, *82*(1), 67–76.
Wu, J., & Cohen, S. M. (2002). Repression of Teashirt marks the initiation of wing development. *Development (Cambridge, England)*, *129*(10), 2411–2418.
Wu, J., Klein, T. J., & Mlodzik, M. (2004). Subcellular localization of frizzled receptors, mediated by their cytoplasmic tails, regulates signaling pathway specificity. *PLoS Biology*, *2*(7), E158. http://doi.org/10.1371/journal.pbio.0020158
Xu, J., Lamouille, S., & Derynck, R. (2009). TGF-β-induced epithelial to mesenchymal transition. *Cell Research*, *19*(2), 156–172. http://doi.org/10.1038/cr.2009.5
Yagi, R., Mayer, F., & Basler, K. (2010). Refined LexA transactivators and their use in combination with the Drosophila Gal4 system. *Proceedings of the National Academy of Sciences of the United States of America*, *107*(37), 16166–16171. http://doi.org/10.1073/pnas.1005957107
Yamazaki, Y., Palmer, L., Alexandre, C., Kakugawa, S., Beckett, K., Gaugue, I., et al. (2016). Godzilla-dependent transcytosis promotes Wingless signalling in Drosophila wing imaginal discs. *Nature Cell Biology*. http://doi.org/10.1038/ncb3325
Yan, D., & Lin, X. (2009). Shaping Morphogen Gradients by Proteoglycans. *Cold Spring Harbor Perspectives in Biology*, *1*(3), a002493–a002493. http://doi.org/10.1101/cshperspect.a002493
Yin, X., Murphy, S. J., Wilkes, M. C., Ji, Y., & Leof, E. B. (2013). Retromer maintains basolateral distribution of the type II TGF-β receptor via the recycling endosome. *Molecular Biology of the Cell*, *24*(14), 2285–2298. http://doi.org/10.1091/mbc.E13-02-0093
Yu, W. (2004). 1-Integrin Orients Epithelial Polarity via Rac1 and Laminin. *Molecular Biology of the Cell*, *16*(2), 433–445. http://doi.org/10.1091/mbc.E04-05-0435
Yu, Z., Ren, M., Wang, Z., Zhang, B., Rong, Y. S., Jiao, R., & Gao, G. (2013). Highly Efficient Genome Modifications Mediated by CRISPR/Cas9 in Drosophila. ….
Zecca, M., & Struhl, G. (2002a). Control of growth and patterning of the Drosophila wing imaginal disc by EGFR-mediated signaling. *Development (Cambridge, England)*, *129*(6), 1369–1376.
Zecca, M., & Struhl, G. (2002b). Subdivision of the Drosophila wing imaginal disc by EGFR-mediated signaling. *Development (Cambridge, England)*, *129*(6), 1357–1368.
Zecca, M., & Struhl, G. (2010). PLOS Biology: A Feed-Forward Circuit Linking Wingless, Fat-Dachsous Signaling, and the Warts-Hippo Pathway to Drosophila Wing Growth. *PLoS Biology*.
Zecca, M., Basler, K., & Struhl, G. (1995). Sequential organizing activities of

engrailed, hedgehog and decapentaplegic in the Drosophila wing. *Development (Cambridge, England)*, *121*(8), 2265–2278.

Zecca, M., Basler, K., & Struhl, G. (1996). Direct and long-range action of a wingless morphogen gradient. *Cell*, *87*(5), 833–844. http://doi.org/10.1016/S0092-8674(00)81991-1

Zelhof, A. C., & Hardy, R. W. (2004). WASp is required for the correct temporal morphogenesis of rhabdomere microvilli. *The Journal of Cell Biology*, *164*(3), 417–426. http://doi.org/10.1083/jcb.200307048

Zheng, X. Y., Zugates, C. T., Lu, Z. Y., Shi, L., Bai, J. M., & Lee, T. (2006). Baboon/dSmad2 TGF-beta signaling is required during late larval stage for development of adult-specific neurons. *The EMBO Journal*, *25*(3), 615–627. http://doi.org/10.1038/sj.emboj.7600962

Zheng, X., Wang, J., Haerry, T. E., Wu, A. Y.-H., Martin, J., O'Connor, M. B., et al. (2003). TGF-beta signaling activates steroid hormone receptor expression during neuronal remodeling in the Drosophila brain. *Cell*, *112*(3), 303–315.

Zhou, S. S., Lo, W.-C. W., Suhalim, J. L. J., Digman, M. A. M., Gratton, E. E., Nie, Q. Q., & Lander, A. D. A. (2012). Free extracellular diffusion creates the Dpp morphogen gradient of the Drosophila wing disc. *Current Biology : CB*, *22*(8), 668–675. http://doi.org/10.1016/j.cub.2012.02.065

Zhou, W., & Hong, Y. (2012). Drosophila Patj plays a supporting role in apical-basal polarity but is essential for viability. *Development (Cambridge, England)*, *139*(16), 2891–2896. http://doi.org/10.1242/dev.083162

Zhu, C. C., Boone, J. Q., Jensen, P. A., Hanna, S., Podemski, L., Locke, J., et al. (2008). Drosophila Activin- and the Activin-like product Dawdle function redundantly to regulate proliferation in the larval brain. *Development (Cambridge, England)*, *135*(3), 513–521. http://doi.org/10.1242/dev.010876

Zou, J., Wang, X., & Wei, X. (2012). Crb apical polarity proteins maintain zebrafish retinal cone mosaics via intercellular binding of their extracellular domains. *Developmental Cell*, *22*(6), 1261–1274. http://doi.org/10.1016/j.devcel.2012.03.007